UCGE Reports

Number 20221

Department of Geomatics Engineering

Remote Estimation of Leaf Area Index in Forested Ecosystems

(URL: http://www.geomatics.ucalgary.ca/links/GradTheses.html)

by

David McAllister

May 2005

UNIVERSITY OF
CALGARY

UNIVERSITY OF CALGARY

Remote Estimation of Leaf Area Index in Forested Ecosystems

by

David Michael McAllister

A THESIS

SUBMITTED TO THE FACULTY OF GRADUATE STUDIES

IN PARTIAL FULFILLMENT OF THE REQUIREMENTS FOR THE

DEGREE OF MASTER OF SCIENCE

DEPARTMENT OF GEOMATICS ENGINEERING

CALGARY, ALBERTA

MAY, 2005

Abstract

Leaf area index (LAI) is defined as the ratio of the foliage area contained within a given area divided by the ground area in question. This quantity is a useful input parameter in various environmental modeling applications. Unfortunately, *in-situ* sampling of LAI is spatially limited and costly; therefore researchers have tried to relate remote sensing measurements to *in-situ* LAI measurements.

Remote sensing models have traditionally attempted to use spectral vegetation indices to model variations in LAI. However, these models have achieved only moderate success because their accuracy is often dependent on the influence of the background. Recently, two promising techniques have been applied for remote LAI estimation: linear spectral mixture analysis and modification of spectral vegetation indices. These techniques offer explicit strategies for the mitigation of background effects. Additional remote estimation techniques have been developed specifically for this study, namely the scale factor and the normalized distance methods

These remote estimation models are derived and compared for a region of montane forest in Kananaskis Country. Analysis has been conducted for both needleleaf and broadleaf vegetation to determine the relative efficacy of the models for each particular vegetation type. Sensitivity analysis has been performed to determine the sensitivity of the derived-models to variation in background spectra and the accuracy of plot locations. Monte Carlo simulations have been performed to determine how various parameters influence the quality of landscape-level LAI estimates. A multi-scale analysis has been performed across a portion of the Upper Elbow River watershed, using MODIS and resampled SPOT imagery, to determine the extent to which the derived relationships are sensor-specific and scale dependent.

The results of this study indicate that the best overall technique for remote LAI estimation is the normalized distance method. The other modeling techniques exhibit varying degrees of modeling success, while evincing significant dependence on vegetation type. This is demonstrated by the contrast between the superior performance of the moisture stress index and the canopy shadow

fraction, for broadleaf and needleleaf vegetation respectively, with their inferior performance for the other vegetation type. The modeling of plot location errors confirmed the validity and accuracy of the plot location algorithm and the georeferencing of the SPOT-4 image. Spatial statistical analyses demonstrated the correlation of the modeling parameters to vary inversely with distance and thereby to demonstrate the validity of the estimation relationships derived. The Monte Carlo simulations determined that the quality of landscape-level LAI estimates depends on the number of pixels under consideration, the quality of the remote estimation model and the landscape variability in terms of LAI. These simulations allowed for the quality of a landscape level LAI estimate to be determined given the particular constraints associated with a given landscape. The multi-scale analysis demonstrated that the remote estimation techniques exhibited significant dependence on scale and imaging platform, almost irrespective of the remote estimation model used.

Acknowledgements

To my family, for the unwavering faith you have shown in me in whatever I have done. I am more grateful than I could ever express.

To my supervisor Dr. Caterina Valeo, without whose guidance and support none of this would have been accomplished

To Rebeca Quinonez-Pinon for her help with the field measurements.

Table of Contents

List of Tables

x

List of Figures

1. Introduction

1.1 Problem Statement

The estimation of leaf area index (LAI) has long been of interest to scientists in a variety of disciplines ranging from hydrology to forestry. LAI has been used as a primary variable of interest in a variety of environmental process models.

Traditionally, measurements of LAI have been performed *in-situ* using a variety of sampling techniques including destructive sampling, allometric methods and optical observation. The primary disadvantage of these particular *in-situ* measurements is that they are geographically limited and considerable effort is required to obtain even the most local characterization of LAI.

Due to the geographic limitation associated with *in-situ* LAI measurement and the modeling requirement for LAI estimates at the regional scale, remote sensing techniques have been developed to estimate LAI. Historically, remote sensing has used a variety of different spectral vegetation indices for the prediction of LAI. This approach has produced mixed and frequently ecosystem specific results due to problems such as saturation and insensitivity of spectral vegetation indices to changes in LAI. The primary advantage of this approach is the simplicity of obtaining spectral vegetation indices over large areas as compared to other more involved techniques.

Two techniques have been developed in recent times in response to the need for higher quality results in remote LAI estimation.

The first technique which has improved upon the use of spectral vegetation indices is the use of adjusted spectral vegetation indices for LAI estimation. Adjustment of spectral vegetation indices involves a scaling of the initial spectral vegetation index by a factor derived from the middle infrared bands. The incorporation of information from the middle infrared bands tends to improve LAI estimation because the middle infrared bands are the most sensitive to changes in LAI. This

sensitivity is thought to be related to observed differences in moisture content for areas of high LAI versus canopies of low LAI (Eklundh *et al.,* 2001).

The second technique that has seen increasing application for LAI estimation is linear spectral mixture analysis. The first task required in spectral mixture analysis involves the definition of classes, in this case typically sunlit canopy, shadowed canopy and background, which are used for LAI estimation. The second task of spectral mixture analysis is the selection of pixels contained within the image in which the classes do not co-exist. The third task is to determine the percentage of each pixel that belongs to each class, typically performed using a constrained least squares approach. Finally, the percentage composition of one of the classes is used for LAI estimation (Peddle *et al., 1999*, Peddle *et al., 2001*).

Spectral mixture analysis and adjustment of spectral vegetation indices have consistently proven to be more effective than traditional remote sensing techniques using unadjusted spectral vegetation indices for LAI estimation (Peddle *et al.,* 1999, Peddle *et al.,* 2001, Peddle and Johnson 2000, Seed and King 2003, Hu *et al.,* 2004). However, few if any explicit comparisons of spectral mixture analysis and adjustment of spectral vegetation indices have been performed. As these techniques exhibit particular advantages and disadvantages it is important to know their relative modeling strengths so that an appropriate method can be selected based on the particular operational context for which estimates are required. Additionally, should neither technique prove sufficiently able to model variations in canopy LAI alternative techniques must be explored.

1.2 General Thesis Objectives

There are three primary objectives for this thesis. These objectives are:
1) To derive and compare the relationships between *in-situ* LAI measurements and input parameters determined using the modification of spectral vegetation indices, linear spectral mixture analysis and methods developed for this study.
2) To determine the sensitivity of these relationships to variations in error and scale.
3) To determine the accuracy of the estimation process across a landscape to determine whether these relationships are useful in the derivation of input data to hydrological, forest management and climatic models

1.3 Thesis Outline

To accomplish the three preceding objectives, several steps have been taken. Firstly, a literature review, presented in Chapter 2, has been conducted to provide a context for the work performed in this study. The relevance of this work is demonstrated through the examination of several process models making extensive use of the LAI parameter.

The second component of the literature review involves an examination of the definition of LAI, due to its ambiguous nature. The various techniques for LAI measurement, along with their advantages and disadvantages, are discussed. Particular attention is paid to the *in-situ* optical and remote sensing techniques due to their application in this study.

Detailed research objectives, along with an analysis of gaps in the literature, are presented in Chapter 3. The specific techniques and instruments that have been employed to collect the data for this study are also discussed.

In Chapter 4, the methodologies described in Chapter 3 are implemented and their performances are validated where necessary.

Chapter 5 discusses the relationships derived between the *in-situ* LAI measurements and the remotely sensed modeling parameters used in this study.

Chapter 6 describes a sensitivity analysis of the relationships derived in Chapter 5 to various known error sources. This sensitivity analysis is performed by analyzing the relationships over a variety of spatial extents and areas.

Chapter 7 provides the conclusions and recommendations of this study

2. Literature Review

2.1 History and Definitions of LAI

2.1.1 Definitions

LAI is a term that has traditionally been defined quite ambiguously because it has been used to refer to quantities which can be similar but not identical (Barclay 1998). The definition of LAI is often dependent on the purpose of the study or the background of the investigator, with some disciplines preferring a certain definition over others.

Historically, the simplest definition of LAI has been the total area of leaves per unit ground area (Nemani *et al.,* 1993). This definition, which was first proposed (Watson*,* 1947) for agricultural purposes, accounts for leaf structure, particularly with respect to shape. This definition of LAI is used throughout this paper when either actual LAI or true LAI is referred to. The adoption of this definition as actual LAI is due to its historical primacy and the fact that has physical meaning.

Another definition of LAI is half of the total area of leaves per unit ground area. This definition is frequently used for studies related to climate change or mass transfer as this definition is representative of the forest's gas exchange potential (Barclay, 1998).

Another definition used within the remote sensing community is the projected area of horizontal leaves per unit ground area. This measurement represents the maximum leaf area observable at nadir (Barclay 1998).

Finally LAI has been defined as the projected area of leaves inclined to the horizontal. This definition is useful for modeling light transmission through a canopy, as it is equal to the foliage area intercepting light. This definition describes LAI observable at nadir. This definition has been slightly modified in many contemporary studies to be half the total surface area of green foliage

per unit of ground area projected on the local horizontal datum. This modification has been made to account for mass and energy transfer within the canopy (Fernandes *et al.,*2004, Chen and Cihlar 1995). This definition will be used for the terms equivalent or effective leaf area as it measures the attenuation of light within the canopy.

2.1.2 Measurement Techniques

The term LAI, as demonstrated in the previous section, possesses many different definitions. Frequently, these definitions have evolved alongside the numerous techniques which have been used to obtain LAI measurements. This section discusses the common techniques for LAI measurement and their associated advantages and disadvantages.

2.1.2.1 Destructive Sampling

Traditionally, LAI has been measured directly through destructive sampling of the vegetation in the area of interest. This involves measuring the surface area of all foliage within a specified area, in addition to whatever necessary parameters such as mean leaf orientation are required by the particular LAI definition being used. Unfortunately, destructive sampling presents several problems related to its time-consuming and environmentally disturbing nature. These problems with direct sampling have prompted the development of alternative methods for LAI measurement.

2.1.2.2 Allometric Equations

The first class of alternative methods has been the definition of allometric relationships for LAI estimation. These methods are indirect, as they are based on well defined relationships between the value of a surrogate and LAI. These surrogates are typically attributes that are easily measured, such as diameter at breast height, and that exhibit strong correlation with LAI. These estimates tend to be species specific and regional in nature because differences in ambient and normal climatic conditions are not otherwise accounted for. Allometric methods are an improvement over

the direct method because they only require destructive sampling to define the initial relationships between LAI and the surrogate. Allometric methods also tend to require substantially less time due to the facility with which the surrogate is generally measured. Unfortunately, despite these advantages, allometric methods are limited by their requirement for *in-situ* measurements and by their regional applicability.

2.1.2.3 Hemispherical Photography

Another technique for LAI determination is the application of hemispherical photography. Hemispherical photography involves analyzing a circular image, covering 180°, taken upwards from the ground level. LAI is determined by measuring canopy gap fraction at various angles (Pontailler *et al.,* 2003). The advent of digital photography has increased the applicability of this technique, rendering measurements more efficient in terms of time and cost. One significant difficulty associated with this method is its limited applicability due to the fact that it can only be applied on overcast days to avoid the scattering of incident radiation. Another disadvantage is that a clumping index (Chen and Cihlar, 1996) must also be determined to account for non-random foliage distribution within the canopy. The estimation of a clumping index is difficult to perform but is required to convert from effective to actual leaf area within a canopy. Hemispherical photography is not recommended for use in tall forests where leaves can be smaller than the size of one pixel resulting in a classic mixed pixel problem (Pontailler *et al.,* 2003).

2.1.2.4 Optical Measurement Techniques

Another class of alternative methods for LAI measurement has been the development of optical techniques. Optical instruments observe incident radiation at the top of the canopy and compare it to that at the height of the instrument. The instrument then uses the known relationship between these two quantities to define an effective LAI.

Prior to discussing the physical relationships which govern optical LAI measurement, it is important to define several concepts, namely canopy gap fraction and canopy gap size distribution.

Canopy gap fraction has been defined as the "…percentage of background area viewed from above (ground or understory), below (sky and clouds), or within a canopy," (Gower *et al.,* 1999). Canopy gap fraction is therefore a primary factor in the determination of the amount of light that would be able to penetrate a canopy.

Canopy gap size distribution has been defined as the "…actual dimension of gaps between individual elements ranging from a fraction of a centimeter to several meters within a canopy," (Gower *et al.,* 1999*).* Canopy gap size distribution is important because gaps are assumed to be randomly distributed within a canopy by most optical measurement techniques. If the assumption of random foliage distribution is violated, errors are likely to be introduced into the estimation of canopy leaf area. Needleleaf canopies have been observed to exhibit foliage agglomeration in several studies (Stenberg *et al.,* 2003, Eklundh *et al.,* 2003). Therefore, adjustments to the initial estimates of leaf area have to be made.

Optical measurement techniques are based on the relationship described in Equation 2.1 (Eklundh *et al.,* 2003, Fernandes *et al.,* 2004)

$$LAI_e = 2 \int_0^{90} -\ln[T(\theta)]\cos(\theta)\sin(\theta)d\theta \qquad\qquad \text{Eq. 2.1}$$

Where *LAI_e* is a measurement of the effective LAI, *T(θ)* is the transmitted non-intercepted radiation and *θ* is the view angle. The integral is taken over the range of zenith angle, from 0 to 90°.

This relationship assumes randomly distributed foliage of convex shape. This relationship is then discretized in Equation 2.2.

$$- \qquad\qquad\qquad\qquad \text{Eq. 2.2}$$

The number and location of the view angles at which the measurements are taken, symbolized by *n*

in the above equation, differs between measurement instruments resulting in slight variances in the observed values when different optical sensors are used.

This effective LAI, sometimes referred to as the plant area index, deviates from the true LAI due to effects associated with both the structure and geometry of individual leaves and the canopy as a whole. These effects are partially mitigated by performing measurements to determine the extent of clumping within the canopy. The knowledge of the extent of clumping within a canopy allows for the quantitative adjustment of the LAI_e so that it can serve as an LAI estimate, as in Equation 2.3.

$$LAI = YLAI_e \qquad\qquad\qquad \text{Eq. 2.3}$$

where Y is the clumping index of the foliage

Optical methods are advantageous because of their global application, non-destructive nature and overall measurement efficiency compared to other methods. Optical methods can also, because of their non-destructive nature, be used to monitor changes in phenological development over time (Eklundh *et al.,* 2003). The primary disadvantage of optical methods is their requirement for *in-situ* measurement, which limits the spatial extent of LAI estimates that can be practically achieved using these methods. Another disadvantage is that optical methods are somewhat limited in their application for non-homogeneous stands. Optical methods also assume that direct solar radiation is the only source of radiation observed beneath the canopy (Gower and Norman, 1991).

2.1.2.5 Radiometric Techniques

Another technique for LAI estimation is through passive radiometric measurement of the spectral reflectance properties of the vegetation of interest. Radiometric sensors have been employed *in-situ* or mounted aboard various vehicles, such as satellites and airplanes, to obtain remote LAI estimates. Radiometric techniques typically employ a combination of several spectral bands, usually located in the red and near-infrared (NIR) ranges of the spectrum to derive spectral vegetation indices. These portions of the electromagnetic spectrum are used because of the

distinctive reflectance properties that vegetation possesses in these bands, as shown in Figure 2.1.
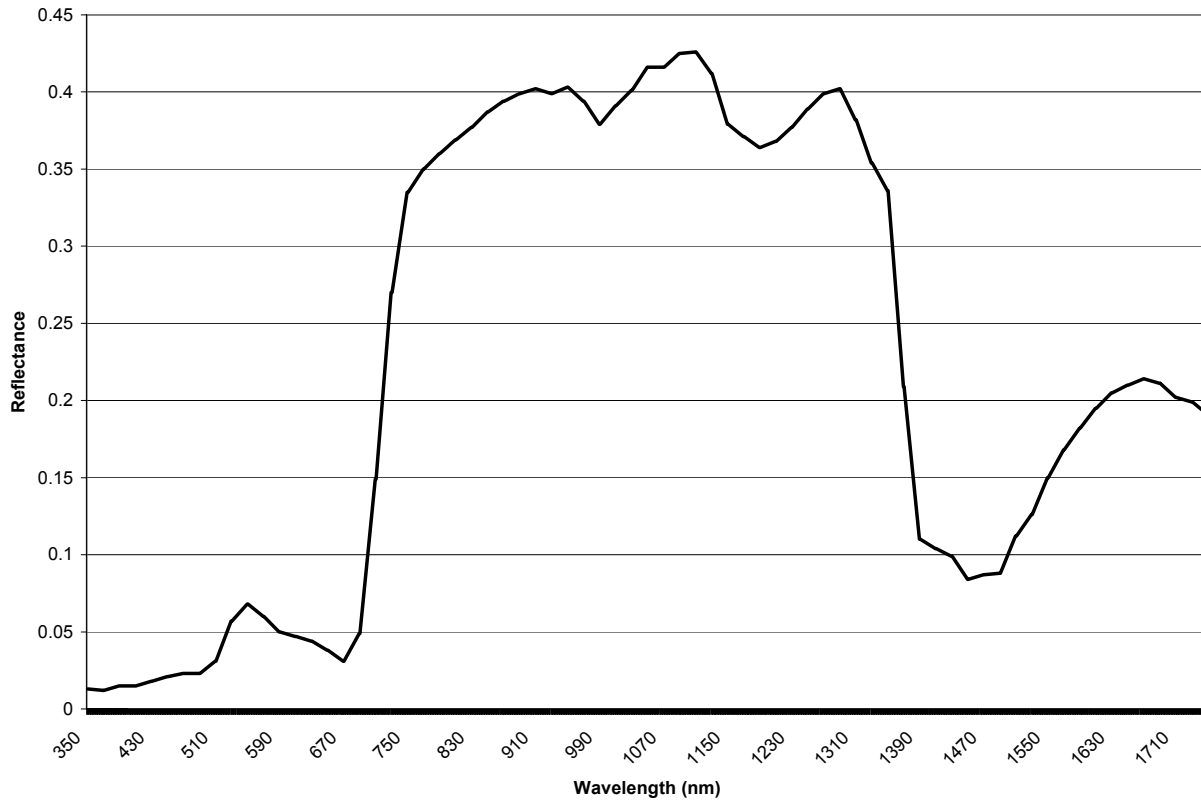
Figure 2.1: Reflectance Spectra of Vegetation Measured by Spectroradiometer

The formulas for the most commonly used spectral vegetation indices are provided in Table 2.1, with RED and NIR representing the values of the reflectance measurements obtained in the red and near-infrared channels respectively.

Table 2.1: A Summary of Vegetation Indices and their Formulas

Name	Originating Study	Acronym	Formula
Normalized Difference Vegetation Index	Rouse *et al.,* ,1973	NDVI	$$\dfrac{RAD_{NIR} - RAD_{RED}}{RAD_{NIR} + RAD_{RED}}$$
Simple Ratio	Jordan, 1969	SR	$$\dfrac{RAD_{NIR}}{RAD_{RED}}$$
Weighted Difference Vegetation Index	Clevers, 1989	WDVI	$RAD_{NIR} - aRAD_{RED}$ where a=is the simple ratio of a pure soil pixel
Soil-Adjusted Vegetation Index	Huete, 1988	SAVI	$$\dfrac{(RAD_{NIR} - RAD_{RED})(1+L)}{(RAD_{NIR} + RAD_{RED} + L)}$$ $$L = 1 - 2.12(NDVI)(WDVI)$$
Transformed Soil-Adjusted Vegetation Index	Baret and Guyot, 1989	TSAVI	$s(RAD_{NIR} - sRAD_{RED} - a) + aRAD_{NIR}$ $+ RAD_{RED} - as + X(1 + s^2)$ where a is the soil line intercept, s is the soil line slope, and X is an adjustment factor which is set to minimize soil noise (0.08 in original papers).
Perpendicular Vegetation Index	Richardson and Wiegand, 1977	PVI	$RAD_{NIR} \sin(a) - RAD_{RED} \cos(a)$ where a is the angle between the soil line and the NIR axis.
Moisture Stress Index	Rock *et al,* 1986	MSI	$$\dfrac{RAD_{MIR}}{RAD_{NIR}}$$

The primary advantage provided by remote sensing techniques is their capacity to estimate LAI in a geographically extensive and non-destructive manner. Remote LAI estimates can be obtained more efficiently in terms of time and cost than the majority of *in-situ* techniques. The primary disadvantage presented by LAI estimation using radiometric measurements is the saturation that is exhibited in certain wavelengths once LAI values exceed certain thresholds.

Another technique applied for LAI estimation, with particular advantages in modeling non-random foliage distribution and its effects on transmitted radiation, is the Monte Carlo method (Kucharik *et al.,* 1998). The authors applied this technique to clumping index estimation in boreal aspen, black spruce and jack pine stands in northern Saskatchewan and Manitoba. The primary goal of this work was to account for canopy architecture which exhibits agglomeration at different scales. The authors noted that there is a minimum element size at which the extent of clumping within a canopy can be measured. Within-shoot clumping can then be difficult to measure in a needleleaf canopy due to the spatial resolution of the sampling method which is often too coarse to observe this effect. The authors used the multiband vegetation imager (MVI) to obtain LAI estimates which had been adjusted for non-random foliage distribution and the effects of branches. They noted that the factors which they computed to account for canopy clumping were entirely dependent on the zenith angle at which the incident radiation penetrated the canopy. The estimates derived from the MVI differed from destructive samples at levels ranging from 10 to 25%. The authors determined that there is a much larger standard deviation associated with LAI measurements in black spruce and jack pine than in aspen which they attributed to lessened range of stem densities in the aspen stands. The authors noted that the difference between the boreal and temperate aspen communities was the lower values of crown closure observed in boreal aspen stands. A significant difference between the needleleaf and broadleaf populations was observed in the contribution of between crown gaps to total gap fraction. The authors determined that 80 to 95% of total measured gap fraction at zenith is due to between crown gaps in conifers while the contribution of aspen varies between 40 to 60%. The authors found that the measurements of the clumping index obtained from the MVI differed by 10 to 15% from those obtained using a tracing radiation and architecture of canopies (TRAC) measurement device for the aspen stands. The estimates of clumping index provided by the two measurement techniques exhibited deviations

which were approximately four times as large as the broadleaf case. The authors used Monte Carlo simulations to determine the extent to which the measured clumping index is dependent on the zenith angle and the clumping index at nadir. They concluded that the use of a clumping index can contribute to more accurate LAI estimates where the foliage distribution within the canopy is not random. The authors also concluded that where *in-situ* measurements of clumping index are not available it can be reasonably approximated using Monte Carlo simulations.

2.1.3 Comparison of *in-situ* techniques for LAI estimation

One study has analyzed the performance of optical measurement techniques for LAI estimation in the Canadian boreal forest (Chen and Cihlar, 1995). The authors noted disadvantages in the use of optical methods including leaf geometry, agglomeration and the contribution of woody material to light attenuation. The most significant of these difficulties was concluded to be agglomeration in conifer stands. This led to the use of a supplementary optical technique to measure gap size information to account for the agglomeration and the resulting underestimation of LAI. The authors concluded that they could accurately determine the agglomeration factor needed to convert the effective LAI to the actual LAI.

Another study comparing the results of optical LAI measurements to allometric LAI estimates was performed in central Finland for Scots Pine stands (Stenberg *et al.,* 2003). The goal of this study was to determine the effect that changes in actual LAI would have on *in-situ* optical measurements. The changes in actual leaf area were implemented through gradual defoliation. The authors noted that the effect of non-random foliage distribution would result in an underestimation of plant area index which could function as a more accurate LAI estimate. They determined that the relationship between changes in actual LAI and changes in LAI measured optically was approximately linear. They concluded that this result was important for applications where the change in LAI is of more interest than its absolute value. The authors concluded that the relationships they were able to derive were accurate predictors of LAI. These relationships tended to be more accurate at lower values of LAI and exhibited increasing divergence as these values increased.

Another study compared LAI estimates obtained from *in-situ* radiometry, hemispherical

photography and optical measurements to destructive measurements for oak stands in Florida (Pontailler *et al.,* 2003). The correspondence between the various LAI estimates and the actual measurements is high, with the coefficient of determination exceeding 0.95 in all cases. This high correspondence is likely due to the limited number of samples. The limited number of samples does not allow for a conclusion to be reached regarding the optimal technique for non-destructive *in-situ* LAI measurement.

Another study related direct measurements of leaf area to estimates which were derived from optical techniques (Gower *et al.,* 1999). Accurate *in-situ* LAI measurements are required to develop effective remote estimation algorithms for LAI, absorption of photosynthetically active radiation and net primary production. Unfortunately, due to the difficulty of measuring these quantities in a rigorous manner, various alternative *in-situ* techniques have been introduced for their measurement. These alternative techniques, such as optical methods for LAI estimation, introduce errors of approximation which intensify as these methods are applied in conditions where their governing assumptions do not hold. The authors note that the most frequently used independent variables for the estimation of leaf area are sapwood cross sectional area or diameter at breast height. These relationships usually are of a power type, frequently transformed to logarithms as follows

$$Y = aX^b \qquad\qquad\qquad \text{Eq.2.4}$$
$$\log(Y) = \log(a) + b\log(X) \qquad\qquad\qquad \text{Eq.2.5}$$

where *X* is the independent variable, *Y* is the dependent variable and *a* and *b* are coefficients determined by regression.

The independent variable, typically diameter at breast height or sapwood area, is an easily measured parameter which evidences a strong relationship with the dependent variable. The dependent variable, typically LAI in this study, is an important quantity which is usually difficult to measure directly and uses a closely related and easily measured variable as a surrogate.

Specific leaf area, the factor relating leaf area to measured biomass, was determined to be

important due to the strong positive correlation it exhibits with maximum rate of photosynthesis and nitrogen concentration in leaves. The authors also noted that the coefficients required to convert from projected leaf area to total leaf area were dependent on the characteristic shape of the leaf. They also determined that differences in the nutrients available to the vegetation could affect the allometric coefficients. After analyzing the optical measurement techniques, the difficulties presented by non-random foliage distribution in needleleaf canopies were explored. The authors hypothesized that instruments which measure clumping within a canopy will not be used frequently. They also noted that these instruments do not generally have sufficiently fine spatial resolution to quantify within-shoot clumping. Values of shoot to total needle ratio are required to normalize the clumping index to account for within-shoot clumping. The authors also noted that optical instruments for LAI measurement do not account for the contribution of woody material, which typically constitutes between 5-35% of total plant area. They noted that similar studies found only 10% of total branch area influenced optical LAI measurements and recommended that the effects of branches be neglected for canopies with large amounts of foliage.

2.2 Role of LAI in Forest Management and Biodiversity

The primary goal of contemporary forest management practice is to effectively plan and implement strategies to manage forest resources in such a way as to maximize profit without compromising the long-term viability of those resources. To accomplish this task, forest managers require data which provide them with insight into the current state of the forest and its associated processes. Knowledge of the current conditions of both vegetation and its processes within a management area allows forest managers to predict future developments in the forest area under their management plan. This allows for effective planning so that forest resources can be harvested optimally. After harvesting has taken place, the area can then be managed so that regeneration of the landscape occurs according to the design of the forest manager.

LAI has been a quantity which has frequently been used by forest managers and researchers alike for the assessment of forest attributes and processes. The role of LAI is examined where it is a relevant indicator or surrogate for a specific forest characteristic or action.

2.2.1 Forest Productivity and Modeling

The role of LAI has been determined to be an important variable in applications related to forest productivity. Forest productivity is a broad term for the expansion state of a forest and is a quantification of its growth rate. Knowledge of the state of current forest productivity can be used to compute its overall potential for growth given additional information such as stand age and species composition.

To determine how and to what extent the canopy leaf area of a forest is related to forest productivity, measures of forest productivity must be discussed. Photosynthesis is the source of all energy available to a forest and it is this energy that makes forest productivity possible. The total energy produced by photosynthesis is reduced by the amount of energy required for respiration, for purposes of cell maintenance, resulting in the net primary productivity. This relationship is summarized in the following equation.

$$E_{NPP} = E_{Photo} - E_{Respir} \qquad\qquad Eq.2.6$$

where E_{NPP} is the energy available for net primary production, E_{Photo} is the energy produced by photosynthesis and E_{Respir} is the amount of energy required by the vegetation for respiration.

The energy remaining for net primary productivity is used in the synthesis of new structures within the forest such as foliage, branches and roots. Therefore, LAI exhibits a direct relationship with net primary productivity. If measurements of leaf area are considered over time, it is possible to determine trends in LAI which can be used as surrogates for trends in net primary productivity. After conducting an assessment of the net primary productivity of a forest, the problem of selecting an optimal harvest time is simplified. As a climax community is reached, net primary productivity decreases until equilibrium is reached between photosynthesis and respiration, apart from any disturbing factors.

A study examined the relationship between LAI and rates of photosynthesis in boreal environments (Bonan, 1993). The author of this study conducted a sensitivity analysis for a model

which estimated rates of photosynthesis based on input values of LAI and species composition. LAI was determined to be an important parameter because it is a primary determining factor for both the absorption of photosynthetically active radiation and stomatal area. The author also noted the tendency of broadleaf species, by a factor of two, to apportion more energy produced from photosynthesis to the development of new foliage than do needleleaf species. Conversely, conifers apportion twice as much photosynthetic energy to the development of root networks than is the case for broadleaf vegetation. Physiological characteristics of needleleaf vegetation were observed to exhibit more substantial difference from those of broadleaf vegetation than between any species which were both members of the same evergreen or broad-leaf class. The results of the sensitivity analysis determined that estimates of photosynthesis exhibited the highest degree of sensitivity to variations in LAI, while exhibiting less sensitivity to differences between species. The author noted that uncertainty in LAI introduced greater errors into the estimation of photosynthesis than did species misclassification. Increased assimilation rates were observed for needleleaf vegetation over broadleaf vegetation due to nitrogen limitation imposed in broadleaf canopies. The author determined that variations in LAI were responsible for 77% of the modeled assimilation rates, in the linear case. It was also noted that LAI exhibited a strong correlation with species type. The variations in species composition and LAI were able to account for approximately 95% of the variance in the estimate of assimilation within the canopy. A coarser delineation into only broadleaf and needleleaf vegetation allowed for the comparison of this quantity with species type. The author found that LAI and vegetation type, whether needleleaf or broadleaf, were responsible for 94% of the deviations in modeled assimilation rate. The authors concluded that uncertainty in LAI can cause errors between 42-70%. It was also concluded that characterization of vegetation type was sufficient, rendering further classification into individual species unnecessary, to provide accurate estimates of assimilation rates in boreal forest canopies.

Another study used remote sensing techniques to estimate LAI within an ecosystem and to use these values to estimate net primary productivity (Franklin *et al* 1997). Information regarding net primary productivity can be used to identify areas where productivity is less than expected given the location and environment of the region and remedial management strategies can then be employed. The study region was located in the Fundy National Forest and LAI estimates were derived from seventeen stands. The authors corrected for geometric errors by using the mean

NDVI of a sampling window centered at the presumed location of the stand for the prediction of that stand's LAI. The authors determined that a weak relationship existed between NDVI and LAI for all stands. A strong relationship, possessing a coefficient of determination of 0.93, was found for the sampled needleleaf stands. The authors determined that the LAI estimate obtained from remote sensing for broadleaf vegetation was consistently underestimated. The authors concluded that forest species composition could be selected based on the extent to which the species optimally used the landscape relative to its potential productivity.

2.2.2 Carbon Budgeting

The estimates of net primary productivity generated above are not only of interest to the forest management community but they are also relevant to those wishing to determine carbon sequestration in forests and incorporate this information into an integrated carbon budget at various scales (Kergoat 1998). Net primary productivity is a measure of the carbon which has been converted in the photosynthetic reaction described in Equation 2.7 and is therefore removed from the atmosphere.

$$SolarRadiation + 6CO_2 + 6H_2O \rightarrow C_6H_{12}O_6 + 6O_2 \qquad Eq.2.7$$
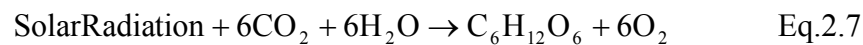
The sequestration of this carbon dioxide results in lower levels of atmospheric carbon dioxide than would be otherwise observed. The lower levels of carbon dioxide in the atmosphere which occur as a result of photosynthesis in forest ecosystems are important to the global carbon budget, particularly given recent trends towards rapid deforestation and increases in anthropogenic emissions of carbon dioxide.

In addition to the relationships determined between net primary productivity and leaf area there are other ways in which leaf area affects carbon sequestration in forests. The canopy is the locus of energy and mass exchange within a forest. The ability to exchange carbon dioxide, water and oxygen is a function of the overall leaf area (Spanner *et al.,* 1990).

The knowledge regarding rates of carbon dioxide exchange and sequestration within the boreal

forests is important, particularly in the Canadian context, as this allows for the analysis of carbon sink potential and an improved bargaining position when negotiating international environmental treaties.

In a series of papers, the FOREST-BGC model was developed to characterize water, carbon and nitrogen balances within forest stands (Running and Gower 1991, Running and Coughlan 1988). In the first study, the authors used LAI as the key parameter for modeling energy and mass exchange. The models were applied to seven distinctly different climatic regions and compared these values to those observed *in-situ*. A sensitivity analysis was performed for each of the environments by varying the LAI value. The authors determined that the ecosystem process and hydrological models that were developed exhibited high levels of sensitivity to the LAI. They noted that they considered LAI to be the most important parameter for modeling vegetation structure at the regional scale and they designed their models accordingly with most of the quantities dependent on LAI. The authors concluded that their model exhibited sufficient relative accuracy when run at the continental scale to characterize regional variations in ecosystem processes without *a-priori* calibration. In the second study, the authors proposed an integrated modeling of the nitrogen and carbon cycles. They noted that the foremost difficulty they encountered was determining the relative allocation of photosynthetic material to roots and foliage. The FOREST-BGC model uses LAI as an attribute for the regulation of ongoing processes within the ecosystem. The boundary conditions of this model were determined by determining the rates at which these processes occur when they are limited by one of the three quantities alone. The authors also noted the relationship between foliage growth and corresponding root development. They concluded that the more efficient sites had higher rates of total photosynthate dedicated to foliage production.

2.2.3 Other Relevant Studies

The canopy leaf area has also been determined to have an effect on vegetation growth and development underneath the canopy. This is primarily due to the varying attenuation of incident radiation associated with variations in the density of foliage (Eklundh *et al.,* 2003). As evidenced by the photosynthetic equation, an inverse relationship would exist between canopy leaf area and

understory growth. This would occur because a greater leaf area would result in increased radiation attenuation resulting in decreased radiation available to understory vegetation for photosynthesis.

The knowledge of LAI is important because without information concerning it or some closely related parameter it will prove difficult to model or monitor the devastation from forest fires. It is also difficult to quantitatively observe regenerated forest landscapes without the introduction of a parameter which models the canopy structure.

2.3. Relationship between LAI and Hydrology

The LAI is an attribute of vegetation that has frequently been used to model hydrological processes because of its relationship to physical and biophysical processes occurring within the vegetation itself.

2.3.1 Evapotranspiration

LAI has been determined to be important for models of evapotranspiration and photosynthesis because it is a measure of the surface available for radiation absorption and material transfer (Kergoat 1998). Variations within the LAI can be indicative of changing moisture conditions and can result in a shift in the water balance due to differences in evaporation and transpiration. The amount of evaporation is dependent on the LAI in terms of the amount of precipitation intercepted and the amount of radiation able to penetrate the canopy. The amount of transpiration depends on the LAI as shown in the Penman-Monteith equation determined in Equation 2.8

$$ET = \frac{\Delta(R_n - G) + \dfrac{P_a C_p \left(E_z^0 - E_z\right)}{R_a}}{\Delta + \gamma\left(1 + \dfrac{R_s}{R_a}\right)} \qquad\qquad Eq.2.8$$

Where Δ is the slope of the saturation vapor pressure curve, R_n is the net radiation, G is the ground

energy flux, P_a is the density of air, C_p is the specific heat of air, E_z^0 is the saturation vapor pressure, E_z is the actual vapor pressure, R_a is the aerodynamic resistance, γ is the psychrometric constant and the surface resistance R_s is a function of stomatal resistance in the canopy.

These typical functions of stomatal resistance are dependent on LAI and examples are contained in Table 2.2.

Table 2.2: Expressions for Canopy Stomatal Resistance

Model	Stomatal Resistance
Zhang *et al., ,*2001	$$R_{st} = \dfrac{1}{\left[\dfrac{f(T)f\left(\left(E_z^0 - E_z\right)\right)f(\psi f(_i)}{D_n}\right]\left[\dfrac{LAI}{r_s}\right]\left[\dfrac{1}{PAR_{SUN}} + \dfrac{1}{PAR_{SHAD}}\right]}$$ where *PAR$_{SUN}$* is photosynthetically active radiation received by sunlit leaves, *PAR$_{SHAD}$* is photosynthetically active radiation received by shaded leaves, *T* is temperature, D_i and D_n are diffusivities, ψ is leaf water potential and r_s is the stomatal resistance for an individual leaf.
Baldocchi *et al,.*1987	$$R_{st} = \dfrac{1}{LAI}$$
Baldocchi *et al.,*1987	$$R_{st} = \dfrac{\left[\dfrac{\sum r_s^i}{n}\right]}{LAI}$$

Transpiration exhibits a curvilinear relationship with LAI (Kergoat. 1998). Overall evapotranspiration maintains a direct relationship with LAI. The LAI exhibits a direct relationship with moisture demand as additional moisture is required to maintain vegetation health when additional foliage occurs within the system. As canopy LAI increases, the level of drought intensifies correspondingly.

Another study related changes in site water yield to variations in evapotranspiration related to changes in LAI. (Watson *et al.,* 1999). The authors initially hypothesized that, through monitoring the changes in LAI across the catchment system over time, they could fully characterize the observed changes in streamflow. They first applied a relationship that had been derived between forest age and water yield. They hypothesized that forest age was really a surrogate parameter for LAI and that leaf area was actually the parameter governing the site water balance. The authors hypothesized LAI to be the governing parameter because of their subordinate hypothesis that both transpiration and interception are characterized by LAI. They noted that the leaf area of the forest canopy exhibits an increased level of control over evapotranspiration, compared to the leaf area of the understory, due to the greater amount of solar radiation it receives. For this reason, the authors chose to separate out the contributions of canopy and understory LAI. A distributed hydrological model based on LAI derived from allometric relationships with stand age was used in this study. Variations in stand age across the watershed were simulated based on known harvesting and forest fire events. The output of the water balance simulation, which incorporated climatic data, was then compared to historical streamflow measurements. The authors concluded that variations in LAI were unable to fully characterize the changes in streamflow over the study period. They subsequently incorporated changes in stomatal conductance due to stand age dynamics. The authors concluded that the incorporation of changing leaf area and stomatal conductance with changes in stand age were able to adequately describe the changes in site water balance.

2.3.2 Rainfall Interception

Intuitively LAI would be thought to exhibit significant correlation with interception and further study has confirmed this initial supposition (Pierce and Running 1988). This study determined that interception was directly proportional to LAI.

One study of interest has primarily focused on the theoretical relationship between interception and LAI (van Dijk and Bruijnzeel 2001). The authors modified the Gash analytical model due to its consistent overestimation of rainfall interception in sparse canopies. The Gash model was reformulated according to several assumptions. Canopy storage capacity was assumed to be

directly proportional to LAI. It was also assumed that the ratio of mean evaporation rate over mean rainfall intensity could be expressed as a function of LAI. The authors noted conflicts with the adjusted Gash model for rainfall interception, which specified that canopy storage capacity was linearly related to crown closure and would therefore exhibit a negative exponential relationship with LAI. These data are usually agglomerated into forest inventory classes according to overall percentage of crown closure. The authors concluded that LAI and canopy storage capacity exhibited a linear relationship in areas with low to medium LAI. It was noted that the only likely condition in which LAI and canopy evaporation would exhibit a linear relationship, according to the Penman-Monteith model, would be due to an increase in LAI resulting in a considerable reduction in aerodynamic resistance of the canopy,.

Another study has applied the reformulated Gash interception model in a northern hardwood stand in Ontario (Carlyle-Moses and Price 1999). The authors observed that canopy interception loss amounted to approximately 19% of incident rainfall. They noted that canopy interception loss is a factor of considerable importance in the determination of evapotranspiration in a forest. In contrast to empirical models which consider interception to be primarily related to intensity and frequency of storm events, the Gash model accounts for additional effects related to forest stand characteristics. The original Gash model has been modified to account for effects such as raindrop size and normalizes all measurements based on the stand's canopy area, not the plot's ground area. The revised Gash model has exhibited improved performance over the original Gash model although sparse forest conditions present difficulty. Predictions of interception to within 0.1 mm were obtained and verified against differences between incident precipitation, throughfall and stemflow. The error in the estimation of interception amounted to less than 1%. The authors concluded that the revised Gash model is an accurate predictor of canopy interception in a northern hardwood stand

Another study examined rainfall interception in a black spruce canopy within the boreal forest in northern Manitoba (Price *et al.,* 1997). Canopy interception efficiency ranged from 0.15 for large rainfall events to 0.60 for small amounts of precipitation. Stemflow was determined not to be a substantial effect, as it was only evident at the largest values of precipitation and accounted for less than 1% of the total precipitation in all cases. Interception efficiency was concluded to be inversely

related to the magnitude of the rainfall event. Interception efficiency was determined to be significantly important irrespective of the magnitude of the rainfall event. The authors noted that the architecture of the spruce canopy contributed to variability in throughfall distribution. Over the study period canopy interception efficiency was measured to be approximately 0.23 of total precipitation at that location. The authors also noted the importance of understory interception, which contributed to further interception losses of 0.21 of incident precipitation at the top of the canopy.

Another study examined the allocation of precipitation to each of throughfall, stemflow and interception in both natural-growth and plantation environments (Huber and Iroume 2001). The authors noted the effects that increasingly large forest operations can have on chemical and material cycling within a watershed. Precipitation was measured using standard rain gauges located in close proximity to the forest's boundaries. Gutters were used in each of the twenty-nine plots for directing throughfall into a measurement tank. Stemflow was measured through the use of collars on the tree stems which were also connected to a measurement tank. Observed throughfall did not differ between needleleaf and broadleaf vegetation at a significance level of 0.05. A linear regression was performed between throughfall and incident precipitation and relationships which were statistically significant at a level of 0.01 were derived. In contrast, stemflow was determined to be significantly different between needleleaf and broadleaf stands at a level of significance of 0.01. Observed values of stemflow varied from 1 to 8% for broadleaf forests and from 1 to 13% for needleleaf forests. Another linear regression was performed and it was concluded that incident precipitation exhibited a statistically significant relationship with stemflow for needleleaf vegetation but not for broadleaf stands. These relationships are presented in Table 2.3 below where I is interception, S is stemflow and P is incident precipitation in mm.

Table 2.3: Equations Resulting from Linear Regressions of Stemflow versus Incident Precipitation for Various Vegetation Types (Modified from Huber and Iroume 2001)

Vegetation Type	Linear Regression Equation	Coefficient of Determination	Measurement Type
Needleleaf	$S = -72.29 + 0.106P$	0.84	Stemflow
Needleleaf	$I = 222.76 + 0.081P$	0.60	Interception
Broadleaf	$S = 20.65 + 0.014P$	0.33	Stemflow
Broadleaf	$I = 44.61 + 0.253P$	0.73	Interception

The authors also noted the effect of interception by multiple canopy layers which has often been assumed to be negligible. They propose that this assumption is only valid in dense canopies which do not allow incident radiation to penetrate sufficiently to evaporate intercepted precipitation at secondary layers of the canopy. The authors concluded that plantations should reduce interception losses due to the lessened contribution of the understory and lower stem density. They were not able to conclude what the overall impact of plantations would be on the water balance as evapotranspiration was not considered within this study. The authors recommended that watersheds which supported plantations should not be homogeneous in terms of age.

Hydrologic measurements have also allowed for the examination of water balance in dense spruce stands in Sweden (Alavi et al., 2001). The primary objective of this study was to quantify interception losses and use these measurements to validate the interception component of the SOIL water balance model. The authors initially hypothesized that a more well-developed leaf area would lead to decreases in soil moisture due to increased interception and evapotranspiration. The development of water balance models, including the Rutter and Gash models, was examined. Throughfall was measured using two devices, roofs and funnel gauges, while precipitation was measured using rain gauges. LAI was measured using an LAI-2000 device which was corrected using the method proposed by Gower and Norman, 1991. The SOIL model was concluded to be reasonably accurate in its predictions of interception losses although it underestimates the interception loss for larger storms and overestimates it for smaller ones. The authors hypothesize that these predictions are in error because different governing factors control the magnitude of interception loss depending on the magnitude of the storm event. Canopy interception efficiency

was determined to vary from 0.30 to 0.60. The maximum storage capacity of the canopy, which was calculated from LAI estimates, was determined to be approximately three times that which was determined graphically. The authors concluded that interception losses can be estimated with reasonable accuracy using only LAI and aerodynamic resistance as input variables, on a seasonal time scale.

2.3.3 Snowfall Interception

In the boreal forest the interception of snow by vegetation and its subsequent sublimation have been identified as important factors contributing to hydrological dynamics within this environment. Global circulation models often implement simple interception and sublimation models. These models are not highly reliable and have often provided unrealistic estimates of interception and sublimation (Pomeroy *et al.,* 1998).

One study which was undertaken in the southern boreal forest near Prince Albert, Saskatchewan measured the interception and sublimation of incident snowfall in a jack pine stand (Pomeroy *et al.,* 1998). The authors attempted to derive energy transfer models which could accurately model interception and sublimation within the canopy. The models were concluded to be moderately accurate predictors of the interception and sublimation occurring within the stand over a range of temporal resolutions. The authors concluded that losses of moisture due to sublimation are considerable, with sublimation occurring in the late-winter achieving particular importance.

Another paper measured the interception of snowfall in the boreal forest near Prince Albert. (Hedstrom and Pomeroy, 1998). The authors attempted to extrapolate from measurements taken on the interception properties of an individual branch to those exhibited by an entire canopy. They wished to derive a model which was independent of the rate of unloading of intercepted snow as previous studies have been primarily conducted where sublimation is high. An inverse relationship was observed between the rate of interception and the total amount of snowfall due to the canopy's structural strength. The authors distinguish between interception in the boreal and temperate forests because intercepted snow generally sublimate more quickly in temperate environments. They observed that the interception capacity of an individual branch depends on its surface area

and the amount of snow already intercepted and remaining on the branch. Snow retention in the canopy results from the combined effects of branch structural strength, the structural strength of previously intercepted snow and snow/branch coherence. As LAI was determined to be an important measure of canopy interception area *in-situ* measurements were made with an LAI-2000 optical measuring device. The LAI determined by the LAI-2000 was not adjusted for clumping as the authors assumed that clumped branches would not intercept snow to the same extent to which they attenuate incident radiation. Therefore the authors concluded that an unadjusted optical LAI measurement was optimal for studies of snow interception in needleleaf canopies. These LAI measurements were stated to be within 10% of their true values. The authors determined that the maximum load of snow that can be supported by the canopy exhibits a direct linear relationship with LAI and can be determined through application of the following formulae:

$$L_{max} = (S)(LAI_e)$$ Eq.2.9

Where *S* is a coefficient determined by species and snow density.

$$\bar{S} = S\left(0.27 + \frac{46}{\rho_s}\right)$$ Eq.2.10

Where ρ_s is the density of fresh snow and S is defined as in equation 2.9.

A sensitivity analysis was conducted to determine to what variations in modeling parameters would affect the models which were derived in this study. The authors observed a decline in interception efficiency as LAI increased. Crown closure exhibited a direct linear relationship with interception efficiency. LAI only affected this relationship in a significant fashion as crown closure exceeded 70%. The authors concluded that the derived interception efficiency models were most sensitive to amount of snowfall, amount of snowfall previously retained, leaf area and time since snowfall. They noted that some variables such as LAI and crown closure are correlated and that this will have important effects on the stand. Mature stands, with more dense canopies, will likely exhibit higher rates of interception than younger stands, which are likely to have more open canopies.

2.4 Temporal and Spatial Variations of LAI

LAI once defined is not a static quantity. Seasonal variations in LAI can vary from minimal for needleleaf vegetation (Spanner *et al.,* 1990) to considerable for broadleaf vegetation. Independent of seasonal variations, changes in environmental factors related to the availability of moisture and sunlight can impact foliage conditions. This dependence is due to the environmental limitations that can be imposed upon biophysical processes which are important to the development and maintenance of healthy foliage.

Substantial differences can also exist between the measured LAI between stands, even among identical species of vegetation at the same time of year. These variations can be attributed to a variety of spatially dependent factors. One important factor in LAI determination is topography because topography largely determines the amount of moisture and sunlight available to a stand. Site conditions independent of topography, such as soil conditions and surrounding vegetation, can also influence foliage development.

One study focused on a quantitative comparison of the allometric and optical methods for LAI measurement (Hall *et al.,* 2003). Optical methods of LAI estimation which measured the fraction of incident radiation penetrating a canopy and then converted this value to a LAI were employed. This study noted that optical methods underestimate LAI whenever foliage is not randomly distributed throughout the canopy. The TRAC approach to optical LAI measurement also considered gap size distribution within its estimation procedure. The authors concluded that the assumption of randomly distributed foliage within a canopy is more valid for broadleaf vegetation with a closed canopy structure than for needleleaf vegetation with an open canopy structure. Due to the non-random distribution of foliage within a canopy structure, they concluded that the extent of foliage clumping is an important parameter to measure for all species under consideration in this study. Significant correlation between spectral vegetation indices and LAI was only obtained in the case of white spruce when LAI was measured optically. All other relationships were determined to be insignificant. This study recommended further research over more varied stand conditions to analyze the applicability of spectral mixture analysis for species other than white spruce.

In another study hemispherical photographs were used at multiple sites in North America and Europe to assess foliage clumping in forest canopies (Walter *et al.,* 2003). Both the clumping index, proposed by Chen and Cihlar, and the coefficient of segregation, proposed by Pielou, were used to quantify the degree of foliage clumping at each study site. The authors of this study defined the basic foliage unit in a needleleaf canopy to be the shoot and therefore needed to measure a species specific within-shoot clumping index. An exponential relationship was obtained between cumulative gap fraction and clumping percentage. The LAI values that were adjusted by the Chen and Cihlar clumping index are reliable at low values of clumping but unreliable as clumping increases. The Pielou coefficient of segregation exhibits acceptable performance at all clumping percentages from 0 to 80%.The estimates predicted using the Chen and Cihlar clumping index are systematically higher than the estimates obtained from the Pielou coefficient of segregation. The authors concluded that the Chen and Cihlar clumping index should be applied when the canopy does not exhibit significant clumping and the Pielou coefficient of segregation should be applied when the canopy exhibits significant clumping.

Another study employed optical techniques for LAI estimation in needleleaf stands in Montana (Pierce and Running,1988). The authors used a sunfleck ceptometer to measure canopy transmittance and then converted this measurement to LAI using the Beer-Lambert law with a constant extinction coefficient of 0.52. The optical LAI estimates were then compared to allometric LAI estimates. The authors validated each of their assumptions regarding a constant extinction coefficient and the independence of measurements from incidence angle variations. Optical LAI estimates exhibited strong correlation with allometric estimates in this study. The authors noted that sampling error for optical techniques exhibited a positive exponential relationship with LAI. The ceptometer was determined to be effective in estimating values of leaf area indices under the following conditions: LAI(1.7-5.3) Stand Density (450-4140 trees/ha) Incidence Angle (32°-57°).

A similar study occurred in Wisconsin in which destructive measurements were compared to optical LAI estimates(Gower and Norman, 1991). The tendency for indirect optical methods to underestimate LAI in needleleaf forest was noted in the results of this study. The correlation

between the destructive measurements and the optical measurements was strong and positive although there was a systematic underestimation of approximately 35-40% due to non-random distribution of foliage. The authors noted that the ratio of total-projected needle area to the shoot-silhouette area for each species was similar. The effect of branches on LAI was determined to be approximately 1% of that of foliage. The LAI-2000 sensor was concluded to possess several advantages over other optical instruments including a larger field of view and better accuracy over a wide range of LAI.

One study investigating the dependence of texture measures on pixel size was performed for boreal forest stands in northwestern Ontario (Gluck and Rempel 1996). Various topologic and geometric metrics, were examined through the comparison of Landsat images with infrared photos at resolutions of 1, 2 and 4m. Patch size metrics were determined to exhibit significant correlation with pixel size. Moderate correlations were evidenced between pixel size and shape. Interspersion, exhibited low levels of correlation with pixel size and was deemed to be scale invariant. These results corresponded to those which were expected *a-priori* except in the case of the patch shape metrics.

2.4.1   Forest Dynamics (Boreal and Montane Forests)

2.4.1.1 A Characterization of the Boreal Forest

The boreal forest spans a considerable portion of the northern hemisphere and is one of the largest global biomes. In Canada the boreal forest comprises approximately 400,000,000 hectares, which is 35% of the national land area (Henry, 2002). The boreal forest is composed primarily of needleleaf vegetation although broad-leaved species can occur especially in the south. The most common needleleaf species in the Canadian boreal forest include jack pine, lodgepole pine, black spruce, white spruce and balsam fir. The prevailing broadleaf species in the Canadian boreal forest are aspen, balsam poplar and paper birch. The broadleaf and needleleaf species can occur in pure stands or in mixed stands.

Although there have been many schemes for the dichotomization of the boreal ecosystem a relatively straightforward delineation has been made between the open and closed boreal ecosystems. The closed boreal ecosystem is characterized by the formation of a canopy whereas the open boreal ecosystem does not form a canopy.

Due to their compositional similarity the boreal forest has historically proven difficult to differentiate from the montane needleleaf forest, which occurs in the western mountain ranges of North America (Henry 2002).

2.4.1.2 Trends in LAI

The species which occur in the boreal forest have been studied extensively in terms of LAI. Typical LAI values have been determined for most species, often with associated variance information. The results obtained for common boreal species are presented in Table 2.4.

Table 2.4: Summary of LAI Values for Various Tree Species

Species	LAI Value	Source
Black Spruce	1.1-3.8	Bonan 1993
Black Spruce	4.1	Hedstrom and Pomeroy 1998
White Spruce	4.4	Bonan 1993
Trembling Aspen	2.3-4.6	Bonan 1993
Lodgepole Pine	1.3-3.7	Kollenberg and O'Hara 1999
Jack Pine	2.2	Hedstrom and Pomeroy 1998

2.5 Relationships between LAI and Remotely Sensed Variables

One of the first tasks for which remote sensing techniques have been applied has been the modeling and monitoring of vegetation and its processes. These techniques have contributed to advances in both methodology and understanding in a variety of scientific disciplines including agriculture, forestry, botany and chemistry.

2.5.1 Remote Sensing of Vegetation

One of the first areas where remote sensing was applied is in the study of vegetation. Prior to the advent of remote sensing techniques vegetation studies were often labor intensive and thus quite limited in scale. Remote sensing provides a unique perspective for vegetation studies on the regional and continental scale that was largely unavailable previously. Historically, remote sensing has primarily used the red and near-infrared portions of the electromagnetic spectrum for characterizing vegetation and its processes. This concentration is due to the well defined spectral features of vegetation associated with these wavelengths demonstrated in Figure 2.1.

2.5.2   Remotely Sensed Relationships for LAI

Since the early 1980s remote sensing techniques have been increasingly applied to the problem of LAI estimation. The techniques and algorithms applied for LAI estimation have evolved considerably over time. The original techniques used for the remote LAI estimation are analyzed to demonstrate how they contributed to the development of the methods undergoing widespread use.

2.5.2.1 Spectral Vegetation Indices

The first studies which attempted to estimate LAI from remote sensing measurements typically involved the derivation of relationships between spectral vegetation indices and *in-situ* LAI measurements. The quality of the relationships which were derived varied substantially, depending considerably on location, environmental conditions and vegetation type. In addition to the variation associated with these methods of prediction, they tended not to be universally applicable due to saturation effects above certain LAI thresholds dependent on the observed vegetation. This technique is still commonly used due to the ease associated with the computation of spectral vegetation indices.

The primary objective of one study was to derive a relationship between structural parameters, which were measured *in-situ*, and spectral vegetation index values associated with Pacific Cordgrass (Phinn *et al.,* 1999). Observations were carried out at high sun angles due to the fact that differences observed in the spectral properties of various vegetation species, caused by differences in structure condition and radiative transfer, are optimally observed at these angles. A preliminary classification of the marsh types using topography was performed to mitigate the measured differences due to factors such as leaf geometry, amount of light penetrating the canopy, orientation and amount of dead biomass. The results of this study concluded that canopy architecture, particularly leaf orientation, had a significant influence on the observed spectral reflectance. Moderate positive correlations were observed between the spectral values and the stem length measurements in all cases except the high marsh and the near-infrared. The one difficulty presented by this study is the fact that the sampling areas for stem length are not similar in size to the pixels defined by the remote sensing system.

Similar relationships have been derived between other metrics of plant canopy structure (Kogan *et al.,* 2003). In this study the Global Vegetation Index (GVI) data set, derived from measurements made by the Advanced Very-High Resolution Radiometer (AVHRR), was used to compute the Vegetation Condition Index (VCI) from 1985 through 1994 for the country of Kazakhstan. *In-situ* measurements of plant density were made and a linear relationship was derived between plant density and VCI during 1991 and 1992. The relationship that was derived was a direct relationship with a coefficient of determination of 0.76. The results derived from this study are important because they demonstrate that spectral vegetation indices can be used as surrogate measurements for the ambient state of vegetation health and productivity.

The primary objective of another study using spectral vegetation indices was to determine a relationship between NDVI and *in-situ* LAI measurements, for a variety of land-cover types (Kite and Spence 1994). The LAI measurements were made using an optical LAI-2000 Plant Analyzer. Corrections were made to these measurements based on the ratio of mean projected needle area to projected needle area to account for the consistent underestimation of LAI resulting from the assumption of uniform foliage distribution within the canopy. The measurements were conducted at the peak of photosynthetic activity in July and August of 1994. The authors of this study noted

several advantages to using a normalized index, including partial mitigation of effects associated with changes in imaging geometry and ambient illumination. This study concluded that LAI estimates for each particular arboreal species did not vary significantly over the analysis period. The authors could not account for the aberrant NDVI values associated with spruce and tundra land-cover types. Additionally, the relationships between LAI and NDVI appeared to be specific to each land-cover type, but significant conclusions could not be made due to the lack of samples required for rigorous statistical analysis.

Another study, relating to the relationship between LAI and NDVI in areas where regeneration after a forest fire had occurred, was performed on the Mediterranean coast of Spain (Videma *et al.,* 1996). This study attempted to relate the increasing LAI of a regenerating plant populations with NDVI derived from a Landsat Image. However, instead of relating NDVI to LAI directly, LAI was replaced with time in an exponential equation. The exponential equation derived in this study accounted for the effects of sensor saturation and soil reflectance at extreme values of LAI

In a similar study in Holland several spectral vegetation indices were compared to determine their ability to estimate LAI and the sensitivity of these predictions to disturbance effects in agricultural applications (Bouman 1992). These disturbance effects include variations in illumination, soil, understory vegetation and canopy conditions. Variations in illumination conditions had the smallest effect on the predictive accuracy, amounting to $0.25 \text{ m}^2\text{m}^{-2}$. This allowed the authors to conclude that no further correction for illumination conditions was required. The errors introduced by the soil background effect ranged from 0.25 to $0.40 \text{ m}^2\text{m}^{-2}$ depending on the spectral vegetation index used. Errors introduced through variations in canopy properties had the largest effect on the LAI estimation accuracy. These errors increased in magnitude as LAI increased, with the WDVI and the PVI outperforming the NDVI and simple ratio by about $3.00 \text{ m}^2\text{m}^{-2}$. The authors concluded that the selection of the most appropriate spectral vegetation index for LAI estimation depended on the variability of the radiance in the visible wavelengths. WDVI was determined to be preferable for large variations in observed radiances in the visible wavelengths and either the simple ratio or the NDVI was preferable for smaller variations in observed radiances.

A similar study involved the use of spectral vegetation indices for LAI and canopy light

attenuation estimation (Baret and Guyot 1991). The authors noted the dependence of spectral vegetation indices on canopy structure, imaging conditions and reflectance properties. Areas with darker soils possessed higher vegetation index values when the amount of the vegetation was constant. A saturation of spectral vegetation indices with increasing LAI was observed. This saturation value varied depending on the spectral vegetation index used for estimation. The appropriate index for LAI estimation was concluded to depend on the characteristics and state of the observed vegetation. The authors concluded that the TSAVI was the best estimator of LAI for all LAI values less than 4. They concluded that for LAI values greater than 4, the NDVI was the best estimator for erect leaves and the PVI was the best estimator for leaves with low inclination. The PVI was determined to be the worst estimator for LAI values greater than 4 with erect leaves. The authors concluded that LAI estimation became increasingly difficult using spectral vegetation indices as these measurements became saturated.

Another study examined the feasibility of using Landsat observations for LAI estimation in a boreal conifer forest in central Sweden (Eklundh *et al.,* 2001). The analysis confirmed other published results in its conclusion that remote estimation models are sensitive to differing ground reflectances, as well as sun angle, in sparse stands. In denser stands the primary determining factor for visible reflectances was the reflectance properties of the leaf as less of the understory or background soil is visible. The density of the stands resulted in different trends occurring in Landsat channels 2 and 4. In dense stands bands 2 and 4 exhibited increasing reflectances contrary to the authors' expectations. The results obtained from the sensitivity analysis allowed the authors to conclude that the middle infrared bands were important to observe forest stand structure. The middle infrared bands were concluded to be important because of their sensitivity to moisture content within the canopy. The authors found that corrected LAI values exhibited the highest correlation with Landsat Band 7, even over adjusted spectral vegetation indices. They concluded that the low correlation of the near infrared channel with LAI is likely the reason for the historically limited success of spectral vegetation indices in LAI estimation. LAI estimation by inverse canopy reflectance modeling was concluded to be difficult in needleleaf stands, due to the large number of parameters required by the models. These parameters are often difficult or time-consuming to measure *in-situ* and values are often taken from literature.

In another study, Landsat TM imagery was used for LAI estimation in broadleaf and needleleaf forests in Sweden (Eklundh *et al.,* 2003). These estimates were compared to field measurements derived from optical, allometric and litter-trap techniques. These field measurements were adjusted according to three different correction methodologies to compare their correlation with remotely sensed LAI estimates. These correction factors accounted for non-random foliage distribution through the use of a clumping index. The contribution of woody material to the LAI estimate was accounted for in two of the methodologies through the incorporation of fractional measurements of woody area to total plant area. The authors compared the estimates obtained using various bands and their combinations as input parameters for LAI prediction models. The correlation coefficients with each adjusted LAI were determined to see correspondence between the remote LAI estimates and the *in-situ* measurements. The authors found that in needleleaf stands no statistically significant correlations were obtained between remotely sensed LAI estimates and *in-situ* measurements which accounted for the effects of non-random foliage distribution and woody contribution. The most significant correlations were observed between the LAI estimates obtained from the Landsat imagery and the *in-situ* measurements which had only been corrected for the non-random distribution of foliage within the canopy. Significant correlations were only observed in the visible bands for the allometric LAI measurements. The authors concluded that their modeling of LAI, which has only been adjusted for non-random foliage distribution, is capable of explaining 30% more of the measured variations in needleleaf stands than in broadleaf stands. Several explanations for this difference were proposed, including the influence of crown closure, understory vegetation, intra-stand species variability, pigment variations and differences in internal structures and saturation thresholds. The authors explained the poor performance of more elaborate adjustments of optical measurements by the inclusion of outlying values which bias the derived model. Adjusted optical measurements were concluded to be only weakly correlated with allometric LAI estimates. In some cases adjusted optical measurements were determined to be negatively correlated with allometric LAI estimates, which is highly problematic. The authors attributed the low correlations between allometric and remote LAI estimates to "…site specific divergence…" from the allometric relationships that were used in this case study. Optical LAI measurements were concluded to be problematic because of the difficulty associated with measuring many of the relevant adjustment parameters *in-situ*. The authors determined that the adjusted optical models were extremely sensitive to the adjustment

parameters, in particular to the clumping index. The highest correspondence was observed between a multiple regression of TM bands 4 and 5 to the optical LAI measurement which had only been adjusted for non-random foliage distribution in the canopy.

One study taking place in the western United States, with study sites located in the montane forest, examined the influence of canopy closure, understory vegetation and background reflectance on remote LAI estimates (Spanner *et al.,* 1990). The authors determined that the influence of understory vegetation and soil background have a significant impact on the spectral properties of a forest stand and correspondingly on remote LAI estimates. They were able to conclude that LAI and near-infrared reflectance were uncorrelated, for stands with less than 89% canopy closure. The authors concluded that the simple ratio was more sensitive to differences in LAI at higher values than the normalized difference index. The normalized difference was more sensitive to LAI at lower values of LAI. The authors also concluded that accurate atmospheric correction is important in the remote sensing of needleleaf forests due to the larger contribution of path radiance to these radiance measurements than for other types of vegetation. It was suggested that spectral mixture models be used in the deconvolution of the spectral signatures of the needleleaf forest and the background.

Another study was undertaken in the boreal forest within Canada to determine the optimal vegetation index for extracting the biophysical parameters of vegetation such as LAI and fractional absorption of photosynthetically active radiation (Chen, 1996). The quality of the estimates provided using each of the spectral vegetation indices was evaluated through a comparison with *in-situ* measurements. The results generated from this comparison demonstrated the advantages and disadvantages of the different spectral vegetation indices in modeling canopy structure and effects. The simple ratio performed the best in LAI estimation and was preferred over the NDVI due to its greater sensitivity and more linear response to changes in vegetation structure. The advantage presented by the NDVI is its fixed functional domain which ranges from negative one to positive one. The authors analyzed the effect of noise on these measurements and determined that the ratio spectral vegetation indices were preferable due to their noise attenuation. Other spectral vegetation indices which are not generated from a ratio may actually amplify the measurement's noise. The coefficients of determination of the relationships derived using other spectral

vegetation indices were negligible. The authors concluded that the use of a ratioing technique was critical in boreal forests due to the low signal to noise ratio within the individual bands. The estimation results depended significantly on the time of year with the best results being obtained in late spring because of the increasing magnitude of understory effects in the late summer.

Another study which used spectral vegetation indices derived from hyperspectral imagery for remote LAI estimation was conducted for Norway spruce stands in the Idarwald study area in Germany (Schlerf *et al.,* 2005). The authors related optical LAI measurements to spectral vegetation indices in samples stratified based on stand age. They observed positive correlations between LAI and reflectance in each of the near infrared, red and middle infrared bands with the strength of the correlation decreasing in that order. The authors concluded that due to the considerable LAI variability within age classes themselves the use of stand age as a surrogate for LAI is not advised. They noted that spectral vegetation indices which adjusted for the effects of background on the observed reflectance properties exhibited superior performance to all others within each of the stand age classes. However, when the whole data set was not stratified into age classes the indices which explicitly accounted for the performance of the background exhibited similar performance to those which did not. The authors compared broadband and narrowband versions of spectral vegetation indices and concluded that narrowband indices outperformed broadband indices in LAI estimation for every spectral vegetation index considered.

Other studies of spectral vegetation indices have performed geostatistical analyses of observed variations in spectral vegetation indices over a variety of scales and topography to characterize the effects of these phenomena. One relevant study examined the effects of analyzing variations in the observed relationships between NDVI and LAI across multiple scales (Friedl *et al.,* 1995). This involved the generation of a virtual image using LAI measurements which were subsequently inserted into the SAIL canopy reflectance model. The authors noted that joining process models at point locations to area extensive models can cause scale dependencies due to non-homogeneity of the land surface at the sub-pixel scale. A strong interrelationship between the structure of clumping in the vegetation was noted which complicates the overall relationship of spectral vegetation indices with LAI. One conclusion was that the relationship between NDVI and LAI is neither scale invariant nor linear. The authors also determined that the simulated NDVI values were not scale

invariant and tended to underestimate the true mean at coarser spatial resolutions. They noted that real world applications are likely to encounter errors of higher magnitude because of variation at the subpixel scale, due primarily to background effects.

2.5.2.2 Geometrical-Optical Reflectance Models

Due to the problems associated with the LAI estimation using spectral vegetation indices, alternative methods were explored. One such method was the use of geometrical-optical reflectance models. These models correlated *in-situ* measurements of modeling parameters, such as leaf orientation, with remote sensing observations of reflectance. These models were then used to compute the LAI that would produce such measurements. The advantage of this technique was that it required minimal *in-situ* measurements to derive LAI measurements across whole landscapes without the problems of saturation associated with spectral vegetation indices. The disadvantages associated with geometrical-optical reflectance models is the fact that they require inversion which means that they can be sensitive to slight variations in input parameters.

Another study relating remotely sensed imagery to LAI measurements in temperate needleleaf forests used simulator data to vary the disturbance factors within a needleleaf forest in Oregon (Peterson *et al.,* 1987). This study focused primarily on canopy structure and concluded that LAI is one of the most significant factors in determining the reflectance properties of the canopy. The other factors affecting the spectral properties of the canopy are vertical foliage distribution, leaf inclination angle, leaf interactions with radiation, foliage aggregation and leaf azimuth angle. The authors noted that the response in the near infrared to increasing leaf area is negligible. They attribute this to the spatial organization and shape of the needles, as needles have rounded cross sections and small lateral dimension enhancing their ability to scatter radiation. Additionally, canopy structure contributes to this effect as canopies often have different heights in natural forests. The authors also noted that the architecture of forest stands can result in the penetration of radiation through the canopy without making contact with any needles. This unimpeded penetration is due to the presence of direct openings at off-nadir angles. Significant correlation was observed between the simple ratio and LAI across a regional gradient. A power relationship with a coefficient of determination of 0.91 was derived between the LAI and the simple ratio.

Forest reflectance models have also been applied for LAI estimation in needleleaf stands in Finland (Rautiainen *et al.,* 2003). The red and near infrared bands of Landsat 7 imagery were used as a basis of comparison for the forest reflectance models. The important role understory vegetation played in the determination of the overall reflectance was noted in this study due to the observed difference between the measured reflectances and those predicted by the model. The authors determined that reflectance models are most useful for measuring differences in LAI. The disadvantages of reflectance models for LAI estimation through an inversion process are primarily related to the accurate estimation of understory parameters which is necessary to obtain meaningful results.

With the recent proliferation of global LAI estimates from satellite measurements a study was undertaken to compare these estimated values with those estimated from data of higher spatial resolution (Fernandes *et al.,* 2004). The Forest Light Interaction Model (FLIM) was implemented on CASI data which had been collected over two areas of boreal forest in Manitoba and Saskatchewan. This data possesses a spatial resolution of 2m and was compared, along with the results obtained using a Landsat TM image, to *in-situ* LAI measurements. This study mitigates the difficulties associated with using optical LAI measurements by using a TRAC instrument to account for foliage clumping. Knowledge of the extent of clumping is necessary to adjust the optical LAI measurement. The authors performed a structural regression due to the similar magnitudes of errors associated with spectral vegetation indices and LAI measurements. They concluded that the common assumption that errors associated with Landsat TM LAI estimates will be smoothed out with resampling to a coarser resolution is not always valid.

Another study used 2m CASI imagery to map effective LAI for black spruce stands in a boreal environment (Fernandes *et al.,* 2002). This study focused on black spruce stands as they are the dominant land cover class within the boreal forests of Canada. The FLIM was used as the geometric-optical model because of the low number of input variables it requires and its effectiveness in other studies for estimating effective LAI in needleleaf stands. The results that were obtained for this estimation were concluded to be highly dependent on the variability of effective LAI. Analysis at multiple scales was performed and it was determined that the simple ratio was strongly correlated to effective LAI at a pixel size of 30m but only weakly correlated at

a pixel size of 90m. The estimates of the FLIM-CLUS algorithm exhibited similar predictive accuracy to those obtained using the simple ratio. The authors concluded that the application of linear mixing models has the potential to account for the majority of variation in effective leaf area across a landscape, given large canopy gaps and lower spatial resolution imagery.

2.5.2.3 Adjusted Spectral Vegetation Indices

Although geometrical-optical models provided an alternative to LAI estimation from spectral vegetation indices, problems associated with inversion and *in-situ* measurements could occur. In response to this, development continued to occur to find spectral vegetation indices which would estimate LAI with greater accuracy. After noting the sensitivity of the middle infrared spectrum to variations in LAI (Eklundh *et al.,* 2001) it became evident that incorporating this information into the estimation process had the potential to considerably improve both the applicability and the accuracy of remote LAI estimates. Several authors attempted to scale vegetation indices by factors derived from middle infrared measurements. The advantages of this technique were that it retained the conceptual simplicity and ease of implementation associated with spectral vegetation indices while greatly increasing the accuracy and applicability of the derived models. The increased robustness of the adjusted spectral vegetation indices was due to the lessened saturation effects they exhibited as LAI values increased within the landscape.

Another study in needleleaf forests in western Montana explored the sensitivity of the modeling of forest processes across a watershed to variations in LAI estimates (Nemani *et al.,* 1993). The authors identified the primary difficulties in LAI estimation in needleleaf forests to be variations in the canopy closure and the contribution of understory vegetation. These variations influence the near-infrared reflectance considerably. The authors concluded that the relationship between NDVI and LAI exhibits poor correlation at typical remote sensing resolution because of the contribution of understory vegetation and soil background in open canopies. A middle infrared band was used to adjust the NDVI to account for these effects. The relationship derived between the adjusted NDVI and the LAI achieved a moderate correlation, possessing a coefficient of determination of 0.64. The mean LAI estimates obtained for the entire watershed from the prediction models for both the corrected and uncorrected NDVI were similar at 2.8 and 2.7 respectively. However, at a

hill slope level the differences in estimated LAI produce more variation in evapotranspiration and net photosynthesis. Simulations using the corrected NDVI for LAI prediction typically resulted in lower estimates of evapotranspiration and net photosynthesis but higher rates of discharge. At the hill slope level the estimates of evapotranspiration and photosynthesis varied by as much as 8 cm and 2 tons of carbon per hectare per year

The adjustment of spectral vegetation indices by factors derived from middle infrared channels has also been applied to the simple ratio for study areas in the boreal forests of Saskatchewan and Manitoba (Brown *et al.,* 2000). The simple ratio was selected due to its superior performance for LAI estimation, when compared to spectral vegetation indices (Chen and Cihlar 1996). LAI predictions were considerably improved and the authors concluded that this was due to the high sensitivity exhibited in the middle infrared to variations in LAI. As well, the middle infrared reflectance is similar across different backgrounds. The authors concluded that adjustment of the simple ratio allowed for improved LAI estimates for both needleleaf and broadleaf species. This result led to the conclusion that one algorithm had the possibility of application in both needleleaf and broadleaf forests. Therefore no prior knowledge of feature class types would be required when this algorithm is applied and mixed pixels are more effectively dealt with. Given the sensitivity of the middle infrared bands to moisture conditions it was proposed that further development include recent climatic data. This climatic data would be incorporated to characterize the moisture conditions in the canopy and the soil to more effectively estimate LAI.

Research has been conducted to determine the scale dependence and topographic specificity associated with relationships derived for modified spectral vegetation indices. One particular study examined the dependence of adjusted NDVI values to terrain variables for a study area located in northwestern Montana (Walsh *et al.,*1997). The authors noted that the primary determining factors of the characteristic scale for analysis were based on the landscape structure and its history extending back to the previous ice age. Three separate models were derived based respectively on elevation alone, elevation and associated topographic variables and spatial statistical measures. The first model displayed an inverse relationship with observed spectral vegetation index as the analysis scale became increasingly coarse. The second model also displayed an inverse relationship however, in contrast to the first model it evinced a stronger

relationship with observed NDVI at finer scales of analysis. The statistical variables exhibited varying degrees of robustness in modeling the variations in NDVI. The coefficient of variation, standard deviation and fractal dimension were the more robust parameters in explaining variation in NDVI. The authors concluded that once the effects associated with feature class coverage are accounted for, there exists only a limited relationship between NDVI and topography at this site. They also noted the direct relationship between NDVI and pixels with high fractal dimension and low Moran values.

2.5.2.4 Spectral Mixture Analysis

Due to the perceived ineffectiveness of LAI estimation from spectral vegetation indices alternative methods have been investigated. One alternative method for LAI estimation that has been applied within the boreal forest in Minnesota is spectral mixture analysis (Peddle *et al.,* 1999). The authors use a linear spectral mixture model because they concluded needleleaf forests do not evidence sufficient multiple scattering to make the response non-linear. The highest coefficient of determination, 0.82, was evidenced between the shadow fraction and the LAI estimated using a spheroid model at a solar zenith angle of approximately 45°. The authors explained the shadow fraction's ability to improve LAI estimates across varying stand densities and solar zenith angles on its heightened sensitivity to tree size and morphology.

A comparison of spectral mixture analysis models and models based on spectral vegetation indices for LAI estimation was undertaken for the Superior National Forest in Minnesota (Peddle *et al.,* 2001). Disadvantages in the use of unadjusted spectral vegetation indices, such as their inability to account for background effects or canopy geometries, were noted in this study and cited as factors necessitating the use of spectral mixture methods. The primary disadvantage of the spectral mixture techniques was determined to be the complexity of their implementation. The authors observed that WDVI exhibited the best results amongst the spectral vegetation indices and this was hypothesized to be due to its capacity to deal with background effects. The spectral mixture analysis outperformed every vegetation index in all categories where significant correlations were observed, including LAI estimation. The authors concluded that, despite the increased difficulty associated with its implementation, spectral mixture analysis was a more appropriate approach for

the estimation of biophysical parameters within boreal forests.

Spectral mixture analysis has also been applied in needleleaf montane forests and compared to methods employing spectral vegetation indices for LAI estimation (Peddle and Johnson 2000). This case study took place near Barrier Lake and used high spatial resolution imagery to estimate LAI. The authors noted that their model provided faulty estimates for entirely homogeneous stands containing one outlier species. They noted an uncharacteristically poor performance of the NDVI for LAI estimation particularly at low values of LAI where it is expected to exhibit optimal performance. The shadow fraction predictor derived from spectral mixture analysis exhibited higher correlation with LAI than did the unadjusted spectral vegetation index, with coefficients of determination of 0.66 and 0.46 respectively. The authors concluded that the results in montane needleleaf forests were inferior to those obtained in boreal environments. This decrease in performance was attributed to factors such as the assumption of homogeneous stands, the need for topographic correction and the lack of radiometric resolution due to the lack of *a-priori* sensor calibration. The most significant conclusion of the authors in this study was that spectral mixture analysis provided superior results in an environment that would be suited to the use of spectral vegetation indices for LAI estimation.

Another relevant study using spectral mixture methods for LAI estimation occurred in a mixedwood boreal forest near Timmins Ontario (Seed and King 2003). The authors identified the primary goal of their research to be the development of an LAI estimation model that would function in a mixedwood environment where *a-priori* stratification of the forest was not performed. One advantage of using spectral mixture analysis for LAI estimation, versus more traditional vegetation index models, is its continued sensitivity to variations in LAI and stand density even at more extreme values. The authors note that although shadow fraction is the primary metric that has been used in spectral mixture analysis, several other shadow metrics exist such as shadow component brightness. Shadow component brightness was used in this study as the authors hypothesized that it would be related to LAI based on light transmission behavior exhibited by the overstory vegetation. The authors noted that scene fraction analysis differs between high and low spatial resolution sensors because at higher resolution it is not necessary to unmix individual pixels. A significant positive correlation was noted between effective LAI and percent composition of

conifers. A significant negative correlation was evidenced between effective LAI and percent composition of broadleaf trees. Effective LAI was also determined to have a significant correlation with canopy closure. The authors observed that the shadow fraction is relatively insensitive to changes in effective LAI at crown closures less than 80% but increased in sensitivity in more closed canopies. Shadow brightness was determined to outperform shadow fraction in the modeling of effective LAI. The authors concluded that the use of shadow fraction may not be advisable in boreal mixedwood environments, a conclusion which is attributable to the non-homogeneity of gap magnitude and occurrence within the canopy. The LAI estimates obtained using shadow brightness as an input parameter were slightly degraded due to unmitigated understory effects. The authors suggest the incorporation of texture information might partially account for the contribution of the understory but note the difficulty associated with this problem. They attempted to combine shadow fraction and shadow brightness information to provide estimates of effective LAI but determined that no additional value would be derived from doing so. The methods of this study were concluded to be valid for imagery of high spatial resolution but would likely be invalid for imagery of lower spatial resolution.

A similar study used spectral mixture analysis to estimate LAI using CASI data degraded to 30m spatial resolution in the boreal forest (Hu *et al.,* 2004). The authors performed an analysis of a winter scene and determined that the fraction of sunlit snow has the strongest correlation with LAI. It was also determined that the fraction of sunlit understory exhibited a strong correlation with *in-situ* LAI measurements in a summer scene. The disadvantage of the spectral mixture analysis method is that it is difficult to extrapolate as the results are site-dependent. The authors conclude that using spectral mixture analysis in either the winter or the summer provides more accurate LAI estimates than the use of spectral vegetation indices did for the same area.

3. Research Objectives

3.1 Gaps Identified in Literature Review

Despite the substantial amount of research conducted on LAI estimation using remote sensing techniques, many areas exist where our understanding remains incomplete. Additionally, many of the techniques which are commonly applied for LAI estimation using remote sensing do not consider or cannot appropriately model certain phenomena which frequently confound LAI estimates.

3.1.1 Background Effects

One confounding phenomenon is the understory or background reflectance conditions which can have a dramatic impact on LAI estimation using remote sensing. The majority of the published literature indicates that the effects caused by understory conditions have not been considered extensively due to the complexity of the problem. These effects have proved difficult to model and in cases where this has been attempted, results which are contrary to measurement have been achieved (Eklundh *et al.,* 2001). Understory effects are particularly prevalent in the open canopy areas characterizing the boreal forest. Although different techniques have attempted to account for the influence of the understory on radiometric measurements, such as the adjustment of spectral vegetation indices by middle infrared bands or spectral mixture analysis, substantial improvement is possible.

3.1.2 *In-Situ* Measurement

Another problem for remote LAI estimation has been related to the manner in which *in-situ* measurements have been obtained. Frequently, remote sensing models for LAI estimation have been derived using *in-situ* measurements which may not have been representative of the true LAI in the canopy. If the remote sensing models were derived based on inaccurate ground truth information, there is little doubt that the estimates obtained from the remote estimation models

would be systematically compromised. When optical techniques have been used for *in-situ* LAI measurement a variety of effects influencing this estimate have not generally been considered. Optical measurement techniques often do not account for effects such as the non-random distribution of foliage and the contribution of woody material to the attenuation of radiation. The use of allometric techniques for LAI estimation has another set of difficulties which are completely different than those which influence the optical measurement. Allometric relationships for LAI estimation have been derived at a specific location and epoch and will only be valid for vegetation whose ambient state approximates those conditions well. Different conditions from those for which the allometric relationships have been defined, whether they be topographic, climatic or temporal, can produce biased ground truth measurements. Allometric relationships can also be inaccurate if vegetation attributes, such as vigor or size, fall outside of the conditions for which the relationship was initially defined. Finally, allometric relationships may not be sufficiently rigorous for LAI estimation due to an insufficient number of samples in their derivation.

3.1.3 Limitations of Traditional Remote Sensing Techniques

Accurate LAI estimation using traditional remote sensing techniques in forested areas has been severely limited by several factors, in addition to the previously discussed inattention to background effects in many studies. The most promising remote sensing techniques, linear spectral mixture analysis and modification of spectral vegetation indices, have rarely been applied simultaneously, so the relative performance of these techniques is not well characterized for different environments, vegetation populations or source imagery. Previous research has also largely neglected the substantial effects which sub-pixel heterogeneity in vegetation parameters can induce into LAI estimates obtained from remote sensing. As most LAI estimates are required over regional geographic extents, coarse resolution satellite imagery is frequently used. The use of such imagery is likely to result in increasing sub-pixel heterogeneity due to agglomerative effects caused by a coarser sampling regime, but this effect has not been substantially quantified.

3.1.4 Limitations of Sensitivity Analysis

After the remote LAI estimation models have been derived their quality needs to be assessed to determine the accuracy and precision associated with LAI estimates and to assess the validity of their application for a given purpose.

The first component of model assessment is an analysis of the geostastistical properties of the modeling parameters. The majority of studies in the literature did not perform analysis on the geostatistical properties of the input variables for their study area. The studies which did analyze the geostatistical properties of spectral vegetation indices did not derive relationships with LAI, therefore minimal assessment has been performed regarding the ability of these indices to predict reliably across multiple scales.

Another component of model assessment is the simulation of known sources of error in the input data to determine the sensitivity of the derived models to this error. Previous studies have largely ignored the impact of known error sources on the models derived, perhaps due to their magnitude which would demonstrate the relative instability of the models. Knowledge pertaining to the expected impact of these error sources on the derived models allows us to assess the stability of the model in question and the validity of its implementation given the requirements of a particular application.

The final component of model assessment is to determine expected values of precision and accuracy for a model when it is applied across a landscape with its associated geographic extent and intrinsic variability in terms of leaf area. In the literature there have been few systematic investigations quantifying the errors expected from propagating a given model for LAI estimation at an individual pixel over a landscape. Without conducting a landscape level analysis, the validity of the implementation of a model for a specific application cannot be meaningfully assessed.

3.2 Detailed Research Objectives

3.2.1 Comparison of Remote Estimation Techniques

The first objective of this thesis is the comparison of models for LAI estimates which use the output from linear spectral mixture analyses, the adjustment of spectral vegetation indices or techniques developed for the purposes of this study as their primary modeling parameters. The estimates from these remote estimation models are then related to *in-situ* LAI measurements. They are then compared to determine their relative quality. This comparison allows for a conclusion to be reached regarding the optimal techniques for the remote estimation of each of the needleleaf and broadleaf vegetation types.

3.2.2 Sensitivity Analysis

The second objective of this research is the determination of the sensitivity of the relationships to known error sources and to variations in scale. This sensitivity analysis is performed through a systematic degradation of the initially derived conditions, in a manner designed to simulate the error sources to which these models are subject. Multi-scale analysis is performed to determine the applicability of the estimation relationships as scale coarsens. The degree of sensitivity of the relationships to variations in the initial conditions determines their relative robustness for diverse application.

3.2.3 Overall Model Quality Assessment

The third objective of this research is to determine the accuracy and precision associated with the estimation models at the landscape scale. An analysis of factors that determine the accuracy and precision associated with the application of these models across a landscape, as well as their relative contributions, is conducted. Completion of this objective allows for the conclusion as to

the suitability of the models for a variety of possible applications as they will be constrained by their performance in this regard.

3.3 Methodology

3.3.1 *In-situ* measurements

3.3.1.1 LAI Measurements

To perform the necessary *in-situ* measurements study plots have been selected according to criteria delineated in Chapter 4. These plots are set out to be squares of approximately 0.36 ha. The absolute locations of these plots are determined using adjusted measurements from the global positioning system so that sufficient positioning accuracy could be achieved. The absolute location is determined with enough precision so that it could be reliably identified on a registered satellite image. The plots were all in a northwest-southeast orientation which has been recommended for LAI measurements using the TRAC sensor (Leblanc *et al.,* 2002). LAI measurements were performed during the same period of time each day. The consistency of measurement occurrence was performed in an attempt to minimize the effect of variations in the imaging conditions.

To perform measurements of both effective LAI and clumping index using the TRAC device, measurement transects were established within the plots. Measurement transects were established at regular intervals within each plot and are oriented northwest-southeast, to be parallel to the plot's boundaries. The overall mean of the measurements of the effective LAI measurements was computed to determine the overall measurement of the effective LAI for each plot. The processing of measurements performed using the TRAC device is conducted in accordance with the TRAC manual (Leblanc *et al.,* 2002).

After the effective leaf area indices have been determined by the TRAC, they are then to be converted to actual LAI through the use of the clumping index measured by the TRAC device according to equation 2.3. The actual LAI is then to be related to the measurements obtained by the

remote sensor.

3.3.1.2 Spectral Measurements

In-situ spectral measurements were conducted to determine the spectral properties of the canopy and the background conditions consisting of understory vegetation and soil. These measurements were taken in the portion of the electromagnetic spectrum between 300 and 2500 nm using the FieldSpec PRO spectroradiometer.

For each of the plots in question, measurements of the spectral properties of the features of interest were always taken in units of reflectance with the maximum reflectance being assumed for the reference target under the ambient light conditions. A measurement of the white target reference spectrum is taken before a measurement of each spectral feature. The spectral averaging and integration times were held constant throughout the sampling.

3.3.2 Remote Sensing Measurements

3.3.2.1 Pre-Processing

After the raw image was obtained from the data providers, as depicted in Figure 3.1 below, several processing steps were performed before these images were subjected to rigorous analysis.
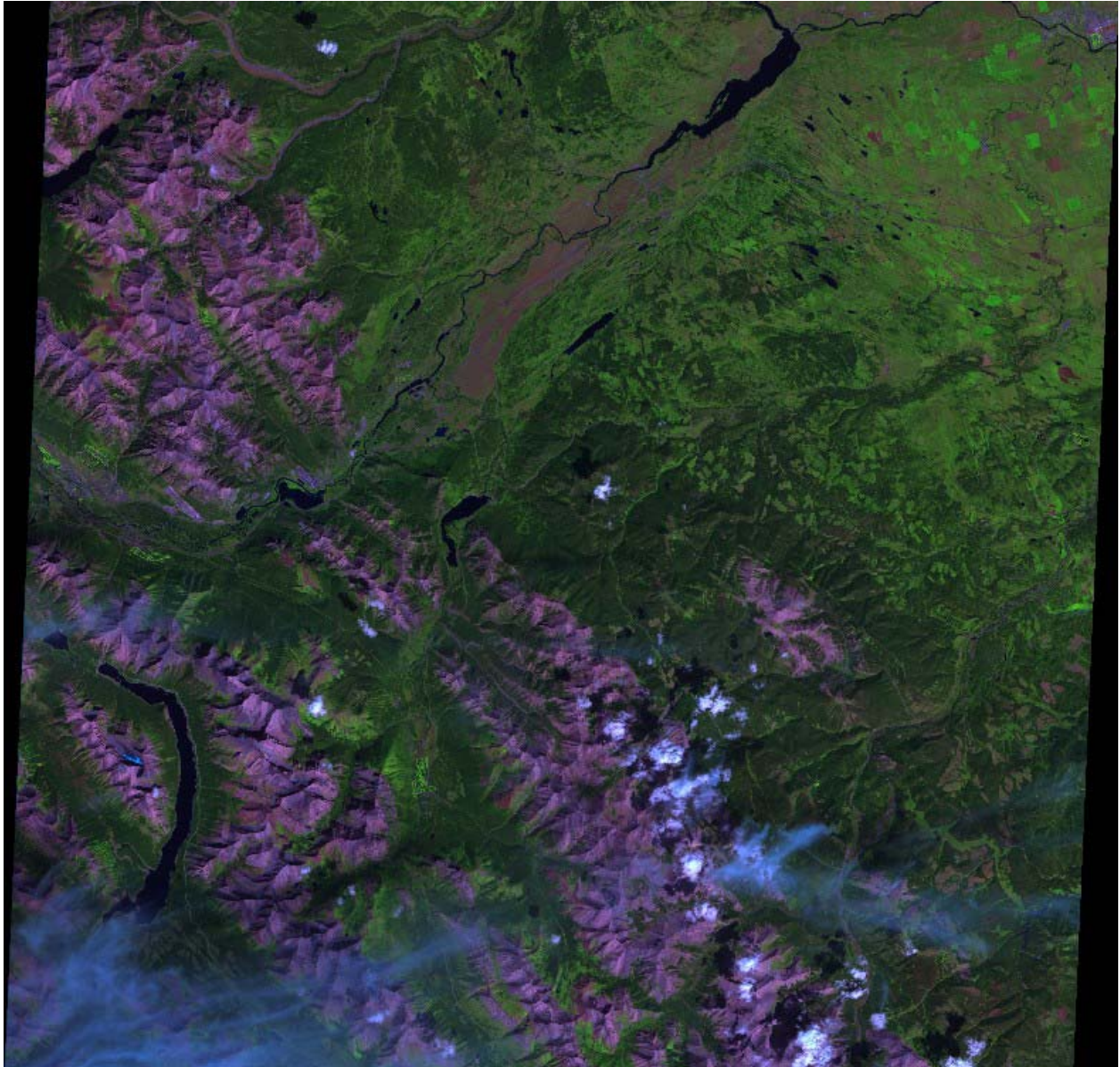
Figure 3.1 SPOT Scene of Study Area Prior to Image Enhancement and Processing with RGB-432

Image registration is necessary to spatially reference the image, as only the raw imagery had been purchased from the data provider. Although the image is available in orthorectified format, this option involves additional cost as well as uncertainty in terms of accuracy as both lower and upper thresholds of accuracy are quoted by the data provider. For these reasons the raw images were obtained and referenced so that an exact measurement of the georeferencing accuracy is obtained. The purchased image is registered to a precisely referenced Landsat image obtained from Geogratis for the same region. This reference image has been precisely orthorectified using an

extensive network of ground control points.

After the image is located spatially, the spectral properties of the image, both before and after atmospheric correction, are compared to *in-situ* measurements taken by a spectroradiometer. This analysis is performed to determine the effectiveness of atmospheric correction for this scene. The atmospheric correction that was applied was the PCI ATCOR2 module.

3.3.2.2 Adjustment of Spectral Vegetation Indices

To perform the adjustment of spectral vegetation indices, the first step is the selection of spectral vegetation indices.

The spectral vegetation indices are computed according to the formulas given in Table 2.1. They are then adjusted, wherever necessary, by the middle infrared band according to the following formula (Nemani *et al.,* 1993).

$$SVI_{ADJ} = SVI\left[1 - \frac{MIR - MIR_{MIN}}{MIR_{MAX} - MIR_{MIN}}\right] \qquad \text{Eq.3.1}$$

where SVI_{ADJ} is the adjusted spectral vegetation index, SVI is the unadjusted spectral vegetation index, MIR is the reflectance of the test plot observed by the remote sensor in the middle infrared band, MIR_{MAX} is the reflectance observed from a completely open canopy in the middle infrared band and MIR_{MIN} is the reflectance observed from a completely closed canopy in the middle infrared band.

3.3.2.3 Spectral Mixture Analysis

To perform spectral mixture analysis the first task that is performed is the selection of our component classes.

After the definition of the input spectral data classes it is necessary to define the endmember spectra. Endmembers are pixels contained within the image that are solely composed of one component class. Endmembers can be selected in a variety of ways. In this study they are selected through the use of spectra measured *in-situ* and the selection of endmembers directly from the image. The minimum and maximum sums of the reflectance from the red, near infrared and middle infrared bands were selected to represent shadowed and sunlit canopy respectively.

After the endmembers are selected, a system of equations is then generated for each pixel which must then be solved to determine the percent composition of each of the plots. The constrained least squares approach is applied to a system of linear equations of the following type:

$$RAD_{OUT}^{i} = \sum \left(RAD_{CLASS}^{i}\right)\left(PC_{CLASS}\right)$$
Eq.3.2

$$1.0 = \sum_{0}^{n} PC_{CLASS}$$
Eq.3.3

where RAD_{CLASS}^{i} is the radiance of the endmember of a specific class in band i, RAD_{OUT}^{i} is the measured radiance of the pixel of interest in band i and PC_{CLASS} is the areal percent composition of the pixel of interest by a specified class.

Once estimates of the percent composition of each of the classes have been determined, these values are then related to the LAI measurements obtained *in-situ*.

3.3.2.4 Independent Investigations

In addition to the promising new techniques previously discussed, further research has been conducted pertaining to the development of other methods for remote LAI estimation. These investigations have resulted in the development of two alternative methods namely the normalized scaling and the normalized distance techniques.

The normalized scaling technique involves the computation of a scaling factor in each of the bands under analysis. This scaling factor is computed in an identical fashion to the scaling factor applied in Equation 3.1. The individual band scaling factors are then either multiplied or divided, in multiple combinations, based on whether the relationship they exhibit with LAI is direct or inverse.

After these values are computed, an area-weighted average is obtained for each plot. Subsequently, *in-situ* LAI measurements are regressed against these area-weighted mean estimates to derive modeling relationships.

To illustrate the appropriate application of this technique a sample calculation is provided for a broadleaf pixel. For broadleaf vegetation it is known that red and middle infrared reflectances are inversely related to leaf area, while near infrared reflectance exhibits a direct relationship with LAI. In this case, the appropriate combination of these bands is the product of the scaling factors in the red and middle infrared bands divided by the scaling factor in the near infrared band. If the initial reflectances are 0.054, 0.227 and 0.125 respectively in the red, near infrared and middle infrared bands, the appropriate scaling factors can be computed using equation 3.1 for each channel. For broadleaf vegetation maximal and minimal reflectance values of MIR_{MAX}=0.163, MIR_{MIN}=0.105, NIR_{MAX}=0.308, NIR_{MIN}=0.209, RED_{MAX}=0.067 and RED_{MIN}=0.044 are used for all SPOT vegetation analyses as these were the maximum and minimum values of these quantities within the measurement plots. Applying these values in equation 3.1 yields scaling factors of F_{RED}=0.563, F_{NIR}=0.813 and F_{MIR}=0.681. Combining these values as described above yields a normalized scaling factor of 0.471.

The normalized distance technique is an expansion of the normalized scaling factor technique. The normalized distance technique involves the computation of the scaling factors and the subsequent computation of the normalized distance for a given pixel as in Equation 3.4.

$$ND = \frac{\sqrt{\sum_{1}^{n}(\frac{1}{0} \pm F_i)^2}}{\sqrt{n}} \qquad \text{Eq. 3.4}$$

where *ND* is the normalized distance, *F* is the scaling factor computed in band *i* and *n* is the number of bands for which the analysis is being performed.

3.3.3 Regression Analysis

To perform regression between *in-situ* measurements and parameters, such as adjusted spectral

vegetation indices and plot fractions, the technique of least squares is applied.

The technique of least squares is used to minimize the sum of the squares of the residuals obtained from fitting a given regression model to a data set as in equation 3.5.

$$\sum \left(\text{Yactual} - \text{Ypredicted} \right)^2 \equiv \text{MIN} \qquad\qquad \text{Eq.3.5}$$

where Y_{Actual} is the measured value of the dependent variable and $Y_{Predicted}$ is the predicted value of the dependent variable.

The method of least squares determines the coefficients which will best fit the data according to the criteria established in equation 3.5. Least-squares analysis is robust in that it leaves the selection of a regression model to the modeler.

In this study both linear, structural and Gaussian regressions are performed as each of these techniques are used extensively in literature. Although structural regression has demonstrable advantages over linear regression (Fernandes *et al.,* 2004), the latter is more intuitive which accounts to a great degree for its continued use.

The properties of the errors obtained for the relationships between remote and *in-situ* measurements are noted so that they could be applied in the sensitivity analysis portion of this research.

3.3.4 Sensitivity Analysis

3.3.4.1 Monte Carlo Simulation

To determine the extent to which errors in both the *in-situ* measurements and radiometric estimates propagate into the subsequent modeling error, a sensitivity analysis was conducted using a Monte Carlo analysis.

Monte Carlo techniques involve the stochastic modeling of phenomena or processes difficult to describe in a deterministic fashion. Monte Carlo simulations are also used to gain an understanding of phenomena whose general characteristics are known but which cannot be experimented on directly due to monetary or temporal constraints.

The Monte Carlo simulations performed for this study introduce typical stochastic errors into models of the parameters of interest. These estimates are then compared to known values.

The determination of the typical errors from the remote sensing models is relatively straightforward after these relationships are derived, due to their known properties. Statistical analysis of the residuals after the least-squares analysis results in the determination of the typical error associated with these measurements.

After specifying a typical error for a particular Monte Carlo simulation, the known parameter is then adjusted by a Gaussian random number produced according to the known standard deviation of the residuals as previously determined. This adjustment is summarized in equation 3.6.

$$PARAM_{ADJ} = PARAM_{KNOWN} + Random \qquad\qquad Eq.3.6$$

where *Random* is the output of the Gaussian random number generator, $PARAM_{KNOWN}$ is the parameter specified for analysis and $PARAM_{ADJ}$ is the estimate with measurement errors incorporated.

3.3.4.2 Plot Location and Georeferencing Errors

To quantify the impact of errors in georeferencing and plot location have upon the derived regression relationships, two techniques have been implemented.

The first technique involves the modeling of a shift of each plot by one pixel in octants, which start and finish due North. The input modeling parameters are computed in the same weighted-area

determination of the mean as performed initially.

The second technique to analyze the effects of location errors involves the performance of a geostatistical analysis to determine to what extent the values of the input modeling parameters used for LAI estimation are spatially correlated. Samples are selected for both broadleaf and needleleaf vegetation in and around the areas where LAI is sampled and the input modeling parameters are computed. Moran's I (Bailey and Gatrell,1995), which is used to quantify the extent of spatial correlation over a variety of lag distances, is then computed using the known values of the input modeling parameters and their spatial locations.

3.3.4.3 Scale and Sensor Effects

To analyze the effects caused by variations in scale and imaging platform, a comparison is performed between the LAI estimates determined across a given landscape using identical estimation relationships for classified MODIS and SPOT imagery at multiple scales.

4 Study Logistics

4. 1 Study Area

4.1.1 Kananaskis Study Area

The study region selected for the derivation of the relationships between remote modeling parameters and *in-situ* LAI measurements is located in Kananaskis Country, near the University of Calgary research station at Barrier Lake (51° 02'N, 115°03'W, Elev 1390m). The entire study area is depicted in Figure 4.1, with maps of the measurement plot areas represented at finer scale in Figures 4.2 and 4.3.
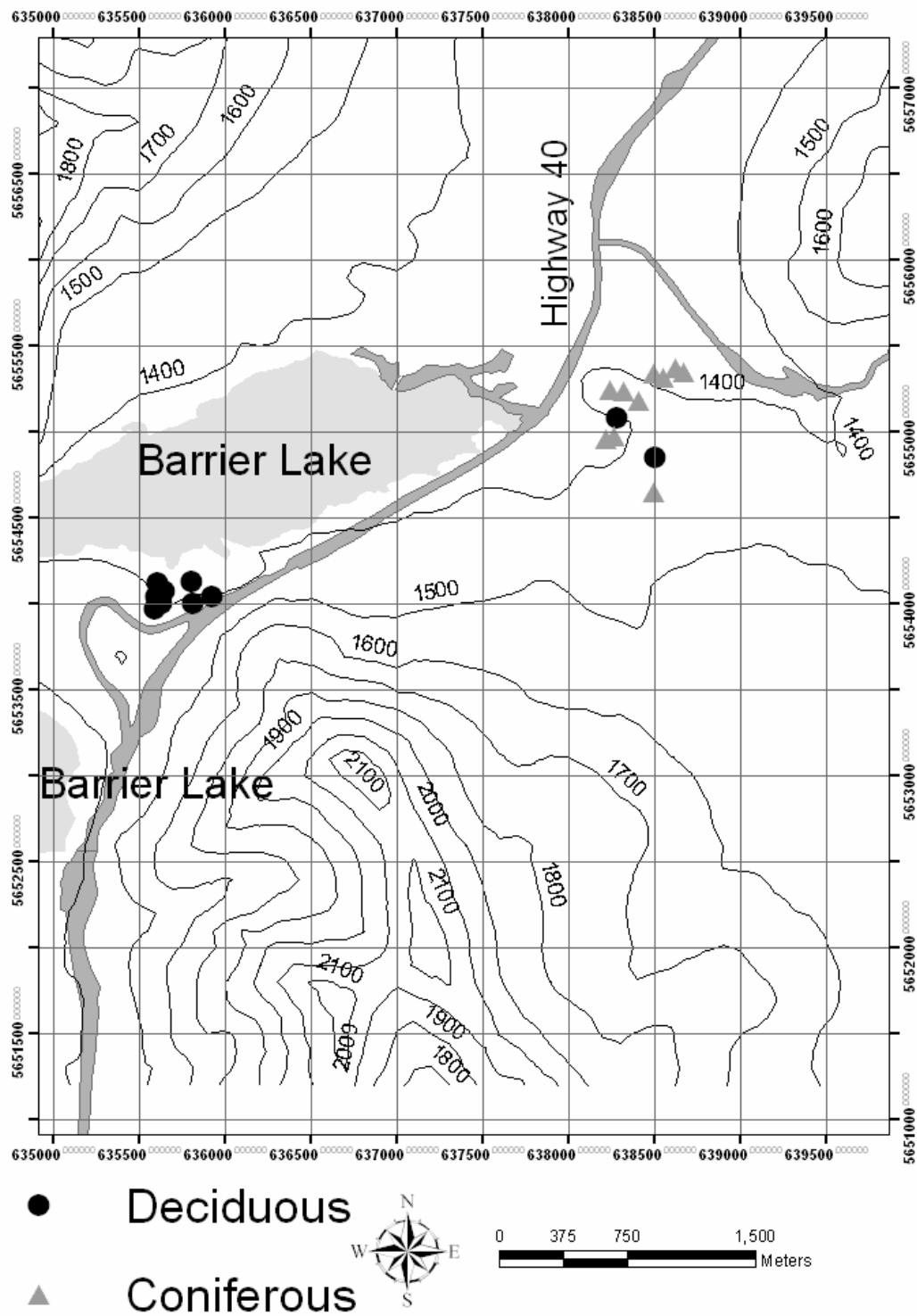
Figure 4.1: Contour Map of the Kananaskis Study Area in UTM Zone 11
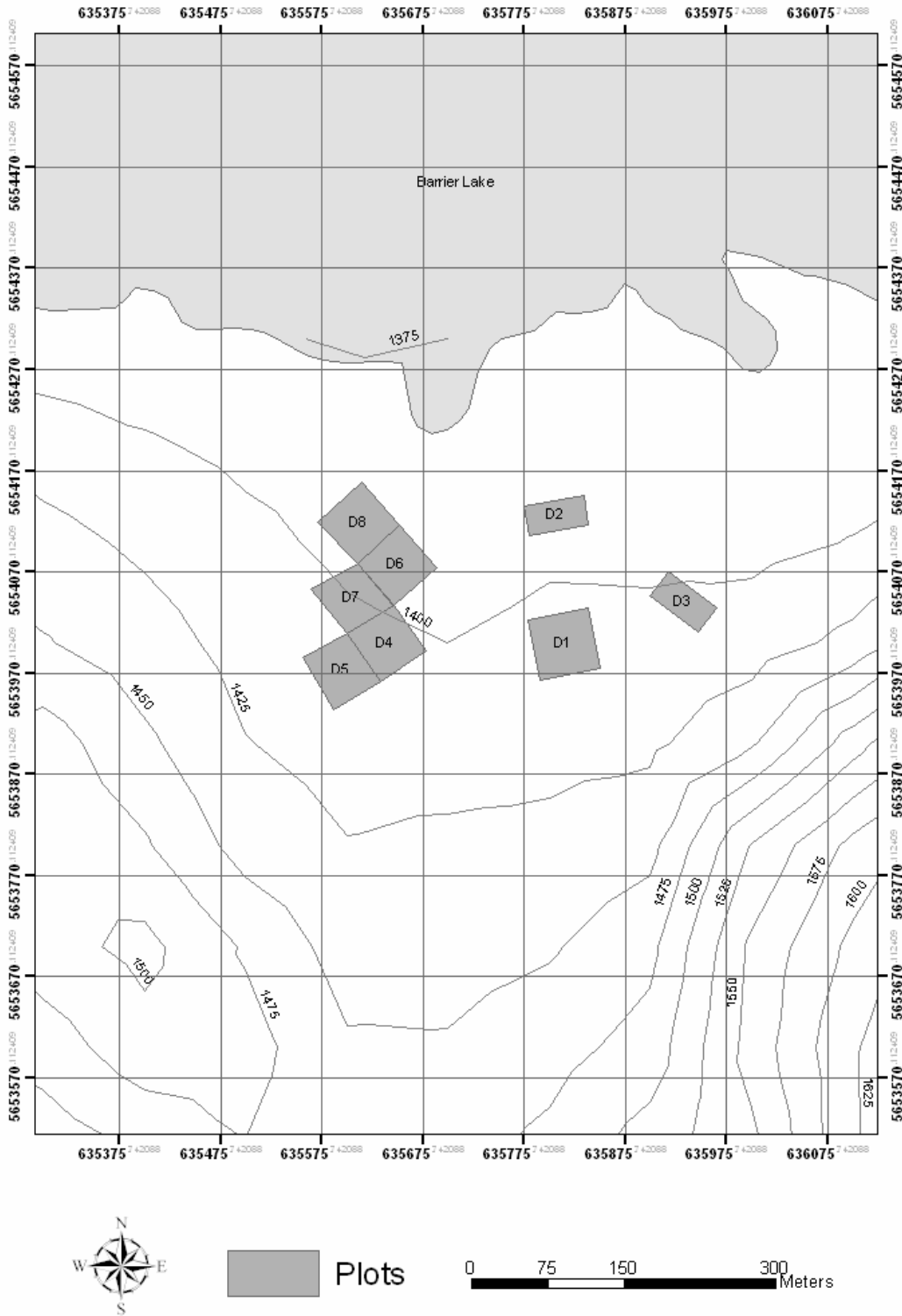
Figure 4.2: Contour Map of the Measurement Plots Located near Barrier Lake in UTM Zone 11
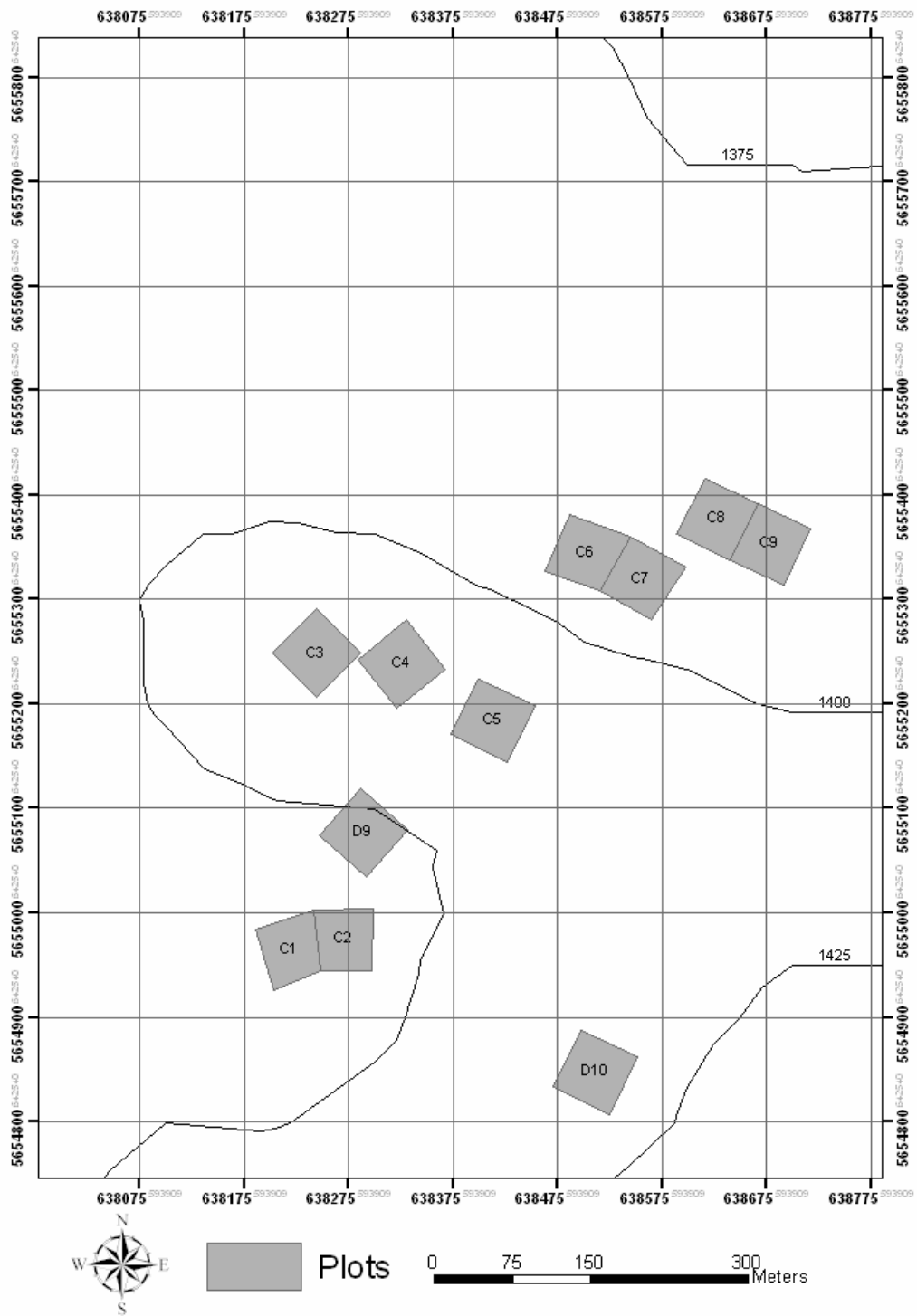
Figure 4.3: Contour Map of the Measurement Plots Located near the Kananaskis Field Station in UTM Zone 11

The forests in this area are primarily needleleaf with a limited number of broadleaf species present. The needleleaf species that occur at this location are predominantly lodgepole pine and white spruce. The broadleaf species that occur most frequently at this location are trembling aspen and balsam poplar.

Climatically the average monthly temperatures range from -7.5°C in January to 14.1°C in August. The majority of the 637.8 mm of annual precipitation occurs from mid-spring through late summer (Environment Canada, 2004).

The choice of this study site is advantageous because the dominant species in this region are also among the most common species in the montane and the boreal forests of Canada. Additionally, this location has been used for other LAI studies (Peddle et al., 2000). This allows for a comparison of results between the two studies. Also Peddle and Johnson's (2000) recommendations to investigate topographic corrections may be considered.

Observations were taken during the periods specified in Table 4.1.

Table 4.1: Schedule of *In-Situ* Measurements Performed in Kananaskis Study Area

Measurement Type	Start Date	End Date
Spectroradiometer	September 1, 2004	September 5,2004
TRAC	August 4,2004	September 5, 2004
GPS Measurements	September 13,2004	September 14,2004
Digital Photographs	September 15,2004	September 16,2004

4.1.2 Upper Elbow River Watershed

The study site for which the multi-scale analysis has been performed is the Upper Elbow River watershed. The watershed is approximately 79 000 hectares in area and contributes to the City of Calgary's water supply. An elevation map of this Watershed is presented in Figure 4.4.
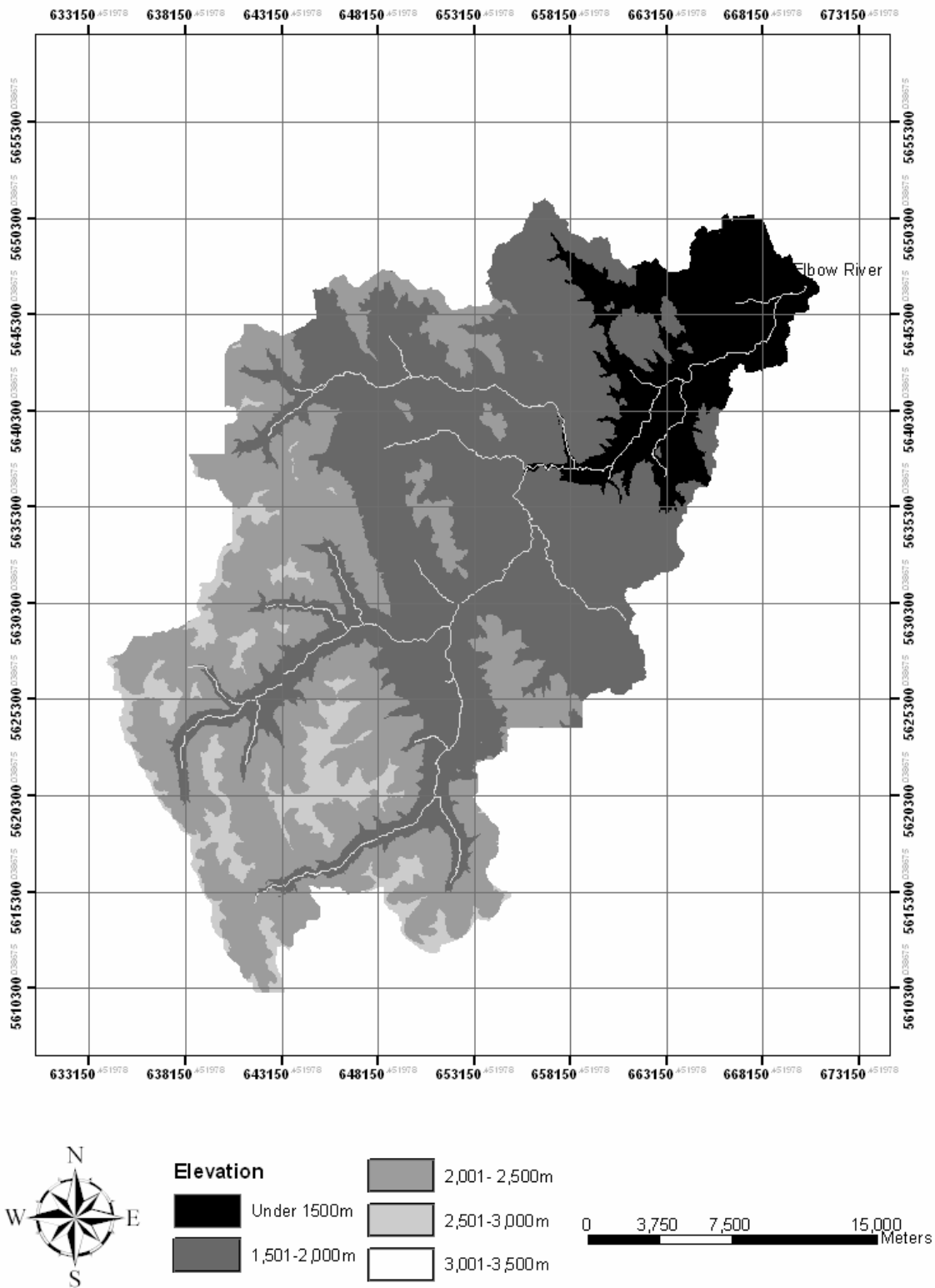
Figure 4.4: Elevation Map of the Upper Elbow River Watershed in UTM Zone 11

The choice of this watershed is advantageous as the original SPOT image used for the derivation of the remote estimation relationships can also be used for the landscape level analysis. The use of the same image is beneficial because no additional processing is necessary to account for various heterogeneous parameters between the two images, which could introduce errors into the modeling. Additionally, the area covered by the watershed has sufficiently similar forest structure to the one for which the remote estimation models have been derived for their implementation to be meaningful.

4.2   Species Selected, Stands and Ages Selected

4.2.1   Species selected

The species selected for this analysis were chosen based on the evaluation of a single criterion; that these species be prevalent in both boreal and montane forest environments. This criterion allows for the derivation of models which will be widely applicable in Canadian forestry applications. The species selected for this study were white spruce, lodgepole pine, and trembling aspen.

4.2.2   Stand Selection

The stands selected for study were chosen based on multiple selection criteria. The selected stands had to be pure in terms of vegetation type. The threshold for the definition of a pure stand is taken as possessing 80% composition of broadleaf or needleleaf vegetation. A value of 80% was selected because it allowed for statistically meaningful and representative samples. The selection of pure stands t allowed for the derivation of higher quality LAI estimation models.

The selected stands are mature communities which have not undergone disturbance. Mature communities are selected because of their predominance within the study area and the extensive studies which have been done in mature communities to validate the remote estimation applied in this study. The requirement that these stands not have undergone disturbance is to remove possible

effects affecting model application such as changes in reflectance properties or stand characteristics associated with disturbance events.

The application of these criteria allowed for the selection of 20 plots. Ten of these plots are purely needleleaf stands and ten are purely broadleaf stands, with some mixing of species within plots of each type. The spatial location and description of each of the plots of interest are specified in Tables 4.2 and 4.3, for the broadleaf and needleleaf plots respectively.

Table 4.2: Center Coordinates and Description of the Broadleaf Plots

Plot Number	E (UTM Zone 11)	N (UTM Zone 11)	Description
1	635815	5653998	Trembling Aspen, Some Balsam Poplar
2	635807	5654126	Trembling Aspen, 30m by 60 m Plot
3	635933	5654040	Trembling Aspen, 30m by 60 m Plot
4	635637	5654001	Trembling Aspen
5	635598	5653975	Trembling Aspen
6	635647	5654075	Trembling Aspen, Lodgepole Pine Outliers.
7	635606	5654044	Trembling Aspen
8	635613	5654117	Trembling Aspen
9	638290	5655077	Mixed Needleleaf and Broadleaf
10	638512	5654848	Trembling Aspen

Table 4.3: Center Coordinates and Description of the Needleleaf Plots

Plot Number	E (UTM Zone 11)	N (UTM Zone 11)	Description
1	638224	5654964	Lodgepole Pine,
2	638193	5654991	Lodgepole Pine,
3	638246	5655249	Lodgepole Pine, Some White Spruce
4	638326	5655239	White Spruce, Some Lodgepole Pine
5	638414	5655185	Lodgepole Pine. Some White Spruce
6	638439	5655349	Lodgepole Pine
7	638266	5655465	Lodgepole Pine
8	638630	5655376	Lodgepole Pine
9	638678	5655355	Lodgepole Pine
10	638503	5654649	Dense leafy green understory, Lodgepole Pine

4.3 Spatial Data Collection

4.3.1 *In-Situ* Measurements

In-situ LAI measurements are required so that relationships can be derived with remote modeling parameters. Due to the uncertainty regarding the correlation between LAI and remote estimation parameters, it is necessary to measure a clumping index so that it is possible to account for non-random foliage distribution. Firstly, optical instruments are used to measure the canopy gap fraction. From these measurements, an effective LAI is computed according to the equations contained in Section 2.2.2.4. Canopy gap distribution measurements are performed to obtain a clumping index to convert effective LAI to actual LAI. To account for the contribution of woody

material to the attenuation of solar radiation the ratio of wooded area to total plant area should be measured. Due to the fact that this ratio is extremely difficult to measure and the sensitivity of LAI estimates to typical values of this ratio is negligible, these values have not been measured but have been obtained from literature.

4.3.2   Remotely Sensed Data

The remote sensing imagery selected for use in this study has been acquired by the SPOT-4 sensor. The SPOT-4 sensor records data in four bands, from the green to the middle infrared, at a spatial resolution of 20m. A description of the band coverage associated with each of the SPOT-4 bands is described in Table 4.4.

Table 4.4: SPOT-4 Imaging Channel Information

Channel Number	Band Coverage (μm)	Spectrum Description
1	0.500-0.590	Green
2	0.610-0.680	Red
3	0.790-0.890	Near Infrared
4	1.580-1.750	Middle Infrared

The selection of SPOT-4 as the imaging platform allows for the application of spectral mixture analysis and adjustment of spectral vegetation index techniques at a spatial resolution suitable for regional climatic, circulation or hydrological studies.

The SPOT-4 image used for analysis in this study was taken on August 13,2004 and is depicted in Figure 4.5.

Figure 4.5: SPOT Scene with RGB-432 with Measurement Plot Locations near Barrier Lake in Kananaskis Country Highlighted in Red

Relationships are derived between the *in-situ* LAI measurements and the radiances observed at the sensor. These relationships are derived for one general case for each vegetation type, whether needleleaf or broadleaf.

Wherever forest inventory information is unavailable, a preliminary classification into broadleaf and needleleaf vegetation still allows for LAI estimation. This classification can usually be performed with a reasonable degree of accuracy (Reese *et al.,* 2002). The application of Bayesian or fuzzy classification instead of the more traditional maximum likelihood method could result in an increased accuracy for remote LAI estimation in areas of heterogeneous species or vegetation type. Remote estimates would also be likely to improve as more regional LAI estimates are required. This would happen as a result of the anticipated smoothing associated with the scaling of this data.

4.3.2.1 Geometric Correction

Image registration was necessary to precisely spatially reference the image, as only the raw imagery had been purchased from the data provider. Although the image was available in orthorectified format, this option involved additional cost as well as uncertainty in terms of accuracy as lower and upper thresholds of accuracy were quoted by the data provider. For these reasons the raw SPOT-4 image was obtained and referenced so that a precise measurement of the spatial measurement accuracies could be obtained. The purchased image was registered to a Landsat-7 image which had been obtained from the Geogratis website. This image, 043024_0101_010923_l7_123457_utm11.pix, was acquired on September 23, 2001. This reference image had been very precisely orthorectified by Natural Resources Canada using an extensive network of ground control points. Twelve control points were selected based on their distinct appearance within both images as well as their spatial distribution across the image. After registration, the geometric accuracy of the pixels was quoted to be approximately 10m in each of Northing and Easting directions for the SPOT image. This amounts to a total registration error less than three quarters of a pixel, which is a reasonable result given the relief associated with the terrain covered by the image.

4.3.2.2 Radiometric Correction

The first step involved in the radiometric processing of the SPOT image was its conversion from digital number to at-sensor radiance. This involved the division of the input digital number by a channel specific scaling factor and the addition of an offset as in equation 4.1 below.

$$RAD_i = \frac{DN_i}{a_i} + b_i$$
Eq 4.1

where *RAD_i* is the radiance observed by the sensor in channel *i*, *a_i* is the scaling factor term and *b_i* is the offset term from the SPOT metadata.

Subsequently the computed radiance in each channel is used to compute the observed reflectance according to equation 4.2

$$REF_i = \frac{RAD_i \pi d^2}{E_i \cos(\theta_s)}$$
Eq 4.2

where *d* is the Earth-Sun distance in atmospheric units, θ_s is the solar zenith angle, and *E_i* is the solar irradiance in channel *i*.

The channel specific coefficients for the SPOT-4 sensor are provided in Table 4.5.

Table 4.5: Radiometric Coefficients of SPOT-4 Satellite on August 13,2004 from Image Metadata

Channel Number	a_i (W/m^2/sr/μm)	b_i (W/m^2/sr/μm)$^{-1}$	E_i W/(m^2*μm)
1	2.16226	0.00000	1843
2	1.81845	0.00000	1568
3	1.24567	0.00000	1052
4	6.02900	0.00000	233

After the image has been converted from digital number to at-sensor reflectance, the spectral

properties of the image, before and after atmospheric correction, were compared to *in-situ* measurements taken by a spectroradiometer. This analysis was performed to determine the efficacy of atmospheric correction for this particular scene. The atmospheric correction that was employed was the PCI ATCOR2 module. The spectra of known feature classes which were observed in the image both prior to and after atmospheric correction were observed and compared in Table 4.6.

Table 4.6: Comparison of Reflectance Spectra within Feature Classes Before and After Atmospheric Correction

Feature Class	Post-Correction Middle-Infrared Reflectance	Post-Correction Near-Infrared Reflectance	Post-Correction Red Reflectance	Pre-Correction Middle-Infrared Reflectance	Pre-Correction Near-Infrared Reflectance	Pre-Correction Red Reflectance
Asphalt	0.14	0.13	0.02	0.19	0.17	0.11
Green Leafy Vegetation	0.09	0.25	0.00	0.13	0.31	0.05
Trail	0.09	0.15	0.00	0.13	0.19	0.06

These values exhibit differences from each other, particularly in terms of the red reflectance which is completely suppressed by the atmospheric correction algorithm for both the green leafy vegetation and trail feature classes.

To determine whether the corrected or uncorrected image should be used the observed reflectance spectra from the image were compared to those measured *in-situ*, which are presented in Table 4.7.

Table 4.7: Reflectances of Various Feature Classes Measured Using a Spectroradiometer in Various Wavelengths

Feature Class	Middle Infrared Reflectance	Near-Infrared	Red Reflectance
Asphalt	0.22	0.15	0.12
Green Leafy Vegetation	0.33	0.46	0.05
Trail	0.18	0.13	0.10

It is evident from the reflectance values presented that the *in-situ* measurements are more similar to the uncorrected image than the corrected image. To validate this conclusion, the sum of the squares of the differences between each of the sets and the *in-situ* measurements has been calculated and the results are presented in Table 4.8.

Table 4.8: Sum of the Squared Differences between *In-Situ* Measurements and Atmospherically Corrected and Uncorrected Reflectances

$\Sigma \, (REF_{CORR}\text{-}REF_{In\text{-}Situ})^2$	$\Sigma \, (REF_{UNCORR}\text{-}REF_{In\text{-}Situ})^2$
0.1395	0.0716

This confirms the validity of the initial assessment that the uncorrected reflectances more closely resemble those of the *in-situ* measurements than do the atmospherically corrected reflectances. This allows us to conclude that it is preferable not to apply atmospheric correction as this will induce additional error. Another factor that leads to this conclusion is the absence of haze or cloud, as determined from the image using the PCI masking function, in the areas surrounding the measurement plots. Finally, if atmospheric correction were to be applied, the majority of the spectral vegetation indices computed in the areas surrounding the plots would be both unrealistic and invariant. This uniformity in the spectral vegetation indices in the atmospherically-corrected image is caused by the complete attenuation of the red signal. The computed NDVI and simple ratio are then uniformly defined with values of one and infinity respectively. This situation does not correspond to the situation observed on the ground and would almost certainly introduce significant problems into LAI estimation using the atmospherically-corrected image.

4.4 Field Methods

There are two primary optical devices which are currently used to measure LAI *in-situ*. These devices are the LAI-2000 Plant Canopy Analyzer and the TRAC device which has been developed by the Canadian Centre for Remote Sensing.

The LAI-2000 Plant Canopy Analyzer has been employed in similar studies to measure effective LAI *in-situ* measurements. The LAI-2000 uses fish-eye optics to measure light intensity over the wavelength spectrum between 320 and 490 nm. This wavelength spectrum is selected because the values of reflectance and transmittance exhibited by foliage are minimized when compared to other potential measurement locations. The LAI-2000 measures over 74° on each side of the zenith. This field of view is divided into five angular ranges with their corresponding detectors arranged in concentric rings. These rings are centered at zenith angles of 7°,22°,38°,53° and 68° respectively. The angles subtended by these rings range from 11° to 13°. The LAI-2000 determines the amount of radiation intercepted by the canopy by taking the ratio of the below canopy measurements to the corresponding above-canopy measurements. This allows for the use of the equations in section 2.2.2.4 to compute the effective LAI.

The TRAC instrument is used for the determination of both the canopy gap fraction and the canopy gap distribution. TRAC measurements record the photosynthetic photon flux density (PPFD) of photosynthetically active radiation, which occurs in the visible spectrum between 400 and 700 nm. Measurements are taken at a frequency of 32 Hz which yields a horizontal measurement resolution of less than one centimeter at the suggested walking speed of 0.3 m/s (Leblanc *et al.,* 2002). PPFD is inversely related to the canopy gap fraction as larger values of PPFD are measured beneath gaps. Since TRAC measurements are obtained while the observer is moving beneath the canopy at a constant rate, the distribution and size of the gaps within the canopy can be characterized. The measured canopy gap fraction is related to the effective LAI as detailed in section 2.2.2.4. Measurements of the canopy gap fraction are then used to determine a clumping index which is used in the computation of the actual LAI.

4.4.1 Verification of *In-Situ* Measurement Devices

Due to the fact that two optical devices for LAI measurement are available for use, a comparison of these two techniques has been undertaken. This comparison is performed to ascertain the similarity between the LAI estimates provided by the individual measurement devices. If the measurements are sufficiently similar between the two devices, then a single device could be selected for the performance of these measurements.

The comparison of the LAI-2000 Plant Canopy Analyzer and the TRAC device is undertaken for one needleleaf stand and one broadleaf stand on the University of Calgary campus. The stands are selected because of their purity in terms of vegetation over an area for which a statistically meaningful sample can be obtained. LAI-2000 measurements are taken in a grid pattern every 5 m within each plot to match the sampling resolution of the TRAC transects. A 90° view cap is used to restrict measurements to the area within the plot.

TRAC measurements are taken along a southeast-northwest transect orientation as prescribed in the literature (Leblanc *et al., 2002*) Iterations where illumination conditions changed are not included in the statistical analysis of the results of the observations.

4.4.1.1 Broadleaf Vegetation

The broadleaf measurements are conducted on a 20 by 20m trembling aspen plot which possessed a relatively heterogeneous canopy due to its low to moderate stand density.

LAI-2000 measurements are performed in the evening in two rounds separated by an hour and a half. The first round of observations consists of 6 iterations of the procedure described above and resulted in a sample mean of 1.498 and a sample standard deviation of approximately 0.040. The second round of observations consists of 3 iterations resulting in a sample mean of 1.340 and a sample standard deviation of 0.020. A two sample pooled t-test is performed using the sample variances to determine whether these samples are significantly different as they appeared to be on the surface. These values are concluded to be significantly different at a 99.9% level of confidence. This result is problematic as over this the time interval the leaf area will have changed negligibly.

However the magnitudes of the sample variances demonstrate that sequential measurements exhibit high degrees of precision.

TRAC measurements are performed as close to local solar noon as possible to achieve optimal imaging conditions. To compare the results of the TRAC and the LAI-2000 it is important to note that effective LAI values observed by the TRAC were employed. This is necessary to compare the individual estimates because the LAI-2000 does not account for non-random foliage distribution or woody contribution to LAI estimates. The estimates are compared on the basis of effective LAI because this quantity is displayed along with actual LAI by the TRAC processing software whereas additional processing would be required to convert the LAI-2000 measurements.

In the aspen plot sampling using the TRAC is performed for five iterations, of which only three provided meaningful measurements. The other two iterations are rejected as outliers; their errors probably caused by changes in imaging conditions associated with cloud cover. The results of the other samples exhibited a mean value of effective LAI of 1.59 and a standard deviation of 0.16. The mean of these three samples does not differ significantly from the mean observed for the LAI-2000 measurements, which are conducted at the same spatial resolution, at a 95% level of confidence. The variances of these samples are also compared using an F-test to determine if the variances of the measurements could be considered to be equal. The results of the F-test allow us to conclude that the variances are not significantly different at a level of significance of 0.10

4.4.1.2 Needleleaf Vegetation

The TRAC and LAI-2000 Plant Canopy Analyzer devices are also compared at 5m spatial sampling resolution for a needleleaf stand on campus. A sample of five iterations using the LAI-2000 yields a sample mean of 3.19 and a sample standard deviation of 0.05. A sample of five iterations taken using the TRAC device yields a sample mean of 3.23 and a sample standard deviation of 0.13. Comparing these results using a two-sample pooled T-test with unknown and unequal variance allows us to conclude that these techniques do not provide significantly different mean estimates at a 95% level of confidence. An F-test resulted in the conclusion that the sample variances were not equal at a 90% level of confidence.

These results allow us to conclude that when sampling at the same spatial resolution under optimal measurement conditions the TRAC and LAI-2000 devices measure to the same level of accuracy. In response to this result it is decided that the TRAC device alone will be employed to measure LAI *in-situ*. This decision is taken primarily because the TRAC measurements are necessary to determine the clumping index within a canopy to convert from effective to true LAI. The TRAC exhibits superior measurement efficiency and logistical ease of use throughout the comparison described here while providing LAI estimates that are not different in terms of accuracy in a statistically significant way from those of the LAI-2000. The use of the LAI-2000 Plant Canopy Analyzer would be both time-consuming and redundant given the efficiency and versatility of the TRAC.

4.4.2 Determination of TRAC Spatial Sampling Resolution

To determine an optimal spatial sampling resolution for the TRAC measurement transects two techniques, namely Monte Carlo simulation and *in-situ* measurement are employed.

4.4.2.1 In-situ Measurement

In-situ LAI measurements using the TRAC device are compared for both the broadleaf and needleleaf stands on the University of Calgary campus at spatial resolutions of 5 and 10m.

In the aspen stand, the means are not determined to be different at a 0.05 level of significance. The precision of the measurements are also concluded not to exhibit significant difference after the performance of an F-test at a 0.10 level of significance. The statistical values resulting from these tests are presented in Table 4.9.

Table 4.9: Statistical Comparison of TRAC Measurements Between 5 and 10m Sampling Intervals for Broadleaf Vegetation

Test Name	Test Statistic	Critical Value
F-Test	1.21	19.00
Two-Sample Pooled T-Test	0.39	2.78

In the needleleaf stand, the means observed at the different spatial resolutions are determined to be significantly different at a 0.05 level of significance. The precisions however did not exhibit significant statistical differences after conducting an F-test at a 0.10 level of significance. The statistical values resulting from these tests are presented in Table 4.10.

Table 4.10: Statistical Comparison of TRAC Measurements Between 5 and 10m Sampling Intervals for Needleleaf Vegetation

Test Name	Test Statistic	Critical Value
F-Test	1.11	6.39
Two-Sample Pooled T-Test	2.82*	2.31

4.4.2.2 Monte Carlo Simulation of LAI Sampling Regimes

To confirm the results obtained using *in-situ* measurement, random LAI landscapes are generated to simulate 1m sampling intervals and different sampling intervals are subsequently implemented on them. Twenty landscapes are generated in a Monte Carlo simulation and sampling intervals of 1, 2, 5, 10 and 20 m are used for analysis. The mean LAI values are computed for each plot at each sampling interval, at which point the values are compared. This comparison involves taking the differences between the means determined for the various sampling intervals for each of the randomly generated surfaces. A statistical analysis of the mean difference values allows conclusions to be made regarding the appropriateness of the various sampling intervals. The mean differences and the standard deviations of these differences between each of the sampling intervals are presented in Tables 4.11 and 4.12

Table 4.11: Mean Values of Mean Differences Resulting from Sampling of Modeled LAI Surfaces at Various Intervals

Sampling Interval	1m	2m	5m	10m	20m
1m	X	0.035	0.100	0.265	0.294
2m	0.035	X	0 .066	0.231	0.260
5m	0.100	0.066	X	0.164	0.193
10m	0.265	0.231	0.164	X	0.029
20m	0.294	0.260	0.193	0.029	X

Table 4.12: Standard Deviations of Mean Differences Resulting from Sampling of Modeled LAI Surfaces at Various Intervals

Sampling Interval	1m	2m	5m	10m	20m
1m	X	0.005	0.007	0.009	0.013
2m	0.005	X	0.008	0.006	0.013
5m	0.007	0.008	X	0.008	0.013
10m	0.009	0.006	0.008	X	0.013
20m	0.013	0.013	0.013	0.013	X

The results indicate that although significant differences exist at 95% levels of confidence between each of the sampling resolutions, the standard deviations on these differences are very small. This allows us to conclude that a relatively constant bias remains present in the observations depending on the spatial sampling resolution selected for implementation.

Given that the evident biases between 5m and finer sampling intervals are less than half the typical standard deviation of the measurements associated with individual TRAC transects, it is reasonable to space the transects at 5m intervals. If a greater level of accuracy is desired, multiple measurements of the TRAC transects would be more advantageous than increasing the sampling interval. Additionally, given the typical footprint associated with the TRAC instrument,

determined by solar zenith angle and canopy height (Leblanc *et al.,* 2002), the selection of 5m sampling intervals exhibits sufficient accuracy for this study.

TRAC measurements are therefore taken according to the orientation and imaging conditions described to be optimal in the TRAC Manual (Leblanc *et al.,* 2002). This involves TRAC measurements along transects located at 5m intervals at a specified northwest-southeast orientation.

4.4.3 Validation of Plot Location Algorithm

To perform relevant analysis the plots set out on the ground must be located accurately on the image. An algorithm for the location of the plots on the remote sensing imagery is developed and subsequently tested using a Monte Carlo simulation to determine whether sufficient accuracy is achieved.

4.4.3.1 Description of Plot Location Algorithm

To locate the plots on the remotely sensed image, the corner points of each of the plots are initially determined using the global positioning system (GPS). The quoted accuracy associated with these points is always less than or equal to 10m as quoted by the receiver. These initial points are used to locate the polygon more accurately in space given its characteristic geometry. Additionally, points appearing to be outliers when initially measured are resurveyed until no outlying values are apparent upon inspection.

The plot location algorithm is implemented by, firstly, computing the azimuths, between each of the adjacent points. These azimuths are then referenced to a single azimuth value by adding or subtracting multiples of 90° and the mean is taken. This referencing to a single azimuth was possible due to the fact that the sides were known to have been set out at angles of 90° to each other. The mean azimuth value was then used to determine the orientation of the plot within the UTM coordinate system in which the measurements were taken.

Secondly, the centroid of the polygon is determined using the initial corner points. This position is determined with higher accuracy than the initial coordinates due to the smoothing of random errors associated with the use of multiple points in this computation and the lessened sensitivity of the centroid of a polygon to random errors in its surrounding points. Given the orientation of the polygon and its central coordinates the coordinates of the plots corners are then computed using their known distance from the center point. The software used to perform this adjustment was developed using Visual C++ and is attached in Appendix A. The corner coordinates resulting from this adjustment are presented in Tables 4.13 and 4.14.

Table 4.13: Summary of Plot Corner Coordinates for Needleleaf Vegetation

Plot Number	Corner Coordinates UTM Zone 11-N Easting	Corner Coordinates UTM Zone 11-N Northing
1	638250 638203 638187 638242	5654945 5654927 5654985 5655003
2	638299 638298 638250 638242	5655005 5654945 5654945 5655003
3	638288 638246 638203 638245	5655249 5655206 5655249 5655291
4	638369 638322 638284 638331	5655234 5655196 5655243 5655280
5	638454 638428 638374 638400	5655199 5655145 5655171 5655225
6	638545 638517 638463 638487	5655361 5655309 5655328 5655382
7	638598 638565 638517 638545	5655331 5655281 5655309 5655361
8	638667 638641 638590 638617	5655392 5655338 5655363 5655417
9	638718 638692 638641 638667	5655369 5655315 5655338 5655392
10	638545 638500 638460 638505	5654646 5654607 5654652 5654691

Table 4.14: Summary of Plot Corner Coordinates for Broadleaf Vegetation

Plot Number	Corner Coordinates UTM Zone 11-N Easting	Corner Coordinates UTM Zone 11-N Northing
1	635851 635792 635780 635839	5653975 5653963 5654022 5654034
2	635839 635780 635775 635834	5654116 5654106 5654136 5654146
3	635900 635918 635966 635948	5654046 5654070 5654035 5654010
4	635678 635633 635600 635647	5653992 5653962 5654009 5654036
5	635633 635587 635557 635600	5653962 5653934 5653986 5654009
6	635690 635647 635611 635652	5654075 5654036 5654078 5654116
7	635647 635600 635565 635611	5654036 5654009 5654053 5654078
8	635652 635605 635571 635616	5654116 5654076 5654119 5654159
9	638332 638292 638248 638288	5655079 5655035 5655075 5655120
10	638552 638526 638472 638498	5654862 5654808 5654834 5654888

4.4.3.2   Monte Carlo Simulation of Plot Location

To determine whether or not the position errors associated with locating the study plots using this algorithm meet the requirements of this study, a Monte Carlo simulation was conducted. The criterion applied to determine the suitability of the positioning solution was to be able to establish the position of the point of interest with an accuracy of less than the size of a pixel 95% of the time. This criterion was selected because the filtering of outlying GPS measurements would ensure that the occurrence of extreme errors would be unlikely to occur.

The Monte Carlo simulation involves specifying an initial case which corresponds to that of the plots and operating conditions present in this work. A square with known initial points, corresponding to the dimensions of the plots, was created. Subsequently, these coordinates are degraded with random errors of magnitudes typical of those associated with the initial GPS measurements. The initial GPS observations are obtained using a 12-channel Garmin eTrex[®] receiver. This measurement unit provided a measure of accuracy associated with the position and measurements are not taken unless this number was 10m or less. Unfortunately, further degradation of the positioning solution had to be accounted for using the dilution of precision associated with the measurement conditions. All measurements are taken between 9:00 a.m. and 6:00 p.m. and GPS constellation analysis software allowed us to evaluate the mean horizontal dilution of precision associated with our measurements. A mean horizontal dilution of precision of 1.19 is determined for the observation period for one of the days on which measurements were performed. This number is used to compute the accuracy of the positioning solution as follows in Equation 4.3.

$$\sigma_{HOR} = (\sigma_{Rec})(\text{HDOP}) \qquad\qquad\qquad \text{Eq.4.3}$$

where σ_{HOR} is the total horizontal positioning error, *HDOP* is the horizontal dilution of precision and σ_{Rec} is the positioning error reported by the receiver.

Applying the values determined from the literature and constellation analysis software yields a

value of 11.9 m.

This value of σ_{HOR} is used as the standard deviation for the generation of random errors employed to degrade the accuracy of the initial coordinates. These degraded coordinates are used as initial conditions for application of the plot location algorithm described above. The resulting corner coordinates are compared to the initial coordinates to determine the typical errors associated with this solution. This process was performed for 50000 iterations to derive a statistically significant sample. The statistics resulting from this Monte Carlo simulation are presented in Table 4.15.

Table 4.15: Summary of Mean and 95% Positioning Errors Resulting from Monte Carlo Simulation of Each Component of the Plot Location Algorithm.

Algorithm Component	Mean Error(m)	95% Error
Centroid Determination	5.42	11.32
Orientation Determination	3.29	8.03
Total(Centroid and Orientation)	6.51	13.45

These statistics demonstrate that the determination of the centroid is the algorithm component that is most sensitive to initial coordinate errors. It is also evident from these statistics that errors in centroid and orientation determination can partially mitigate each other as is evident from the mean and 95% errors being less than the natural sum of their algorithm components.

To gain a more complete understanding of the distribution of the total horizontal positioning error, the histogram of the Monte Carlo simulation results is presented in Figure 4.6.
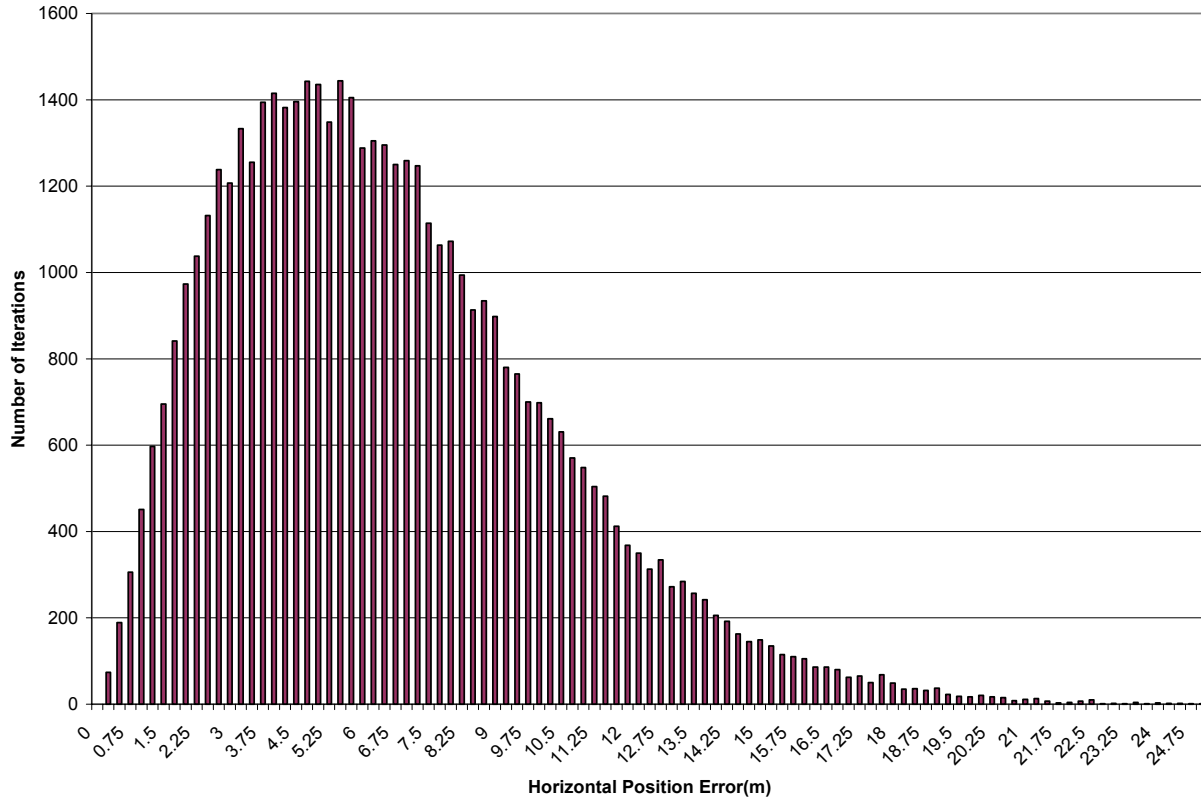
Figure 4.6: Histogram of the Position Errors Computed from Monte Carlo Simulation Using Standard Deviation of 10m, HDOP of 1.19 and 50000 Iterations

After analysis of the Monte Carlo simulation results it is evident that the plot location algorithm exhibits a positioning accuracy consistently less than the 20m spatial resolution associated with the SPOT image. This is even more demonstrably the case when considering the removal of apparent outliers which would have biased the positioning solution to the greatest degree. Therefore, it can be concluded that using the initial GPS coordinates with outlier removal within the plot location algorithm previously described allows for location of the plots with sufficient accuracy for the purpose of this study.

4.4.4 Determination of Background Composition and Spectral Properties

To successfully implement the linear spectral mixture analysis technique, an accurate

determination of the spectra associated with features beneath the canopy, referred to as the background spectra, is required for each plot in the study area. There are two primary components involved in the determination of the overall background spectra, one related to the spectral properties of the designated feature classes which constitute the overall background signature and the other related to the relative abundance of these feature classes.

4.4.4.1 Determination of Spectral Properties

The measurement of the spectral properties of the background is necessary to perform linear spectral mixture analysis. Without background measurements the algorithm is unable to differentiate between the contributions of the canopy and the underlying soil and vegetation to the overall radiation reflected by the target and measured by the radiometer.

The measurement of the spectral properties of the background feature classes is also important because it is these properties which influence the remotely sensed measurement when a pixel contains more than one feature type. An observation of the background, which can consist of many different feature class types, allows for a quantification of the background effects in each channel of interest. The effects of the background have been determined to be one of the most significant problems in remote LAI estimation and even its partial mitigation would result in worthwhile improvement. Additionally *in-situ* spectral measurements would verify that appropriate atmospheric correction had been applied to the image. An appropriate atmospheric correction is particularly important for this study given that needleleaf vegetation is among the most adversely affected feature classes due to its generally lower reflectance spectrum (Spanner *et al.,* 1990).

There are several methods by which background spectra can be obtained for linear spectral mixture analysis. One method is the determination of background spectra directly from the image itself. Another method is the use of standard library spectra obtained for feature classes similar to those encountered in the study area. A third method is *in-situ* spectral measurement of the background

The method of *in-situ* spectral measurement of the background feature classes is selected for this study. This method is selected because it accounts for local variations in the background's spectral properties because measurements are taken at a specific location in the study area, rather than the more general area associated with library spectra. Another reason *in-situ* measurement is selected was due to the observed differences between understory composition and spectral properties observable beneath the canopy and in clearings where background spectra would be taken from the image. This observed difference is likely to introduce errors into the determined background spectra and subsequently into the spectral mixture analysis as representative and characteristic samples of the background are less likely to be obtained.

In this study a FieldSpec Pro FR spectroradiometer is used for *in-situ* spectral measurement of the background feature classes. This spectroradiometer can measure the spectral properties of the background feature classes in wavelengths ranging from the ultraviolet through the middle infrared portion of the electromagnetic radiation spectrum. Measurements across these spectral bands are necessary due to the importance of the middle infrared spectrum for accurate LAI estimation (Eklundh *et al.,* 2001).

Measurements are taken at two different sites for each of the needleleaf and broadleaf canopies. Statistical testing is performed to determine whether the spectral properties exhibited by each feature class are significantly different, between each of the sample locations and feature class types.

For the sites possessing broadleaf canopies the overall results are presented in Table 4.16 in terms of reflectance.

Table 4.16: Summary of Reflectances Measured by FieldSpec Pro Spectroradiometer for Feature Classes at Various Locations with Broadleaf Overstory.

Feature Class	Sample Location	Mean Reflectance (0.61-0.68 μm)	Mean Reflectance (0.79-0.89 μm)	Mean Reflectance (1.58-1.75 μm)
Green Vegetation	Broadleaf One	0.056	0.509	0.280
Yellow Vegetation and Soil	Broadleaf One	0.055	0.149	0.256
Green Vegetation	Broadleaf Two	0.058	0.583	0.298
Yellow Vegetation and Soil	Broadleaf Two	0.055	0.237	0.269

Two-sample pooled t-tests are performed and the test statistics from the intra feature class comparisons are presented in Tables 4.17 and 4.18 for the observed reflectances in each of the red, near infrared and middle infrared bands.

Table 4.17: Summary of T-test Statistics with 0.05 Level of Significance for Mean Reflectances of Green Vegetation Compared at Sampling Locations with Broadleaf Canopies

T-test Statistic for Mean Reflectance (0.61-0.68 μm)	T-test Statistic for Mean Reflectance (0.79-0.89 μm)	T-test Statistic for Mean Reflectance (1.58-1.75 μm)	Critical Value
0.166	0.856	0.393	2.571

Table 4.18: Summary of T-test Statistics with 0.05 Level of Significance for Mean Reflectances of Yellow Vegetation and Soil Compared at Sampling Locations with Broadleaf Canopies

T-test Statistic for Mean Reflectance (0.61-0.68 μm)	T-test Statistic for Mean Reflectance (0.79-0.89 μm)	T-test Statistic for Mean Reflectance (1.58-1.75 μm)	Critical Value
0.043	2.777*	0.682	2.306

The results in Tables 4.17 and 4.18 allow us to conclude that the spectral properties of green vegetation do not vary significantly between the sampling sites with broadleaf canopies in any of the imaging bands. However, the yellow vegetation and soil feature class exhibit significant variation between the two sampling locations with broadleaf canopies in the near-infrared channel. This variation allows us to conclude that the spectral properties exhibited by yellow vegetation and soil in the near-infrared bands are not homogeneous for the sites having broadleaf canopies for this study area. The significant difference in these values indicates that care should be taken in their application.

The final step is to determine whether the feature classes under broadleaf canopies exhibit sufficiently different spectral properties for discrimination between them. The ability to discriminate between these classes was determined by performing a comparison of the mean spectral properties observed for the green and yellow vegetation respectively. Two-sample pooled T-tests are conducted using the measurements for each feature class type after the measurements from the two sampling locations had been unified to form one set. The results of this statistical testing are presented in Table 4.19.

Table 4.19: Results of Two Sample Pooled T-tests Comparing Feature Class Spectral Properties for a Broadleaf Overstory

T-test Statistic for Mean Reflectance (0.61-0.68 μm)	T-test Statistic for Mean Reflectance (0.79-0.89 μm)	T-test Statistic for Mean Reflectance (1.58-1.75 μm)	Critical Value
0.219	8.314*	1.178	2.131

These results lead to the conclusion that the feature classes under a broadleaf canopy are sufficiently different to allow for separation solely in the near-infrared portion of the electromagnetic spectrum. The homogeneity of the spectral properties of these two feature classes in the middle infrared and red portions of the spectrum could allow for their treatment as one entity within the modeling process, simplifying it dramatically.

For the needleleaf sites the overall results are presented in Table 4.20 in terms of reflectance.

Table 4.20: Summary of Reflectances Measured by FieldSpec Pro Spectroradiometer for Feature Classes at Various Locations for a Needleleaf Overstory.

Feature Class	Sample Location	Mean Reflectance (0.61-0.68 μm)	Mean Reflectance (0.79-0.89 μm)	Mean Reflectance (1.58-1.75 μm)
Green Vegetation	Needleleaf One	0.058	0.555	0.371
Yellow Vegetation and Soil	Needleleaf One	0.155	0.272	0.466
Green Vegetation	Needleleaf Two	0.042	0.355	0.280
Yellow Vegetation and Soil	Needleleaf Two	0.075	0.205	0.323

Two-sample pooled t-tests are performed and the test statistics from the comparisons of the sets within each feature class are presented in Tables 4.21 and 4.22 for the reflectances recorded for each of the red, near infrared and middle infrared bands.

Table 4.21: Summary of T-test Statistics at Level of Significance 0.05 for Mean Reflectances of Green Vegetation Compared at Sampling Locations with Needleleaf Overstory

T-test Statistic for Mean Reflectance (0.61-0.68 μm)	T-test Statistic for Mean Reflectance (0.79-0.89 μm)	T-test Statistic for Mean Reflectance (1.58-1.75 μm)	Critical Value
1.586	4.547*	2.243	2.262

Table 4.22: Summary of T-test Statistics for Mean Reflectances of Yellow Vegetation and Soil Compared at Sampling Locations with Needleleaf Overstory

T-test Statistic for Mean Reflectance (0.61-0.68 μm)	T-test Statistic for Mean Reflectance (0.79-0.89 μm)	T-test Statistic for Mean Reflectance (1.58-1.75 μm)	Critical Value
3.723*	1.898	1.961	2.306

The results in Tables 4.21 and 4.22 allow us to conclude that, for sites with needleleaf canopies, the spectral properties of green vegetation exhibit significant variance between the sampling sites in the near infrared bands while the yellow vegetation exhibits significant variation in the red bands. This variation allows us to conclude that the spectral properties of the feature classes are not homogeneous in all bands and the results occurring from the application of these measurements must be carefully scrutinized to see that their inclusion has not affected the quality of the results.

The last step is to ascertain whether the feature classes with needleleaf canopies exhibited sufficient difference in their spectral properties for them to be mutually distinguished. Two-sample pooled T-tests are performed and the results of this statistical testing are presented in Table 4.23.

Table 4.23: Results of Two Sample Pooled T-tests at 0.05 Level of Significance Comparing Feature Class Spectral Properties for Needleleaf Overstory Conditions

T-test Statistic for Mean Reflectance (0.61-0.68 μm)	T-test Statistic for Mean Reflectance (0.79-0.89 μm)	T-test Statistic for Mean Reflectance (1.58-1.75 μm)	Critical Value
4.214*	4.977*	1.641	2.093

The above testing permits us to conclude that the spectral properties of the feature classes under a needleleaf overstory exhibit significant differences in their reflectances in the red and near-infrared wavelengths. Due to the substantial nature of these differences it is reasonable to conclude that these feature classes should be distinguishable within these wavelengths. The similarity of the spectral properties of the feature classes in the middle infrared bans could allow for the agglomeration of these classes for modeling purposes.

4.4.4.2 Determination of Feature Class Composition

To determine the overall spectral properties of the background it is necessary to determine the relative abundance of each of the feature classes contained within each particular study plot. The relative abundance of each of the feature classes determines the contribution of each respective feature class to the overall spectral signature of the background for that specific location.

The relative composition of each feature class is determined in the following manner. Digital photos were collected at 20m intervals within each plot on September 15th and 16th, 2004. This sampling regime resulted in a total of nine digital photos for each 60m by 60m plot. These photos are subsequently converted from JPEG to PIX file format to be analyzed in PCI. After the file format conversion, subset areas of the resulting images are taken for analysis. These subset areas are selected visually so as to comprise the largest representative area that could be obtained from the initial image, while minimizing the presence of overstory features in the image.

Once the subset areas are obtained the initial red, green, blue (RGB) values obtained from the digital camera are transformed using an intensity, hue, saturation (IHS) transformation. This transform is used because of the substantial variability in light intensity under the canopy. These variations are evident in the images from the presence of shadows associated with overstory shading rendering members of the same feature class indistinguishable using a classification algorithm on the initial RGB channels. However, application of the IHS transform mitigates these difficulties to some extent due to its extraction of the intensity component. Further processing is required after the IHS transform due to the scaling of the hue value, which is modeled to be circular, on a linear eight bit scale. This processing involves the separation of the hue into an X and Y component based on either the sine or cosine of its magnitude.

After this initial processing an unsupervised classification is performed using the X and Y components of the hue value as input parameters. The input feature classes are then identified in the image, along with the output classification clusters they correspond to. The relative abundance is calculated by determining the proportion of the image which is occupied by each feature class. This process is performed for each photo within a plot. The results of these classifications are compiled at the plot level to determine the differences between the mean background compositions and the local background compositions. The classification results are compiled for broadleaf or needleleaf canopies, as variation between the spectral properties of the background feature classes is sufficient for separate analysis.

In Figures 4.7 and 4.8 photographs of typical needleleaf and broadleaf understory conditions are presented.

Figure 4.7: Typical Understory Conditions Beneath a Broadleaf Canopy

Figure 4.8: Typical Understory Conditions Beneath a Needleleaf Canopy

It is evident from the above photographs that the understory conditions associated with broadleaf and needleleaf canopies are distinct from each other. Beneath the broadleaf canopy, an abundance of leafy green vegetation is evident, with leafy yellow vegetation scarcely evident. Underneath the needleleaf canopy smaller needleleaf shrubs, in addition to an increased incidence of bare soil is evident. Although some leafy green vegetation is visible, an increased proportion of green understory vegetation is composed of weeds and mosses.

In Tables 4.24 and 4.25 the statistics regarding feature class composition are presented for both the needleleaf and broadleaf canopy conditions.

Table 4.24: Feature Class Composition for Sites with Broadleaf Overstory

Plot Number	Percent Composition of Green Vegetation Feature Class	Percent Composition of Yellow Vegetation Feature Class
1	60	40
2	55	45
3	55	45
4	55	45
5	55	45
6	50	50
7	50	50
8	60	40
9	55	45
10	60	40
Total	55	45

Table 4.25: Feature Class Composition for Sites with Needleleaf Overstory

Plot Number	Percent Composition of Green Vegetation Feature Class	Percent Composition of Yellow Vegetation Feature Class
1	35	65
2	40	60
3	65	35
4	50	50
5	65	35
6	60	40
7	65	35
8	50	50
9	55	45
10	50	50
Total	55	45

It is evident from these statistics that the understory is approximately equally composed of the two feature classes which were defined for the analysis for needleleaf and broadleaf vegetation. It is also evident that the needleleaf sites exhibit substantially more variance in the understory composition, their standard deviation being larger by a factor of approximately three, than do those of the broadleaf sites.

5. Regression Analysis

The regression analysis using any modeling parameter employed in this study is performed in the same way. The values for each pixel contained within the boundaries of an individual plot are incorporated into the final estimate of the plot-wide LAI estimate. The contribution of each of the pixel values is weighted based on the area of the plot contained within that pixel to the total area of the plot. Once the overall parameter values are determined, after application of the weighting function, these values are regressed against *in-situ* LAI measurements.

5.1 Spectral Vegetation Indices

As previously discussed in Chapter 3 several spectral vegetation indices, both traditional and modified, are computed for each plot. These indices are compared to determine which one evinced the highest capacity to model the observed LAI variations for each vegetation type. This analysis is subdivided into needleleaf and broadleaf vegetation respectively to facilitate analysis and comparison. This subdivision also allows for a determination whether the optimal relationships derived for each vegetation type differs in terms of strength, accuracy or modeling inputs.

5.1.1 Needleleaf Vegetation

Relationships are derived between reflectance values, generic spectral vegetation indices, along with scaled versions of these indices incorporating middle infrared reflectance, and measured LAI. Linear and power relationships are derived between each spectral vegetation index and the LAI measurements. The results of these regressions are presented in Table 5.1.

Table 5.1: Coefficients of Determination for Spectral Vegetation Indices and LAI Measurements

Input Parameter	Linear Relationship	Coefficient of Determination of Linear Relationship	Power Relationship	Coefficient of Determination of Power Relationship
Red Reflectance (REF_{RED})	$LAI = -359.42 REF_{RED} + 19.57$	0.50	$LAI = \dfrac{8E-05}{REF_{RED}^{3.45}}$	0.44
Near Infrared Reflectance (REF_{NIR})	$LAI = -57.30 REF_{NIR} + 12.68$	0.80	$LAI = \dfrac{0.11}{REF_{NIR}^{1.89}}$	0.73
Middle Infrared Reflectance (REF_{MIR})	$LAI = -84.76 REF_{MIR} + 11.25$	0.75	$LAI = \dfrac{0.099}{REF_{MIR}^{1.49}}$	0.65
$\dfrac{MIR}{RED}$ $BAND_{QUO}$	$LAI = -4.31 BAND_{QUO} + 12.68$	0.63	$LAI = \dfrac{14.91}{BAND_{QUO}^{1.94}}$	0.59
$MIR * RED$ $BAND_{PROD}$	$LAI = -1581.7 BAND_{PROD} + 9.8$	0.76	$LAI = \dfrac{0.007}{BAND_{PROD}^{1.13}}$	0.64
NDVI	$LAI = -27.43 NDVI + 19.34$	0.54	$LAI = 0.45 NDVI^{-3.70}$	0.54
SR	$LAI = -2.76 SR + 13.85$	0.56	$LAI = 77.61 SR^{-2.36}$	0.56
MSI	$LAI = -32.33 MSI + 22.54$	0.27	$LAI = 0.42 MSI^{-4.01}$	0.22
$NDVI_{ADJ}$	$LAI = -14.46 NDVI_{ADJ} - 0.61$	0.77	$LAI = 17.18 NDVI_{ADJ}^{1.30}$	0.79
SR_{ADJ}	$LAI = 2.64 SR_{ADJ} - 1.30$	0.76	$LAI = 1.40 SR_{ADJ}^{1.46}$	0.77

The relationships derived from the structural regressions are presented in Figures 5.1 through 5.10 to facilitate interpretation.
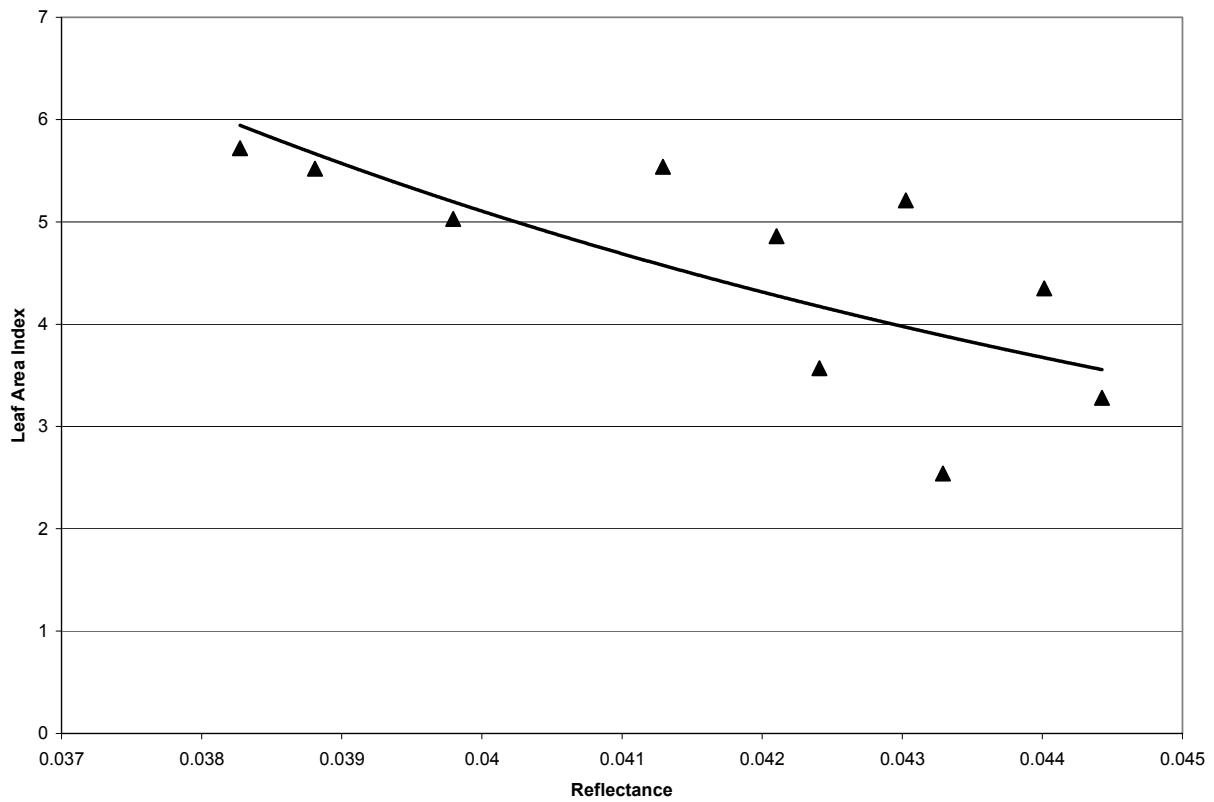
Figure 5.1: Graph of LAI versus Measured Reflectance between 0.610 and 0.680 μm for Needleleaf Vegetation
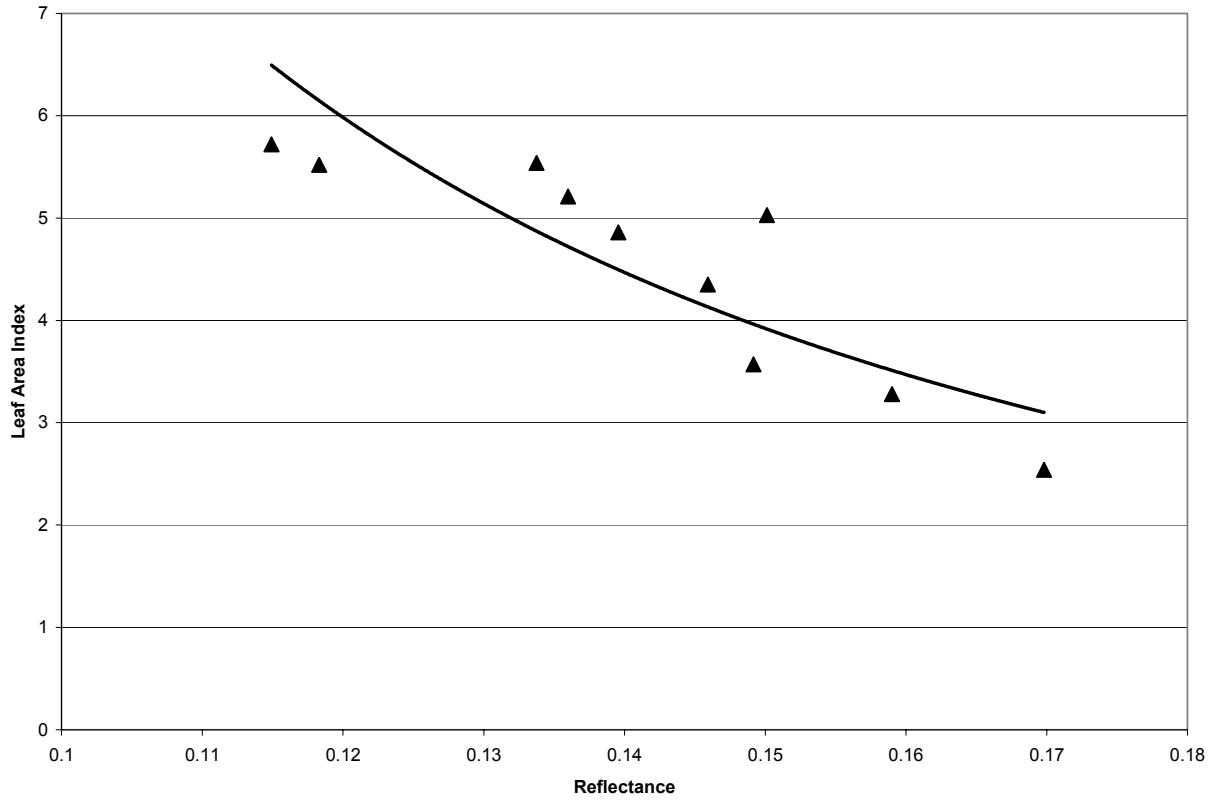
Figure 5.2: Graph of LAI versus Measured Reflectance between 0.790 and 0.890 μm for Needleleaf Vegetation
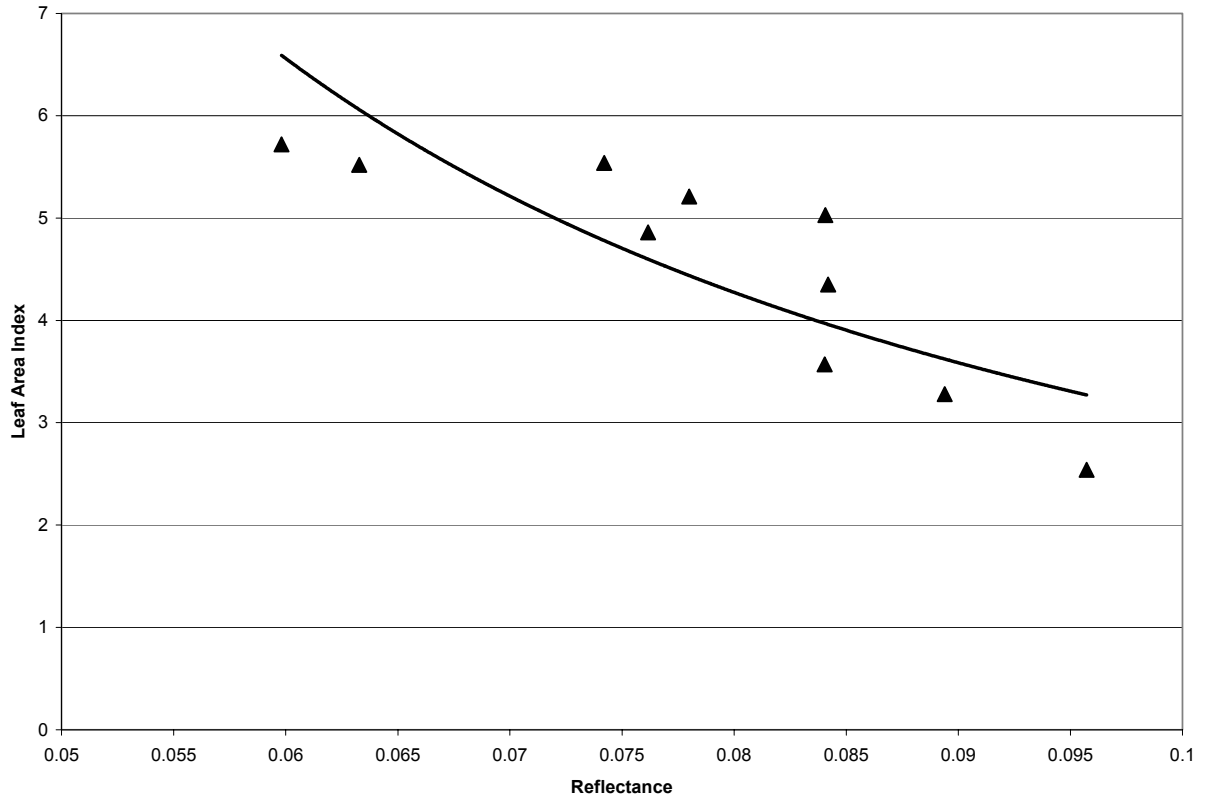
Figure 5.3: Graph of LAI versus Measured Reflectance between 1.580 and 1.730 μm for Needleleaf Vegetation
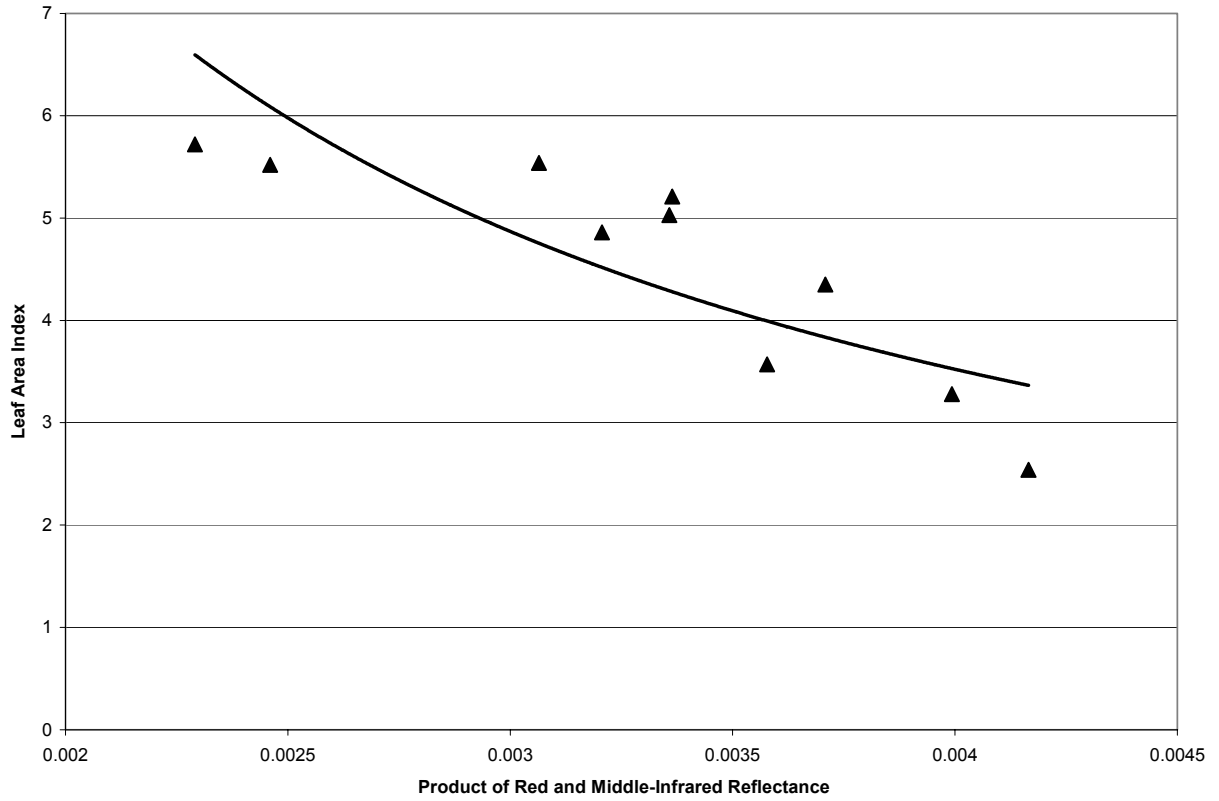
Figure 5.4 Graph of LAI versus the Product of the Observed Reflectances in the Red and Middle-Infrared Bands for Needleleaf Vegetation
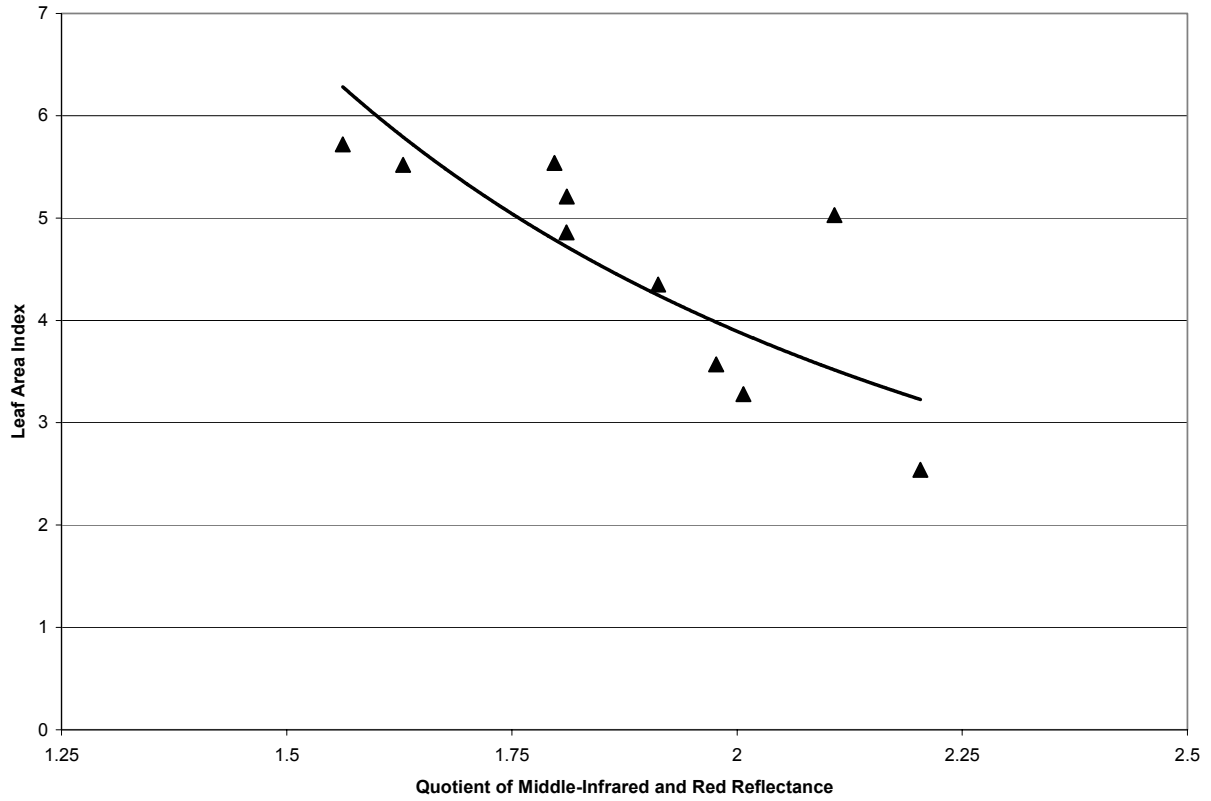
Figure 5.5 Graph of LAI versus the Quotient of Middle-Infrared Reflectance Divided by Red Reflectance for Needleleaf Vegetation
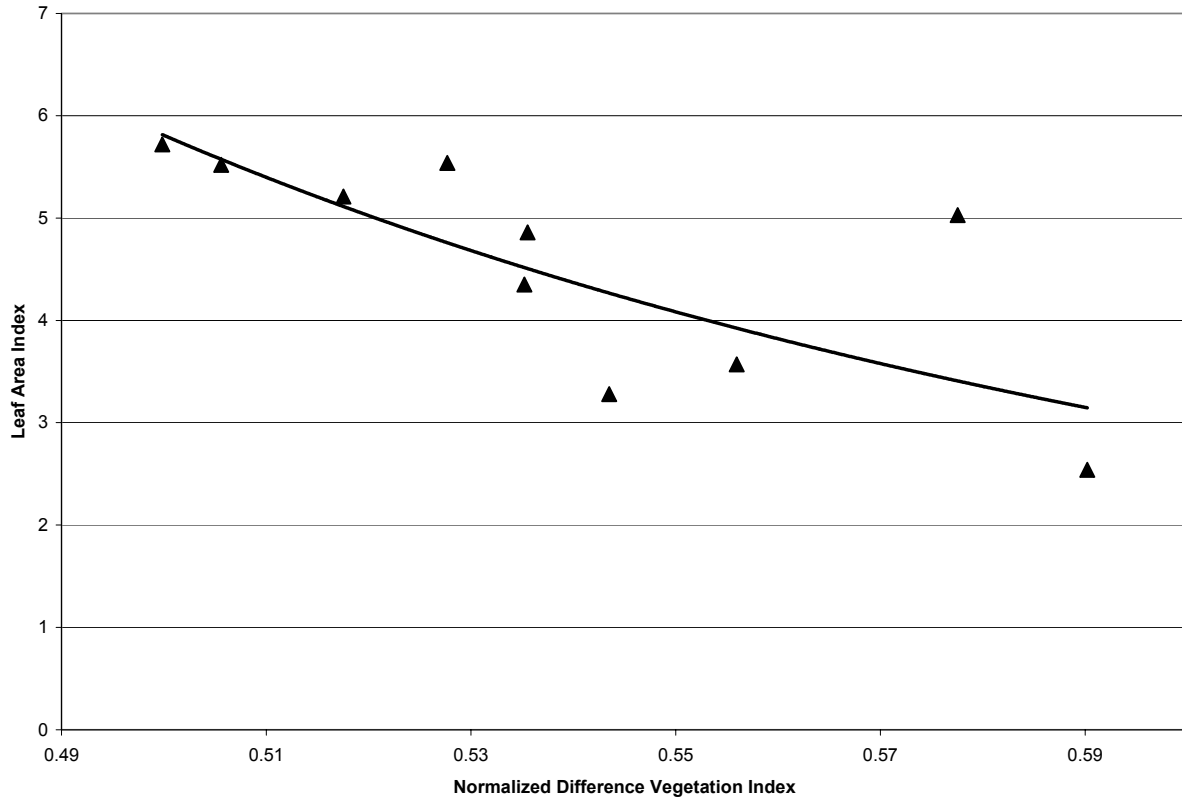
Figure 5.6: Graph of LAI versus Normalized Difference Vegetation Index for Needleleaf Vegetation
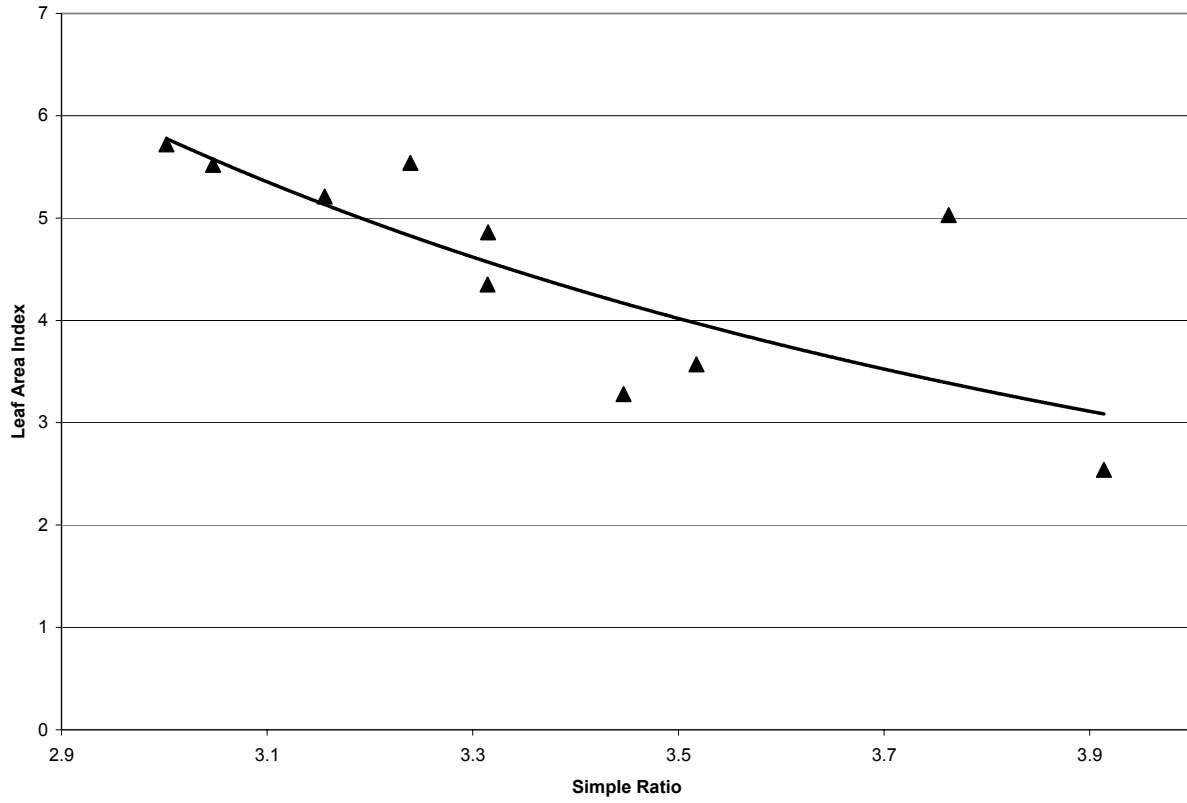
Figure 5.7: Graph of LAI versus Simple Ratio for Needleleaf Vegetation
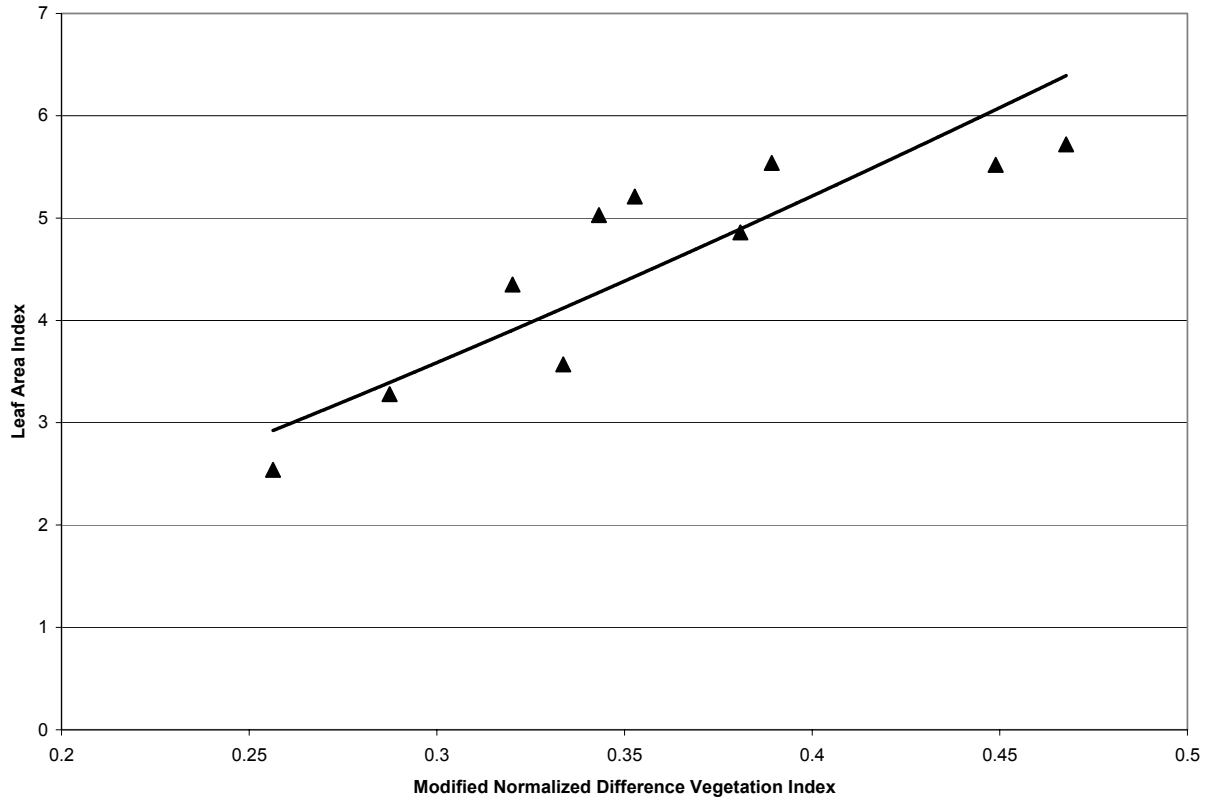
Figure 5.8: Graph of LAI versus Modified Normalized Difference Vegetation Index for Needleleaf Vegetation
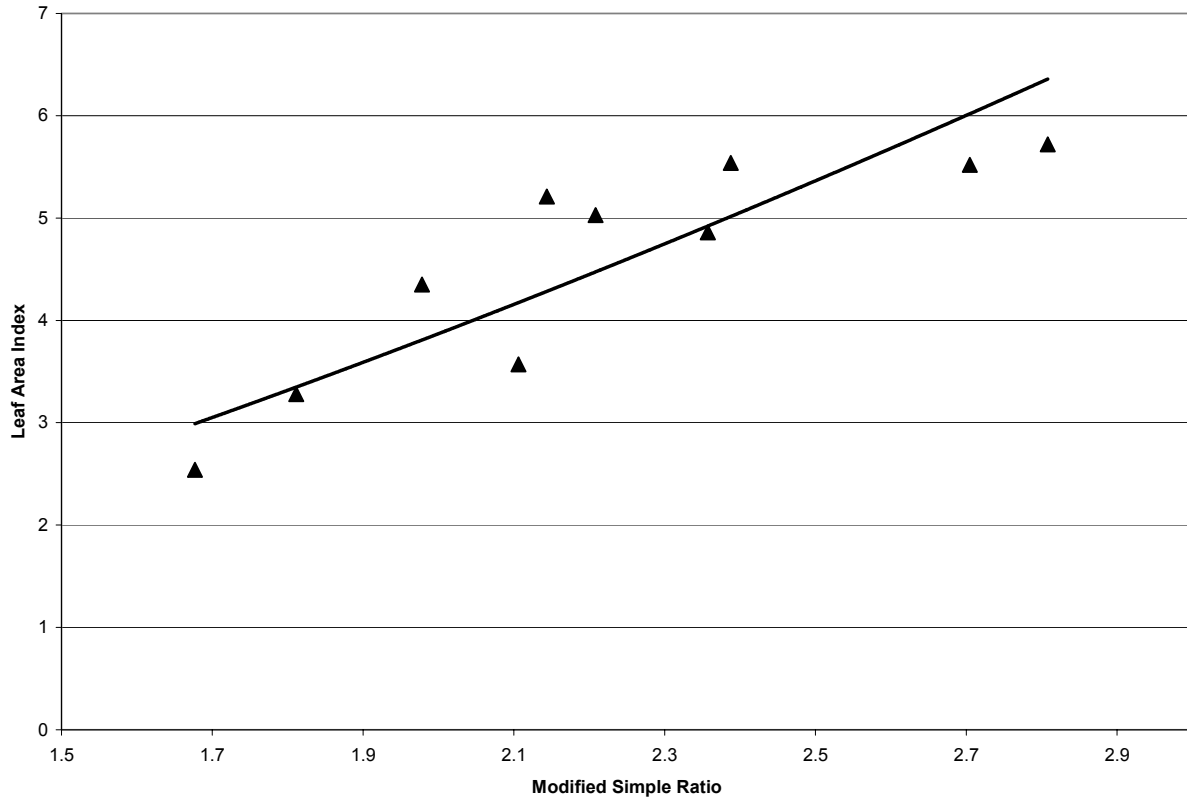
Figure 5.9: Graph of LAI versus Modified Simple Ratio for Needleleaf Vegetation
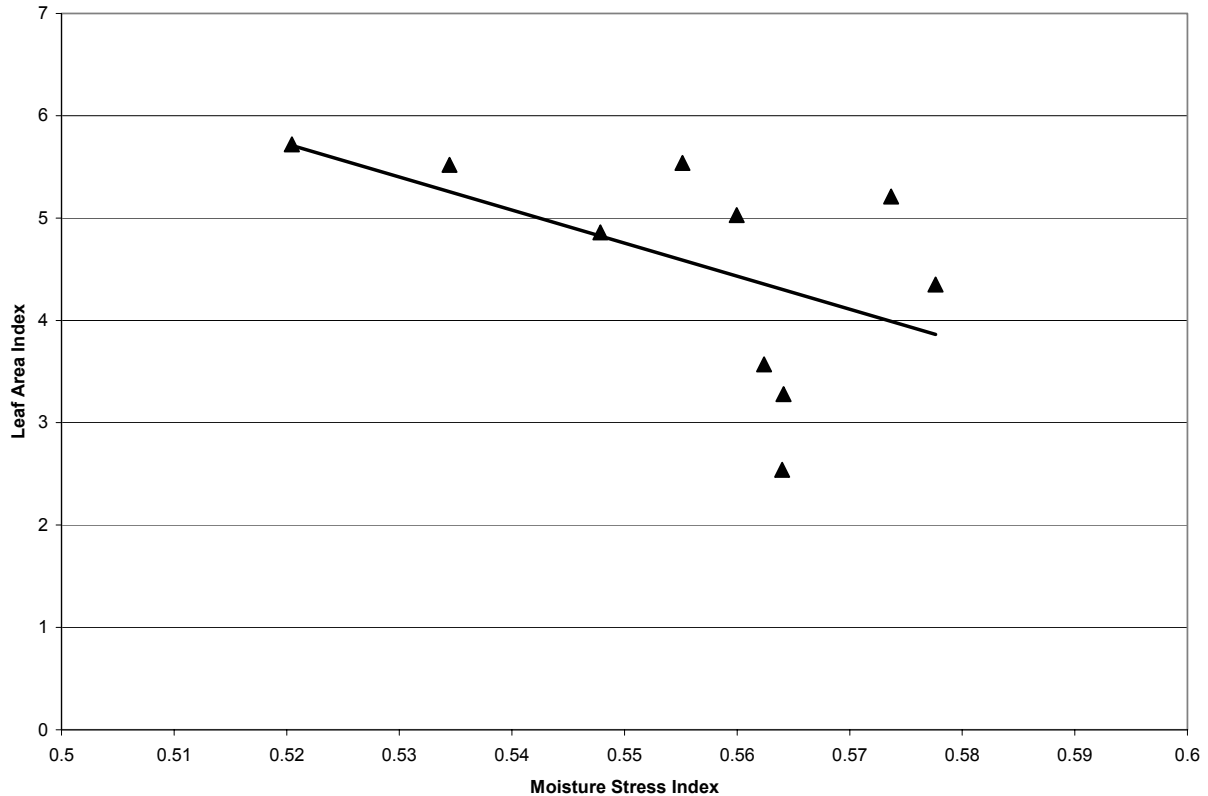
Figure 5.10: Graph of LAI versus Moisture Stress Index for Needleleaf Vegetation

For needleleaf vegetation the spectral vegetation indices which exhibited the strongest relationships with measured LAI, incorporated measurements in each of the red, near-infrared and middle-infrared bands.

One interesting feature of the needleleaf vegetation in this study, is the unexpected inverse relationship observed between NDVI and LAI measurements. Such behavior in traditional LAI estimators, which generally assume positive correlations with NDVI, almost certainly results in the introduction of errors into the modeling which propagate across the landscape. This inverse relationship is likely due to the reflectance properties of the understory, which differ from those of the needleleaf overstory as it is composed of green leafy vegetation. This is due to the visibility of understory vegetation by the sensor in sparser canopies. The presence of leafy green vegetation likely contributes to an increase in NDVI.

5.1.2 Broadleaf Vegetation

As in the case of needleleaf vegetation already discussed, relationships are derived between *in-situ* LAI measurements and each of the modified and unmodified spectral vegetation indices. Linear and power relationships are derived between the spectral vegetation indices and the LAI measurements. It should be noted that only nine plots of the original ten are employed for the regression analysis. This decision has been made because the plot that is not being used, plot number 9, was significantly more mixed in terms of species composition than the other plots and substantially degraded the results in terms of quality and sampling uniformity. In Table 5.2 the coefficients of determination for each of the relationships are presented.

Table 5.2: Regression-Derived Coefficients of Determination between Spectral Vegetation Indices and LAI Measurements for Broadleaf Vegetation

Input Parameter	Linear Relationship	Coeffic-ient of Determ-ination of Linear Relation-ship	Power Relationship	Coefficient of Determination of Power Relationsh-ip
Red Reflectance (REF_{RED})	$LAI = -111.90REF_{RED} + 8.23$	0.43	$LAI = \dfrac{0.0035}{REF_{RED}^{2.21}}$	0.44
Near Infrared Reflectance (REF_{NIR})	$LAI = 8.52REF_{NIR} + 0.38$	0.11	$LAI = 7.22REF_{NIR}^{0.76}$	0.08
Middle Infrared Reflectance (REF_{MIR})	$LAI = -26.07REF_{MIR} + 5.98$	0.47	$LAI = 0.16REF_{MIR}^{-1.38}$	0.49
$\dfrac{MIR}{RED}$ ($BAND_{QUO}$)	$LAI = -1.12BAND_{QUO} + 5.62$	0.48	$LAI = \dfrac{7.42}{Band_{QUO}^{1.14}}$	0.48
$MIR*RED$ ($BAND_{PROD}$)	$LAI = -338.87BAND_{PROD} + 4.81$	0.49	$LAI = \dfrac{0.031}{BAND_{PROD}^{0.88}}$	0.49
NDVI	$LAI = 14.05NDVI - 7.01$	0.46	$LAI = 10.43NDVI^{3.68}$	0.43
SR	$LAI = 0.70SR - 1.16$	0.43	$LAI = 0.23SR^{1.43}$	0.38
MSI	$LAI = -7.20MSI + 6.04$	0.63	$LAI = 0.93MSI^{-1.37}$	0.64
$NDVI_{ADJ}$	$LAI = 2.23NDVI_{ADJ} + 1.72$	0.51	$LAI = 3.55NDVI_{ADJ}^{0.33}$	0.59
SR_{ADJ}	$LAI = 0.28SR_{ADJ} + 1.70$	0.56	$LAI = 1.79SR_{ADJ}^{0.33}$	0.63

The graphical results determined by structural regression are presented in Figures 5.11 through 5.20.
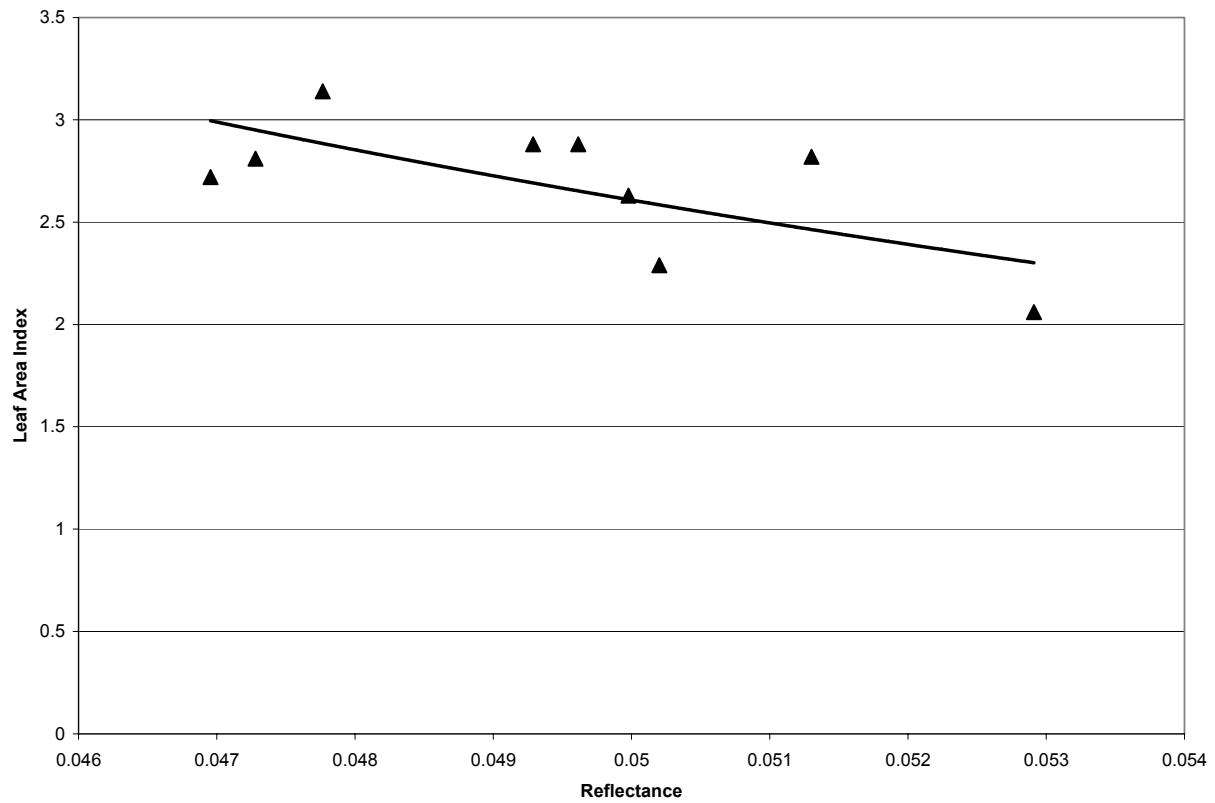
Figure 5.11: Graph of LAI versus Measured Reflectance between 0.610 and 0.680 µm for Broadleaf Vegetation
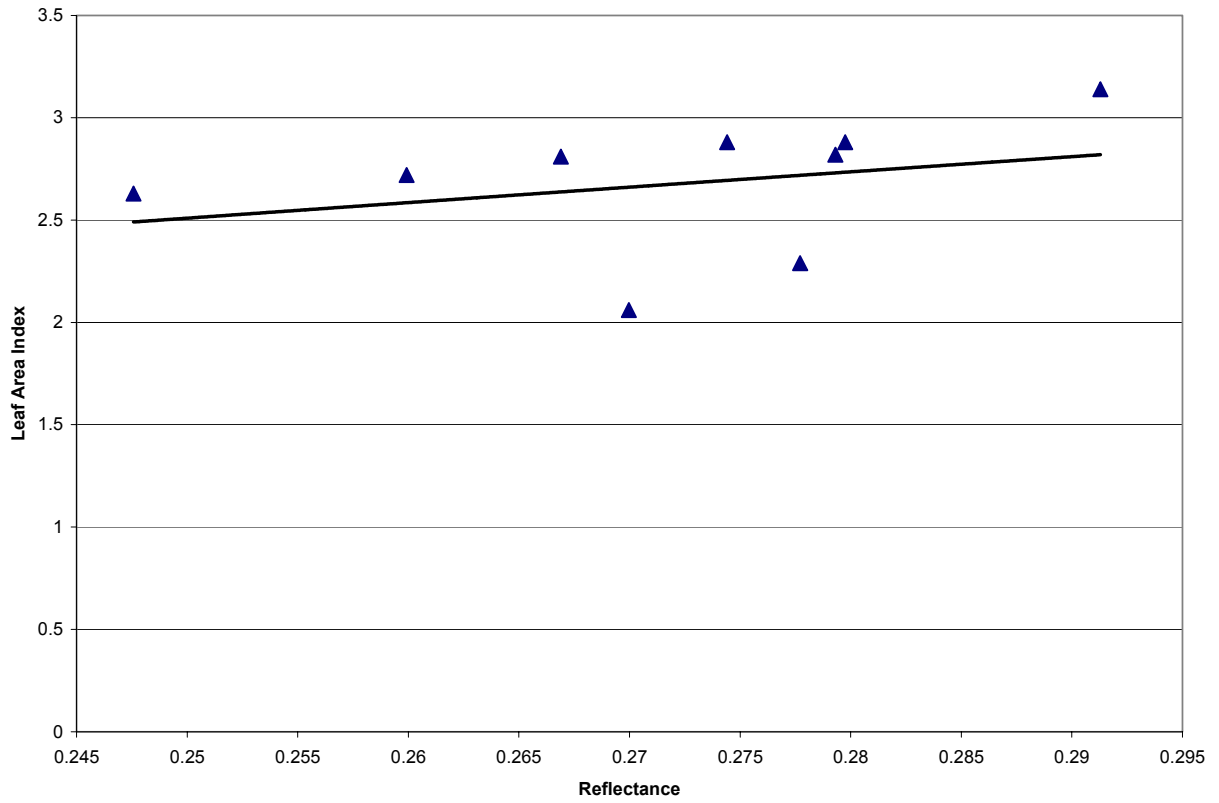
Figure 5.12: Graph of LAI versus Measured Reflectance between 0.790 and 0.890 μm for Broadleaf Vegetation
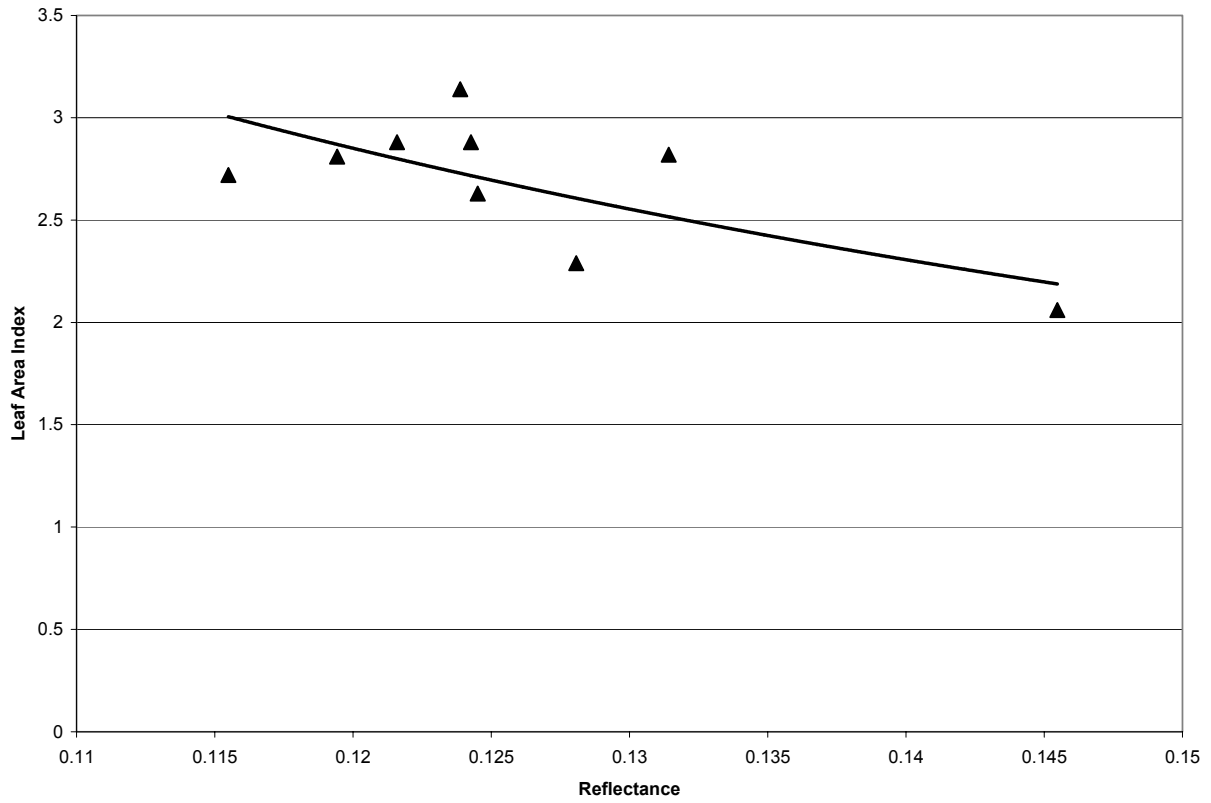
Figure 5.13: Graph of LAI versus Measured Reflectance between 1.580 and 1.730 μm for Broadleaf Vegetation
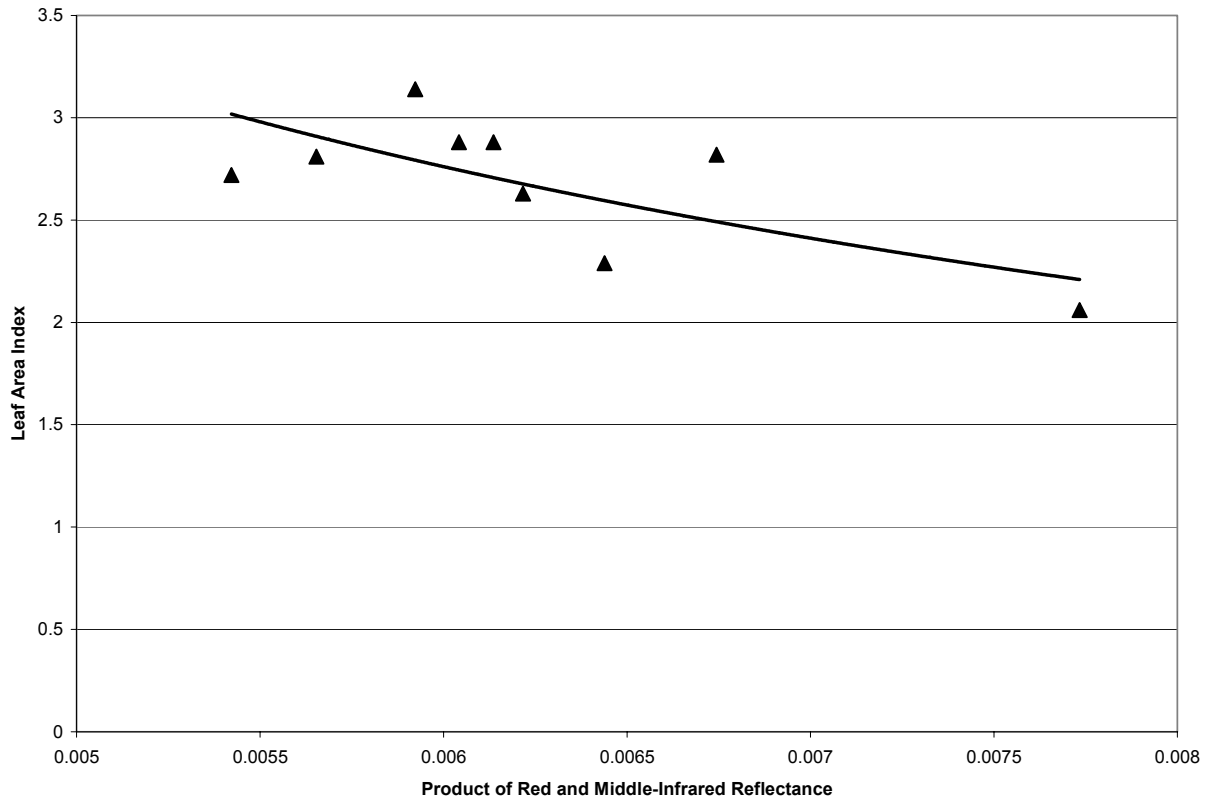
Figure 5.14 Graph of LAI versus the Product of the Observed Reflectances in the Red and Middle-Infrared Bands for Needleleaf Vegetation
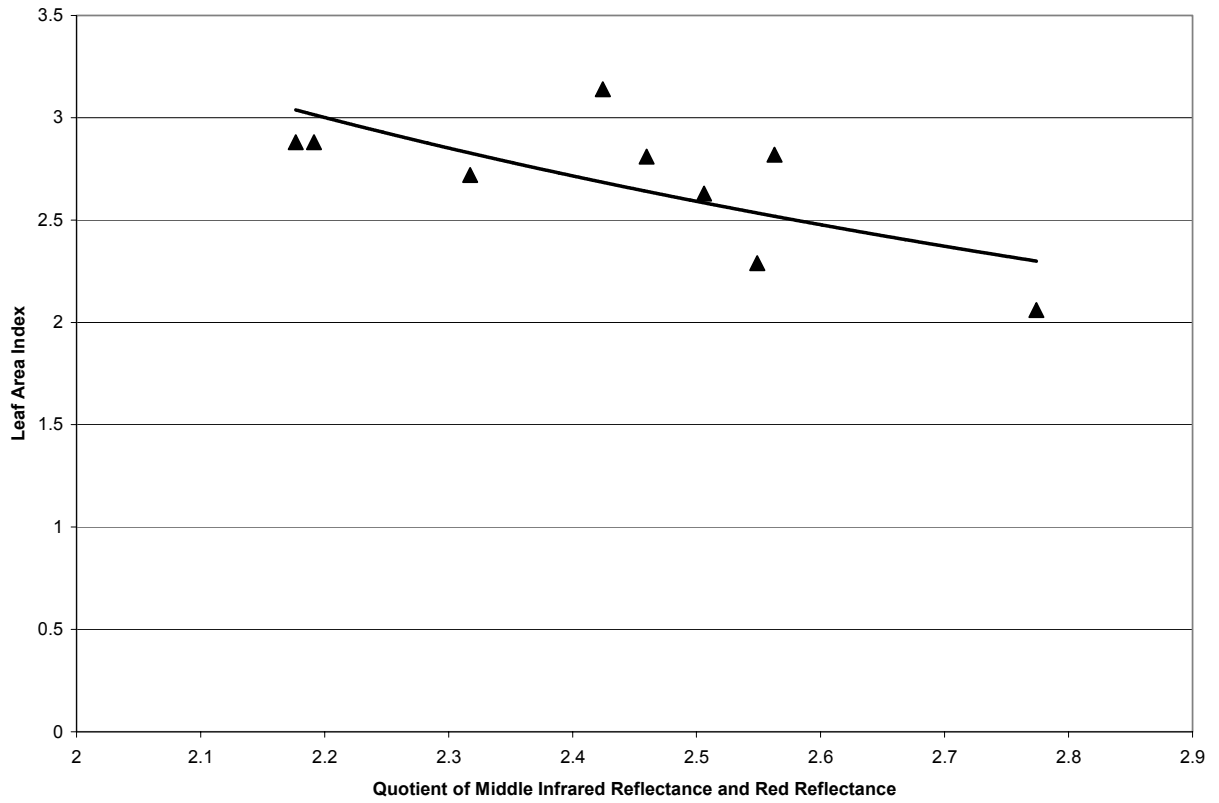
Figure 5.15 Graph of LAI versus the Quotient of Middle-Infrared Reflectance Divided by Red Reflectance for Needleleaf Vegetation
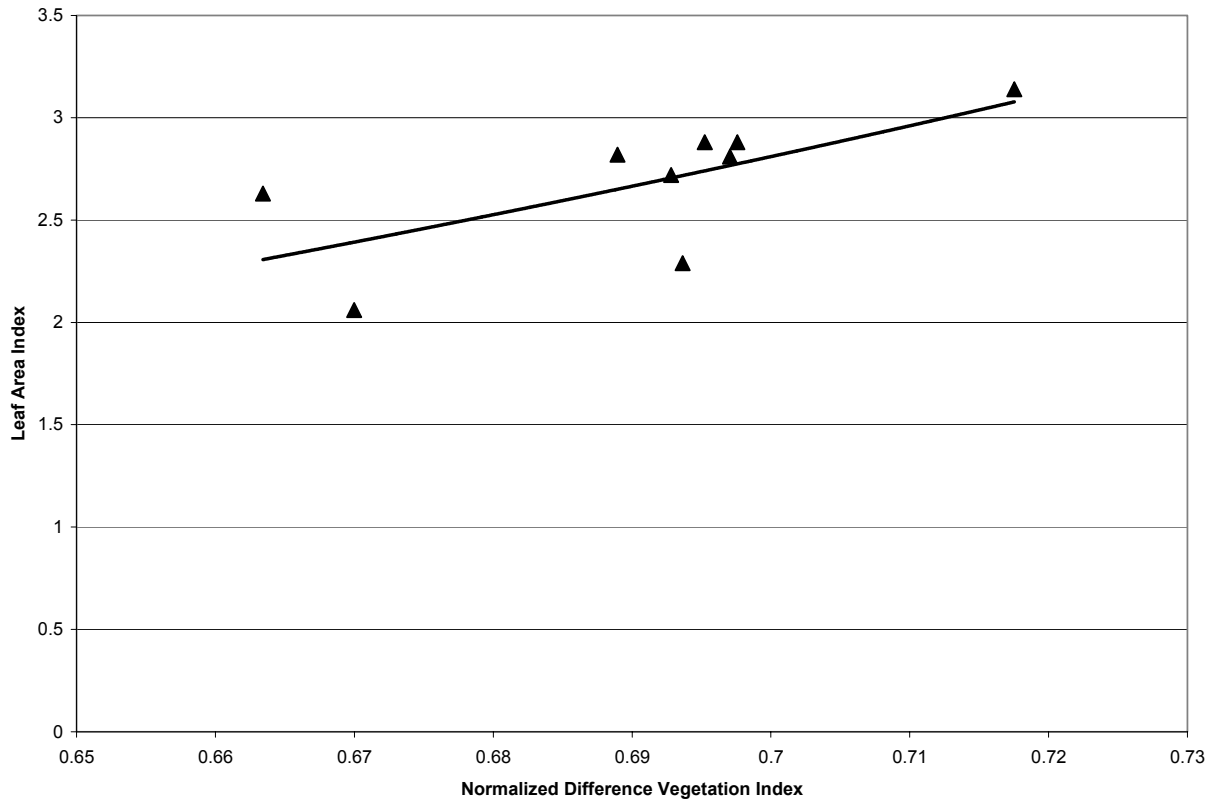
Figure 5.16: Graph of LAI versus Normalized Difference Vegetation Index for Broadleaf Vegetation
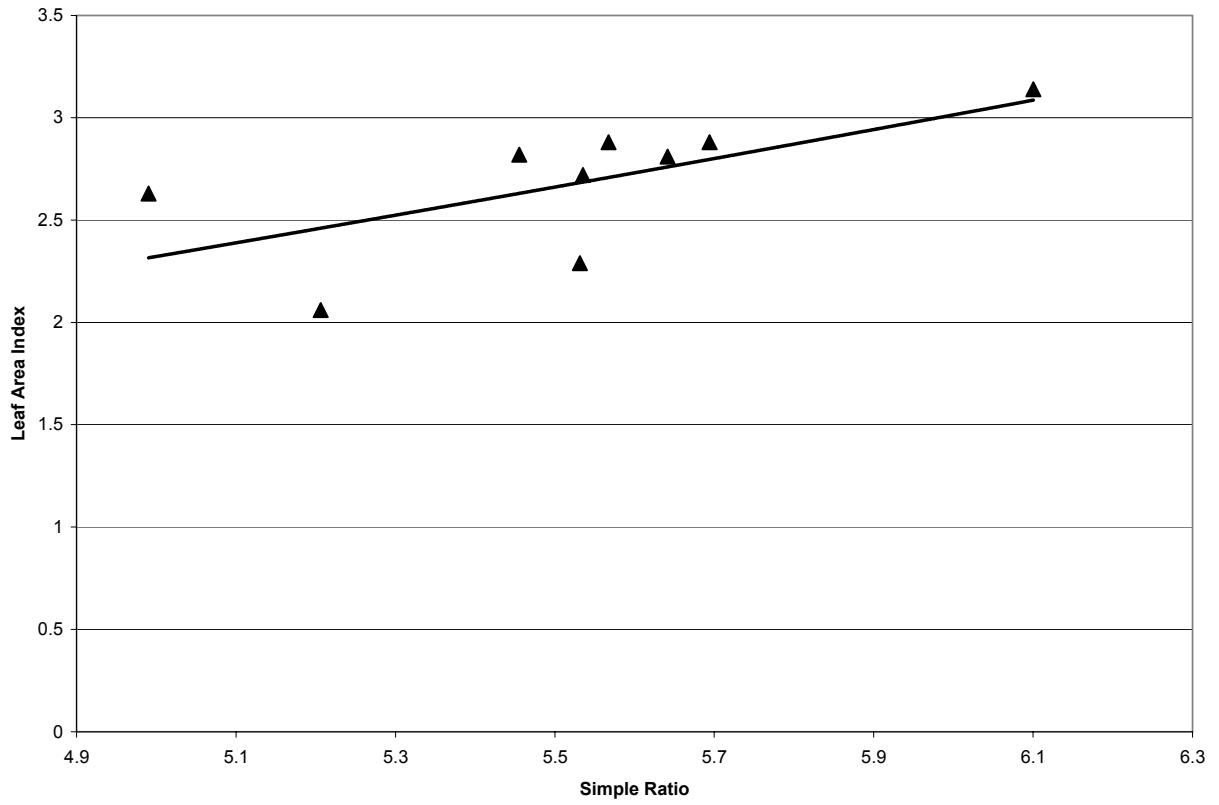
Figure 5.17: Graph of LAI versus Simple Ratio for Broadleaf Vegetation
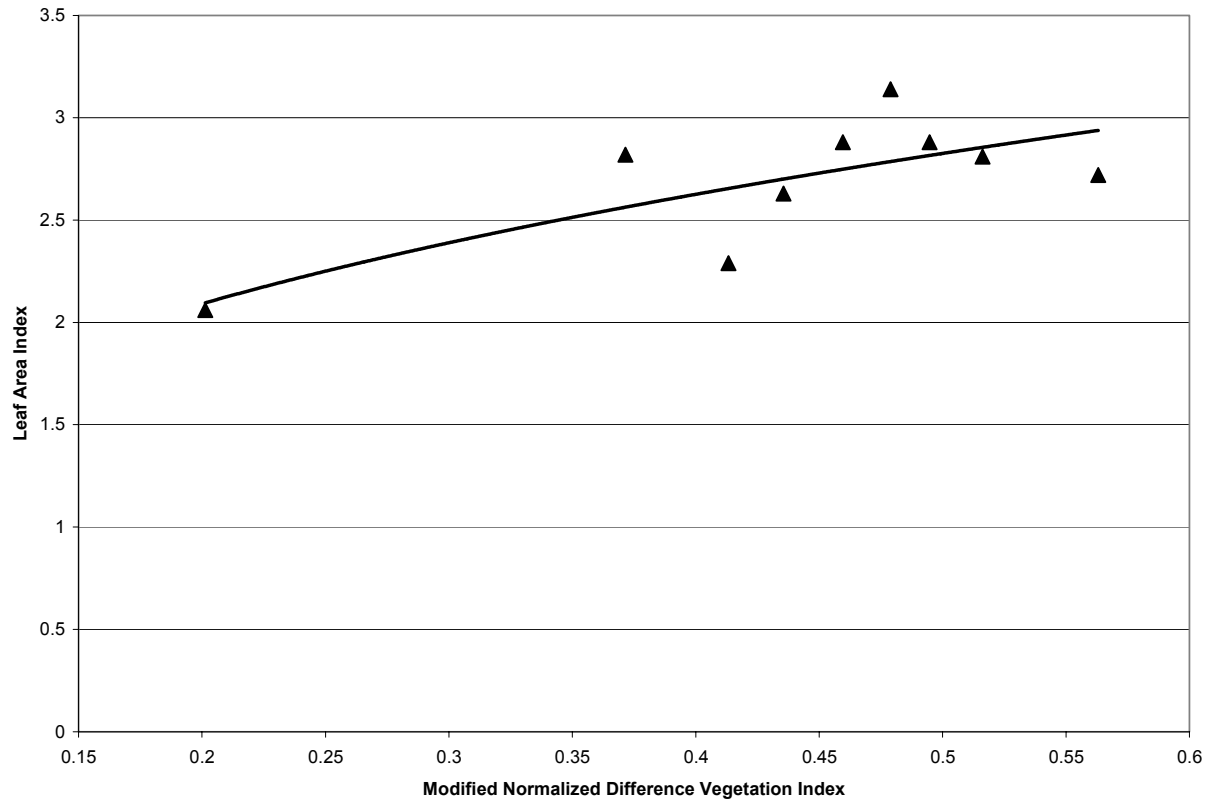
Figure 5.18: Graph of LAI versus Modified Normalized Difference Vegetation Index for Broadleaf Vegetation
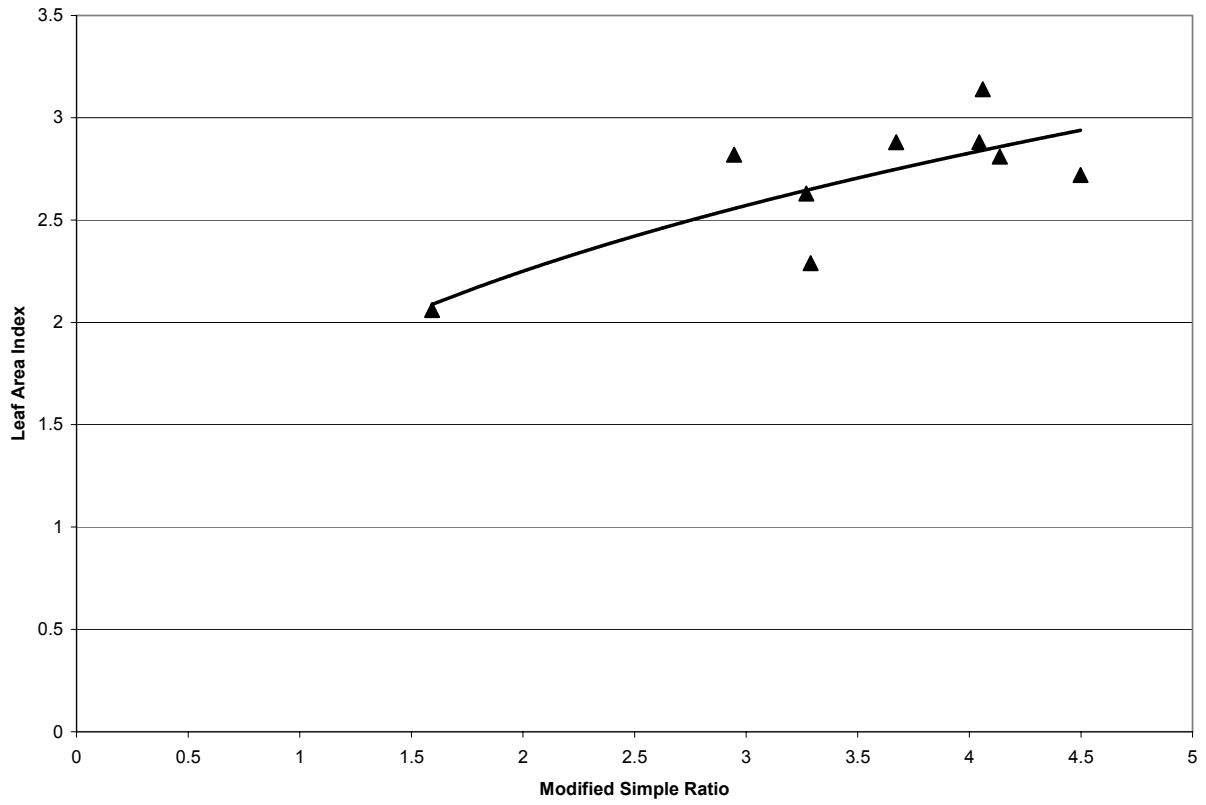
Figure 5.19: Graph of LAI versus Modified Simple Ratio for Broadleaf Vegetation
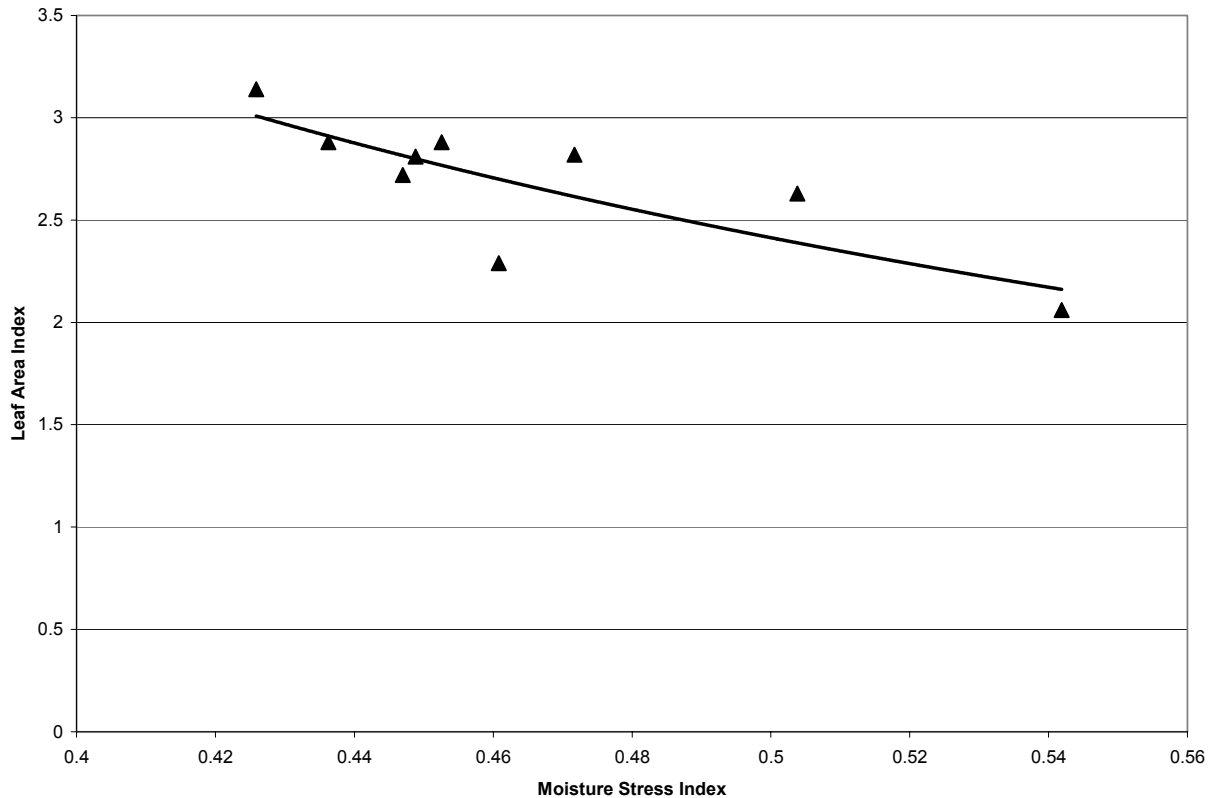
Figure 5.20: Graph of LAI versus Moisture Stress Index for Broadleaf Vegetation

It is evident that the strongest relationships are derived between measured LAI and spectral vegetation indices which incorporate middle-infrared information. The unmodified spectral vegetation indices, namely the normalized difference vegetation index and the simple ratio, exhibit the poorest performance in modeling LAI in broadleaf canopies.

These results differ from those of the needleleaf canopy in that the moisture stress index, which exhibits the weakest relationship with LAI in the needleleaf case, is now the parameter which best models LAI. The variable performance of the moisture stress index in its ability to reliably model LAI is likely attributable to the differing spectral properties of needleleaf and broadleaf canopies, particularly in the middle infrared bands. The variations in reflectance observed in the middle infrared are primarily due to the relative moisture content. Given the different moisture storage mechanisms associated with needleleaf and broadleaf vegetation, it is therefore not surprising that the performance of the models employing the moisture stress index as the input parameter exhibit

varying performance.

5.2 Linear Spectral Mixture Analysis

As previously discussed in Chapter 3, techniques of linear spectral mixture analysis are employed to determine the relative composition of each pixel of interest in terms of predefined feature classes. The three feature classes defined for this study are sunlit canopy, shaded canopy and background. These classes are selected as the majority of studies implementing spectral mixture analysis techniques for LAI estimation in boreal or montane forests have used these specific classes. (Peddle *et al* 2001, Peddle *et al.,* 1999) The shaded canopy is also referred to as the shadow fraction.

Spectral endmembers for each of the needleleaf and broadleaf cases are determined in the same way. The sum of the observed reflectances of the red, near-infrared and middle-infrared are taken for each pixel observed and contained within a plot of a given overstory type. The pixels possessing the minimum and maximum values of these sums are determined and then specified as endmembers. The pixel with the minimum value for the reflectance sum is taken to be the shaded canopy endmember, as a decrease in observed reflectance is expected with increasing shade. The pixel with the maximum value for the reflectance sum is taken to be the sunlit canopy endmember, as an increase in observed reflectance is expected with minimal shading.

To determine the impact of variations in the remote estimation models based on the method of determination of background spectra, two different background values are employed. One background spectrum has been determined from *in-situ* spectral and composition measurements of feature classes, while the other has been selected directly from the image. Regression analysis between measured LAI and shadow fraction is conducted to determine whether a significant relationship exists.

To ensure convergent solutions that satisfied the preliminary constraints of non-negative percent compositions, which computed over all feature classes sums to one, the application of both analytical and numerical solution techniques is necessary. The analytical solution consisted of a

parametric least-squares algorithm designed to determine the optimal composition to generate the observed reflectance for a particular pixel. If the analytical solution satisfied the initial constraints it was accepted, however if it violated the initial constraints a numerical solution algorithm was implemented. The numerical solution algorithm implemented a constrained solution where the errors generated by particular values of pixel composition are to be evaluated. The values of pixel composition are varied at uniform intervals across the domain specified by the initial constraints. The pixel composition which minimizes the differences between the observed and modeled reflectances is selected as the solution. The numerical method is specified to have an evaluation interval of 0.5%. Due to the voluminous computations associated with the numerical method, employing a finer sampling regime would have necessitated non-linear increases in computational time without corresponding increases in accuracy. Although the numerical solution has lower accuracy than the analytical solution, the extent to which it affects the solution is an order of magnitude less than the evaluation interval.

5.2.1 Needleleaf Vegetation

In the needleleaf case, the relationships determined between the shadow fraction (SF) and the LAI are stronger than those derived using the technique of modified spectral vegetation indices.

The results obtained from the use of different background spectra produced are similar overall, although the background spectra derived from *in-situ* spectral sampling slightly outperforms that determined from the image for both the linear and power relationships. Additionally, the power relationship appears to exhibit increased robustness in its modeling of LAI, for needleleaf canopies, than does a linear model. This is evident from Table 5.3 and Figures 5.21 and 5.22.

Table 5.3: Coefficients of Determination Determined from Regression of LAI against Shadow Fraction for Needleleaf Vegetation

Background Spectra Derivation Type	Linear Relationship	Coefficient of Determination of Linear Relationship	Power Relationship	Coefficient of Determination of Power Relationship
Spectroradiometer	$LAI = 7.15SF - 0.80$	0.81	$LAI = 6.59SF^{1.31}$	0.83
Image	$LAI = 6.38SF + 0.13$	0.78	$LAI = 6.81SF^{1.11}$	0.82
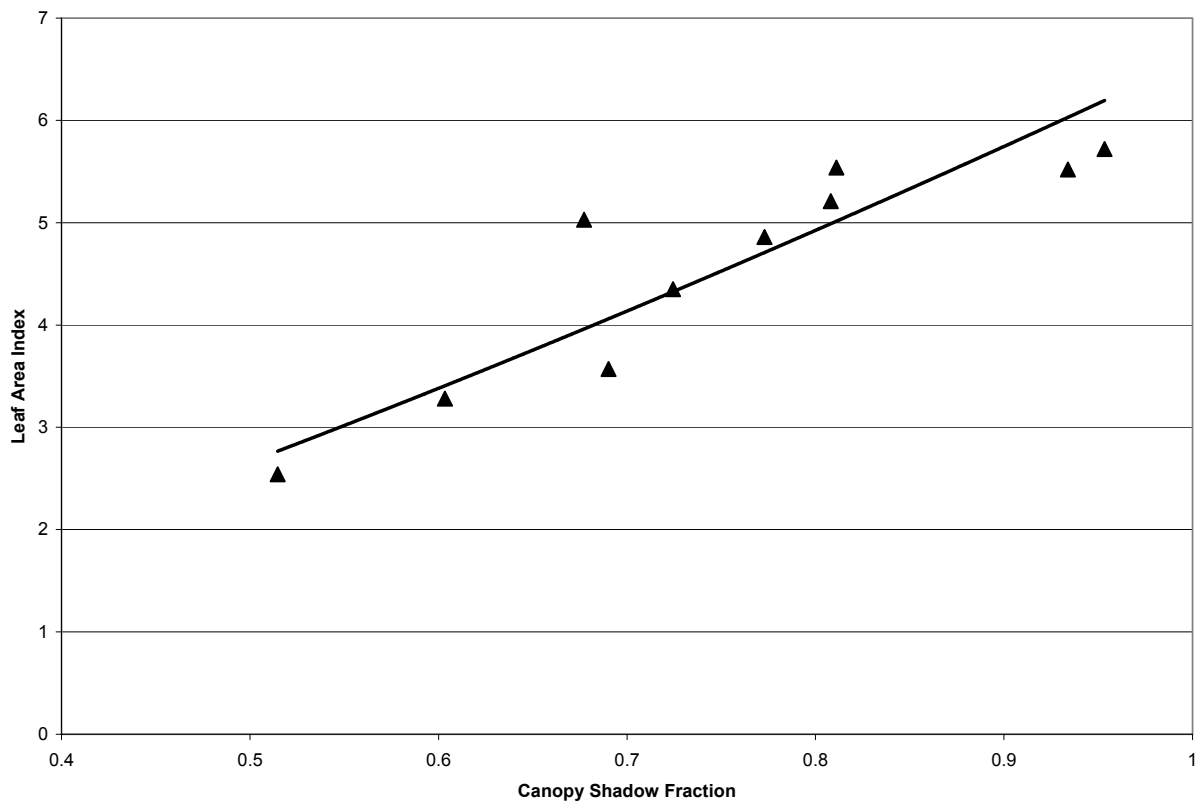
Figure 5.21: Graph of LAI versus Shadow Fraction for Needleleaf Vegetation Using Background Spectra Derived from *In-Situ* Spectroradiometer Measurements
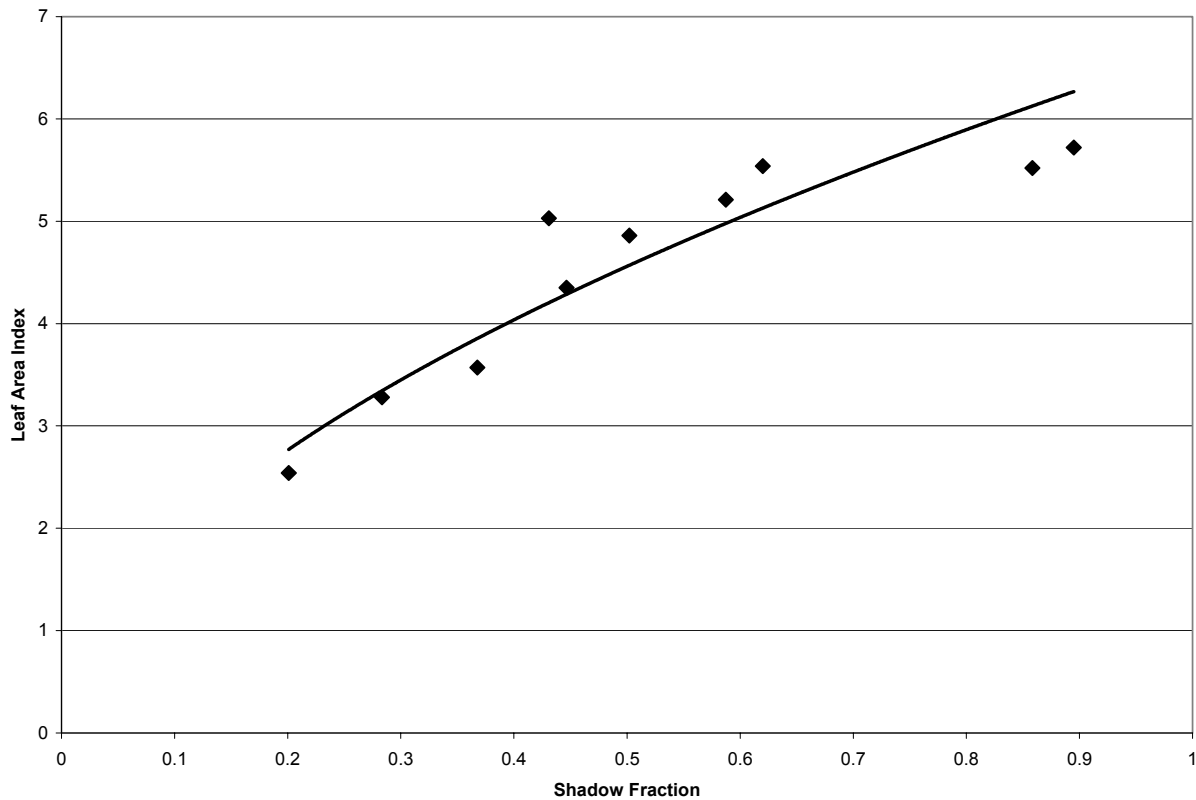
Figure 5.22: Graph of LAI versus Shadow Fraction for Needleleaf Vegetation Using Image-Derived Background Spectra

5.2.2 Broadleaf Vegetation

For broadleaf canopies the relationship derived between *in-situ* LAI measurements and the shadow fraction computed using linear spectral mixture is extremely weak, barely exceeding that of complete randomness. In contrast to the needleleaf case, the employment of the background spectra derived from the image resulted in a stronger relationship with LAI than did the application of the background spectra derived from *in-situ* measurement. Power relationships again exhibit an increased capability to accurately model LAI over more traditional linear relationships in a broadleaf canopy as demonstrated in Table 5.4.

Table 5.4: Coefficients of Determination Determined from Regression of LAI against Shadow Fraction for Broadleaf Vegetation

Background Spectra Derivation Type	Linear Relationship	Coefficient of Determination of Linear Relationship	Power Relationship	Coefficient of Determination of Power Relationship
Spectroradiometer	$LAI = 0.049SF + 2.67$	0.00	$LAI = 2.72SF^{0.014}$	0.00
Image	$LAI = 0.37SF + 2.58$	0.02	$LAI = 2.96SF^{0.079}$	0.08
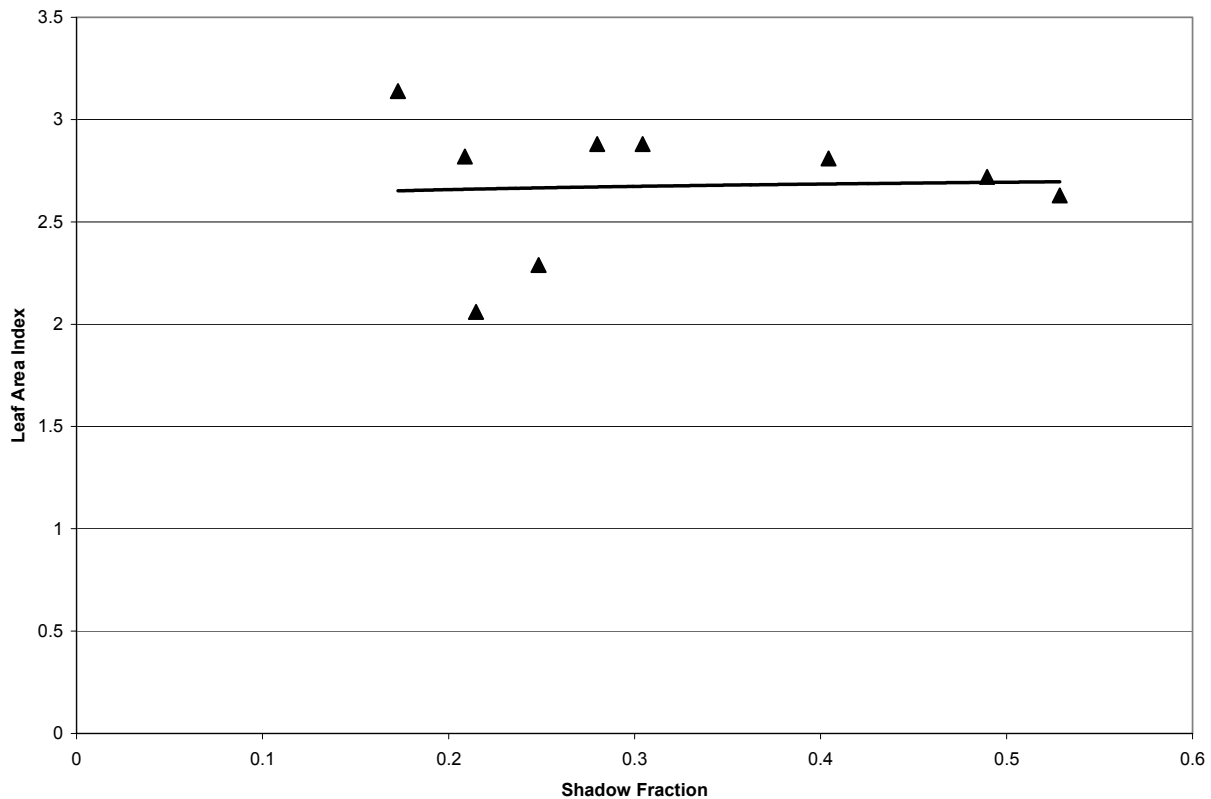
Figure 5.23: Graph of LAI versus Shadow Fraction for Broadleaf Vegetation Using Background Spectra Derived from *In-Situ* Spectroradiometer Measurements
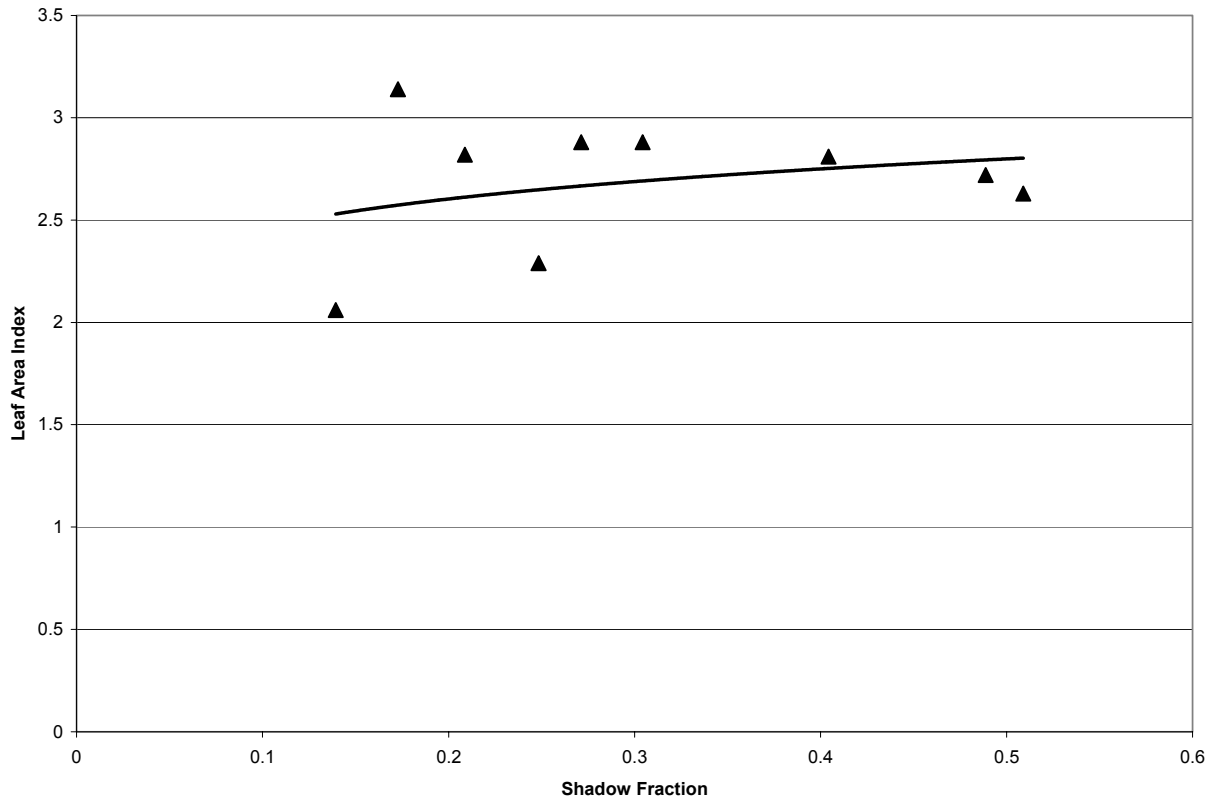
Figure 5.24: Graph of LAI versus Shadow Fraction for Broadleaf Vegetation Using Image-Derived Background Spectra

5.3 Independent Investigations

5.3.1 Scale Factor Method

To compute the normalized scale factor (NSF) the product of the middle-infrared and the red factor was divided by the near-infrared factor in the broadleaf case and multiplied by this factor in the case of needleleaf vegetation. This change in methodology is performed due to the differences in the observed relationships between LAI and near-infrared reflectance for needleleaf and broadleaf vegetation at this particular study site.

After an area-weighted mean of the overall scale factor is computed for each plot, a regression against *in-situ* LAI measurements is performed.

The results of the application of the normalized scaling algorithm are presented in Figures 5.25 through 5.28 and Table 5.5.

Table 5.5: Regression Relationships Determined between *In-Situ* measurements of LAI and Scale Factor for Various Vegetation Types

Scale Factor Formula	Derived Power Relationship	Coefficient of Determination	Vegetation Type
$NSF = (F_{RED})(F_{NIR})(F_{MIR})$	$LAI = 7.06NSF^{0.46}$	0.74	Needleleaf
$NSF = (F_{RED})(F_{MIR})$	$LAI = 6.99NSF^{0.64}$	0.69	Needleleaf
$NSF = \dfrac{(F_{RED})(F_{MIR})}{F_{NIR}}$	$LAI = 2.45NSF^{0.14}$	0.59	Broadleaf
$NSF = (F_{RED})(F_{MIR})$	$LAI = 3.24NSF^{0.27}$	0.54	Broadleaf
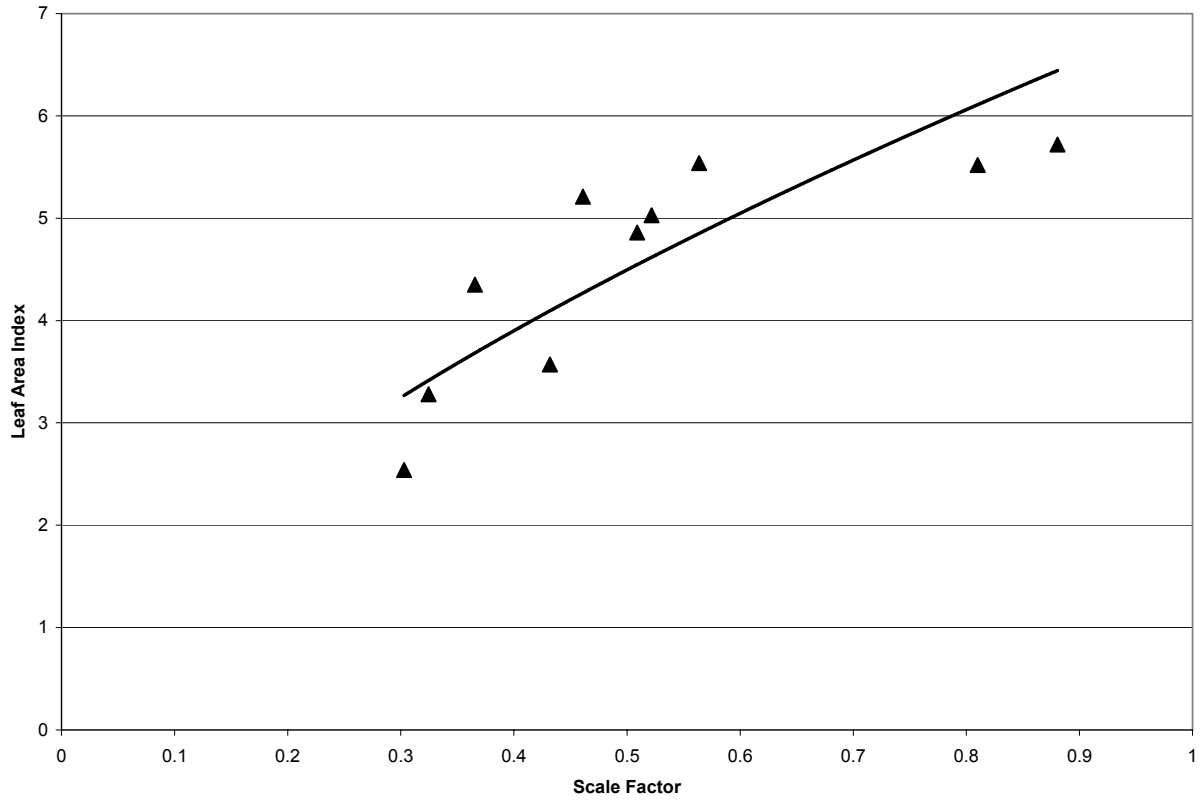
Figure 5.25: Graph of LAI Against Scale Factor Determined Using Red and Middle-Infrared Channels for Needleleaf Vegetation
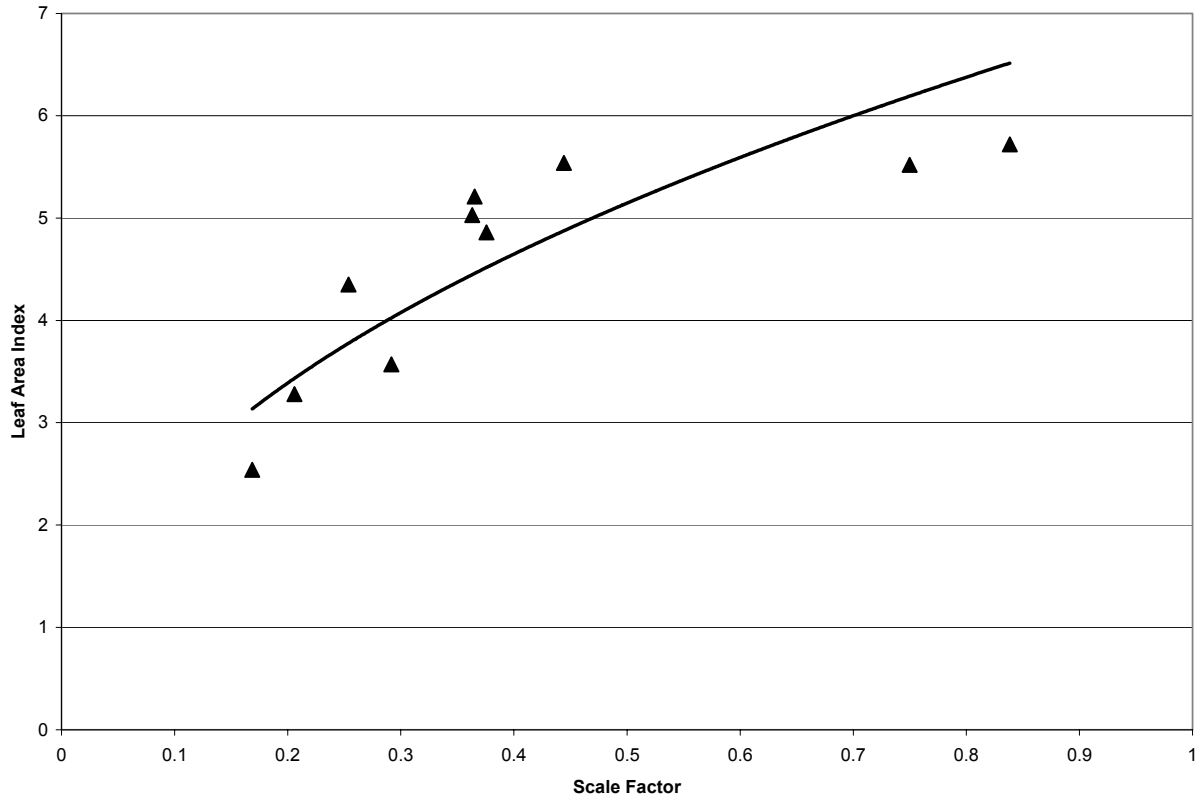
Figure 5.26: Graph of LAI Against Scale Factor Determined Using Red, Near-Infrared and Middle-Infrared Channels for Needleleaf Vegetation
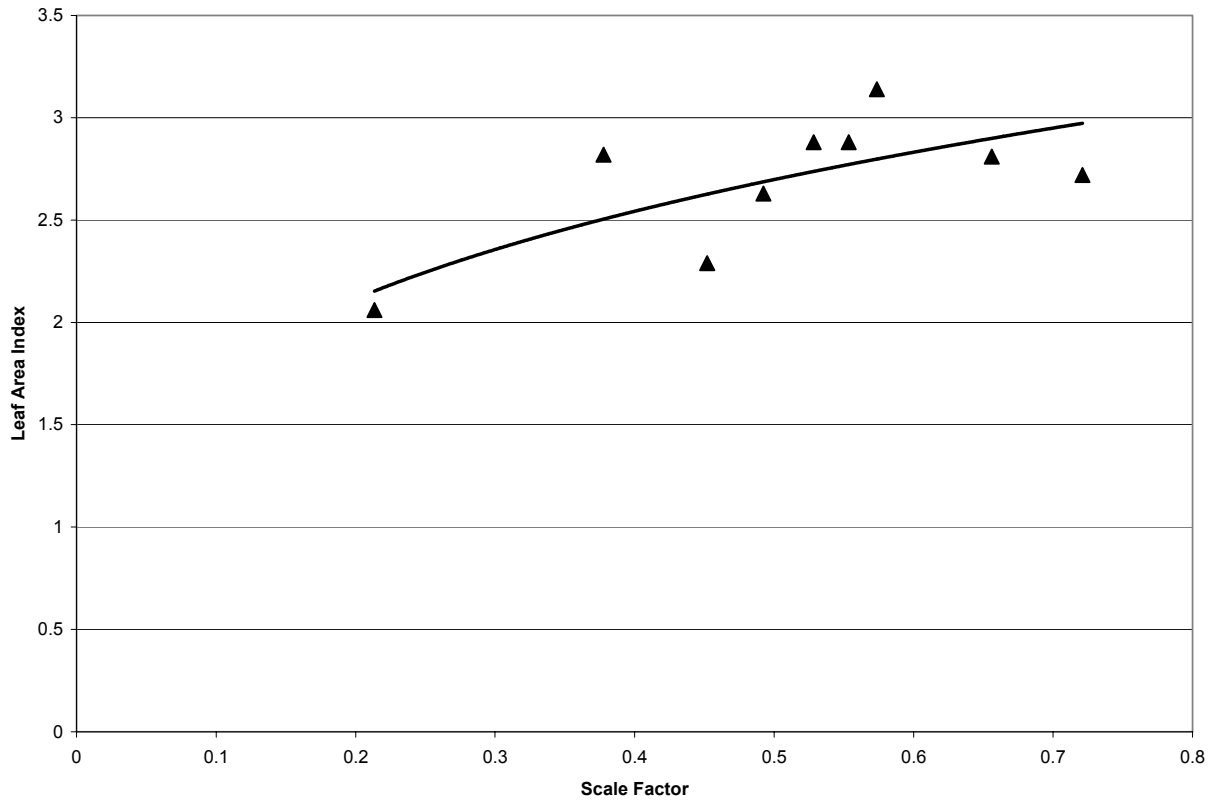
Figure 5.27: Graph of LAI Against Scale Factor Determined Using Red and Middle-Infrared Channels for Broadleaf Vegetation
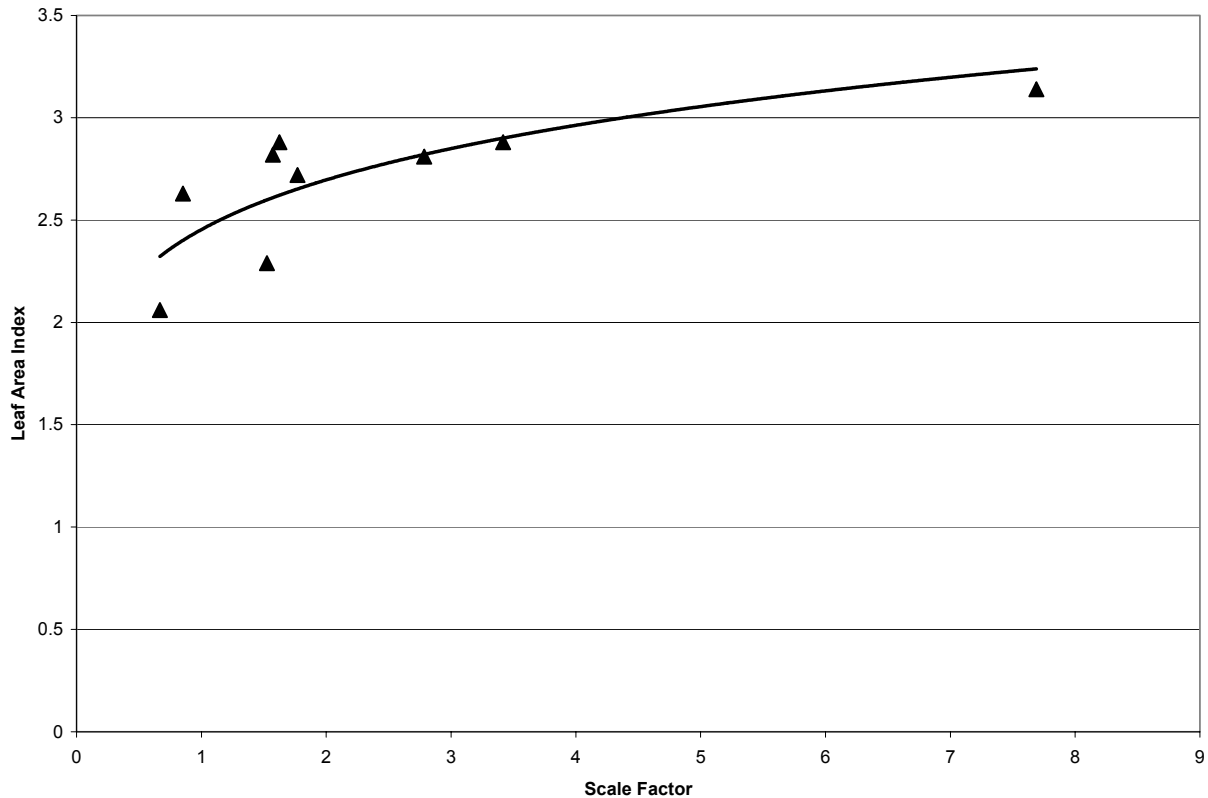
Figure 5.28: Graph of LAI Against Scale Factor Index Determined Using Red, Near-Infrared and Middle-Infrared Channels for Broadleaf Vegetation

It is evident from these results that the scaling technique exhibits slightly inferior performance when compared to the parameters which most robustly model LAI. However, the results derived from the scale factor technique are still a considerable improvement over the results obtained using the unadjusted vegetation indices. It should also be noted that it may be advantageous to use the two band scaling factor versus the three band scaling factor as the results do not degrade substantially. This decision might be prudent based on the sensitivity of observed reflectance in the near-infrared channel to the influence of the background spectra, particularly in the case of needleleaf vegetation.

5.3.2 Normalized Distance

The results obtained from applying the normalized distance method are presented in Table 5.6 and Figures 5.29 through 5.32.

Table 5.6: Regression Relationships Determined between *In-Situ* measurements of LAI and Normalized Distance for Various Vegetation Types

Normalized Distance Formula	Derived Relationship	Coefficient of Determination	Vegetation Type
$ND = \dfrac{\sqrt{\left(1 - F_{RED}\right)^2 + \left(1 - F_{NIR}\right)^2 + \left(1 - F_{MIR}\right)^2}}{\sqrt{3}}$	$LAI = 6.29e^{-3.30ND^2}$	0.86	Needleleaf
$ND = \dfrac{\sqrt{\left(1 - F_{RED}\right)^2 + \left(1 - F_{MIR}\right)^2}}{\sqrt{2}}$	$LAI = 6.32e^{-3.35ND^2}$	0.79	Needleleaf
$ND = \dfrac{\sqrt{\left(1 - F_{RED}\right)^2 + \left(F_{NIR}\right)^2 + \left(1 - F_{MIR}\right)^2}}{\sqrt{3}}$	$LAI = 3.28e^{-1.53ND^2}$	0.65	Broadleaf
$ND = \dfrac{\sqrt{\left(1 - F_{RED}\right)^2 + \left(1 - F_{MIR}\right)^2}}{\sqrt{2}}$	$LAI = 3.00e^{-1.06ND^2}$	0.58	Broadleaf
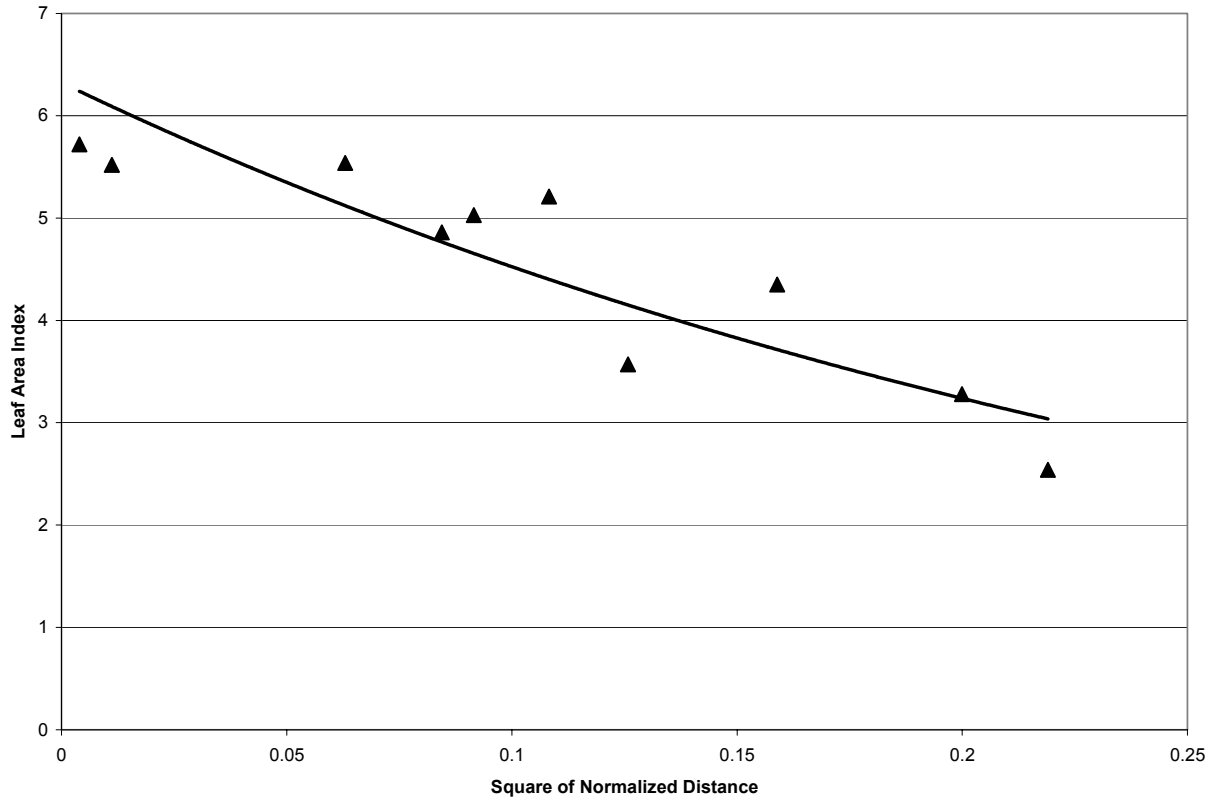
Figure 5.29: Graph of LAI Against the Square of Normalized Distance Determined Using Red and Middle-Infrared Channels for Needleleaf Vegetation
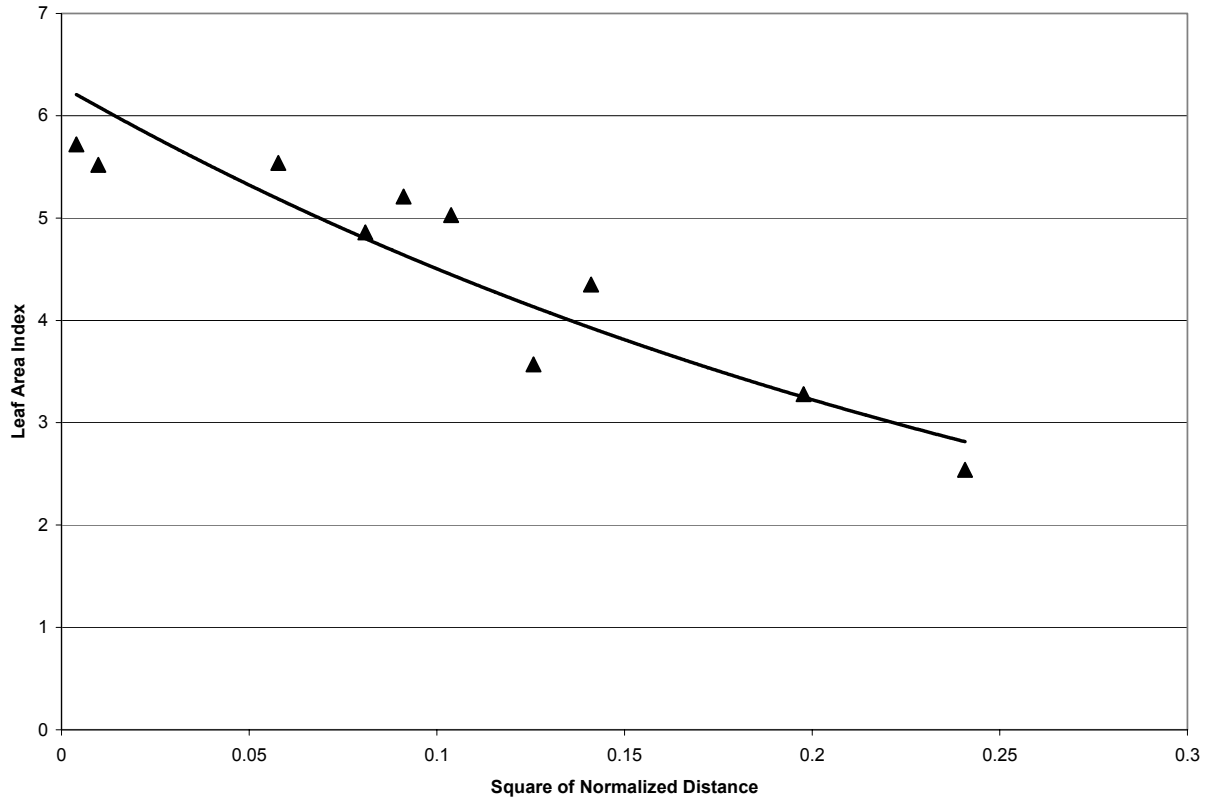
Figure 5.30: Graph of LAI Against the Square of Normalized Distance Determined Using Red, Near-Infrared and Middle-Infrared Channels for Needleleaf Vegetation
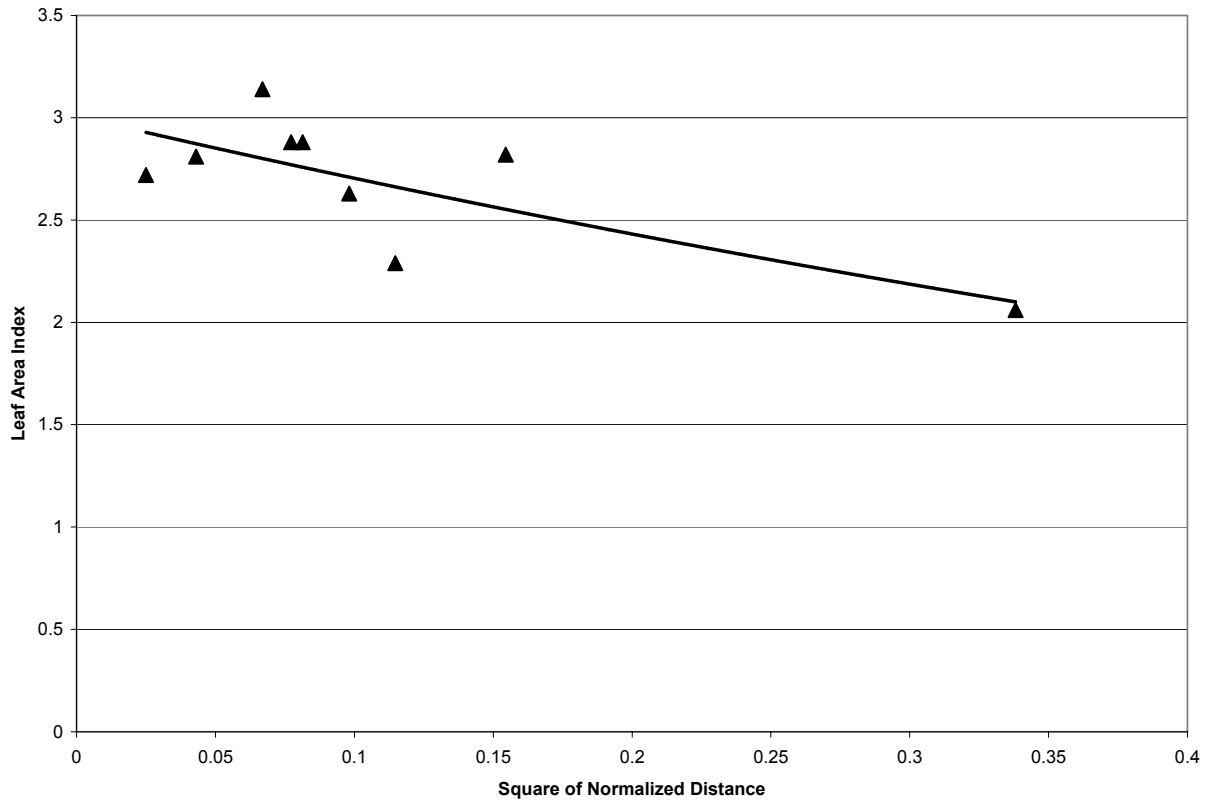
Figure 5.31: Graph of LAI Against the Square of Normalized Distance Determined Using Red and Middle-Infrared Channels for Broadleaf Vegetation
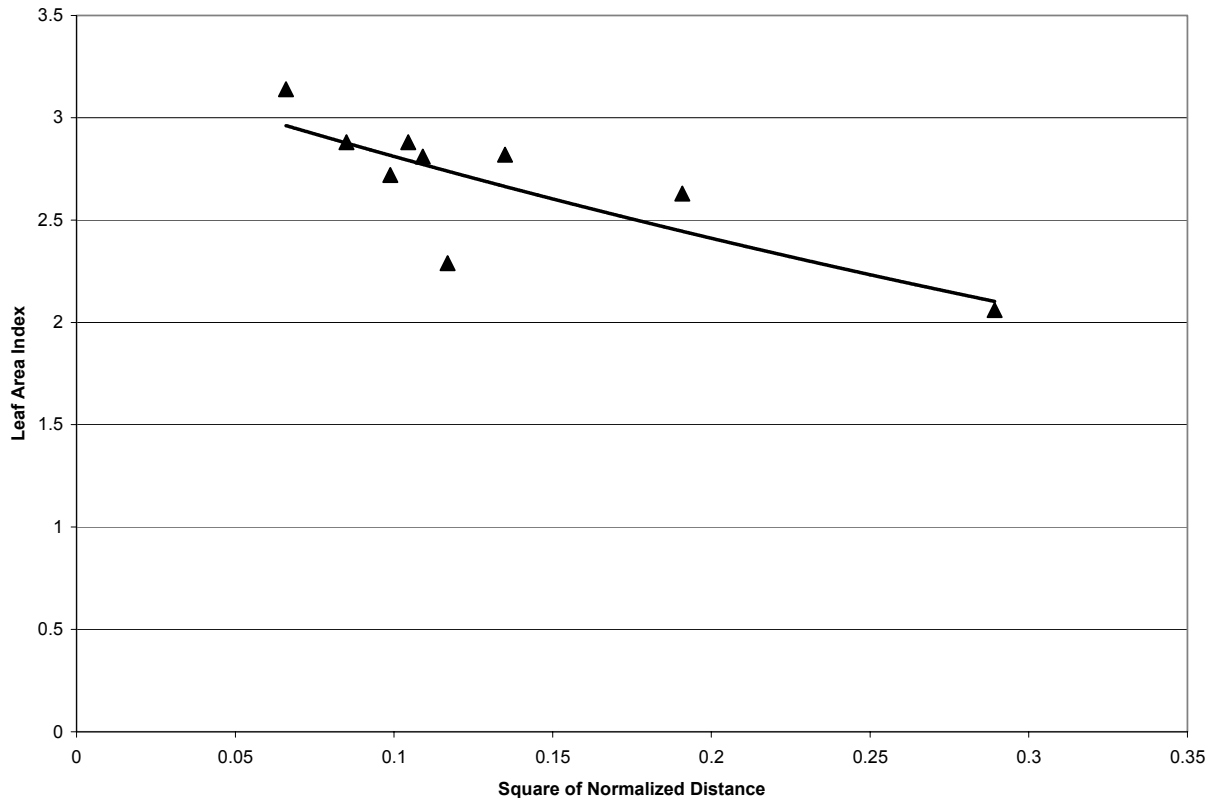
Figure 5.32: Graph of LAI Against the Square of Normalized Distance Determined Using Red, Near-Infrared and Middle-Infrared Channels for Broadleaf Vegetation

It is evident from theses results that the Gaussian relationships derived between the normalized distances and the *in-situ* LAI measurements exhibit superior performance to any regression relationships derived in this study for both needleleaf and broadleaf vegetation. One advantage of the regression relationships derived using normalized distances is their inherently bounded nature over the range of input values for which they are defined, as well as the more realistic values which they exhibit over this entire range. Another advantage presented by this technique is the between the relationships derived using two and three channels, particularly for needleleaf vegetation, which may prove useful in situations where the reflectances in the near-infrared band are highly dependent on the influence of the background.

It is also evident that the incorporation of additional spectral information is beneficial, as evidenced for both needleleaf and broadleaf vegetation, where the superior performance of normalized distances for three spectral bands is compared with those derived using two spectral

bands. However, the normalized distances derived using two spectral bands exhibit superior modeling performance for LAI as compared to other input modeling parameters derived using two spectral bands except for the moisture stress index in the broadleaf case. This generally superior performance in the special case where two spectral channels are used is evidence of the overall robustness of the normalized distance technique in LAI modeling for needleleaf and broadleaf vegetation. It should be noted in the needleleaf case that the two spectral channel normalized distance model may be preferred in areas where the background effects are not well characterized.

6 Sensitivity Analysis

To determine the relevance and suitability of the LAI estimation models developed in the previous section, given the typical errors associated with them, several simulations are conducted.

The first simulation involves testing the sensitivity of the model derivation process to errors in spatial location. This analysis is composed of two distinct approaches. The first approach employs a simulation of a uniform spatial shift in each of the cardinal directions and then computes the input parameter upon which models are then derived. The variability and quality of the models are then compared to the initial models. The second approach implements a spatial statistical analysis to determine the magnitude and distance over which modeling parameters are spatially correlated. These two approaches allow us to conclude whether the derived models are valid and whether the contribution of errors in spatial location to errors in the models is significant.

The simulations employ the remote estimation algorithms for LAI in an application for which these values are required as input parameters with certain levels of accuracy. The first of these simulations is a Monte Carlo simulation which examines the magnitude of the difference between the known and estimated LAI, given the known errors of the remote estimation model and randomly generated surfaces.

6.1 Sensitivity Analysis for Location Accuracy

6.1.1 Spatial Error Analysis

To determine the sensitivity of the derived models to errors in location, due to errors in plot location or in georeferencing, a shift of each plot by one pixel in octants, which start and finish due north, is modeled. The input modeling parameters are recomputed to find the area-weighted mean value for the shifted plot location.

To decrease the computational volume of the regression combinations by orders of magnitude, resampling is performed to determine estimates in each of the cardinal directions. This resampling is conducted by resampling the weighted means in each of the octant directions to each of the cardinal directions, as described in Table 6.1, to incorporate all of the information from the various octants.

Table 6.1: Resampling Equations from Octants into Cardinal Directions

Cardinal Direction	Formula
West	$\dfrac{VAL_{nw} + 2VAL_w + VAL_{sw}}{4}$
East	$\dfrac{VAL_{ne} + 2VAL_e + VAL_{se}}{4}$
North	$\dfrac{VAL_{nw} + 2VAL_n + VAL_{ne}}{4}$
South	$\dfrac{VAL_{se} + 2VAL_s + VAL_{sw}}{4}$

This resampling is justified, despite some data smoothing, quantified in the statistics of Tables 6.2 and 6.3, due to the size of the remaining statistical sample and the strength of conclusions derived from the analysis.

Table 6.2: Statistics of Input Parameters with Modeled Location Errors in Broadleaf Sites

Input Parameter	Mean Plot Standard Deviation Octant	Maximum Plot Standard Deviation Octant	Mean Plot Standard Deviation Cardinal	Maximum Plot Standard Deviation Cardinal
NDVI	0.018	0.036	0.014	0.027
Simple Ratio	0.321	0.562	0.255	0.422
Modified NDVI	0.058	0.032	0.045	0.047
Modified Simple Ratio	0.469	1.030	0.377	0.849
Moisture Stress Index	0.023	0.042	0.018	0.036
Shadow Fraction	0.112	0.174	0.087	0.145

Table 6.3: Statistics of Input Parameters with Modeled Location Errors in Needleleaf Sites

Input Parameter	Mean Plot Standard Deviation Octant	Maximum Plot Standard Deviation Octant	Mean Plot Standard Deviation Cardinal	Maximum Plot Standard Deviation Cardinal
NDVI	0.0129	0.0221	0.0104	0.0180
Simple Ratio	0.135	0.256	0.109	0.209
Modified NDVI	0.0294	0.0812	0.0241	0.0660
Modified Simple Ratio	0.172	0.492	0.140	0.398
Moisture Stress Index	0.0147	0.0271	0.0118	0.0229
Shadow Fraction	0.068	0.134	0.055	0.111

It is evident from the results that the resampling decreases the standard deviation in all cases, in the majority of cases by approximately 20%. The effect of this resampling is an increase in the modeling accuracy due to noise reduction and a greater proportion of accurate results due to the marked decrease, over 99% in all cases, in the number of samples. It should be noted that the plots with the highest standard deviations associated with the modeled location errors, were those surrounded or partially bounded by land cover distinct from the vegetation type. This is expected as the spectral properties in these boundary regions are the most variable due to their non-homogeneous composition and therefore have the potential to induce considerable error if they are mistakenly included in the modeling areas due to errors in spatial location. Comparisons between the initial results and the results with induced spatial error, determined by the coefficients of determination, are presented in Tables 6.4 and 6.5.

Table 6.4: Comparison of Initial Coefficient of Determination with Coefficients of Determination Derived with Induced Location Error for Broadleaf Canopies

Input Parameter	Mean Coefficient of Determination Linear Model	Standard Deviation Coefficient of Determination Linear Model	Initial Coefficient of Determination Linear Model	Mean Coefficient of Determination Power Model	Standard Deviation Coefficient of Determination Power Model	Initial Coefficient of Determination Power Model
NDVI	0.27	0.22	0.46	0.26	0.23	0.43
Simple Ratio	0.27	0.21	0.43	0.25	0.22	0.38
Modified NDVI	0.37	0.18	0.51	0.43	0.21	0.59
Modified Simple Ratio	0.41	0.19	0.56	0.45	0.22	0.63
Moisture Stress Index	0.43	0.19	0.63	0.43	0.19	0.64
Shadow Fraction	0.64	0.14	0.81	0.64	0.16	0.83

Table 6.5: Comparison of Initial Coefficients of Determination with Coefficients of Determination Derived with Induced Location Error for Needleleaf Canopies

Input Parameter	Mean Coefficient of Determinat-ion Linear Model	Standard Deviation Coefficient of Determinat-ion Linear Model	Initial Coefficient of Determinat i-on Linear Model	Mean Coefficient of Determinat-ion Power Model	Standard Deviation Coefficient of Determinat-ion Power Model	Initial Coefficient of Determinat -ion Power Model
NDVI	0.53	0.13	0.54	0.51	0.13	0.54
Simple Ratio	0.53	0.15	0.56	0.51	0.15	0.56
Modified NDVI	0.62	0.14	0.77	0.61	0.17	0.79
Modified Simple Ratio	0.59	0.15	0.76	0.59	0.18	0.77
Moisture Stress Index	0.18	0.15	0.27	0.16	0.14	0.22
Shadow Fraction	0.04	0.06	0.00	0.06	0.08	0.00

These statistics demonstrate the validity of the initial models as they outperform the majority of the models derived with enhanced data in a reduced sample size. The initial modeling is even more marked in its success for the modeling parameters which exhibited the highest initial correlation with measured values of LAI, exceeding one standard deviation above the mean in some cases. The validity of this solution is indicative that the measurements plots are located with sufficient accuracy to derive meaningful results and that the known positioning errors did not substantially

compromise the initial estimation models. It also demonstrates how errors in the spatial location of plots can degrade the measurements from which models are derived, even after the effects of the reduced sample size and measurement smoothing have been considered.

6.1.2 Spatial Statistics

Although the previous section demonstrates that errors in the location of plots influence the quality of the models derived, an explicit relationship between the magnitude of the spatial location error and the magnitude of its effect on the models has not been derived. This effect is landscape specific and therefore relationships between modeling parameters should be examined for the extent of spatial correlation they exhibit to determine the relative impact of location error on the derived models.

6.1.2.1 Broadleaf Vegetation

The values of Moran's I determined for each of the modeling parameters over various lag distances are presented graphically in Figures 6.1 through 6.7.
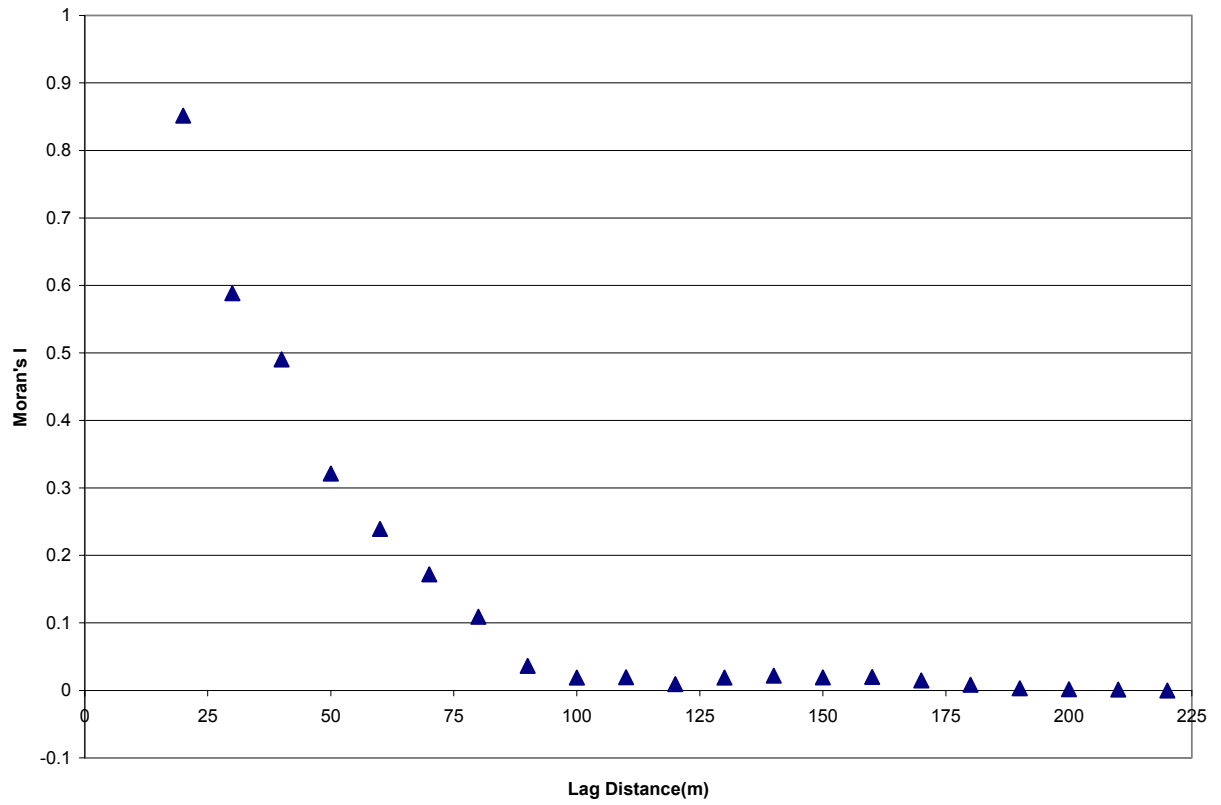
Figure 6.1: Plot of Moran's I versus Lag Distance for Normalized Difference Vegetation Index for Broadleaf Vegetation
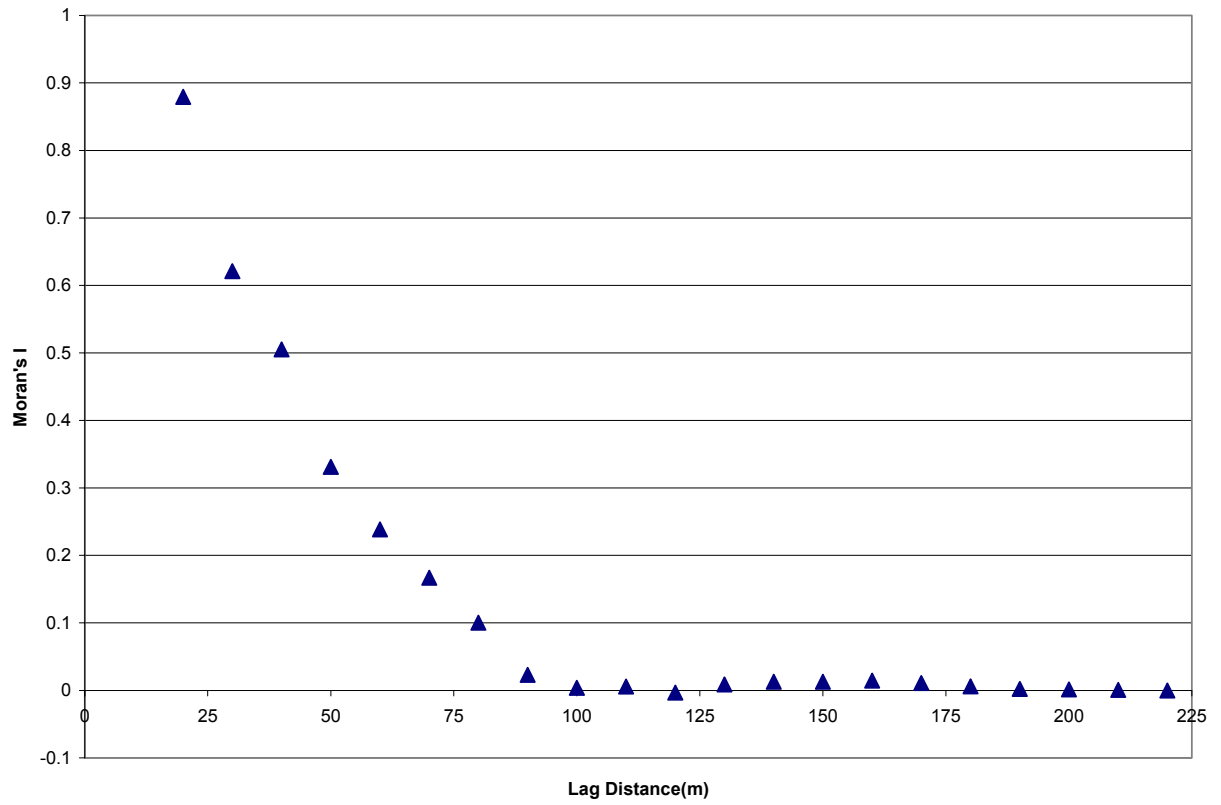
Figure 6.2: Plot of Moran's I versus Lag Distance for Simple Ratio for Broadleaf Vegetation
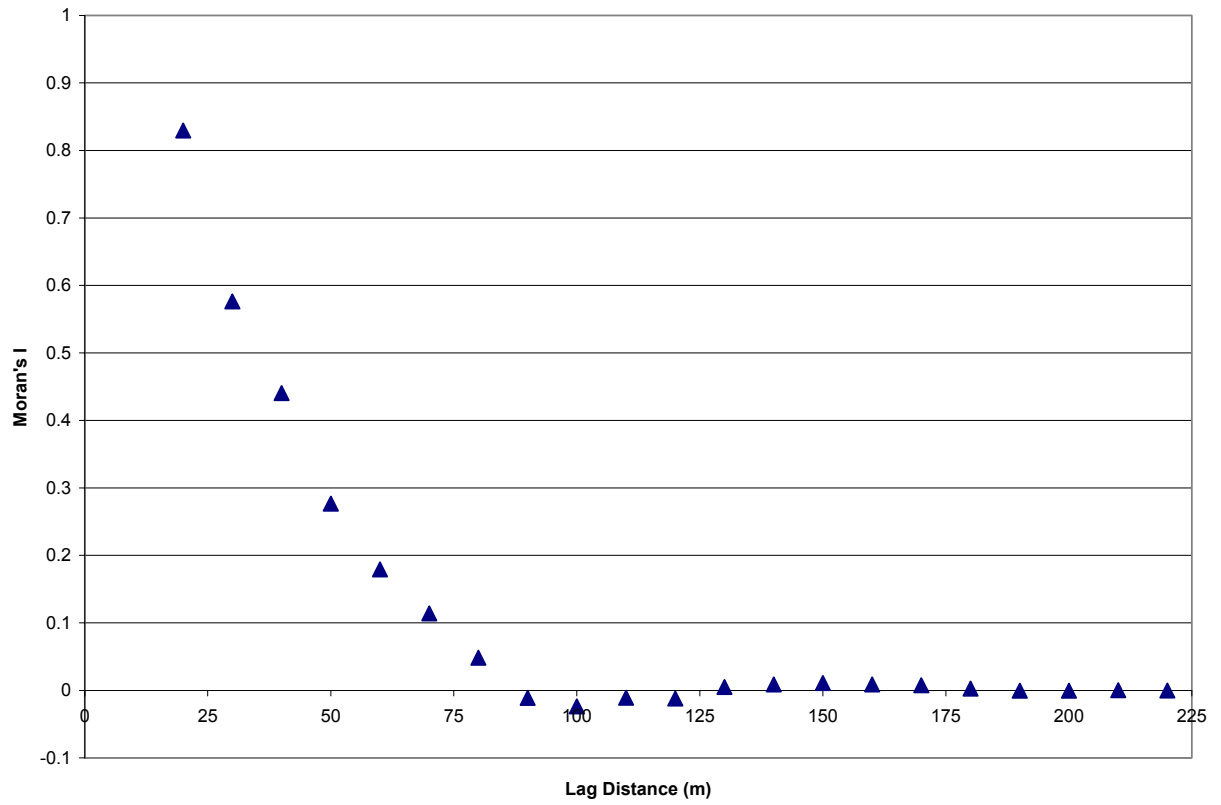
Figure 6.3: Plot of Moran's I versus Lag Distance for Moisture Stress Index for Broadleaf Vegetation
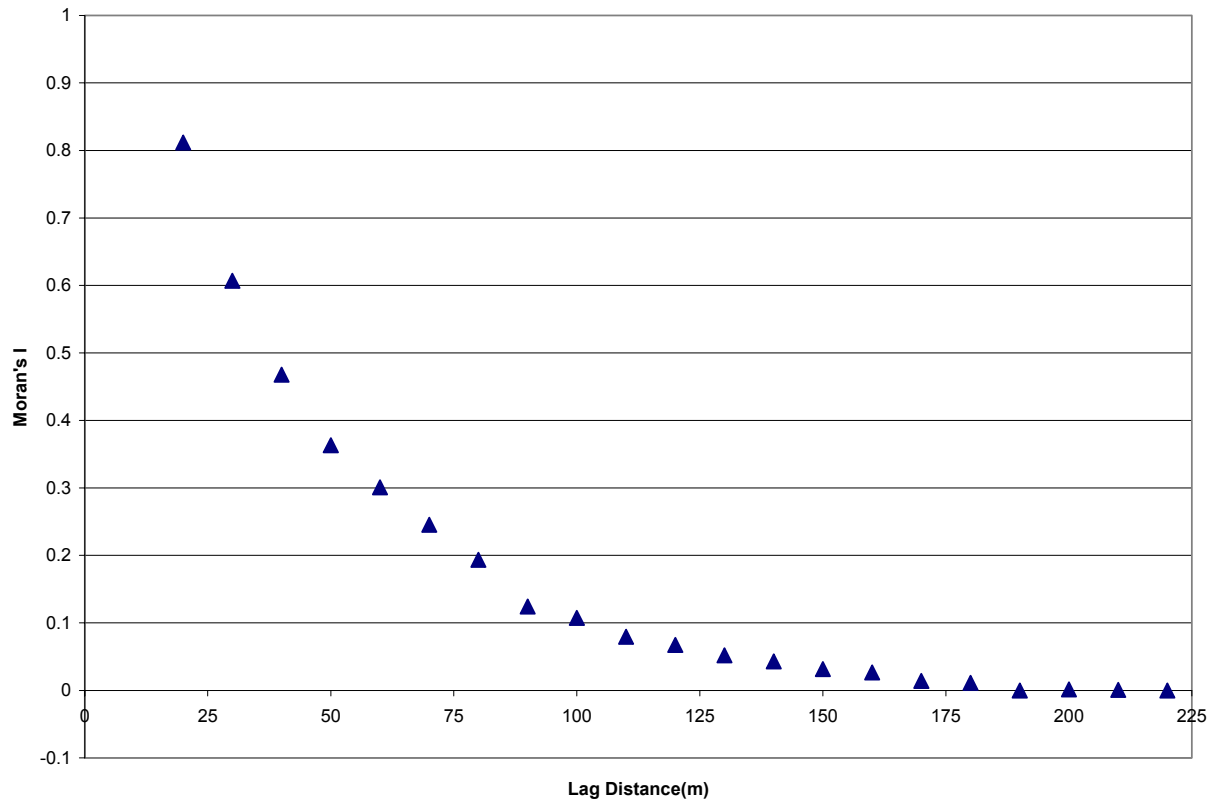
Figure 6.4: Plot of Moran's I versus Lag Distance for Modified Normalized Difference Vegetation Index for Broadleaf Vegetation
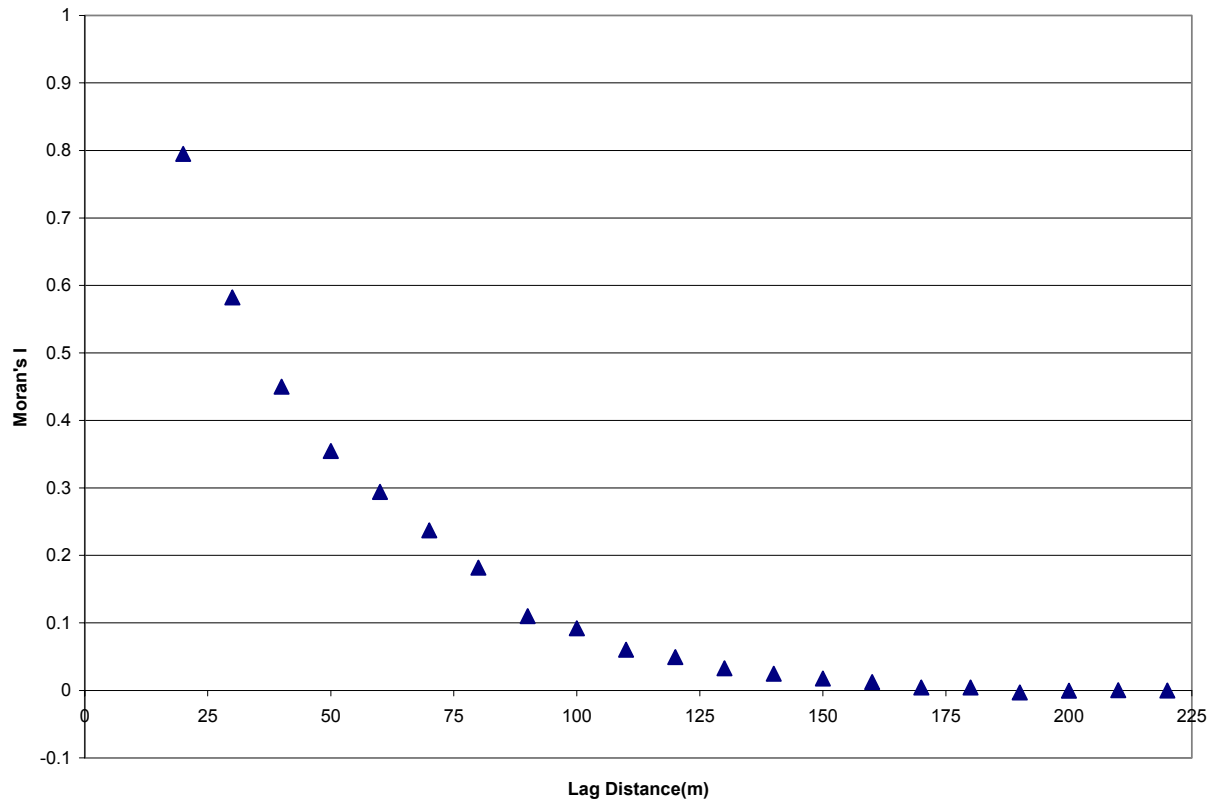
Figure 6.5: Plot of Moran's I versus Lag Distance for Modified Simple Ratio for Broadleaf Vegetation
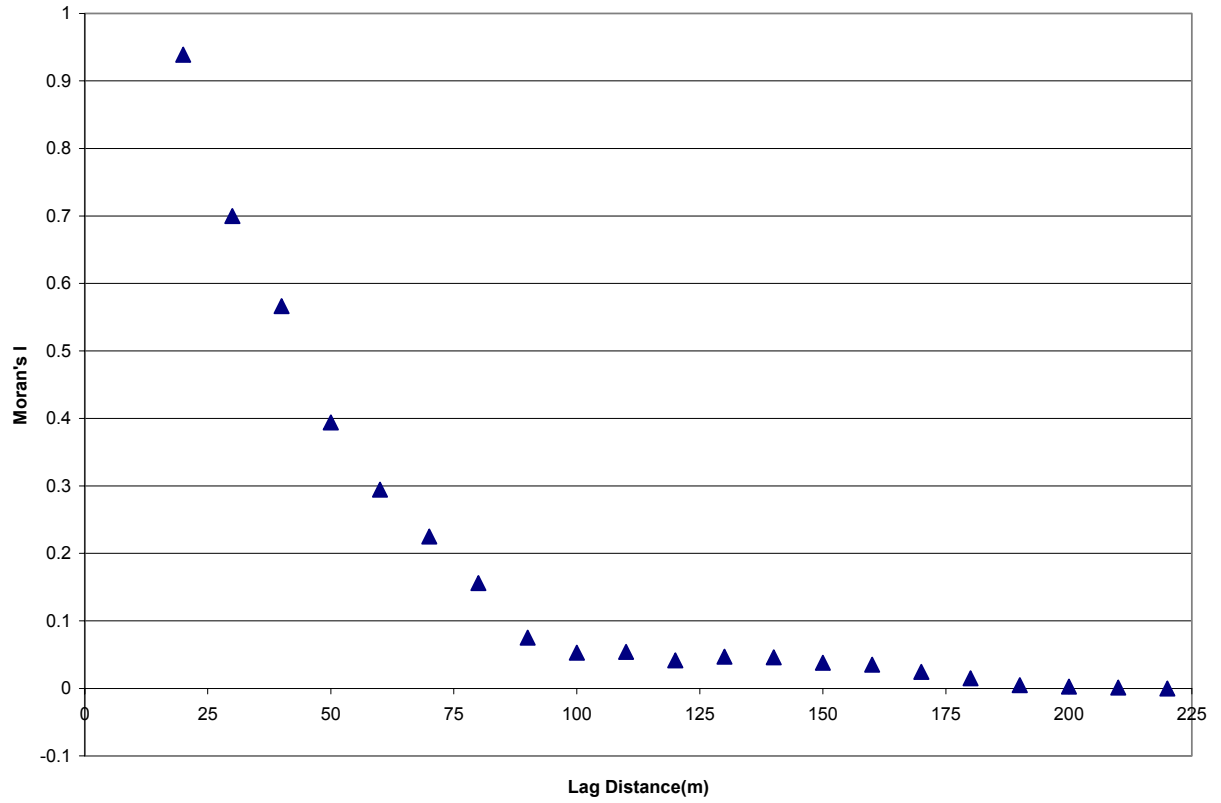
Figure 6.6: Plot of Moran's I versus Lag Distance for Shadow Fraction for Broadleaf Vegetation
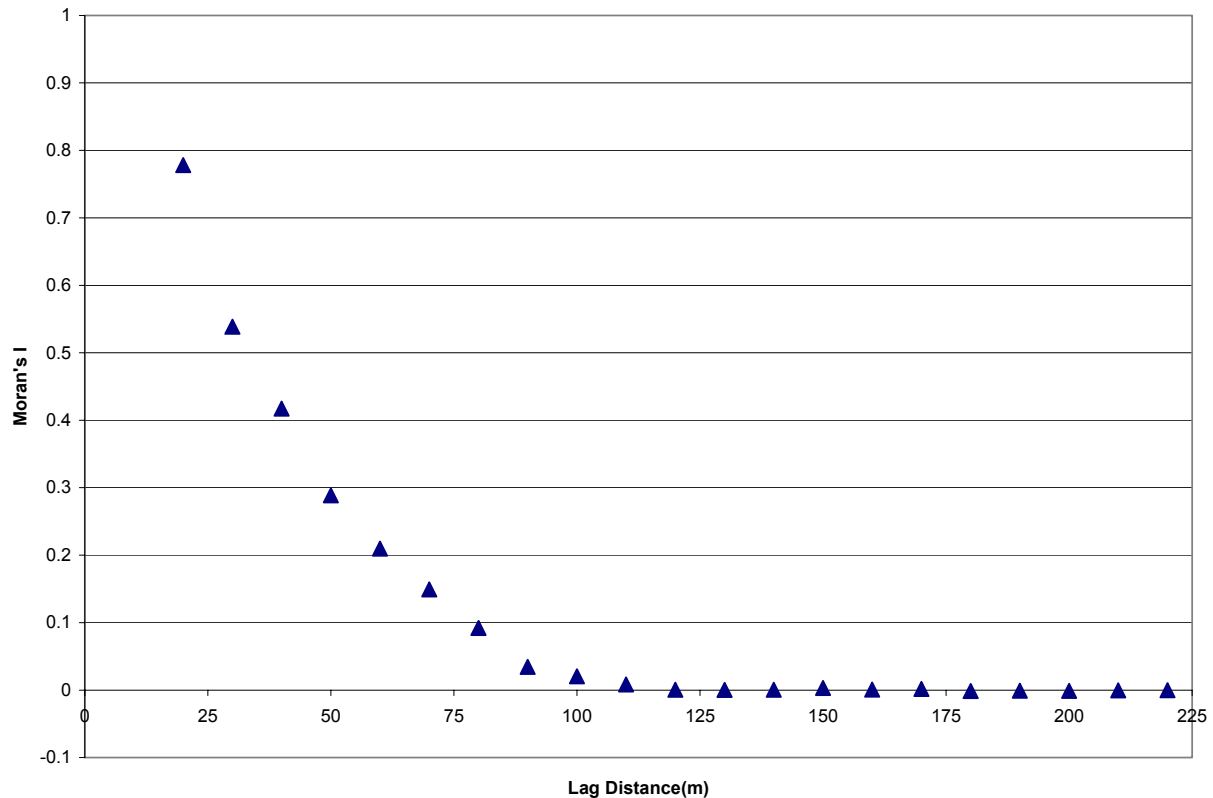
Figure 6.7: Plot of Moran's I versus Lag Distance for Normalized Distance Computed Using Middle Infrared, Near Infrared and Red Channels for Broadleaf Vegetation

One feature evident from the figures is the inverse relationship that Moran's I values maintain with lag distance. Substantial positive correlation is observed over shorter distances, as demonstrated by the values of the nearest spatial neighbors which range from a minimum of 0.78 for the normalized distance to a maximum of 0.94 for the canopy shadow fraction. Values of all the modeling parameters except the shadow fraction become weakly correlated at distances of 50m. The approximate range of the relationships varies from a value of 100m for the normalized difference vegetation index and the simple ratio to 190 m for the modified normalized difference vegetation index and the shadow fraction. Complete spatial randomness occurs within broadleaf patches at the range value for the observed relationship. Another interesting feature is the presence of negative Moran's I values in relation to some of the vegetation indices. Negative values of Moran's I typically suggest inter-event repulsion however the negative values are so close to zero that they are more likely due to a modeling artifact.

6.1.2.2 Needleleaf Vegetation

Moran's I values for each of the modeling parameters are also evaluated over a range of lag distances for needleleaf vegetation. The results are presented in Figures 6.8 through 6.14.
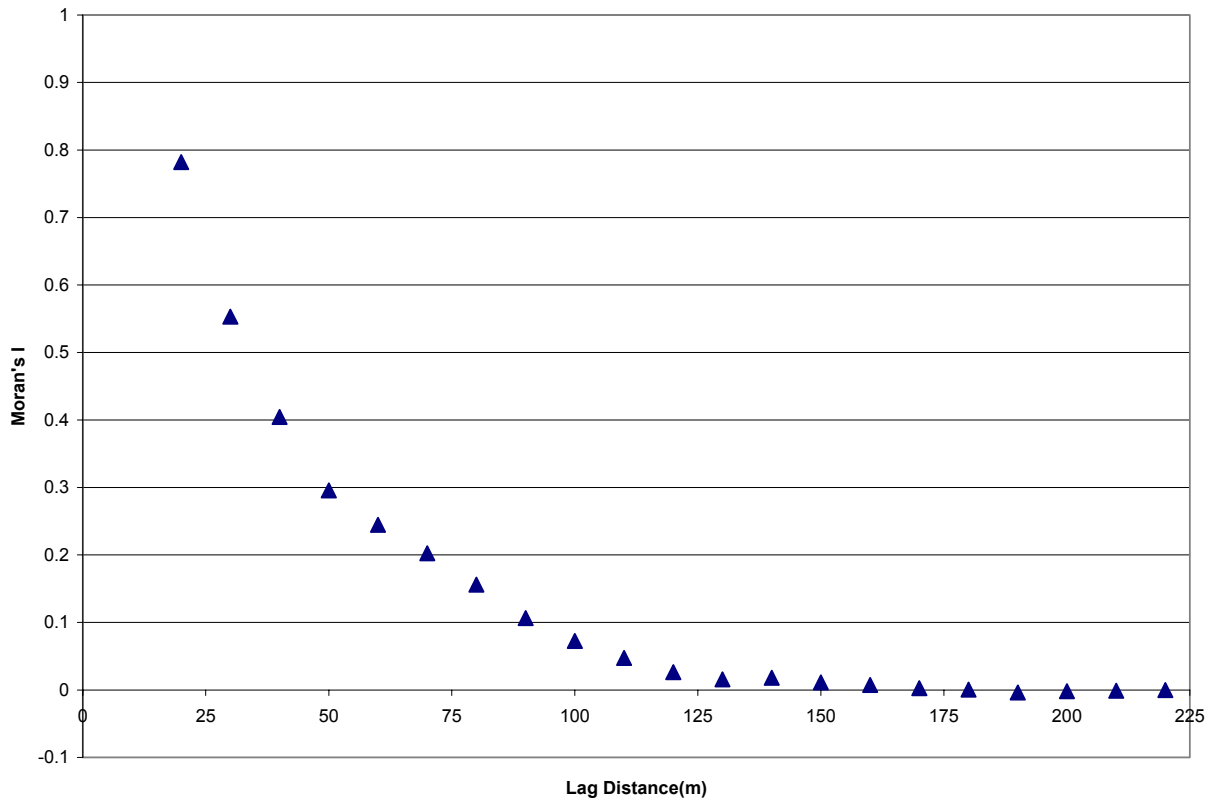
Figure 6.8: Plot of Moran's I versus Lag Distance for Normalized Difference Vegetation Index for Needleleaf Vegetation
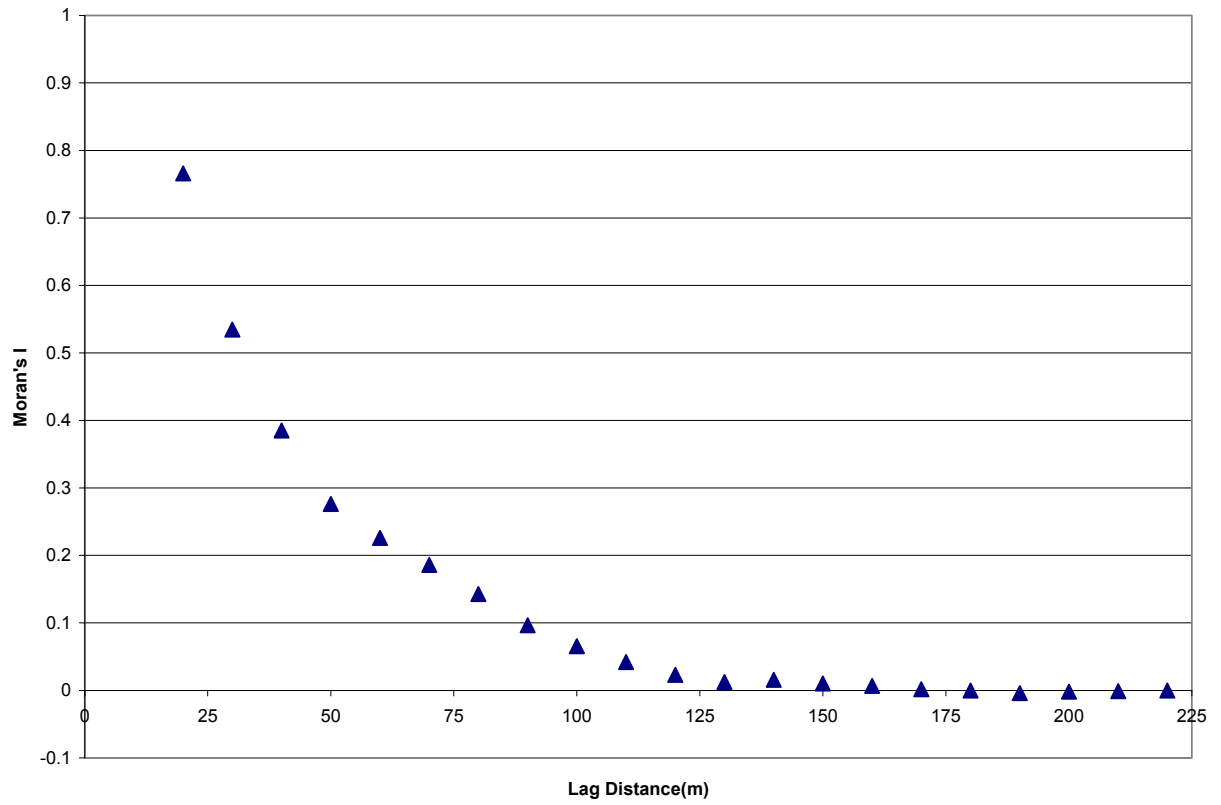
Figure 6.9: Plot of Moran's I versus Lag Distance for Simple Ratio for Needleleaf Vegetation
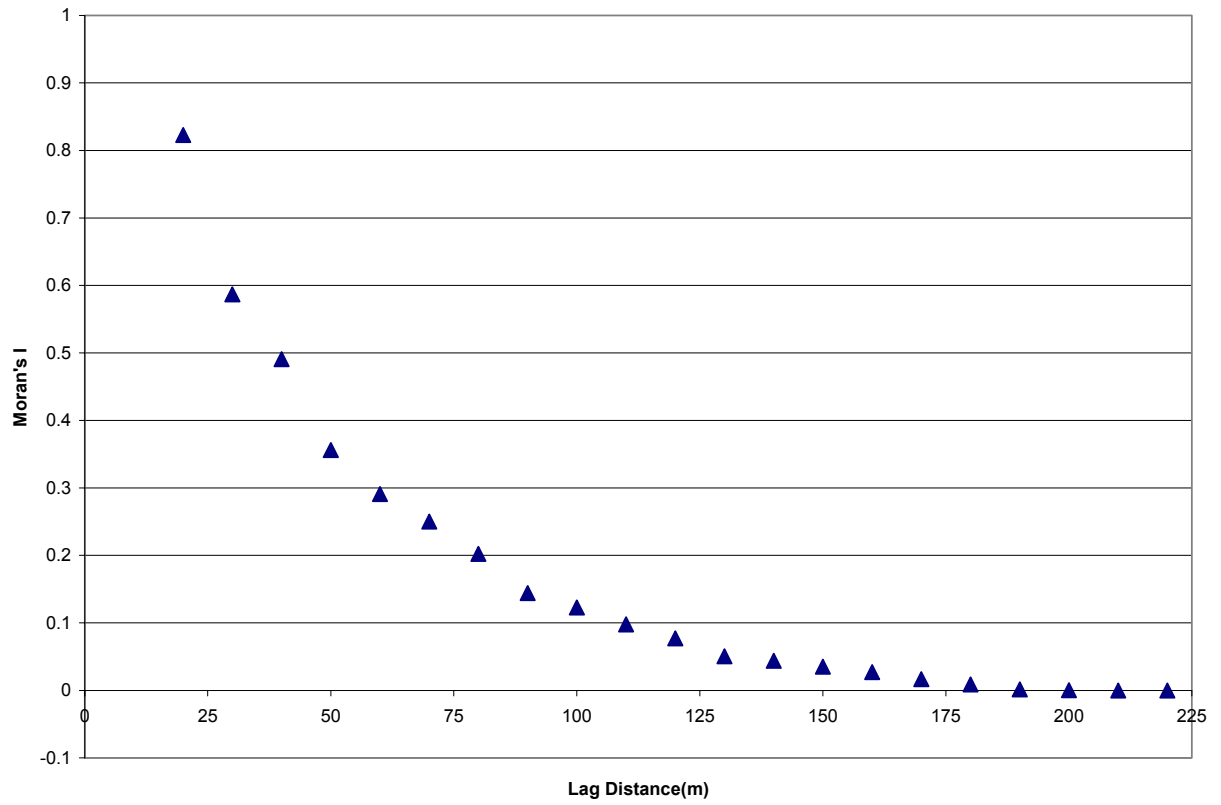
Figure 6.10: Plot of Moran's I versus Lag Distance for Moisture Stress Index for Needleleaf Vegetation
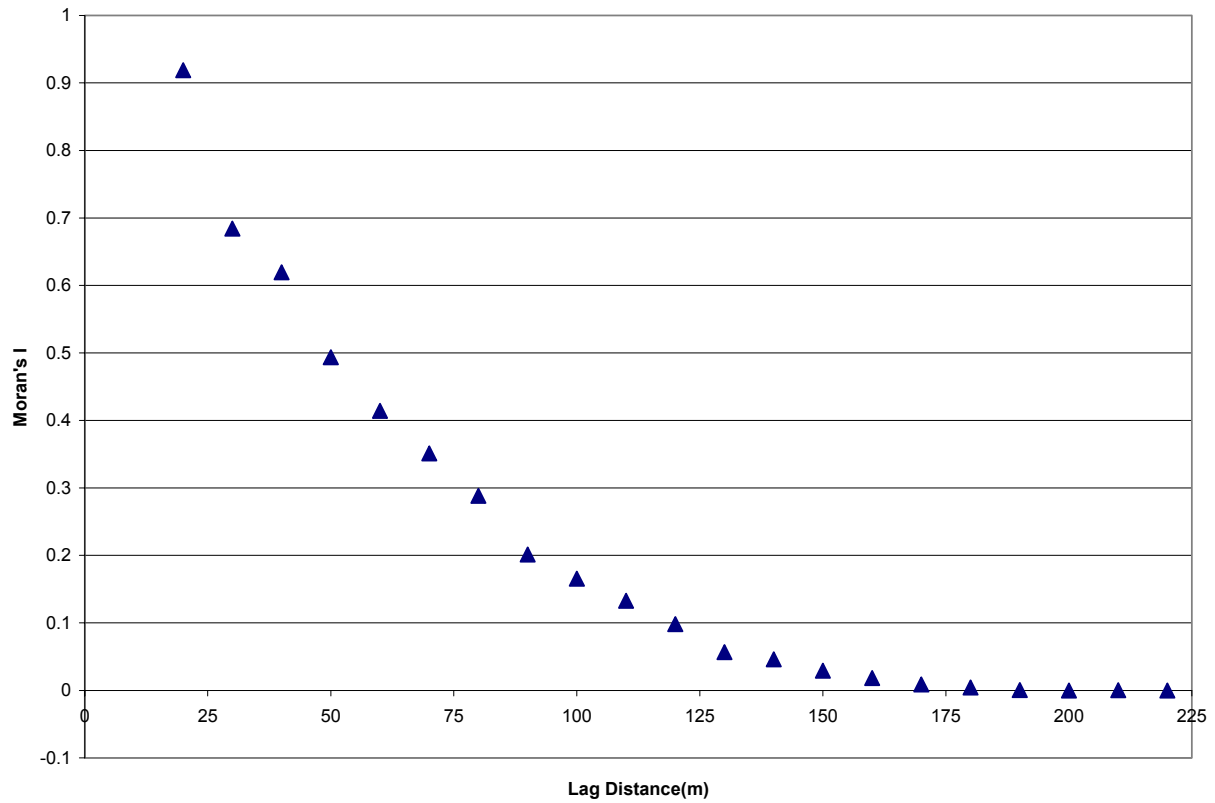
Figure 6.11: Plot of Moran's I versus Lag Distance for Modified Normalized Difference Vegetation Index for Needleleaf Vegetation
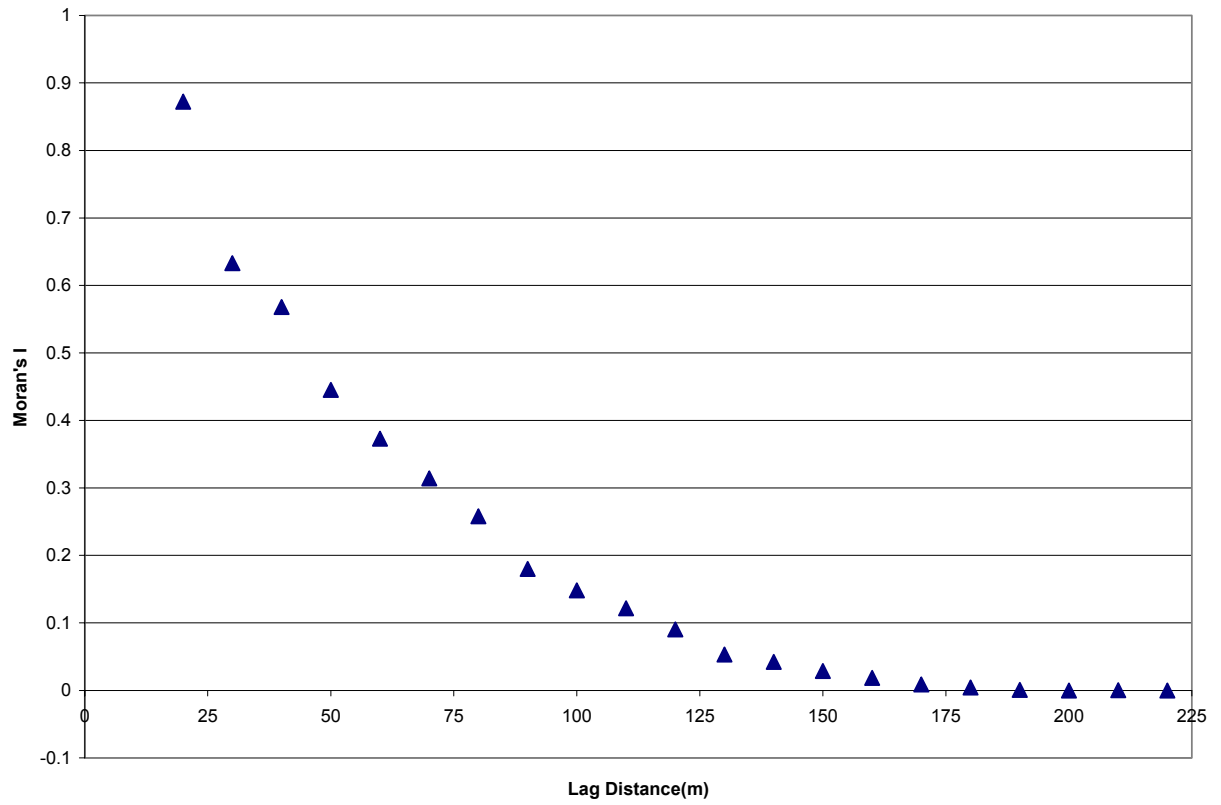
Figure 6.12: Plot of Moran's I versus Lag Distance for Modified Simple Ratio for Needleleaf Vegetation
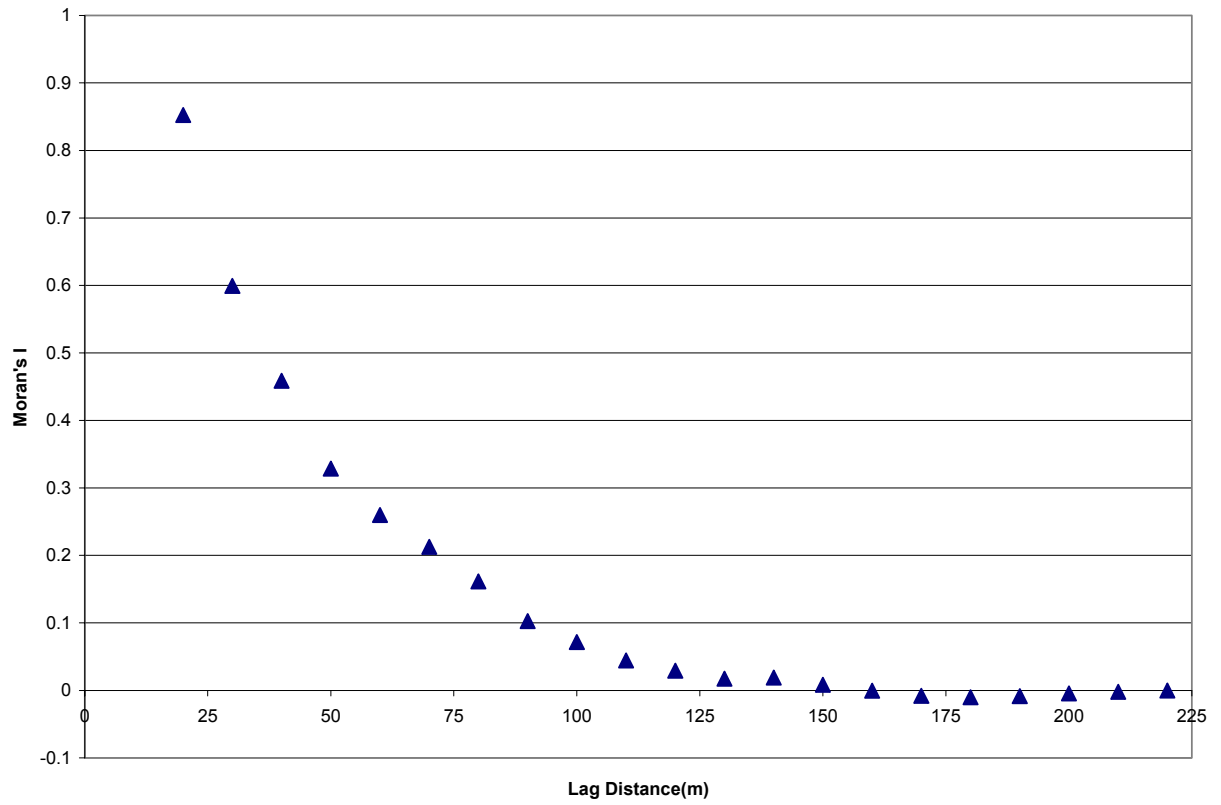
Figure 6.13: Plot of Moran's I versus Lag Distance for Shadow Fraction for Needleleaf Vegetation
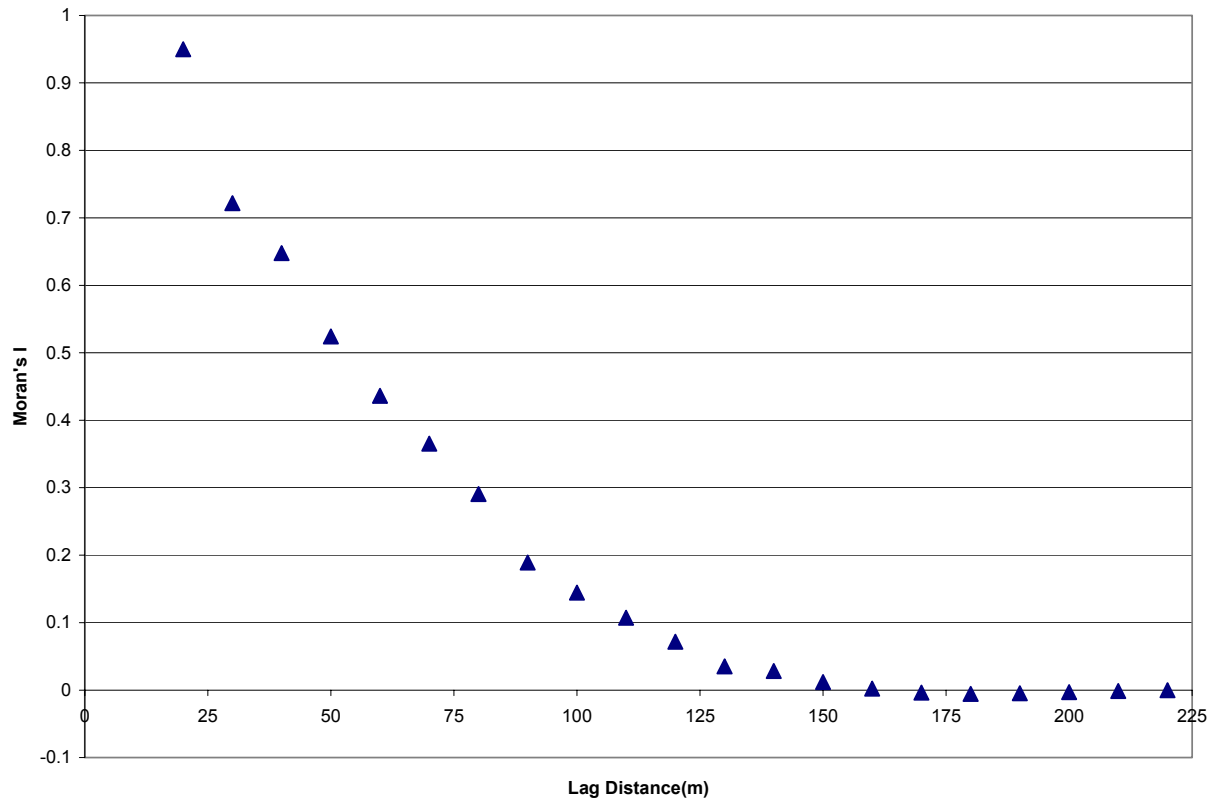
Figure 6.14: Plot of Moran's I versus Lag Distance for Normalized Distance Computed Using Middle Infrared, Near Infrared and Red Channels for Needleleaf Vegetation

As in the broadleaf case, Moran's I values for each modeling parameter evinced an inverse relationship with lag distance. The correlations at the shortest lag distance vary from a minimum of 0.77 for the simple ratio to a value of 0.95 for the normalized distance method. The range varies from a value of 130m for both the NDVI and the simple ratio to 190m for the modified versions of these indices. Complete spatial randomness is again achieved when the lag distance exceeds the range. Insubstantial negative values of Moran's I are again observed and are attributable to modeling artifacts.

6.1.2.3 Discussion of Spatial Statistical Analysis

The overall results generated from the analysis of the spatial statistics have implications in two areas, namely the impact of geo-referencing and plot location accuracy on the relationships

159

derived as well as characterizing the spatial correlation observed between modeling parameters and consequently on LAI estimates.

The results from the analysis of the spatial statistics confirm that the effects of errors in location are minimal. Given the typical accuracies associated with plot location, presented in Table 4.15, and geo-referencing, presented in section 4.3.2.1, the measurements determined by these relationships do not vary substantially enough to dramatically shift the relationships derived in Chapter 5. Additionally, given the known location of the plots in terms of their distance to trails and other easily-identifiable features it is apparent from the image that errors in the locations of plots are not substantial.

In terms of spatial autocorrelation, one result of interest is the evident difference in the spatial autocorrelation values evidenced for the normalized distance model between the needleleaf and broadleaf cases. In needleleaf vegetation the highest initial spatial correlation is observed between neighboring indices whereas for broadleaf vegetation the lowest initial spatial correlation is observed. Additionally, the needleleaf model exhibits a longer range, of approximately 50m. These differences are likely indicative of the varying degrees of similarity exhibited by forest structures of different type observed by remote sensing at this particular scale. This result is more compelling particularly given the robustness of the normalized distance model for modeling LAI in both needleleaf and broadleaf vegetation.

6.2 Monte Carlo Simulation

Monte Carlo simulation consists of multiple determinations of the difference in mean LAI between the known value for the randomly generated surface and that derived from an estimate with modeling precision identical to that of the derived models. There are two quantities of interest which are determined through the Monte Carlo simulation, namely the accuracy and precision of the model over a given landscape. The modeling accuracy is quantified through an examination of the difference in the means computed over a landscape with a given number of samples. The modeling precision is determined through an examination of the standard deviation of the errors of the differences of the actual and modeled LAI across a landscape.

There are three primary factors which largely determine the precision and accuracy that can be generated in a given situation. These factors are the number of samples, the variability of the landscape in terms of LAI and the quality of the initial model.

6.2.1 Number of Samples

It is evident from the Monte Carlo simulations that for constant landscape variability and uniform modeling there is a strong dependence of the overall modeling precision on the number of samples. The number of samples exhibits a direct relationship to the size of the region in question.

To demonstrate this effect, Monte Carlo simulations are performed with varying sample sizes, ranging from 100 to 1000 to demonstrate the effect of increasing sampling size on modeling precision. Two values of underlying variability are used, each of which was derived from the *in-situ* LAI measurements, to simulate each of the broadleaf and needleleaf cases.

These simulations produce the graphical results displayed in Figures 6.15 and 6.16.
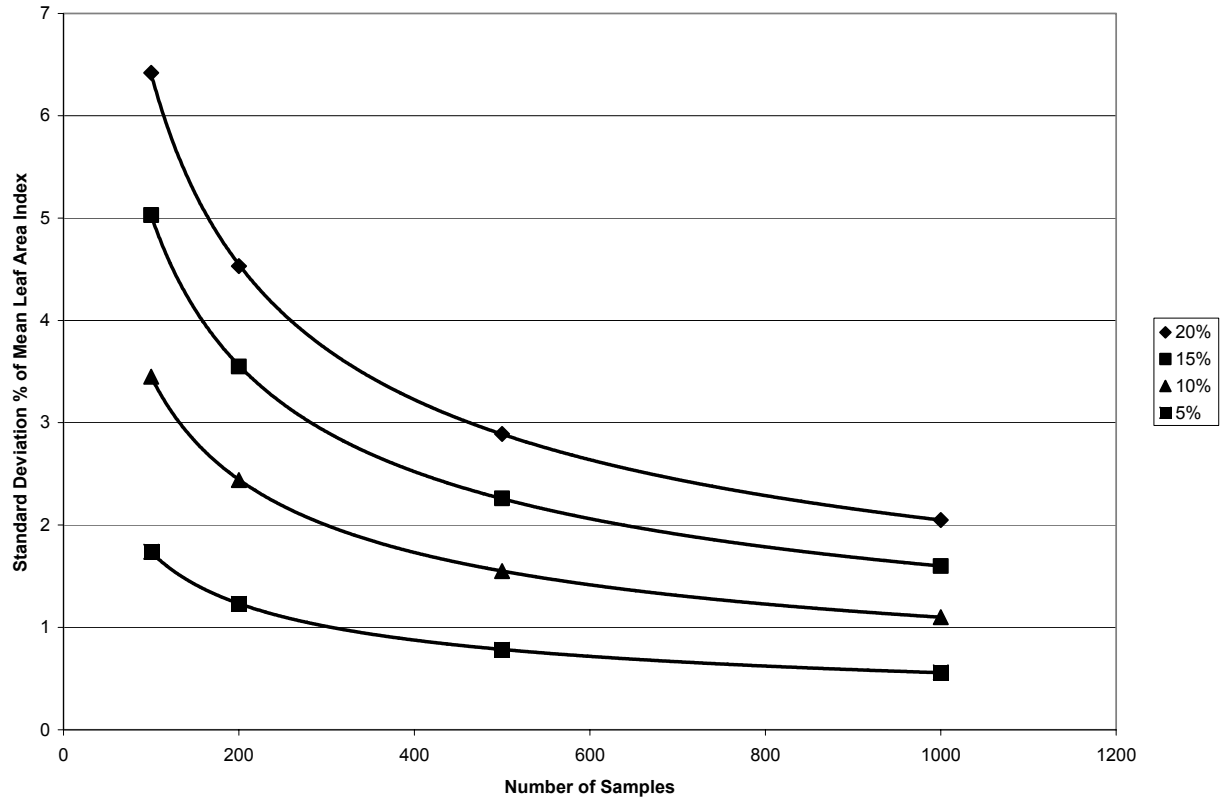
Figure 6.15: Typical Standard Deviation of Mean Differences in LAI Expressed as Percent of Mean Resulting from Monte Carlo Simulations with Varying Number of Samples for Broadleaf Vegetation with 50000 Iterations.
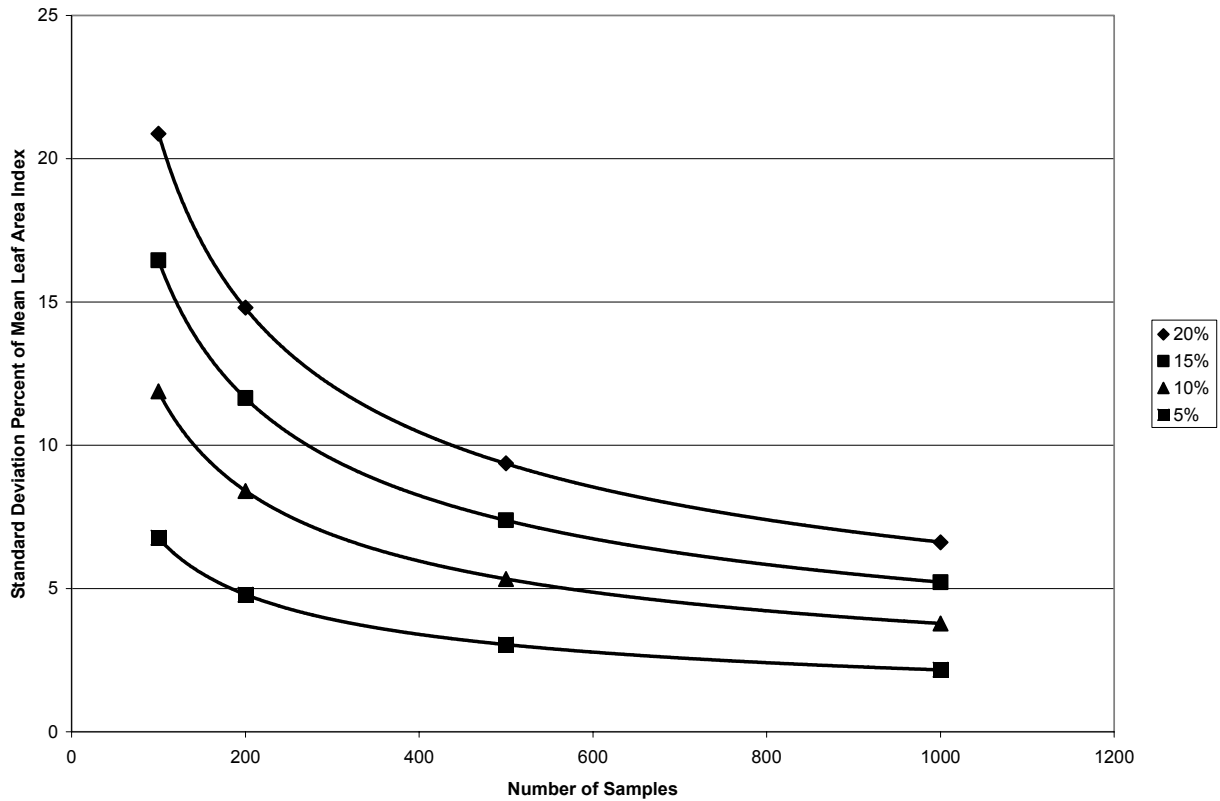
Figure 6.16: Typical Standard Deviation of Mean Differences in LAI Expressed as Percent of Mean Resulting from Monte Carlo Simulations with Varying Number of Samples for Needleleaf Vegetation with 50000 Iterations.

It is evident from Figures 6.15 and 6.16 that a well-defined power relationship exists between the number of samples and the standard deviation associated with the derivation of landscape level LAI estimates. This allows us to conclude that given the number of samples the component of the overall precision of the mean LAI determined by the sampling size can be estimated.

In contrast, modeling accuracy seems to be largely independent of sample size. This is evident from Figures 6.17 and 6.18.
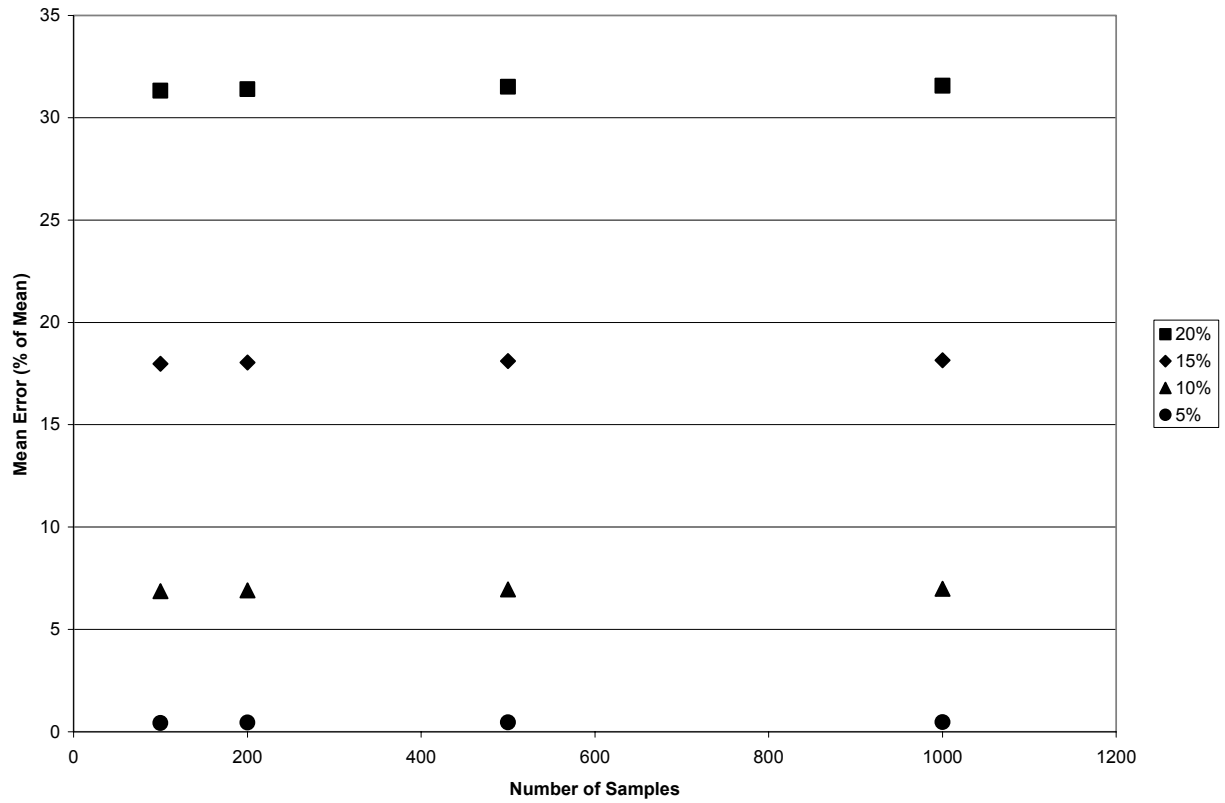
Figure 6.17: Mean Error of Mean Differences in LAI Expressed as Percent of Mean Resulting from Monte Carlo Simulations with Varying Number of Samples for Needleleaf Vegetation with 50000 Iterations.
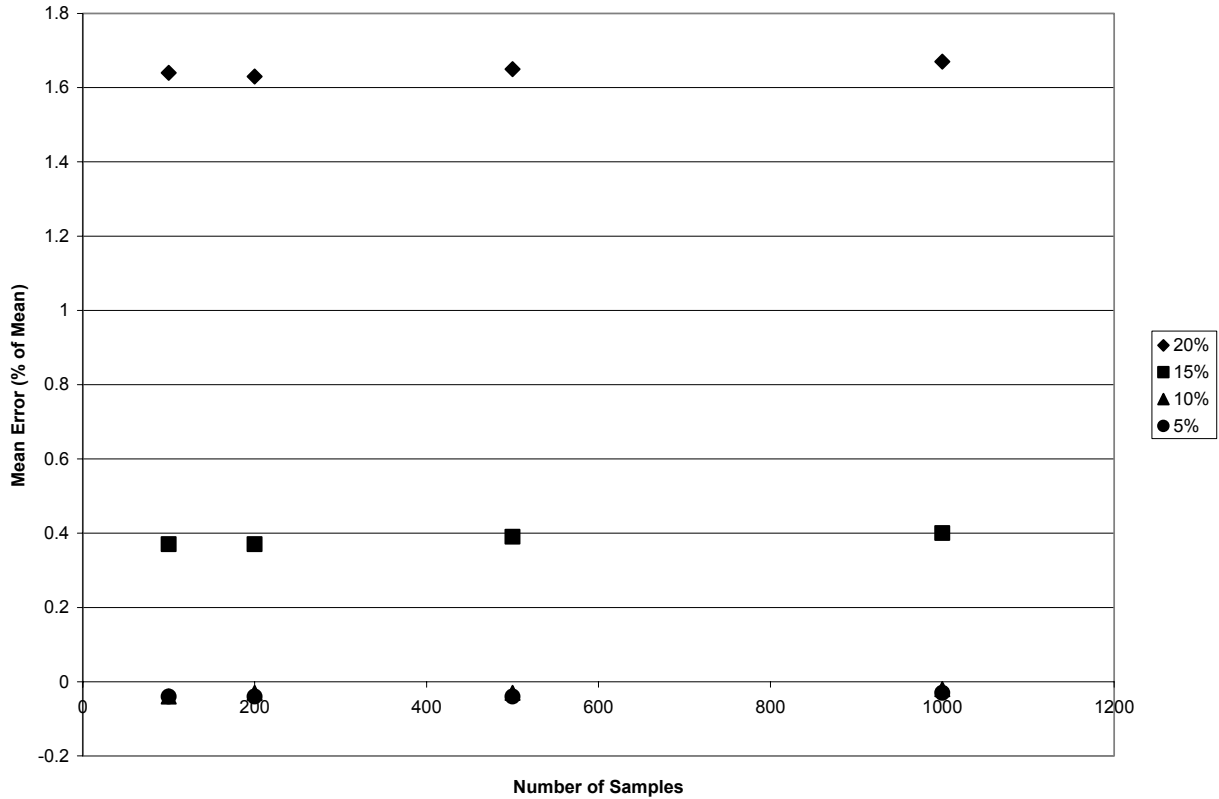
Figure 6.18: Mean Error of Mean Differences in LAI Expressed as Percent of Mean Resulting from Monte Carlo Simulations with Varying Number of Samples for Broadleaf Vegetation with 50000 Iterations.

The figures demonstrate that the mean accuracy is largely insensitive to variation in the number of samples. This permits the conclusion that the number of samples is an important quantity in determining the precision of the modeling results but is of little importance in the determination of the accuracy of these results.

6.2.2 Initial Model Quality

To examine the effects of the quality of the initial model on the overall modeling accuracy and precision in isolation, the data from the simulations performed above is analyzed.

The overall modeling accuracy exhibits the expected direct relationship with initial model quality

for the simulated landscapes, as demonstrated in Figures 6.19 and 6.20.
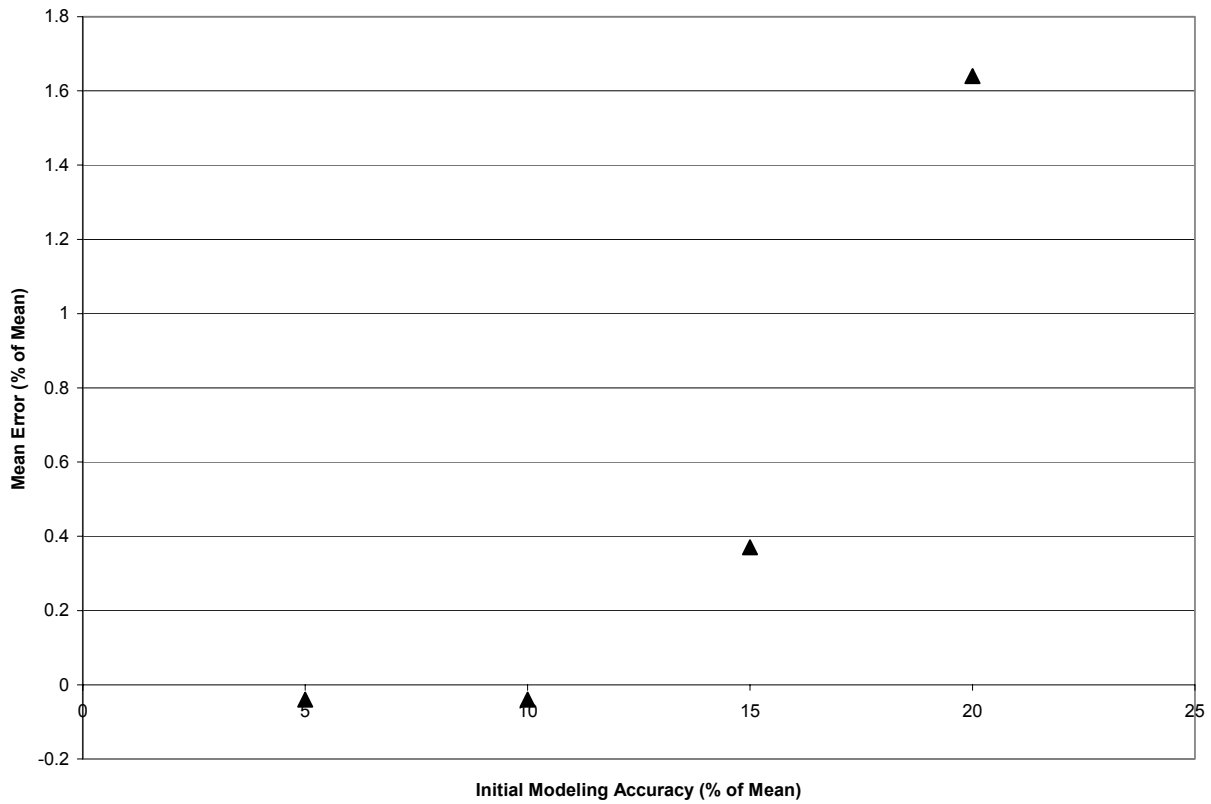
Figure 6.19: Mean Error of Mean Differences in LAI Expressed as Percent of Mean Resulting from Monte Carlo Simulations with Varying Initial Modeling Accuracies for Broadleaf Vegetation with 50000 Iterations and 100 Samples.
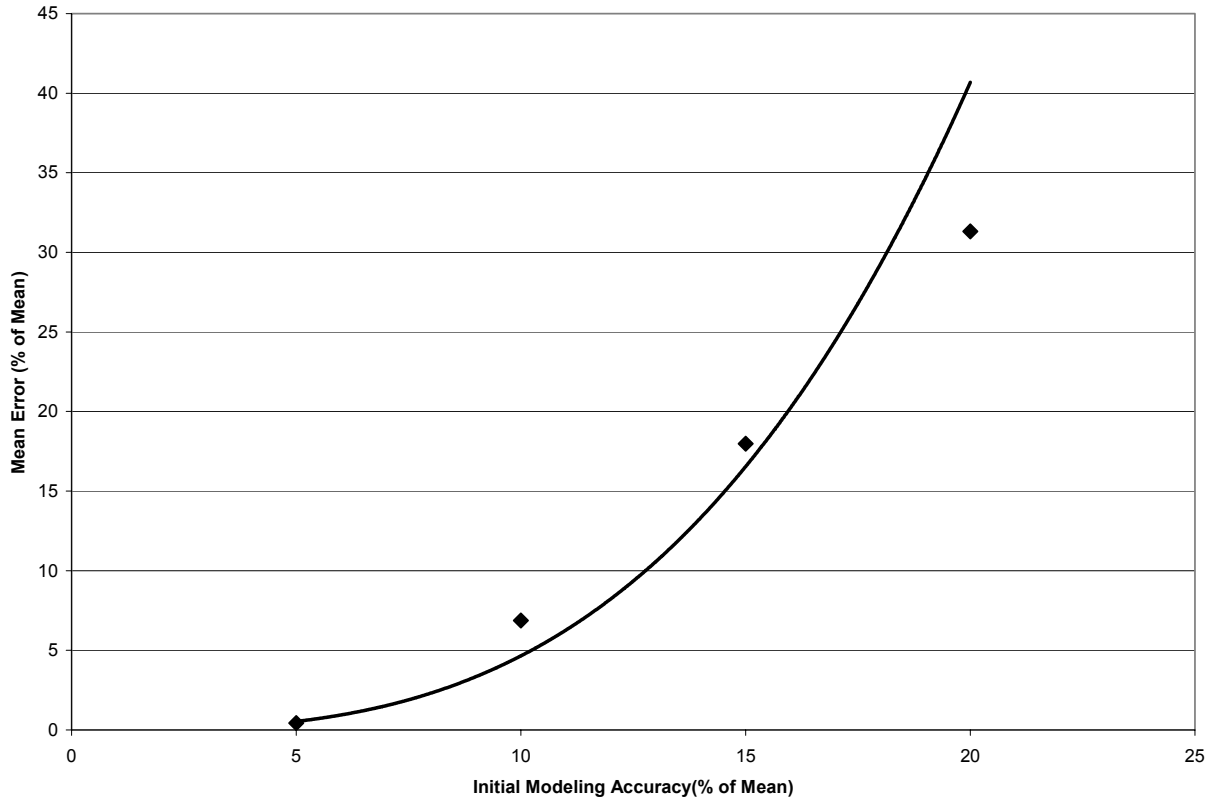
Figure 6.20: Mean Error of Mean Differences in LAI Expressed as Percent of Mean Resulting from Monte Carlo Simulations with Varying Initial Modeling Accuracies for Needleleaf Vegetation with 50000 Iterations and 100 Samples.

It is evident from Figures 6.19 and 6.20 that the initial modeling accuracy displays a strong power relationship with the overall mean error, although the introduction of a bias term may be necessary depending on the underlying variability of the landscape.

In terms of modeling precision, the results from the Monte Carlo simulation evince the anticipated direct relationship between the overall modeling precision and the accuracy associated with the initial model. This relationship is most appropriately modeled linearly as in Figures 6.21 and 6.22.
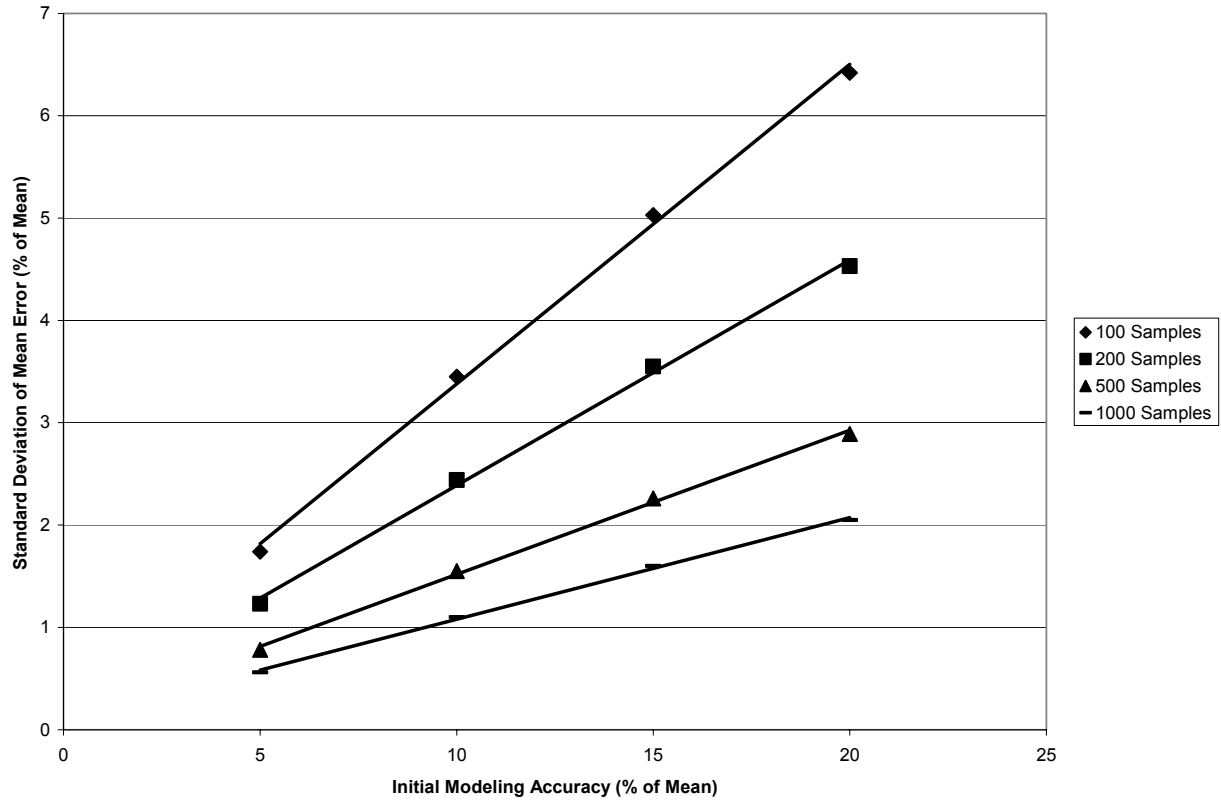
Figure 6.21: Standard Deviations of Errors of Mean Differences in LAI Expressed as Percent of Mean Resulting from Monte Carlo Simulations with Varying Initial Modeling Accuracies for Broadleaf Vegetation with 50000 Iterations.
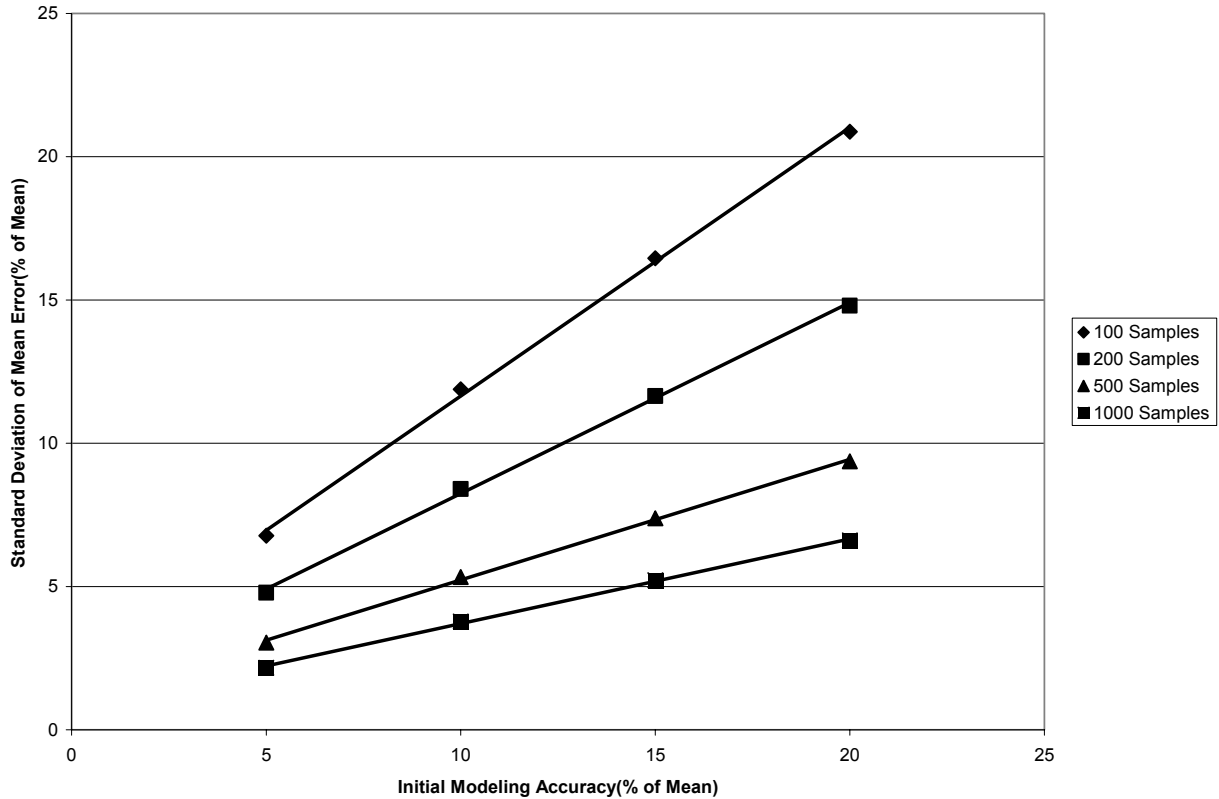
Figure 6.22: Standard Deviations of Errors of Mean Differences in LAI Expressed as Percent of Mean Resulting from Monte Carlo Simulations with Varying Initial Modeling Accuracies for Needleleaf Vegetation with 50000 Iterations.

The results from the Monte Carlo simulations indicate the strong dependence of both the overall modeling precision and accuracy on the quality of the initial model. These results also provide a basis of comparison against which to analyze the models derived in Chapter 5 for a given landscape.

6.2.3 Landscape Variability

The third primary factor that substantially contributes to the determination of the overall modeling accuracy and precision is the inherent variability in LAI associated with a particular landscape. In the previous simulations, canopies with variability in LAI similar to those found in the study region are simulated using variability parameters determined from the *in-situ* LAI measurements.

In this result the variability of the landscape in question is systematically altered, while holding the other primary determining factors constant, and the results generated are therefore independent of vegetation type.

Figure 6.23 demonstrates that, for a given model and number of samples, a linear relationship is evident between the degree of landscape variability and the resulting standard deviation of the observed differences in mean LAI computed by the Monte Carlo simulation
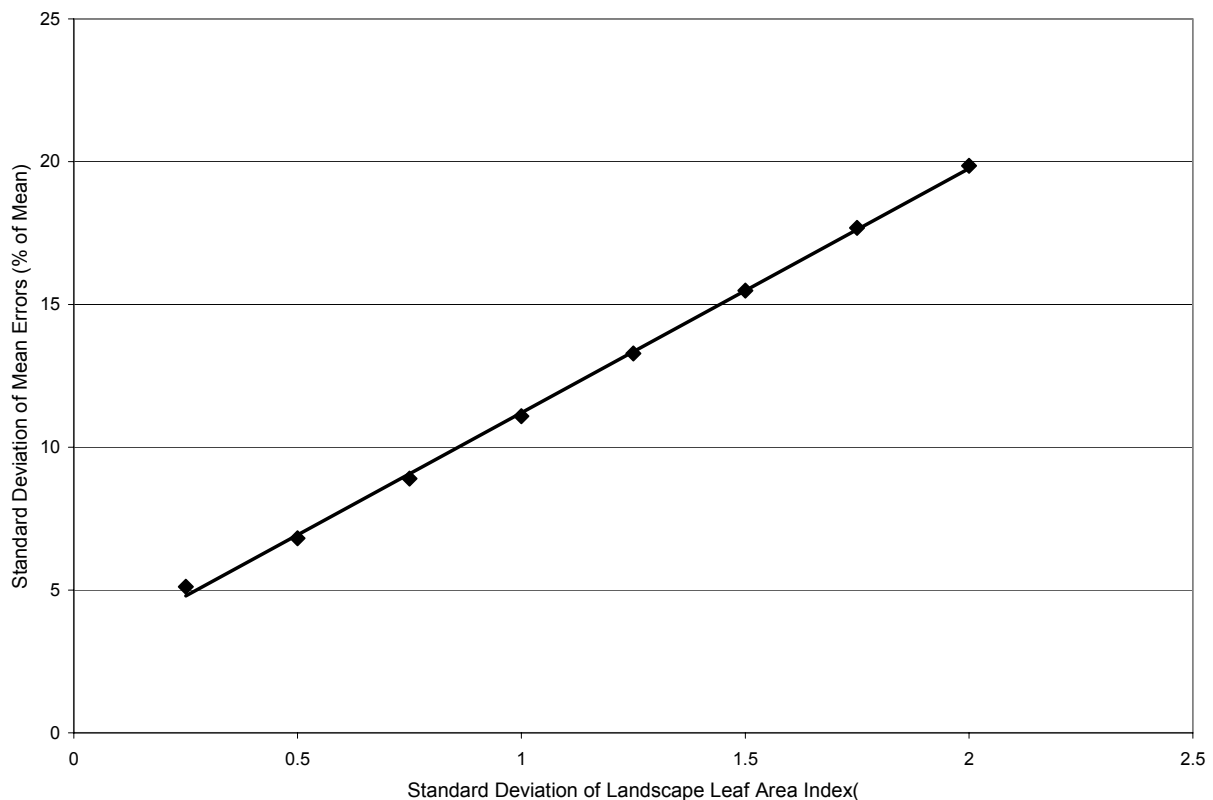
Figure 6.23: Standard Deviations of Mean Differences in LAI Expressed as Percent of Mean Resulting from Monte Carlo Simulations with Varying Degrees of Landscape Variability for Modeling Quality of 10%, Mean LAI of 4.56 and 50000 Iterations.

The observed linear relationship between the degree of landscape variability and the overall modeling precision is quite strong and well-defined.

In terms of overall modeling accuracy, another direct relationship is observed although in this case it is best modeled as a power relationship, as in Figure 6.24.
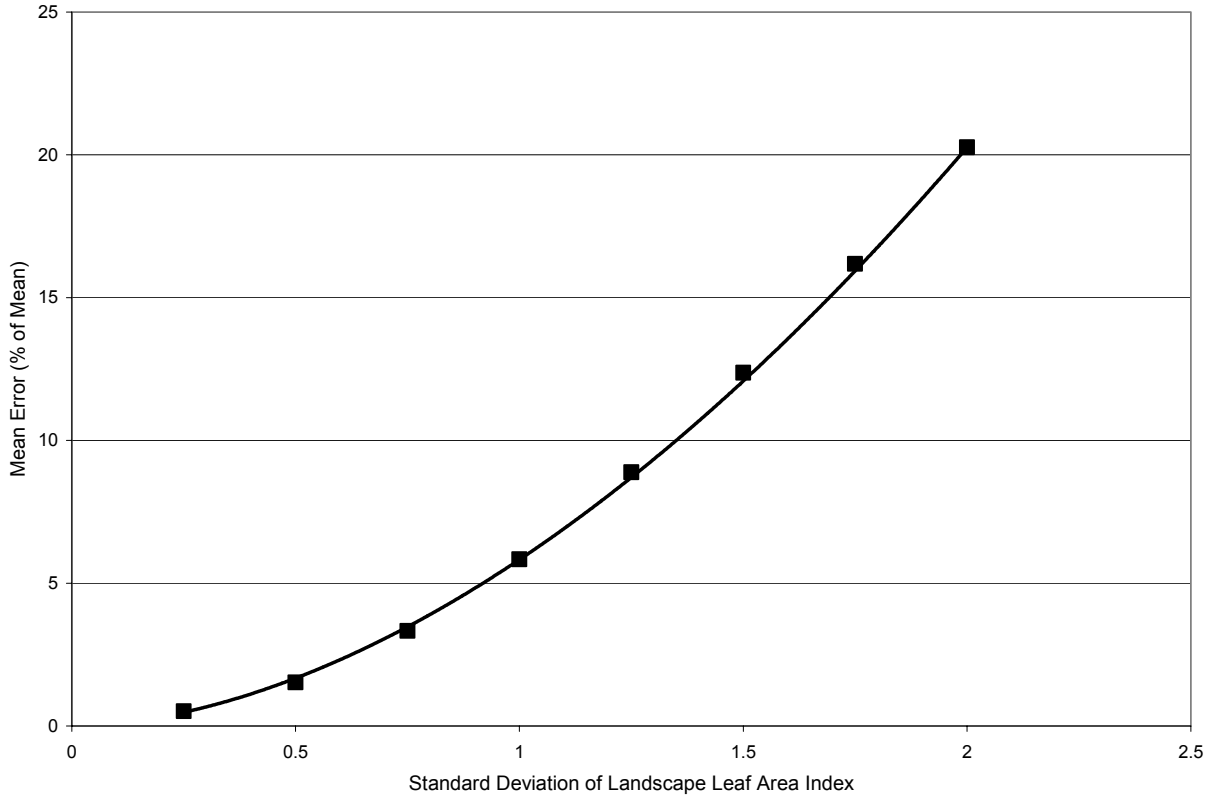
Figure 6.24: Mean Errors of Mean Differences in LAI Expressed as Percent of Mean Resulting from Monte Carlo Simulations with Varying Degrees of Landscape Variability for Modeling Quality of 10%, Mean LAI of 4.56 and 50000 Iterations.

The strength of these relationships allows for the conclusion that knowledge of the variability of the landscape allows for a quantification of the impact which LAI possesses on expected modeling precision and accuracy.

6.3 Adjustment of Mean Error

Due to the presence of a residual modeling error, which is almost solely dependent on the variability of LAI across a landscape, further analysis has been performed to determine whether

the effect of the variability of the landscape can be mitigated through mathematical adjustment of the initial model output. The power relationship, displayed graphically in Figure 6.10, is used to determine an appropriate adjustment factor for a given landscape variability.

In Equation 6.1 through 6.3 the relationship between the mean leaf area indices estimated by a model for a given landscape at a given accuracy are characterized as follows:

$$LAI_{True} \cong LAI_{Model} - LAI_{True} * LV_{Error} \qquad \text{Eq.6.1}$$

$$LAI_{True} + LAI_{True} * LV_{Error} \cong LAI_{Model} \qquad \text{Eq.6.2}$$

$$LAI_{True} \cong \frac{LAI_{Model}}{\left(1 + LV_{Error}\right)} \qquad \text{Eq.6.3}$$

where LAI_{True} is the true mean LAI of the landscape, LAI_{Model} is the mean estimate generated by a given prediction model and LV_{Error} is the predicted error in the mean based on the degree of variability in measured LAI for the sample in question.

Monte Carlo simulations are performed to determine the mean error with and without adjustment, using Equation 6.1 and the derived mean error prediction function from section 6.3 to determine the adjustment factor. Values of landscape variability that are not used in the derivation of the mean error prediction function are used for this task. The results of this analysis are presented in Table 6.6.

Table 6.6: Statistical Results of Monte Carlo Simulations at Various Values of Landscape Variability with Adjusted and Unadjusted Mean Values for Mean LAI of 4.56, Modeling Quality of 10% and 100 Samples

Variability of LAI	Mean Error of Unadjusted Mean Difference (% of Mean)	Standard Deviation of Unadjusted Mean Difference (% of Mean)	Mean Error of Adjusted Mean Difference (% of Mean)	Standard Deviation of Adjusted Mean Difference (% of Mean)
0.17	0.35	4.75	0.11	4.74
0.33	0.76	5.59	-0.04	5.54
0.67	2.67	8.21	-0.16	7.99
0.83	4.07	9.59	-0.1	9.21
1.17	7.86	12.58	0.12	11.68
1.33	9.96	13.99	0.21	12.75
1.67	14.93	16.98	0.24	14.81
1.83	17.46	18.37	0.16	15.67

It is evident from these results that the adjustment of mean differences is effective in reducing the observed mean error by one to two orders of magnitude in the majority of cases tested. The resulting mean errors appear to be non-systematic, due to their oscillation and the absence of any apparent trend. The standard deviations of the samples with adjusted means had reduced magnitudes as compared to those of the unadjusted sample, providing an ancillary benefit to the adjustment procedure.

6.4 Simulation Conclusions

By combining knowledge regarding the sample size of the region of interest, for a given model, with accompanying analysis of the degree of canopy variability across a landscape, it is possible to quantify both the magnitude and characteristics of the error associated with the predictions of the models. This quantification of error allows for a definitive conclusion to be drawn regarding the suitability of the implementation of a given model for a particular area with certain accuracy

specifications. It should be noted that standard normal distributions were assumed for LAI across a landscape. This allowed for a general validation of the technique, while permitting rigorous modeling of the landscape variability. In general, however, such rigid control of landscape variability is not possible and the distribution of LAI values must be considered in the derivation of models for the application of similar techniques to those described above.

6.5 Multi-Scale Analysis

To determine the scale dependence that the remote estimation relationships for LAI exhibit these relationships are implemented across a landscape. The selected landscape, which covers a portion of the Upper Elbow River watershed, is similar to the one for which these relationships are derived, as evidenced in Figures 6.25 and 6.26.

Figure 6.25: MODIS Image of the Upper Elbow River Watershed
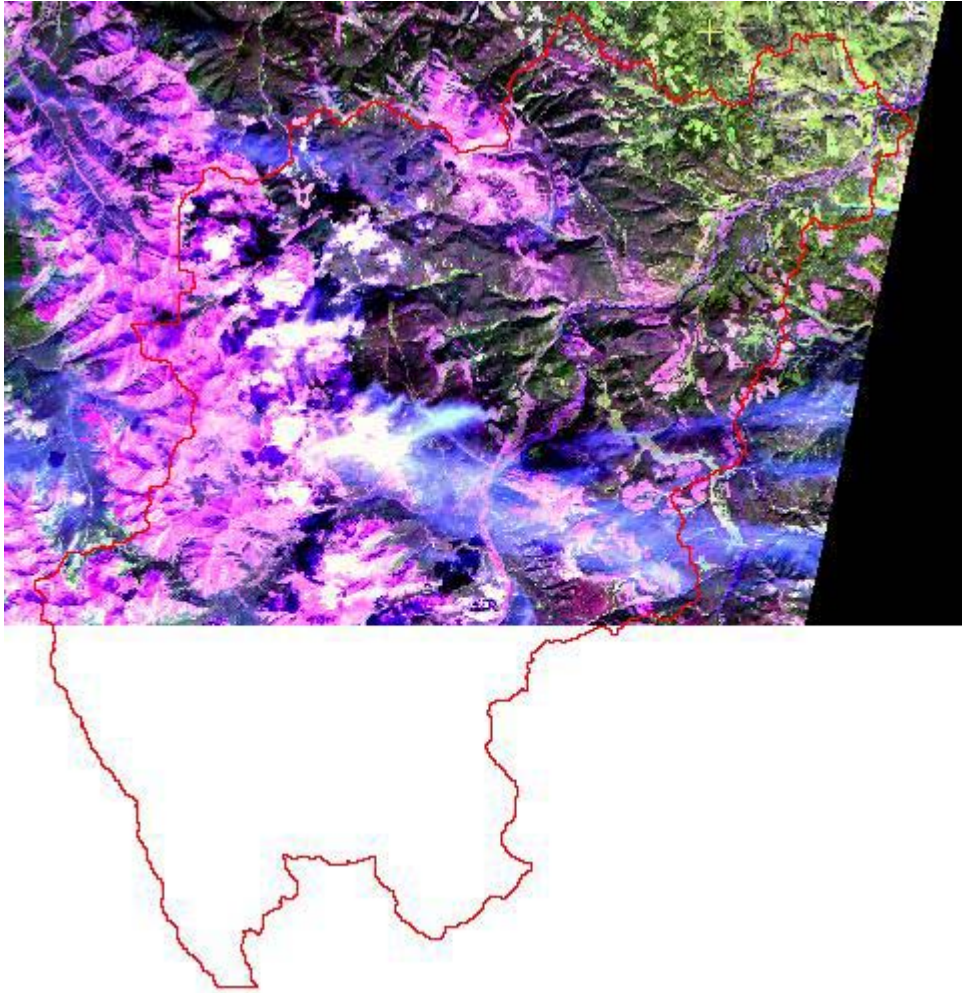
Figure 6.26: SPOT Image at 20m Spatial Resolution of Upper Elbow River Watershed

 To analyze the sensitivity of these relationships to sampling resolution, a MODIS satellite image is acquired and the SPOT image is resampled to 1200 m spatial resolution, to approximate the spatial resolution of the MODIS sensor, using a mean resampling approach. The acquired image is the MODIS surface reflectance product which is used to compute the input parameters necessary for estimation of the LAI. The MODIS channels are summarized in Table 6.7.

Table 6.7: MODIS Sensor Channel Information

Channel Number	Band Coverage (μm)	Spectrum Description
1	0.620-0.670	Red
2	0.841-0.876	Near-Infrared
3	0.459-0.479	Blue
4	0.545-0.565	Green
5	1.230-1.250	Middle-Infrared
6	1.628-1.652	Middle-Infrared
7	2.105-2.155	Middle-Infrared

Channels one, two and six are selected for this analysis as they correspond most closely to the portions of the spectrum, as determined by the width and location of the spectral channels, whose measurements are used in the initial models.

To determine the appropriate model for application within a given area, a maximum likelihood classification is performed on each of the images that have been analyzed. In terms of classification parameters both the normalized difference vegetation index and the middle infrared channel are selected as this combination effectively differentiates vegetation from the surrounding landscape and needleleaf vegetation from broadleaf vegetation. Another reason for the selection of these quantities is their relatively low correlation, which contributes to the robustness of the solution. Training areas are selected for the desired output classes of needleleaf and broadleaf vegetation. A null class is also required in this classification as no discrimination is needed between other feature class types.

For each image the modeling types which exhibit the most robustness in their modeling of variations in LAI for each of the vegetation types are applied. Based on this criterion, needleleaf vegetation uses the models derived based on shadow fraction, modified NDVI and normalized distance. Broadleaf vegetation uses the models derived based on the moisture stress index, modified NDVI and normalized distance. These models are analyzed separately to determine their individual performance.

6.5.1 Broadleaf Vegetation

The results derived from application of the moisture stress index, modified NDVI and normalized distance models for the estimation of LAI in broadleaf vegetation for SPOT and MODIS imagery are presented in Table 6.8.

Table 6.8: Statistics of LAI Computed Using Various Imagery Types for the Upper Elbow Watershed for Broadleaf Vegetation

Image Type	Mean LAI	Median LAI	Standard Deviation of LAI	Maximum LAI	Minimum LAI	Modeling Parameter
SPOT -20m	2.35	2.33	0.23	3.94	1.79	Moisture Stress Index
MODIS	1.87	1.86	0.29	2.90	1.05	Moisture Stress Index
SPOT-1200m	1.63	1.66	0.18	1.95	1.17	Moisture Stress Index
SPOT-20m	2.65	2.66	0.22	3.16	2.12	Modified NDVI
MODIS	2.55	2.64	0.50	3.36	0.00	Modified NDVI
SPOT-1200m	2.49	2.58	0.45	2.92	0.00	Modified NDVI
SPOT-20m	2.35	2.35	0.24	3.18	1.84	Normalized Distance
MODIS	2.23	2.27	0.35	3.08	1.37	Normalized Distance
SPOT-1200m	2.21	2.18	0.36	2.93	1.17	Normalized Distance

It is evident from the statistics in Table 6.8 that the models derived in Chapter 5 exhibit varying degrees of robustness in LAI estimation for broadleaf vegetation. The overall error in the mean LAI determined using the observations at coarser resolutions underestimates the mean LAI of the landscape, obtained from the original SPOT imagery, by between 3 to 30%. The presence of this

mean error is indicative of degraded performance exceeding that anticipated by Monte Carlo simulations due to the marked decrease in the number of samples used to compute the mean LAI for the coarser resolution data sets.

It is interesting to note the high degree of similarity between the statistical values computed for the moisture stress index model and the normalized distance model. This high similarity is indicative of the underlying stability and modeling robustness of these models and is a partial confirmation of the results expected from the Monte Carlo simulation.

The standard deviations in Table 6.8 appear dissimilar between the estimates at finer and coarser spatial resolution and an F-test is conducted on these standard deviations to determine whether this variation is statistically significant. The results of the F-tests allow the conclusion that the variances of the coarser resolution images are significantly different from the original SPOT imagery fro all models at a level of significance of 0.10. This dissimilarity in standard deviations is indicative of non-uniformity in the overall precision exhibited by the model in using each of the input data sets.

It is also important to consider whether the frequency distribution of LAI is scale invariant for broadleaf vegetation. This is done first through a comparison of the LAI histograms determined for each case and then through a χ^2 goodness-of-fit test of the coarser resolution data to the frequency distribution observed for the original SPOT image. The LAI histograms are presented in Figures 6.27 through 6.35.
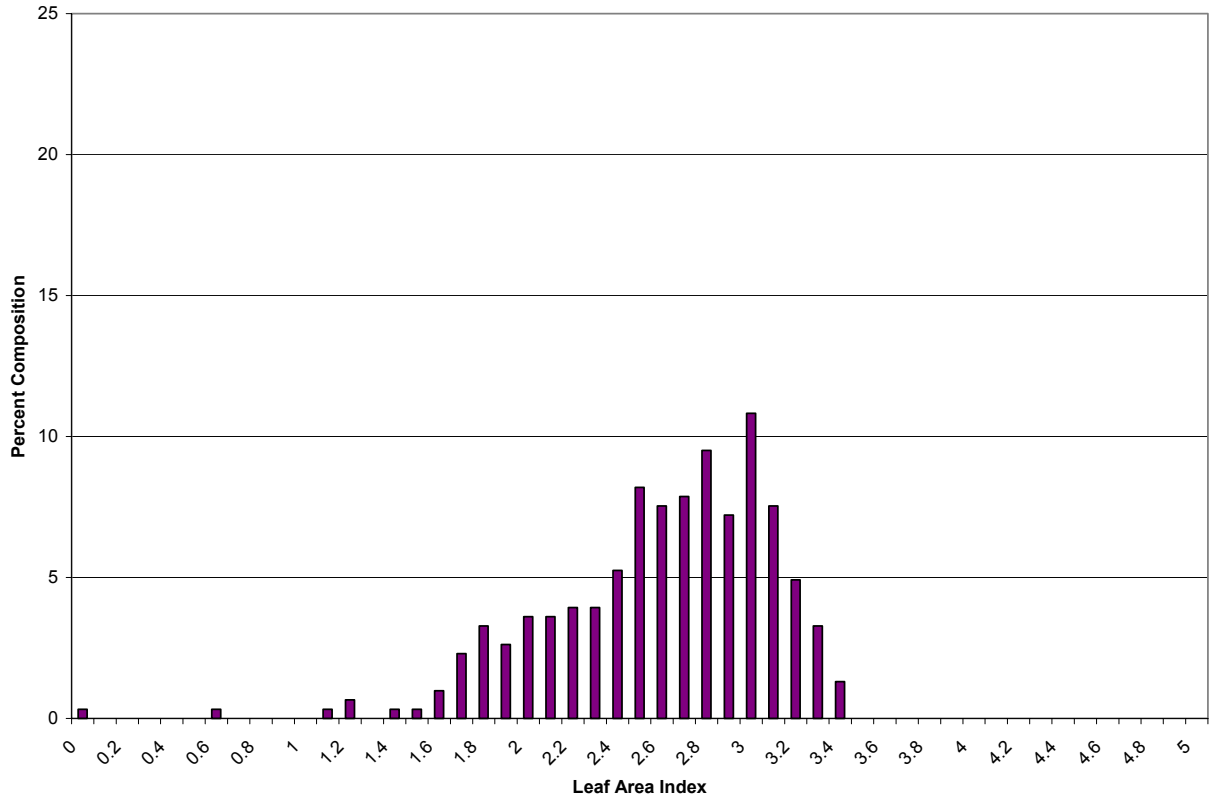
Figure 6.27: Histogram of LAI Estimated Using Modified Normalized Difference Vegetation Index Values from MODIS Imagery
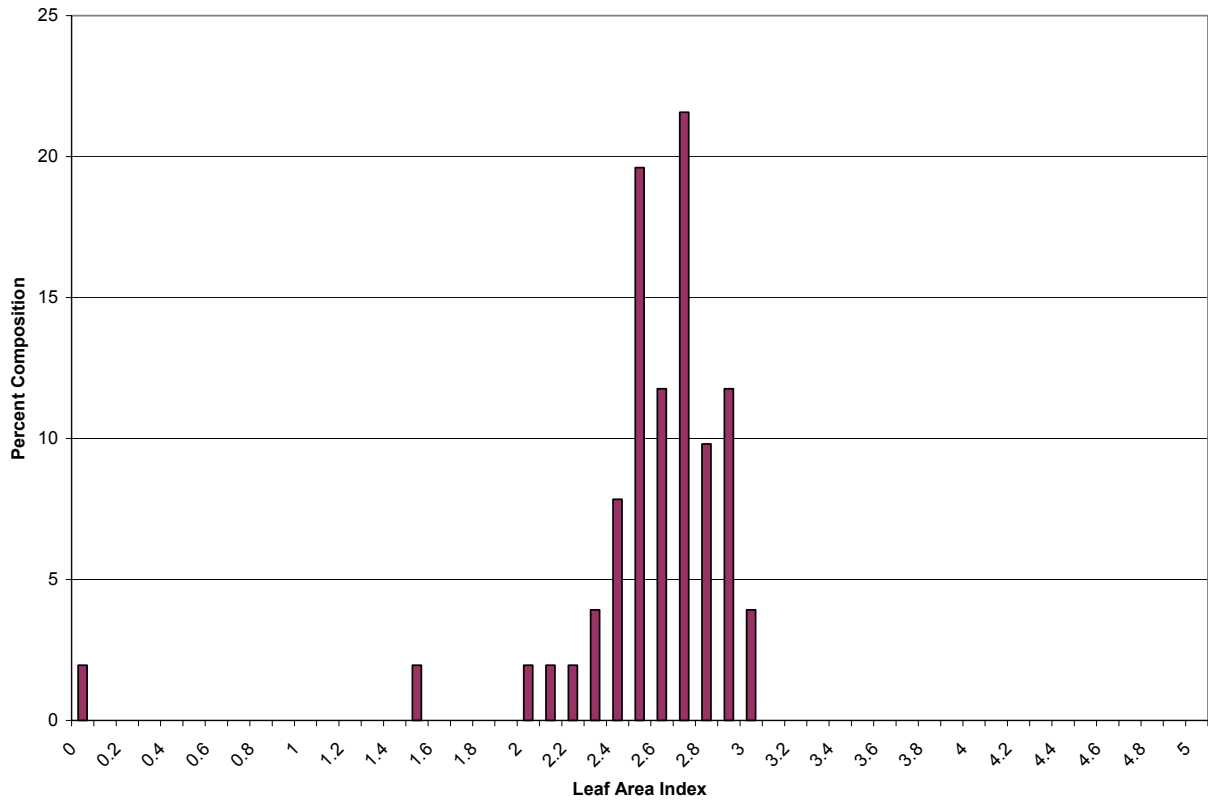
Figure 6.28: Histogram of LAI Estimated Using Modified Normalized Difference Vegetation Index Values from SPOT Imagery at 1200m Spatial Resolution
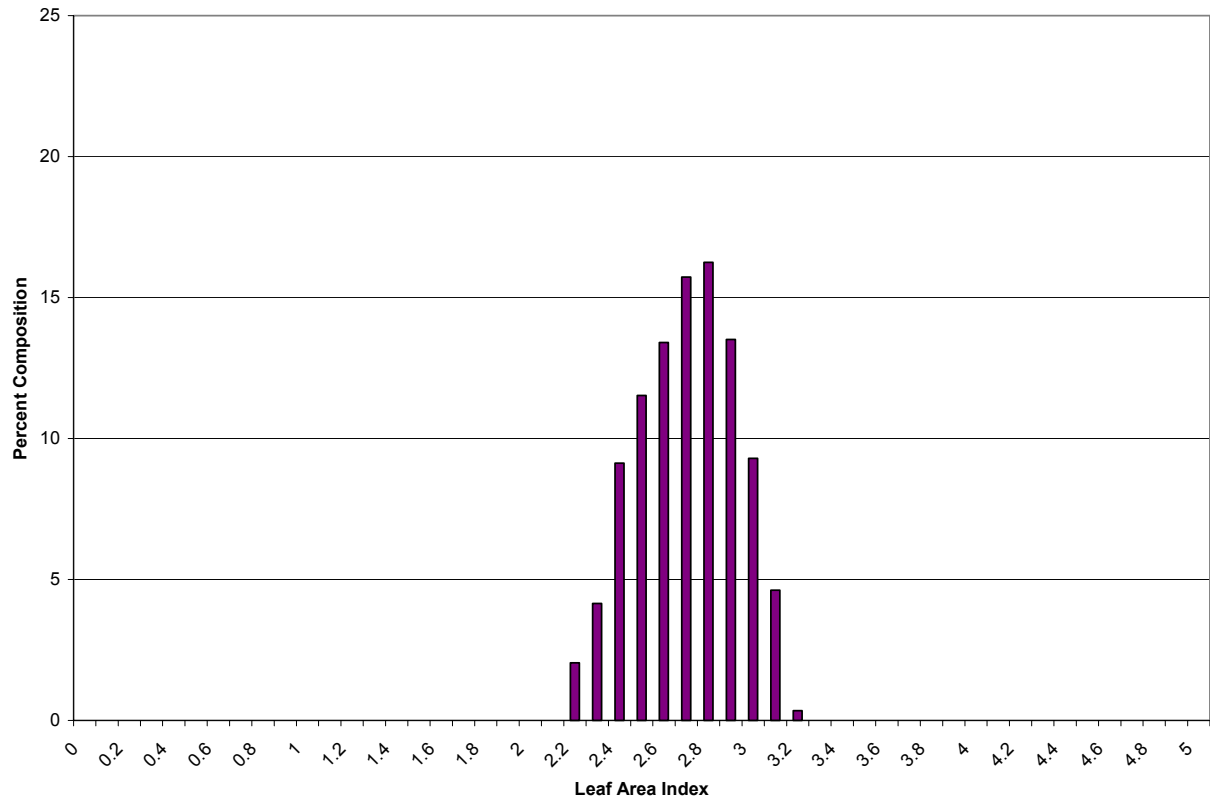
Figure 6.29: Histogram of LAI Estimated Using Modified Normalized Difference Vegetation Index Values from SPOT Imagery at 20m Spatial Resolution
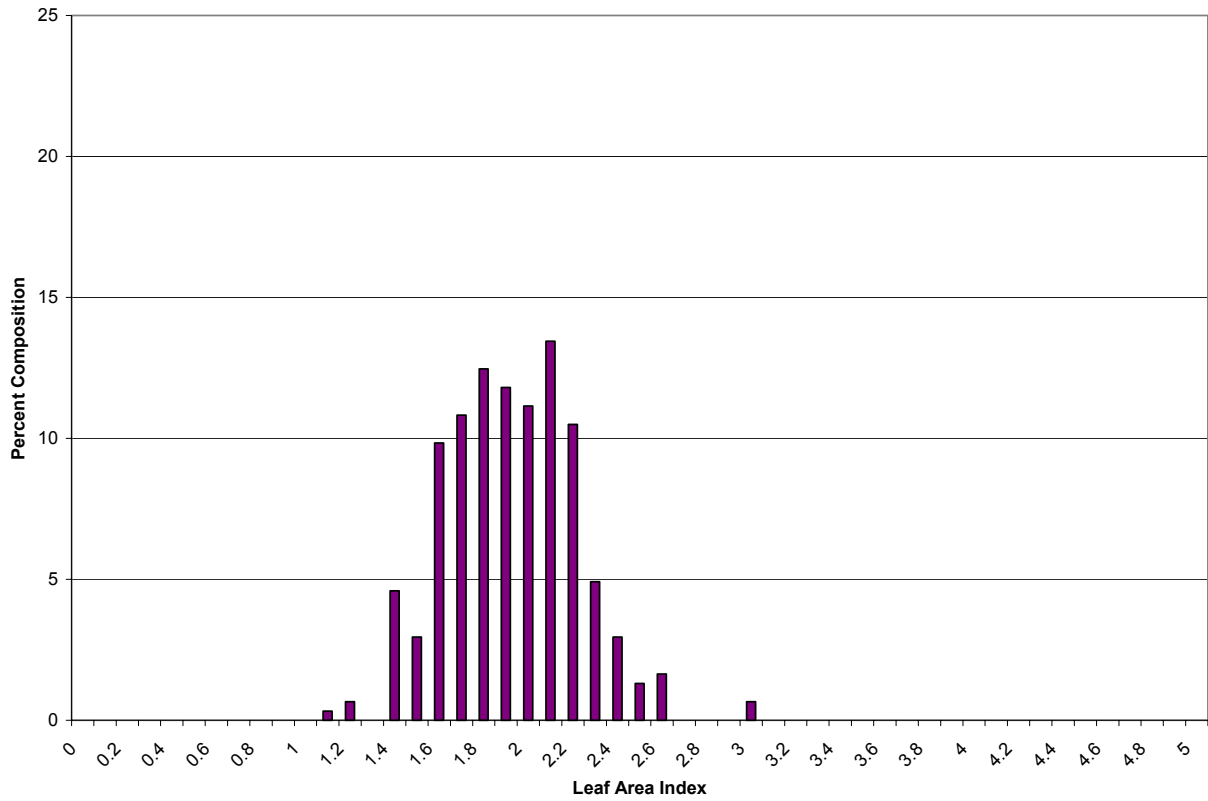
Figure 6.30: Histogram of LAI Estimated Using Moisture Stress Index Values from MODIS Imagery
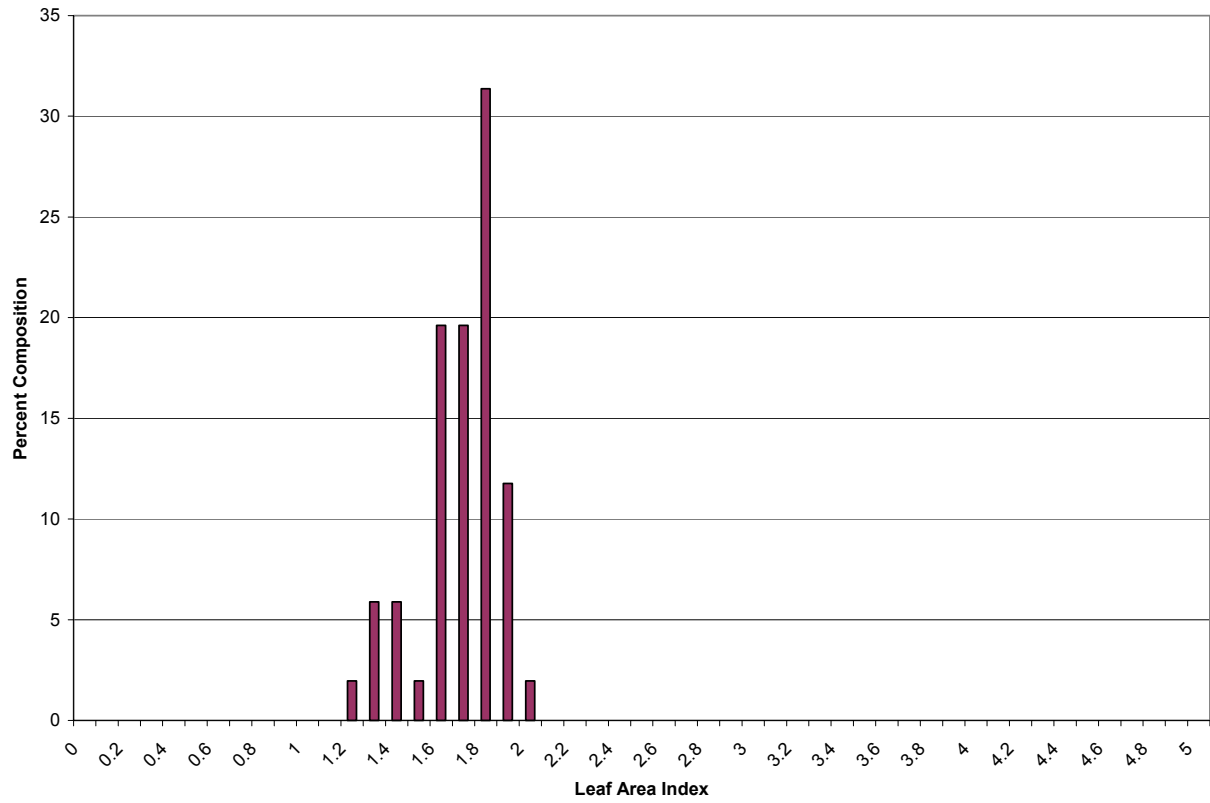
Figure 6.31: Histogram of LAI Estimated Using Moisture Stress Index Values from SPOT Imagery at 1200m Spatial Resolution
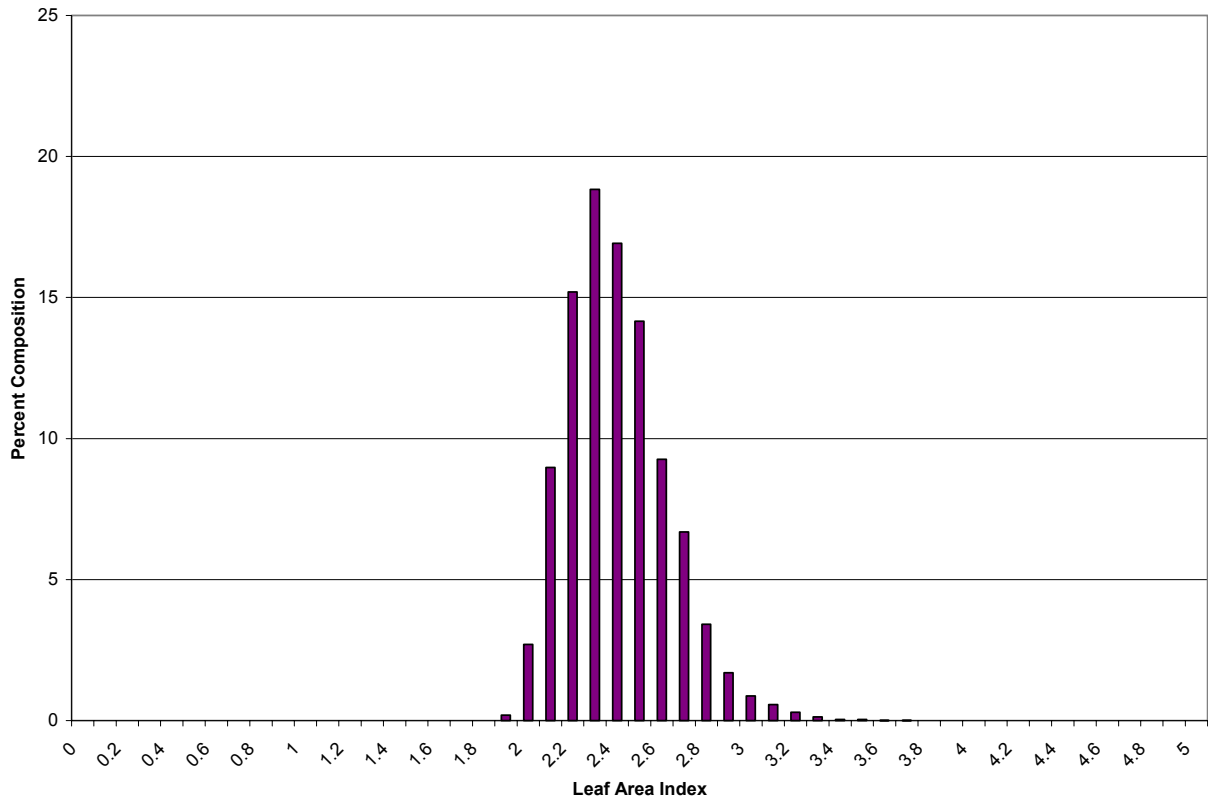
Figure 6.32: Histogram of LAI Estimated Using Moisture Stress Index Values from SPOT Imagery at 20m Spatial Resolution
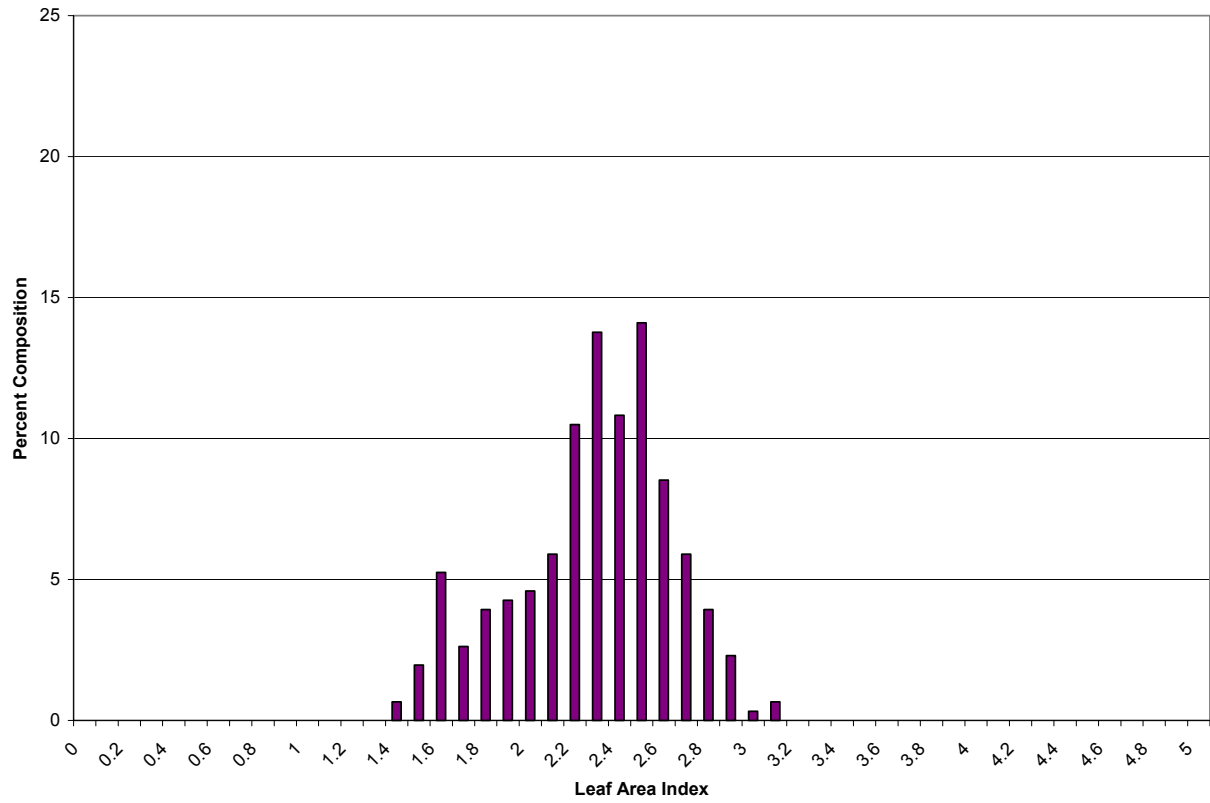
Figure 6.33: Histogram of LAI Estimated Using Normalized Distance Values from MODIS Imagery
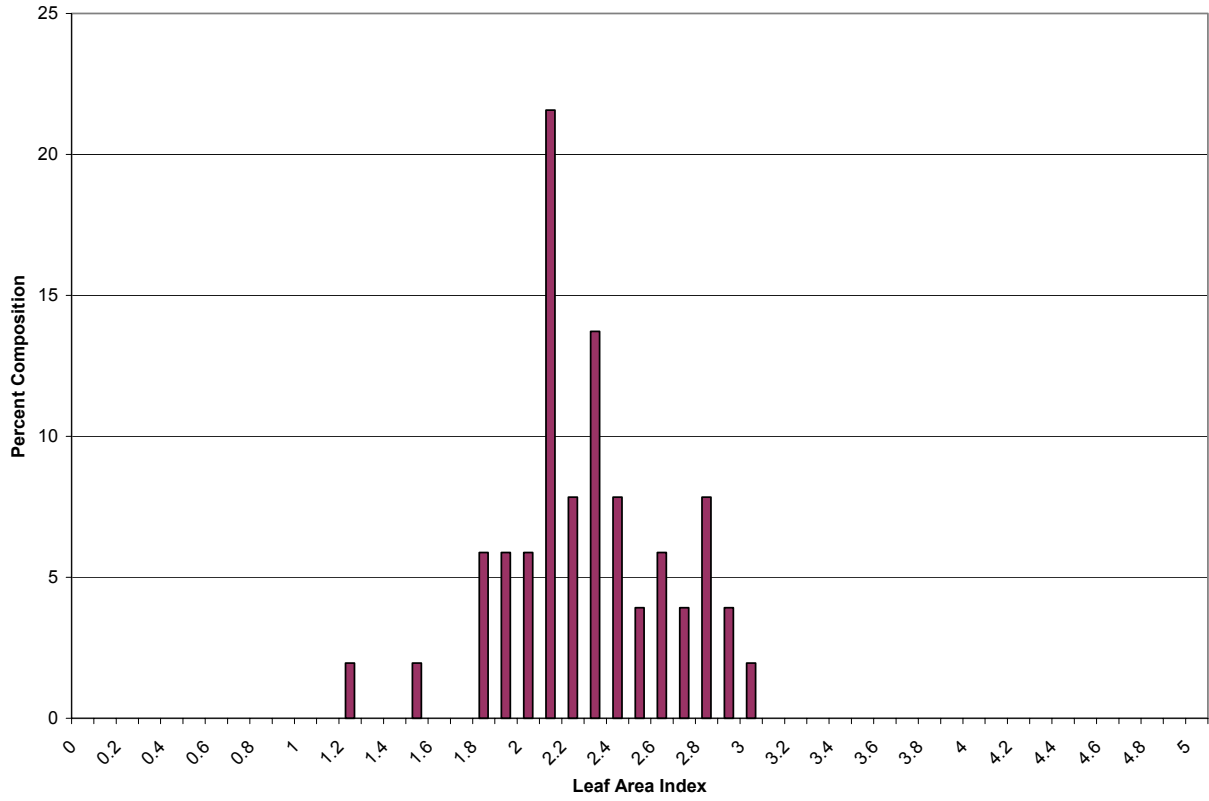
Figure 6.34 Histogram of LAI Estimated Using Normalized Distance Values from SPOT Imagery at 1200m Spatial Resolution
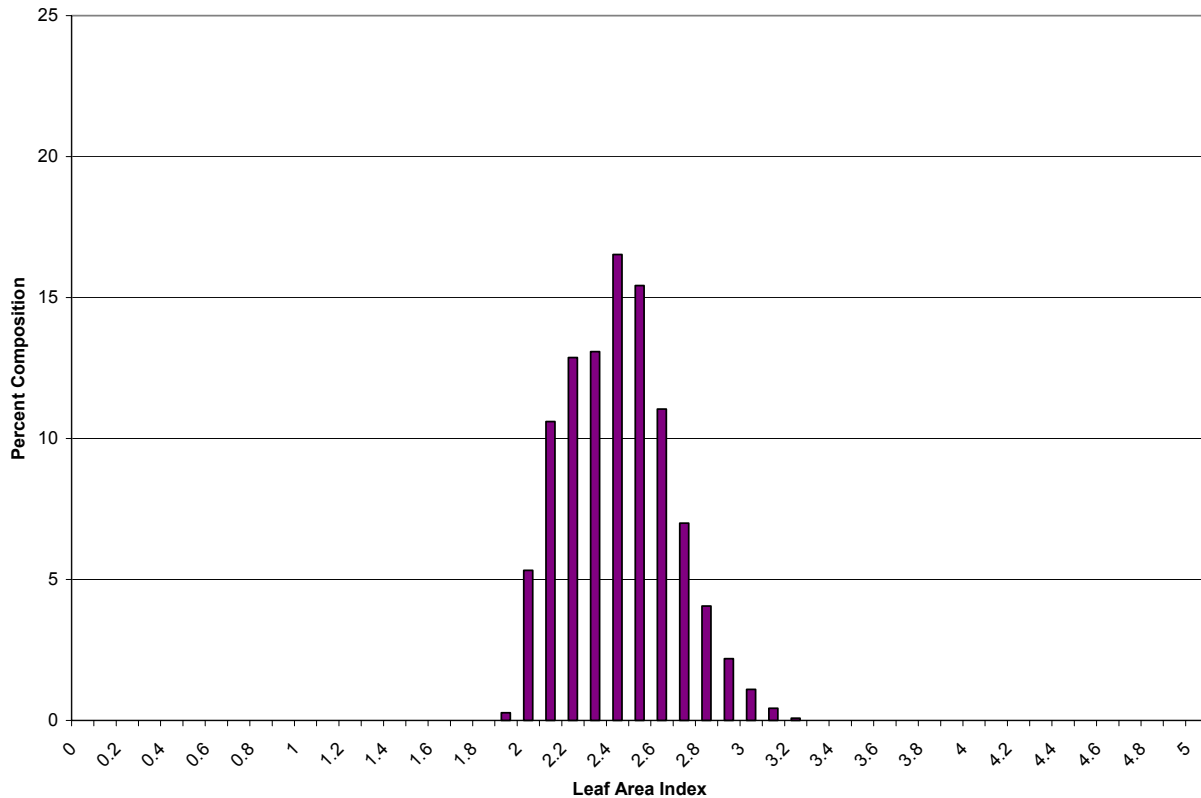
Figure 6.35: Histogram of LAI Estimated Using Normalized Distance Values from SPOT Imagery at 20m Spatial Resolution

It seems apparent from the above figures that the LAI distributions possess similar shapes, despite the statistical differences noted above. This could be attributable to the presence of systematic bias between the estimation models when they are applied at different scales Fewer high frequency oscillations in percent composition are noticed in the original SPOT image as compared to the coarser resolution imagery, which is expected due to its increased sample size.

To determine quantitatively whether the frequency distributions of LAI values are significantly different a χ^2 goodness-of-fit test is performed between the two distributions. This goodness-of-fit test uses the frequency distribution of the initial SPOT image to determine the expected rate of occurrence over a specific range of LAI values and then compares this to that observed in the coarser resolution imagery. The χ^2 test determines the frequency distributions of LAI to be significantly different at a level of significance of 0.05 with two degrees of freedom for the MODIS cases and the coarser resolution SPOT estimates using the moisture stress index and the

189

normalized distance model. However, the estimate computed using the modified NDVI cannot be concluded to follow different distributions at a level of significance of 0.05 with two degrees of freedom between the SPOT images.

Spatial statistical analysis demonstrates that these modeling parameters still possesses the capacity to model LAI at coarser scales. This is evident from the plots of Moran's I versus distance in Figures 6.36 through 6.41 which demonstrate similar behavior to those initially derived using the original SPOT data.
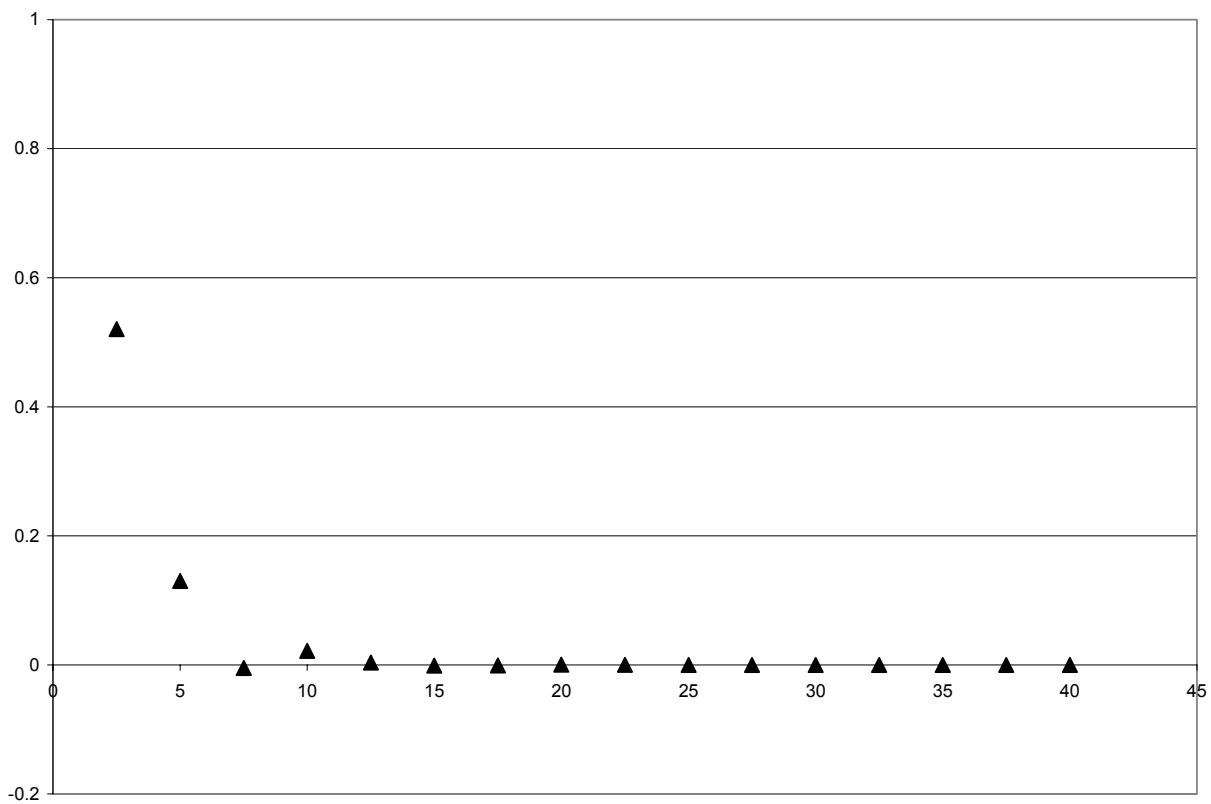
Figure 6.36: Plot of Moran's I versus Lag Distance for Moisture Stress Index Values Computed from SPOT Imagery at 1200m Spatial Resolution
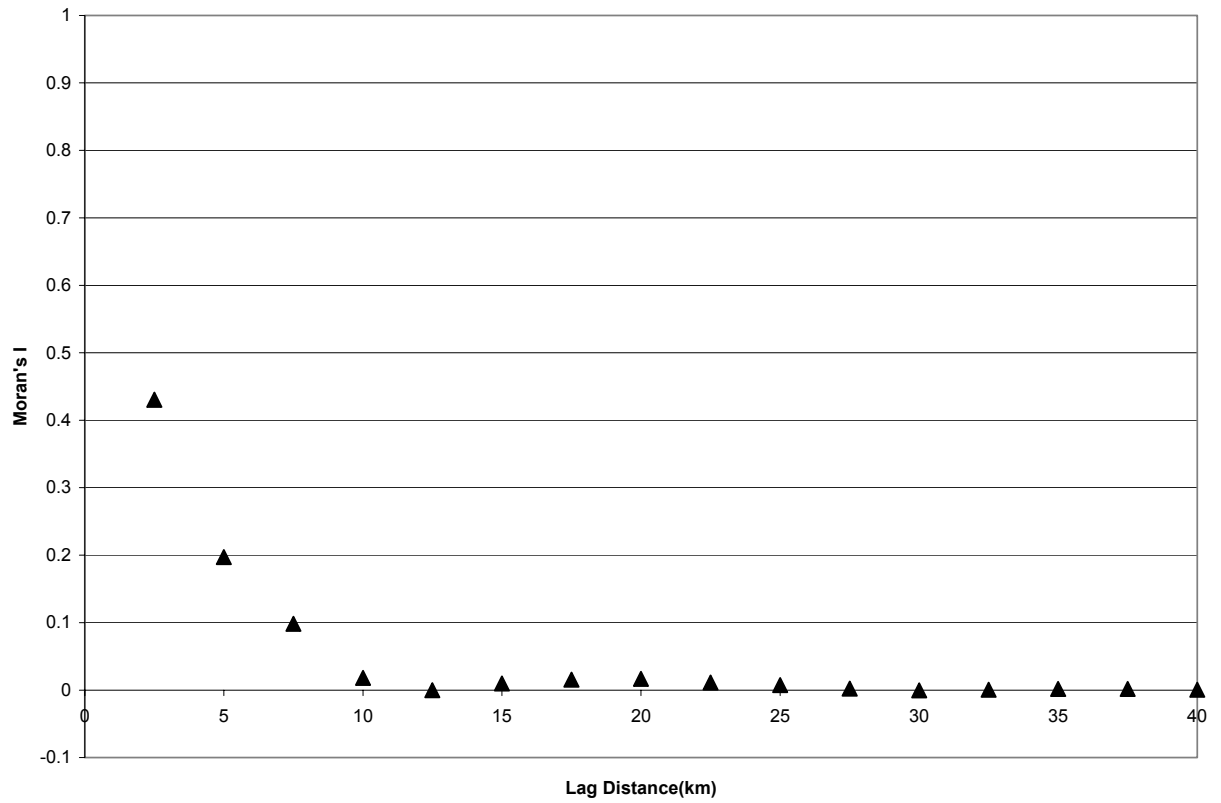
Figure 6.37: Plot of Moran's I versus Lag Distance for Moisture Stress Index Values Computed from MODIS Imagery
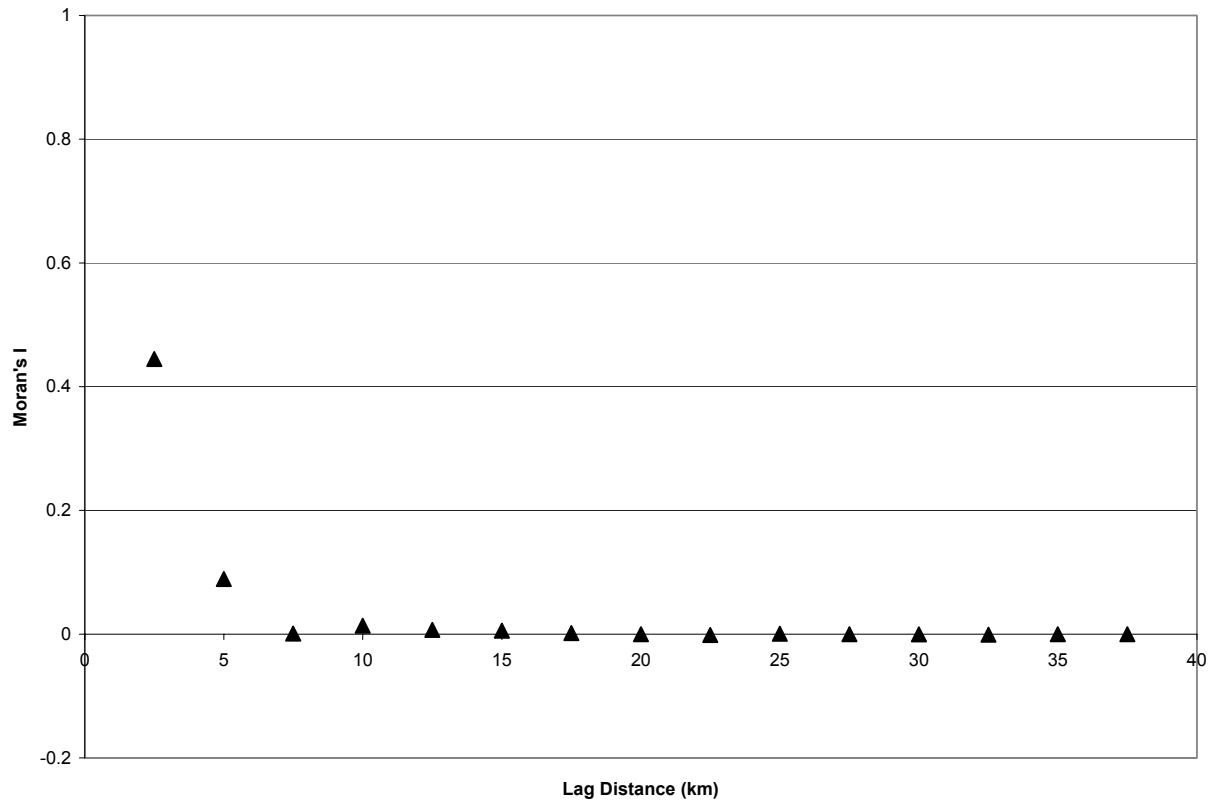
Figure 6.38: Plot of Moran's I versus Lag Distance for Modified Normalized Difference Vegetation Index Values Computed from SPOT Imagery at 1200m Spatial Resolution
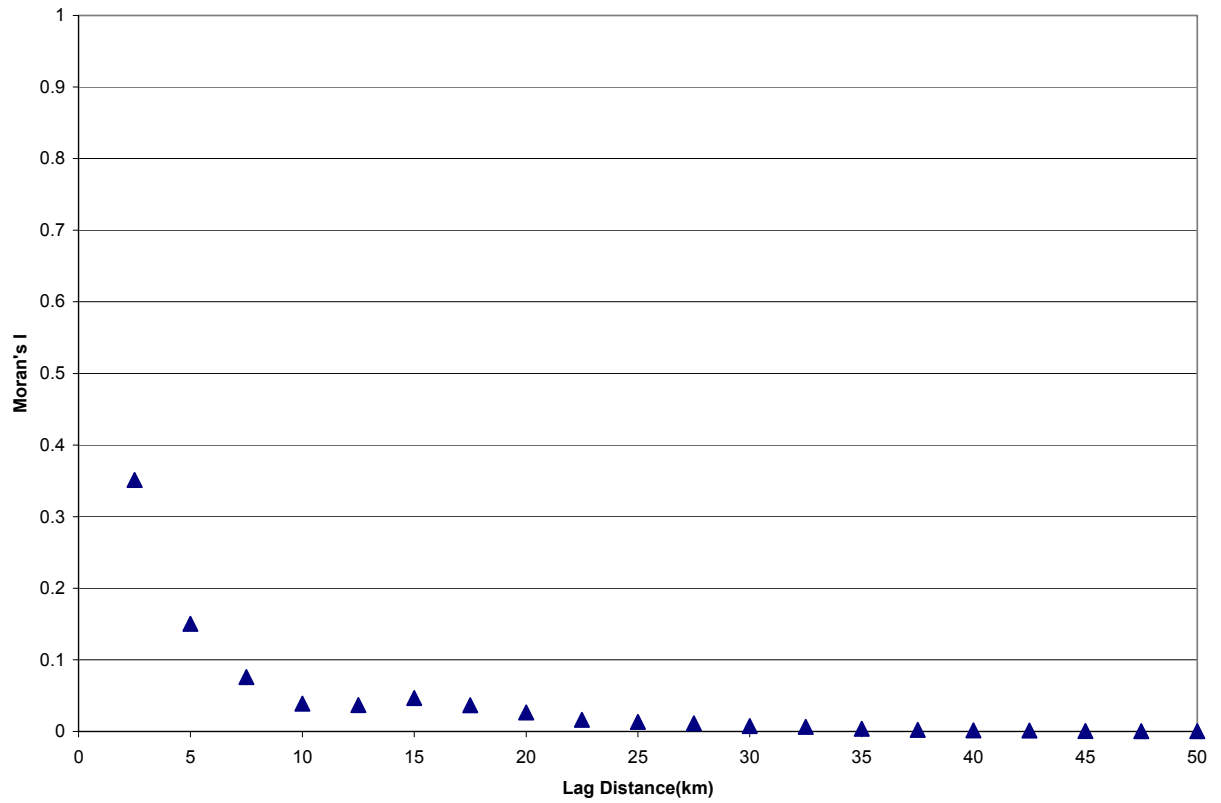
Figure 6.39: Plot of Moran's I versus Lag Distance for Modified Normalized Difference Vegetation Index Values Computed from MODIS Imagery
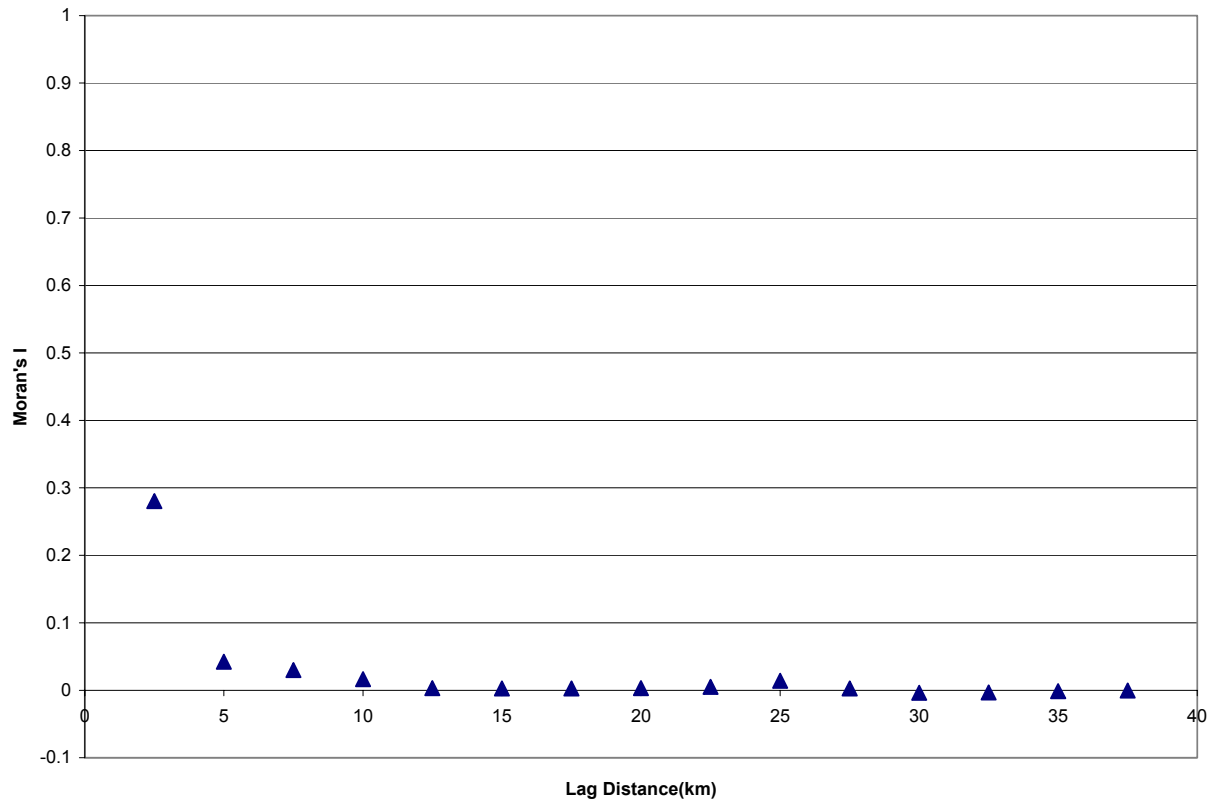
Figure 6.40: Plot of Moran's I versus Lag Distance for Normalized Distance Values Computed from SPOT Imagery at 1200m Spatial Resolution
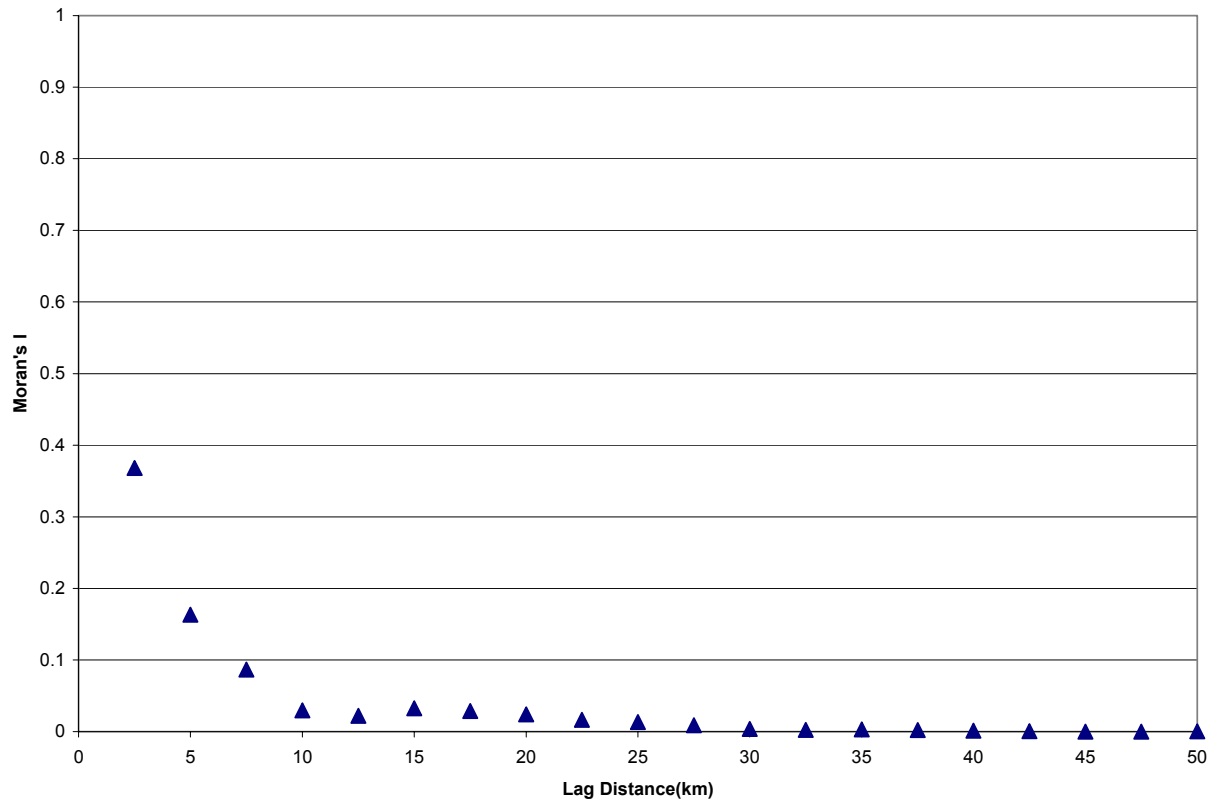
Figure 6.41: Plot of Moran's I versus Lag Distance for Normalized Distance Values Computed from MODIS Imagery

In similar fashion to Figure 6.3 the Moran's I values consistently decrease until complete spatial randomness is reached. The fact that complete spatial randomness is reached at different values for each spatial resolution is important. It is indicative of the extent to which the processes determining LAI vary depending on the scale of analysis for broadleaf vegetation. The fact that the imagery with coarser spatial resolution evidences correlation in Moran's I values over lag distances exceeding the range observed for the initial SPOT imagery is further evidence that analysis of the processes that determine variations in the input modeling parameter is scale dependent. This means that estimation relationships derived for use with a given imagery type at a given scale cannot necessarily be reliably applied for even the same imagery type at another scale.

Additionally, it should be noted that the initial correlations observed between values are in all cases lower than those observed at finer scales. This is likely indicative of increasingly

heterogeneous pixel composition at coarser scale, perhaps with non-linear mixing, and generally increasing dissimilarity between the spectral properties within a vegetation type as distance increases.

6.5.2 Needleleaf Vegetation

The results derived from application of the remote estimation models for both MODIS and SPOT imagery are presented in Table 6.9.

Table 6.9: Statistics of LAI Computed Using Various Imagery Types for Needleleaf Vegetation

Image Type	Mean LAI	Median LAI	Standard Deviation of LAI	Maximum LAI	Minimum LAI	Model Type
SPOT-20m	4.81	4.84	0.96	6.46	1.37	Shadow Fraction
MODIS	2.59	2.25	1.37	6.59	0.00	Shadow Fraction
SPOT-1200m	2.15	2.00	1.36	6.59	0.00	Shadow Fraction
SPOT-20m	4.86	4.81	0.88	7.52	3.26	Modified NDVI
MODIS	5.57	5.71	2.91	12.42	0.00	Modified NDVI
SPOT-1200m	2.25	1.84	1.60	7.90	0.00	Modified NDVI
SPOT-20m	4.67	4.77	0.96	6.27	0.96	Normalized Distance
MODIS	3.08	2.99	1.49	6.27	0.41	Normalized Distance
SPOT-1200m	1.65	1.33	1.16	5.70	0.38	Normalized Distance

In comparison to the broadleaf case the shadow fraction model proved less robust in its estimation of the mean LAI exhibiting an error of between 12 to 65% for the coarser resolution imagery. The presence of a residual mean error above that which is predicted by Monte Carlo simulation is likely attributable to variance in the derived relationships as the resolution of the input imagery decreases, as well as a decreased number of samples.

The same high similarity between landscape level estimates of mean LAI exhibited for broadleaf vegetation is also present for needleleaf vegetation. The mean estimates are within at least 5% of

each other which is indicative of the quality of the remote estimation models. The correspondence between the statistical properties of landscape level LAI estimates is in line with the results predicted by Monte Carlo simulation.

An F-Test is performed to determine whether the apparent differences between the observed standard deviations are statistically significant. The results of the F-Test indicate that the LAI sample variances indices are different at a level of significance of 0.10 when comparisons are made between each of the coarser spatial resolution images and the original SPOT image for all remote estimation models. This indicates that the precision of LAI estimation is not scale-invariant.

The frequency distributions of LAI values are examined first qualitatively and then quantitatively to determine whether they are scale invariant. In qualitative terms, the frequency distributions exhibit a greater degree of variation in the needleleaf case than in the broadleaf case, as evidenced in Figures 6.42 through 6.50.
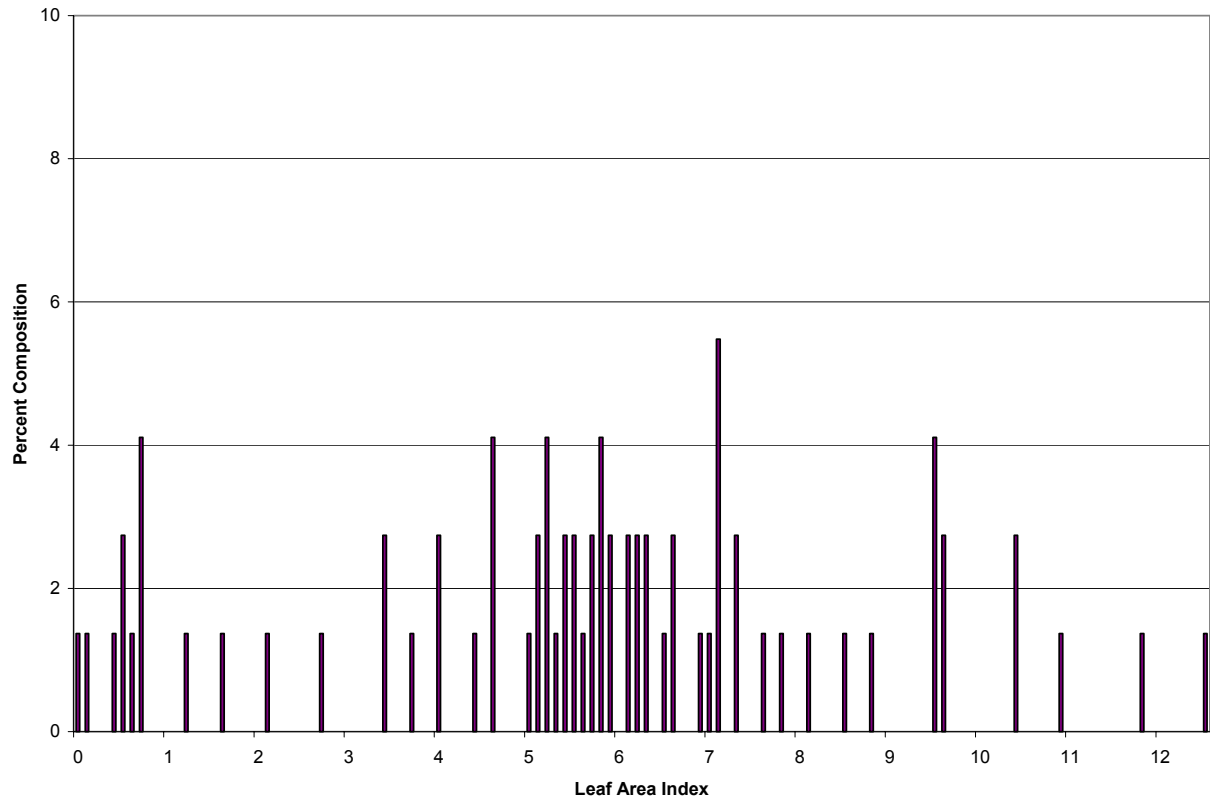
Figure 6.42: Histogram of LAI Estimated Using Modified Normalized Difference Vegetation Index Values from MODIS Imagery
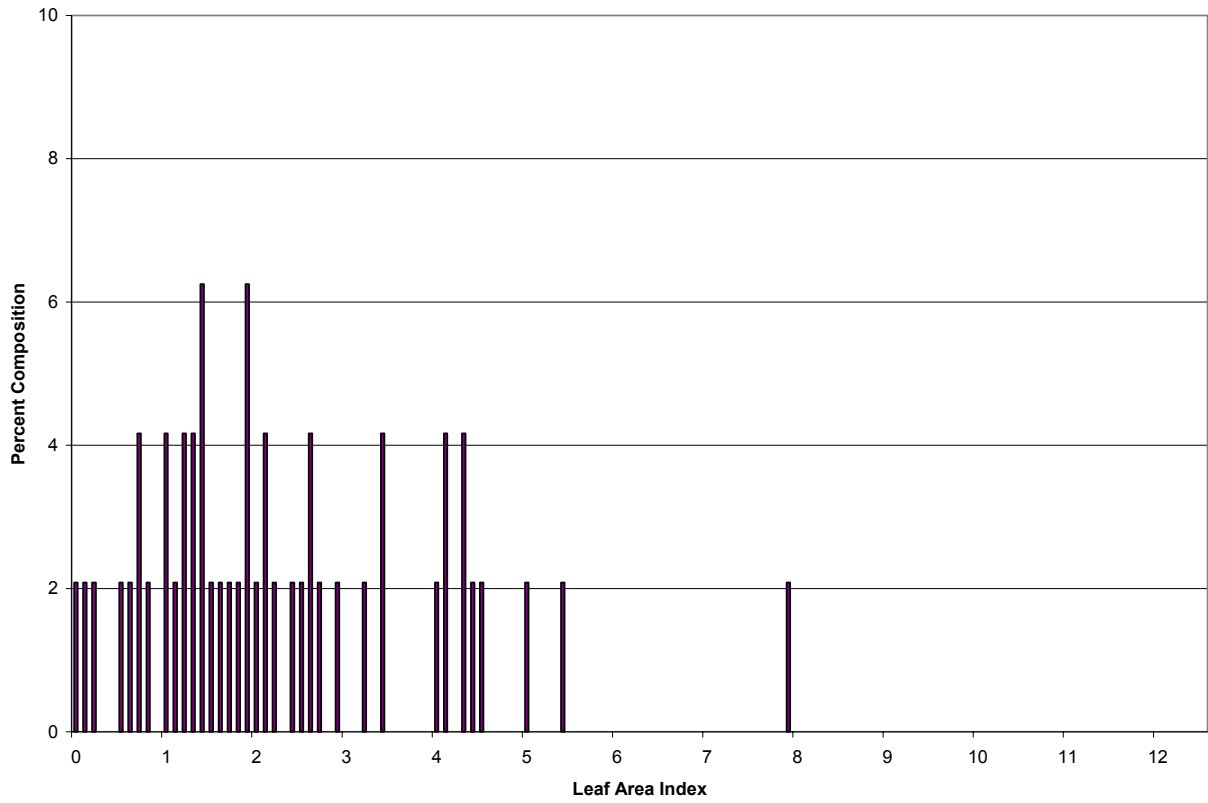
Figure 6.43: Histogram of LAI Estimated Using Modified Normalized Difference Vegetation Index Values from SPOT Imagery at 1200m Spatial Resolution
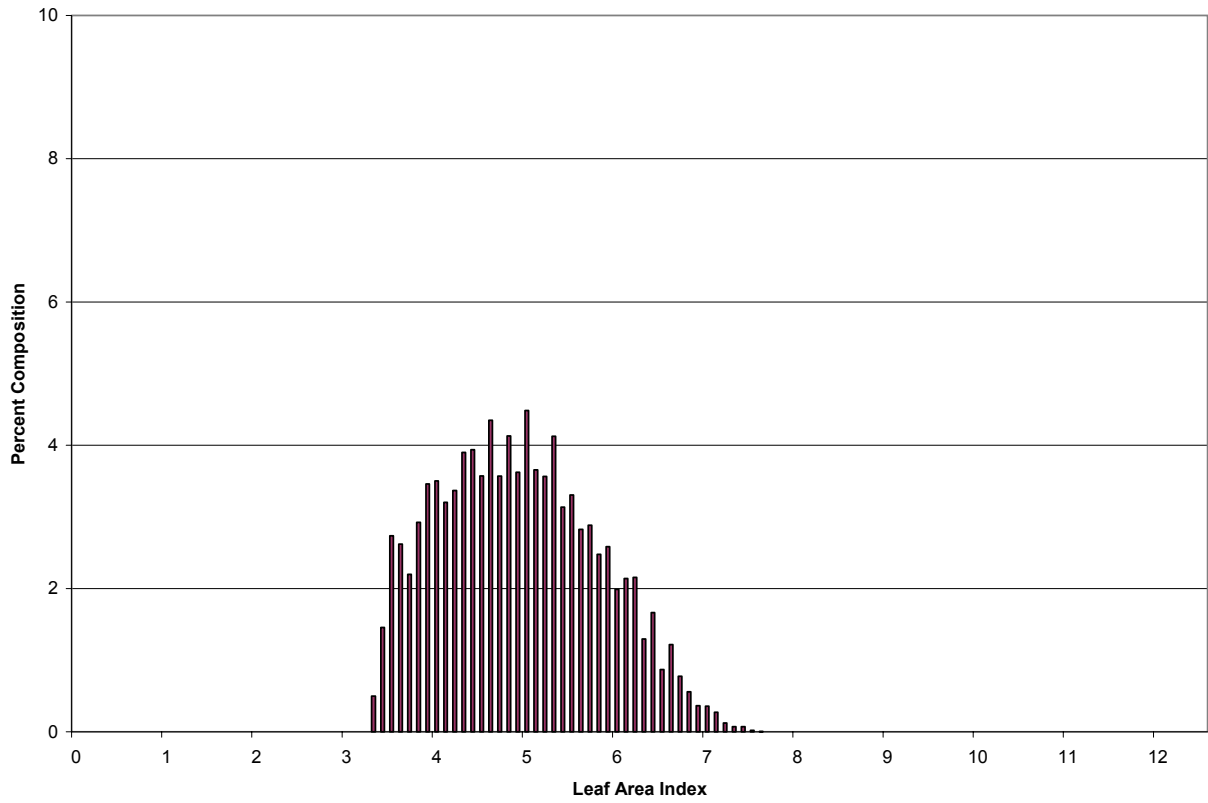
Figure 6.44: Histogram of LAI Estimated Using Modified Normalized Difference Vegetation Index Values from SPOT Imagery at 20m Spatial Resolution
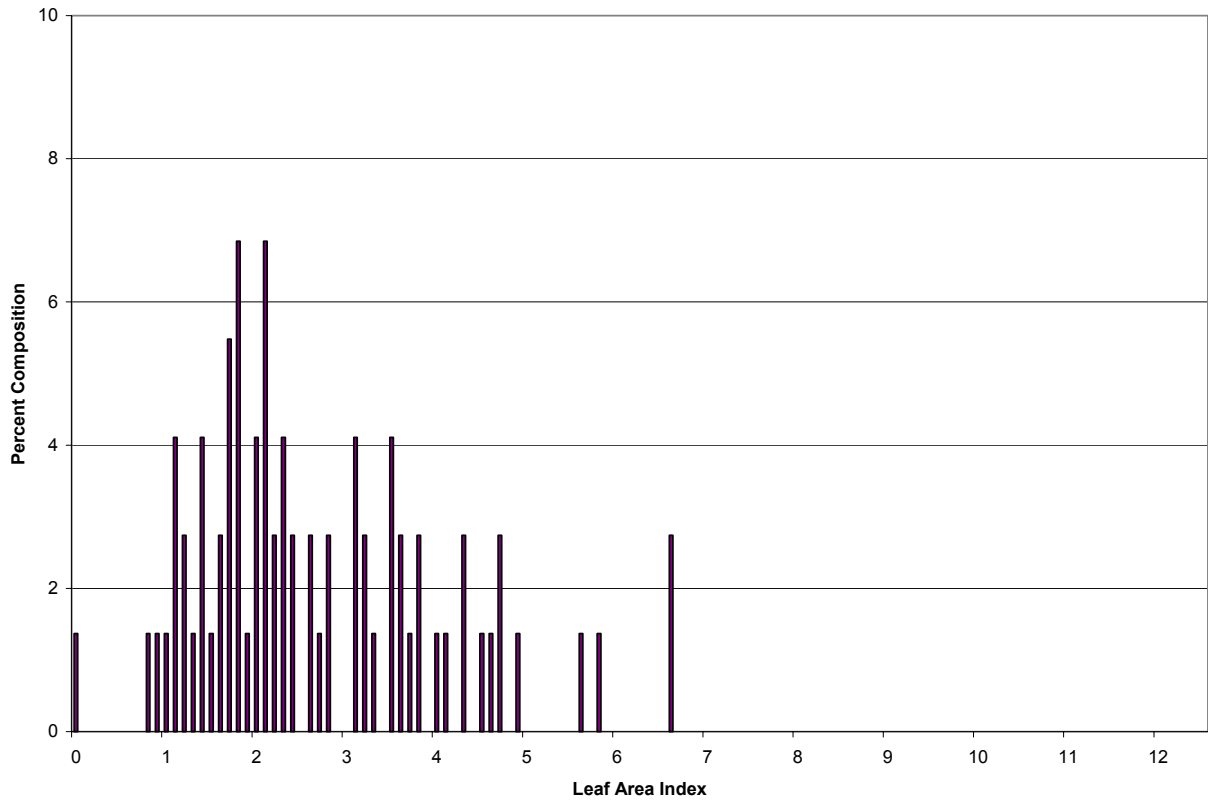
Figure 6.45: Histogram of LAI Estimated Using Canopy Shadow Fraction Values from MODIS Imagery
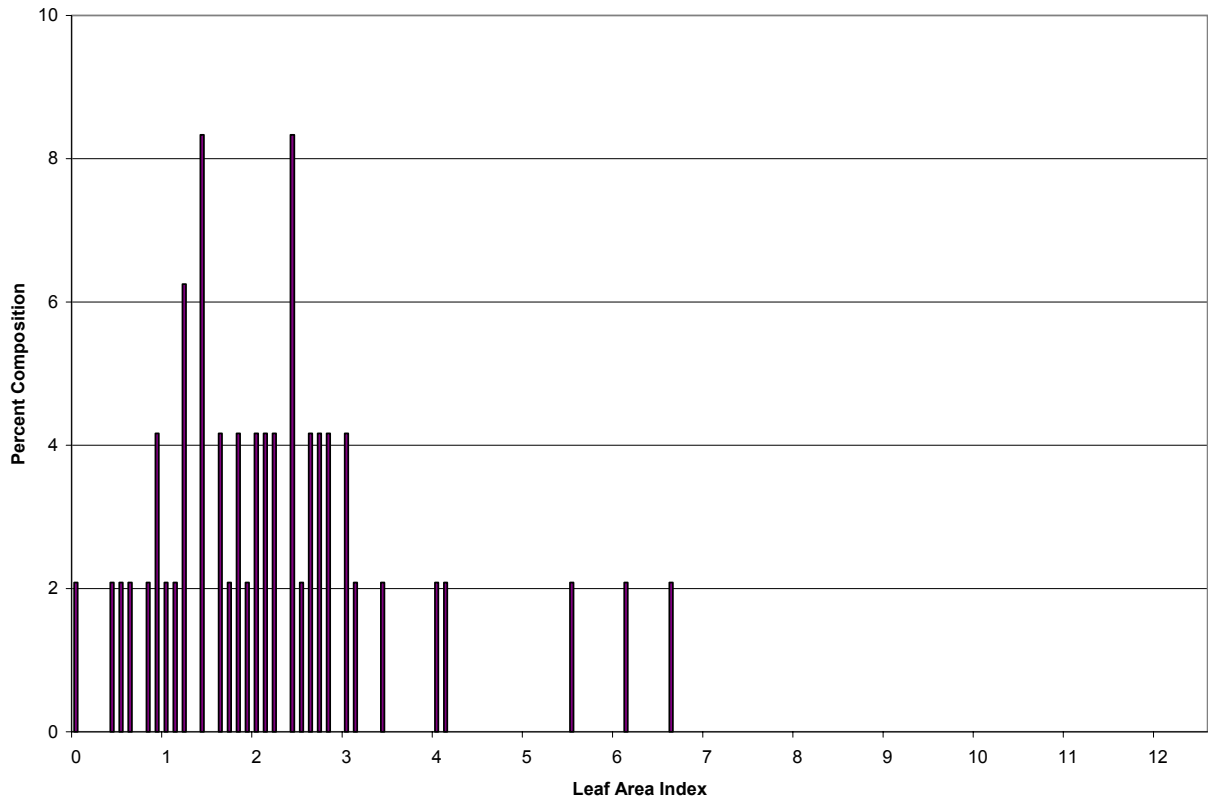
Figure 6.46: Histogram of LAI Estimated Using Canopy Shadow Fraction Values from SPOT Imagery at 1200 m Spatial Resolution
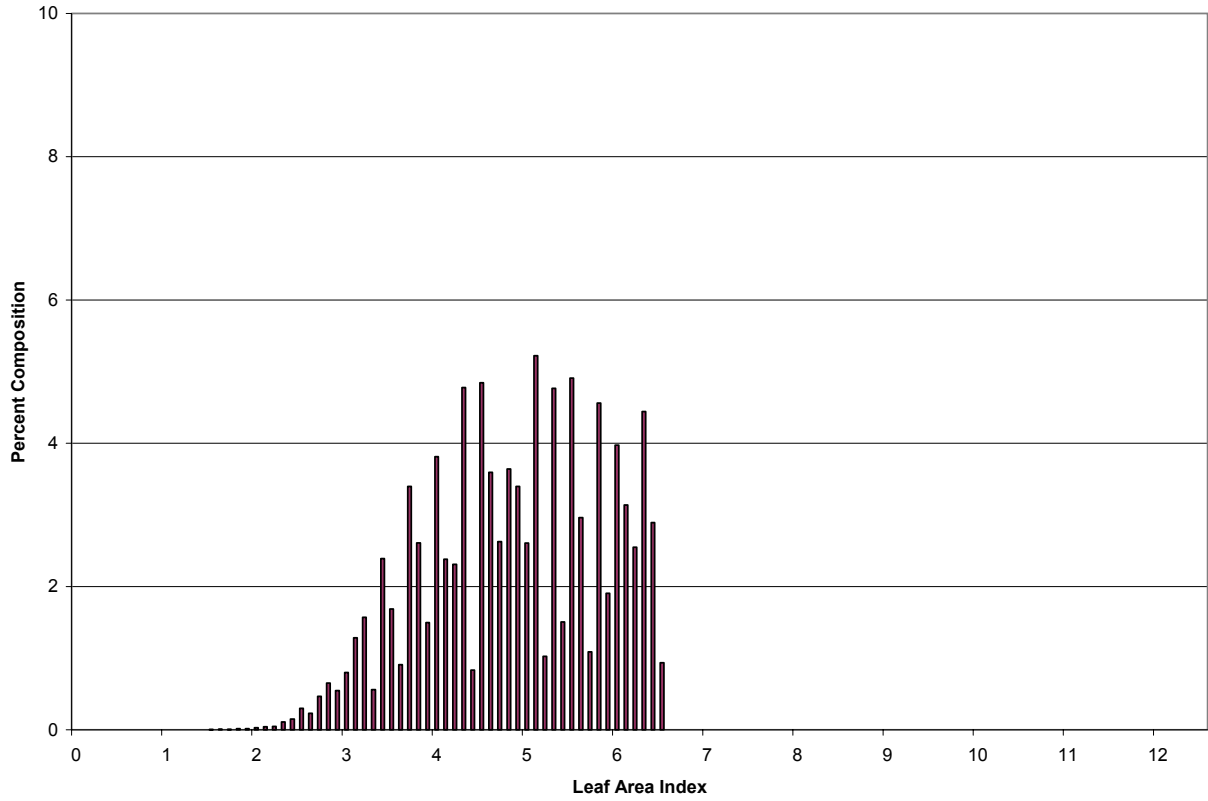
Figure 6.47: Histogram of LAI Estimated Using Canopy Shadow Fraction Values from SPOT
Imagery at 20 m Spatial Resolution
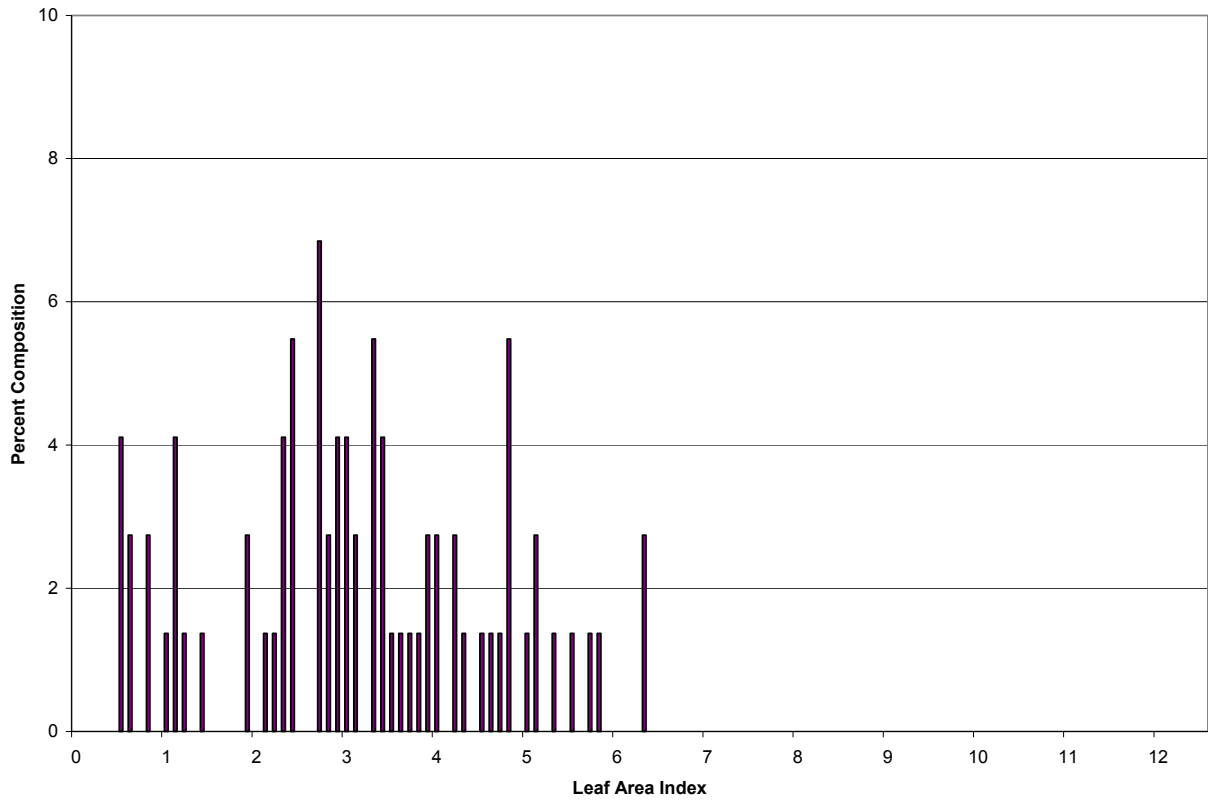
Figure 6.48: Histogram of LAI Estimated Using Normalized Distance Values from MODIS Imagery
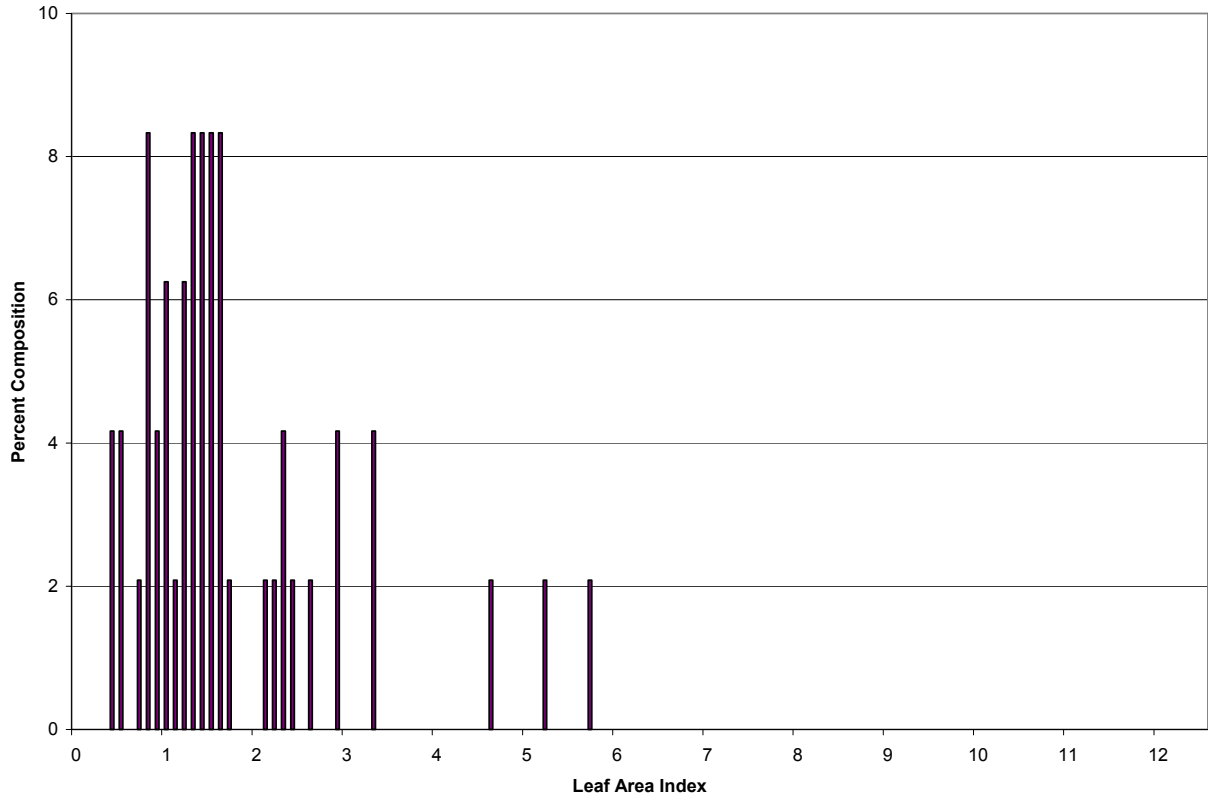
Figure 6.49: Histogram of LAI Estimated Using Normalized Distance Values from SPOT Imagery at 1200m Spatial Resolution

206
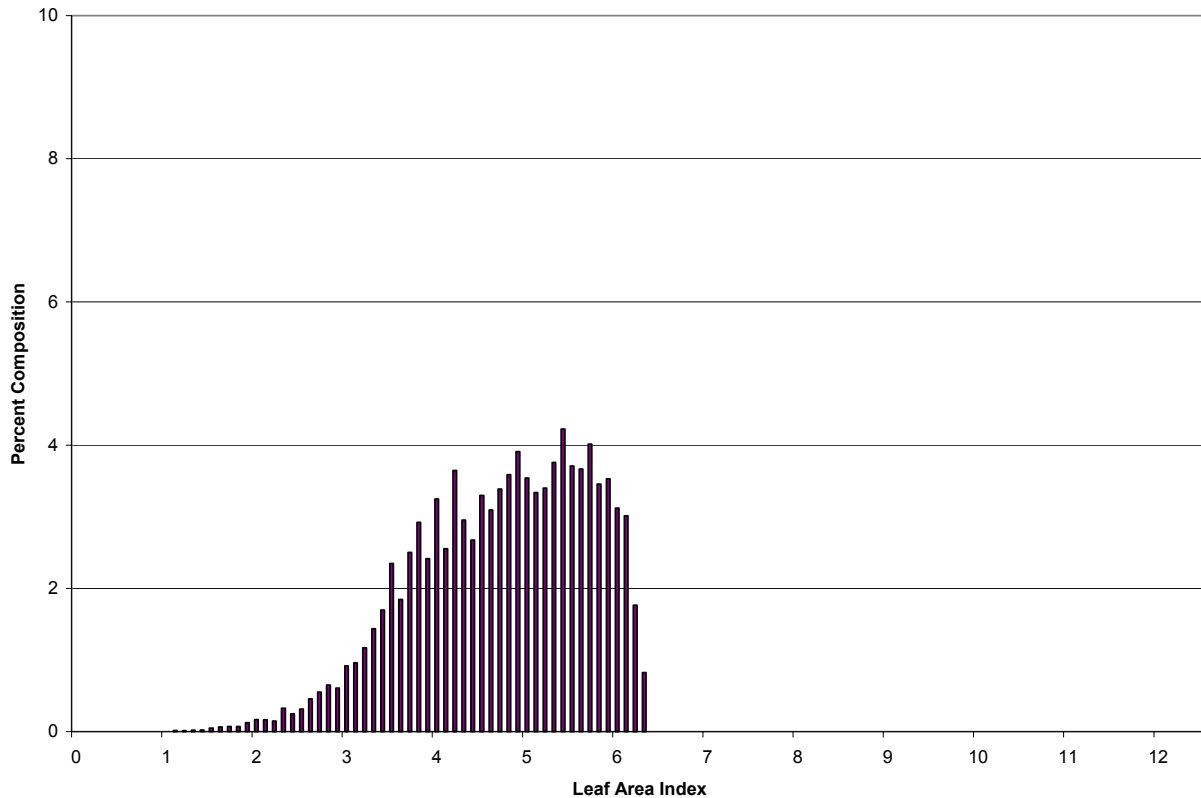
Figure 6.50: Histogram of LAI Estimated Using Normalized Distance Values from SPOT Imagery at 20m Spatial Resolution

The histograms of the functions appear much less smooth when compared to the broadleaf case. This is likely due to the nature of the estimation models and their requirement for robust endmember selection. As sample sizes decrease and spatial agglomeration effects contribute to increasingly mixed pixels the ability to define reasonable endmembers decreases markedly and likely contributes to the degraded LAI estimates for needleleaf vegetation derived from imagery with coarser spatial resolution.

In similar fashion to the broadleaf case, a χ^2 goodness-of-fit test is performed to quantitatively compare the frequency distributions of LAI of each image. For needleleaf vegetation the χ^2 test found that the LAI distributions o are significantly different at a level of significance of 0.05 with two degrees of freedom between each of the coarser resolution images and the original SPOT image.

The scale dependence of the measurements can again be evaluated through a geostatistical analysis of the input modeling parameters as in Figures 6.51 through 6.56.
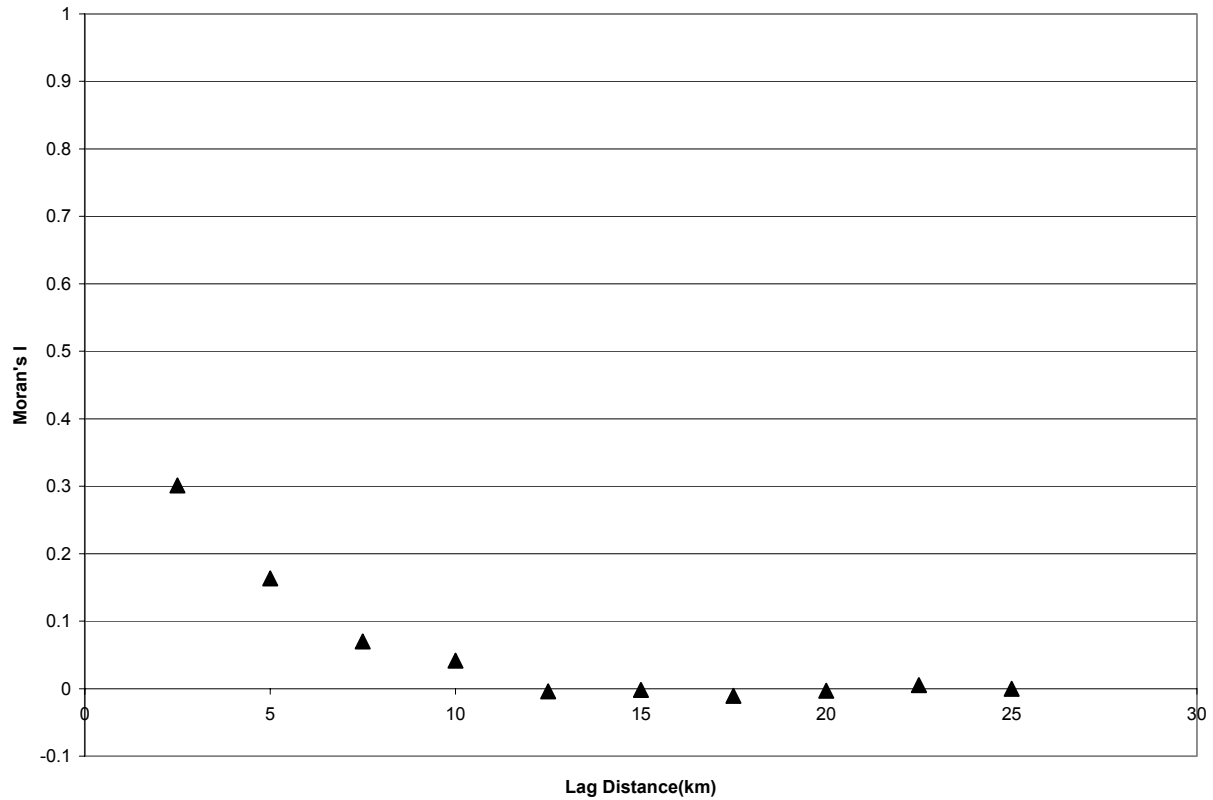
Figure 6.51: Plot of Moran's I versus Lag Distance for Shadow Fraction Values Computed from MODIS data
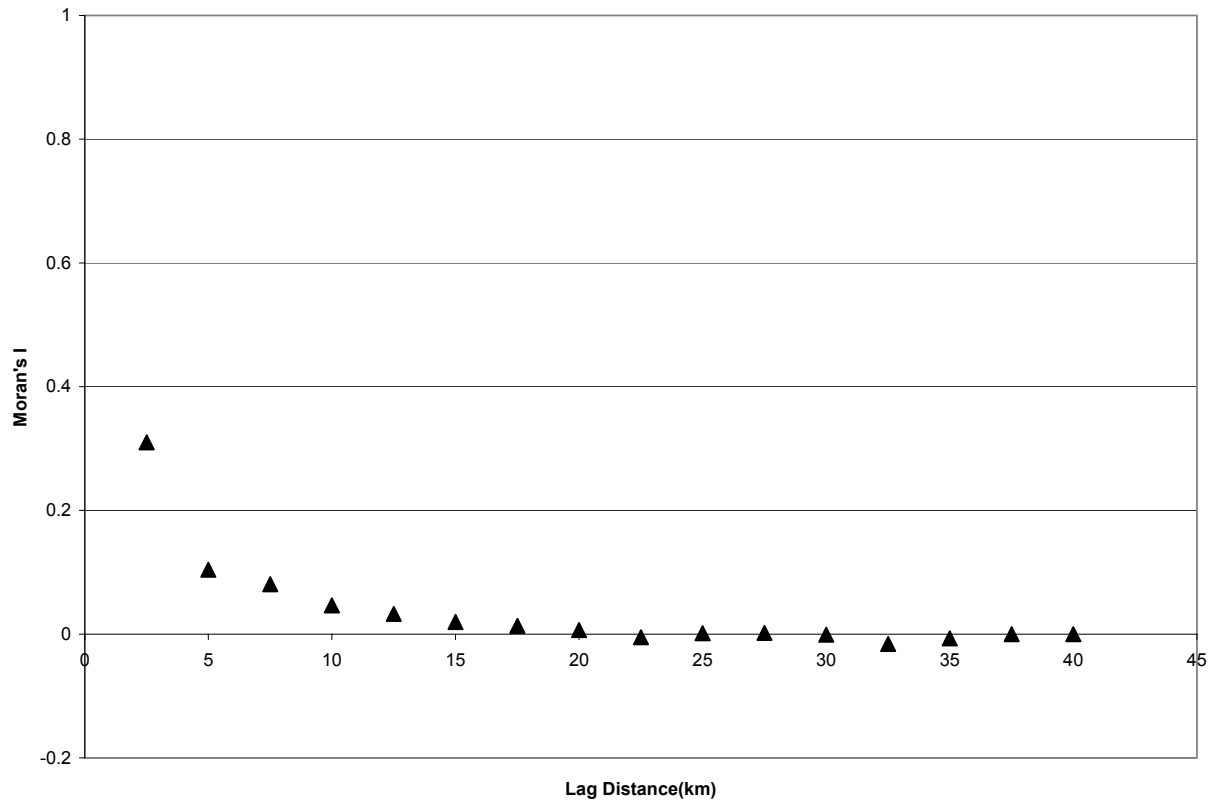
Figure 6.52: Plot of Moran's I versus Lag Distance for Shadow Fraction Values Computed from SPOT Imagery at 1200m Spatial Resolution
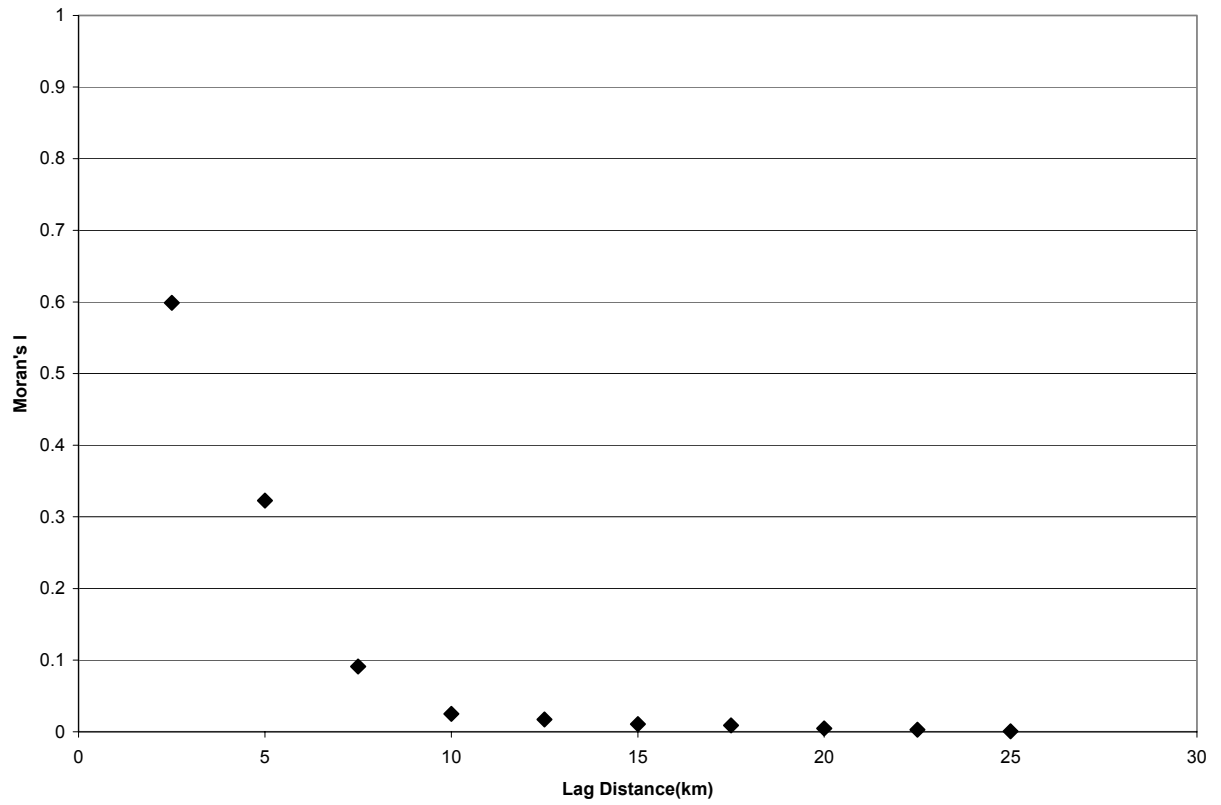
Figure 6.53: Plot of Moran's I versus Lag Distance for Modified Normalized Difference Vegetation Index Values Computed from MODIS data
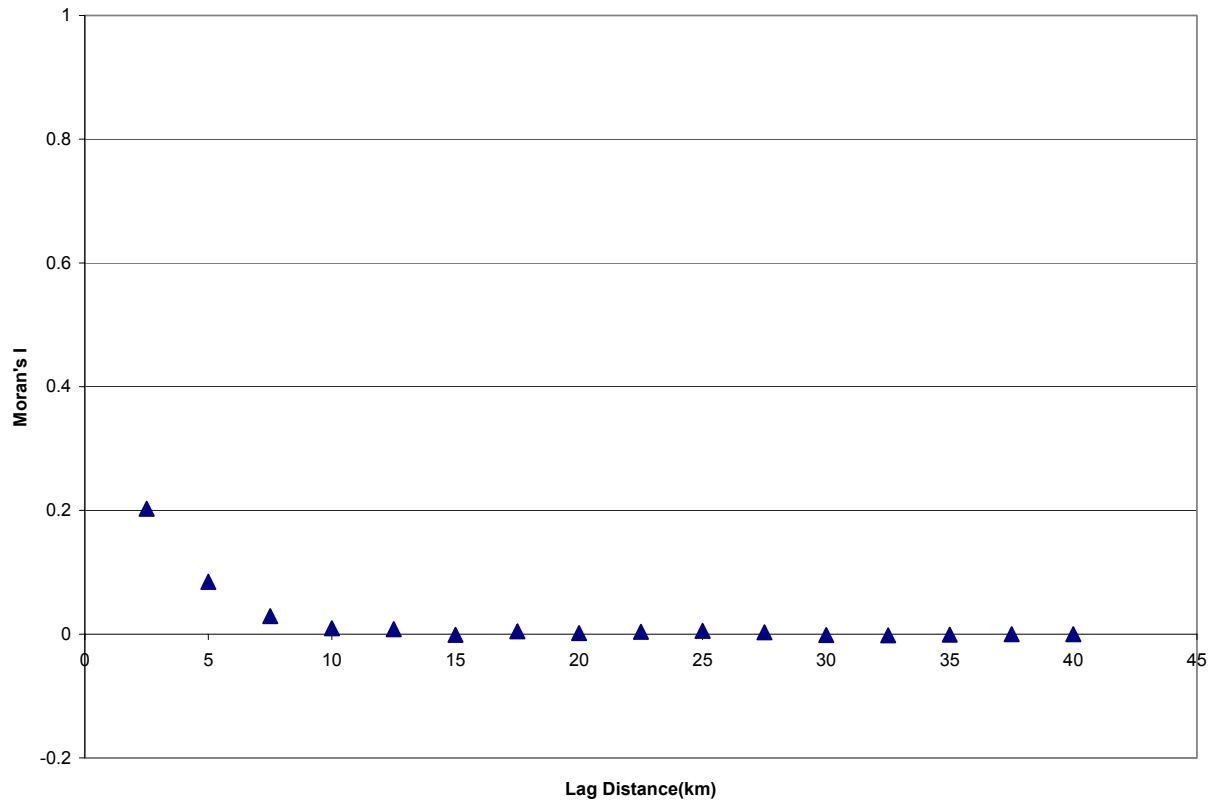
Figure 6.54: Plot of Moran's I versus Lag Distance for Modified Normalized Difference Vegetation Index Values Computed from SPOT Imagery at 1200m Spatial Resolution
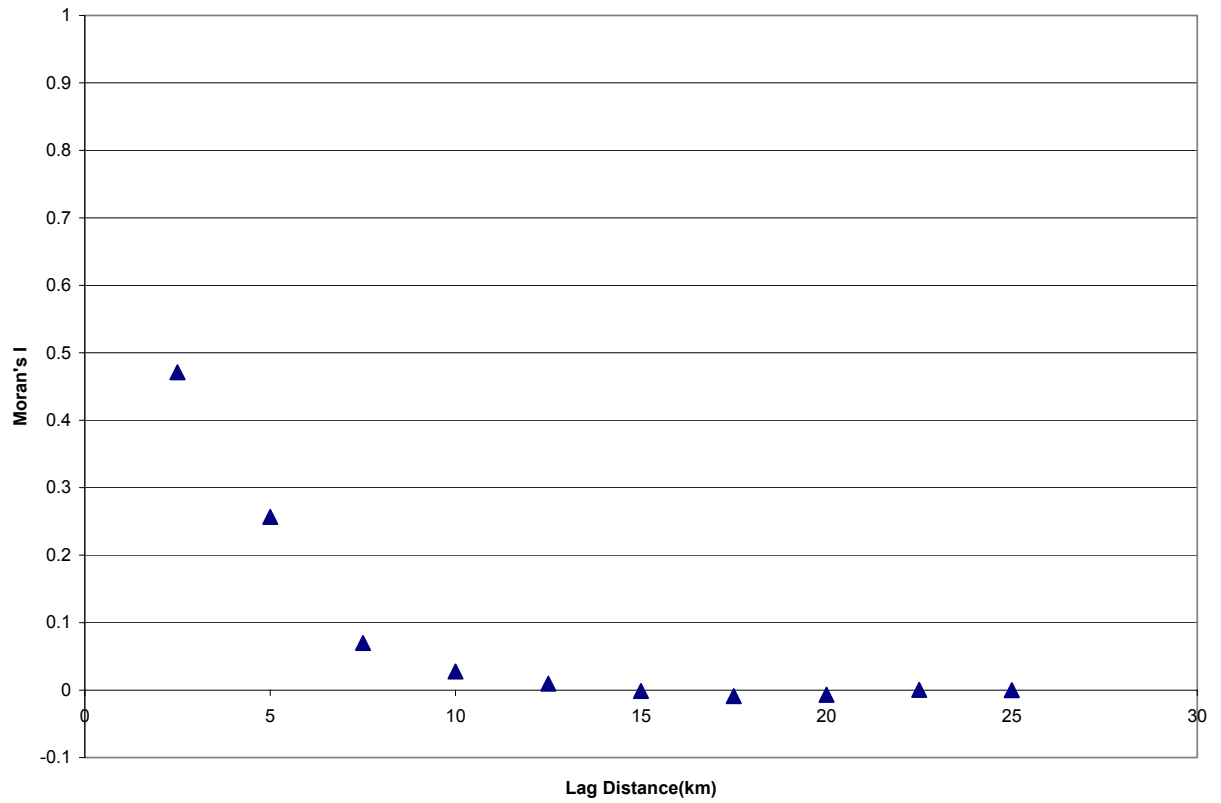
Figure 6.55: Plot of Moran's I versus Lag Distance for Normalized Distance Values Computed from MODIS data
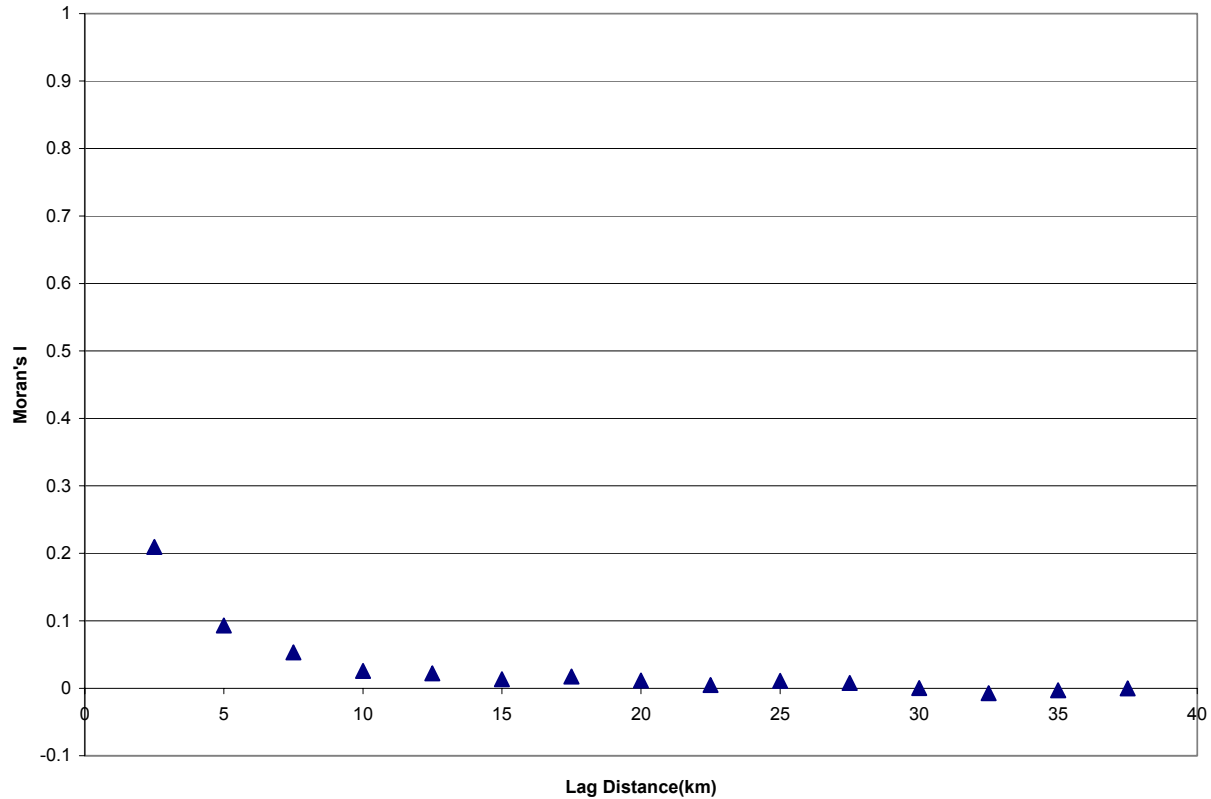
Figure 6.56: Plot of Moran's I versus Lag Distance for Normalized Distance Values Computed from SPOT Imagery at 1200m Spatial Resolution

These figures demonstrate the same decreasing trend as the original modeling parameters did for the original SPOT data at 20m spatial resolution. It is evident that complete spatial randomness is achieved at a much higher value of lag distance than for the initial SPOT image. It is also evident that strong correlation is observed between certain input modeling parameters for coarser spatial resolution at values of lag distance for which complete spatial randomness is achieved in the original SPOT image. In similar fashion to the broadleaf case this variation in the range observed between the coarser and finer spatial resolution imagery is indicative that the processes determining the observed values of the input modeling parameters are scale dependent. This scale dependence arises from factors such as increasing sub-pixel heterogeneity and increasingly heterogeneous properties of vegetation spectra as sampling intervals coarsen.

7 Conclusions and Recommendations

7.1 Conclusions

There are several conclusions which can be drawn from the results obtained in this study and the implications which they possess for further applications of, and research related to, remote LAI estimation.

7.1.1 General Conclusions

One conclusion that can be drawn from the results obtained in this study is that the selection of an appropriate method for the remote LAI estimation is, to a large extent, application and resource dependent. The advantages exhibited by the modified spectral vegetation indices are their robust modeling of both needleleaf and broadleaf vegetation and their ease of use. The linear spectral mixture analysis method, despite the difficulties it possesses related to the subjectivity of end-member selection, outperformed all the modified spectral vegetation index models derived for needleleaf vegetation. The normalized distance technique, despite the considerable promise it has demonstrated in remote LAI estimation for both broadleaf and needleleaf vegetation in this study, requires further validation before it can be concluded to exhibit generally superior LAI estimates. Therefore, model selection must be made on the basis of factors such as the required accuracy of LAI estimation, resource availability and composition of the landscape in question.

7.1.2 Conclusions Related to Remote Sensing

One conclusion that is evident from the results of this study is that the observed reflectance properties associated with a pixel can be substantially influenced by the background spectral properties, particularly in forested areas of reduced crown closure. This phenomenon is made apparent in the needleleaf vegetation by the counter-intuitive decrease in each of the normalized differenced vegetation index, simple ratio and near infrared reflectance. This deviation from the results obtained in similar studies (Spanner *et al.,* 1990) is indicative of the presence of a leafy

understory, which is visible to the sensor and introduces bias into the measurements. A corollary to this conclusion is that any relationships for remote LAI estimation that have been presented in literature for a particular environment have the potential to be invalid for different environments or epochs unless explicit techniques have been applied to account for the influence of understory or background conditions.

A second conclusion that can be drawn from the remote estimation relationships is that similar to results obtained in literature (Fernandes *et al.,* 2004), structural regressions generally exhibited increased modeling robustness when compared to the results of standard linear regression. The enhanced capabilities of power relationships versus their linear counterparts are most importantly demonstrated for the input parameters which exhibited the strongest relationships with LAI. In addition to the enhanced modeling robustness structural regressions result in LAI estimates that possess physically meaningful lower boundaries. Possible disadvantage to the use of power relationships is their non-linear transformation of the distribution associated with the input modeling parameters when used for LAI estimation and rapid divergence in application environments for which the models are ill-suited.

A third conclusion is that reflectance information in the middle-infrared portion of the electromagnetic spectrum can substantially contribute to remote LAI estimation. For both needleleaf and broadleaf vegetation the most robust and accurate estimation relationships incorporated the middle-infrared bands in some capacity. This is particularly evident in the results achieved by the modified spectral vegetation index method, when the modified indices are compared to their unadjusted counterparts. The marked improvement in the ability to model LAI from the original spectral vegetation indices to the modified spectral vegetation indices is indicative of the substantial information contained in the middle-infrared band.

One final conclusion that can be reached based on the results in Chapter 5 is that the linear spectral mixture analysis method appears to be relatively insensitive to the method of determination of the background member spectrum. This conclusion is important because if it possesses general validity it removes the necessity for *in-situ* sampling of background reflectance. The general validity of this conclusion would permit people without access to *in-situ* spectroradiometers to

implement these models without constraint.

7.1.3 Conclusions Related to Sensitivity Analysis

7.1.3.1 Monte Carlo Sensitivity Analysis

One conclusion derived from the results of the Monte Carlo sensitivity analysis is that, almost irrespective of the accuracy and precision associated with a remote model, the quality of the solution for a mean value of LAI across a landscape is constrained by the size and inherent variability of that landscape in terms of LAI Although these constraints can be estimated and ,to some extent, mitigated, particularly as this relates to the anticipated mean error, the resulting accuracy and precision of regional LAI estimates will always be limited by these factors.

7.1.3.2 Spatial Statistics

Despite the fact that the degree of spatial correlation observed between values of the various modeling parameters at a variety of lag distances is in all cases relatively uniform, certain conclusions can be drawn. It is evident from the analysis that the highest degrees of spatial correlation with a pixel and its nearest neighbors are observed for the unmodified spectral vegetation indices in both the broadleaf and needleleaf cases. As the unmodified spectral vegetation indices generally exhibit the least robustness in LAI modeling, these results are indicative as to the reason for this. This modeling deficit for the unadjusted spectral vegetation indices versus the adjusted spectral vegetation indices is likely attributable to the variability of these indices for adjacent pixels possessing different LAI values. This greater sensitivity to variations observed between a pixel and its nearest neighbors for the modified spectral vegetation indices is indicative of the enhanced capability of these indices to capture variations in leaf area. One codicil to this enhanced modeling is that due to the lessened degree of spatial correlation, greater accuracy may be required in the determination of the location of the plots. Another feature of interest is the decreased ranges associated with the unmodified spectral vegetation indices, which are exceeded by those of the modified spectral vegetation indices for both needleleaf and

broadleaf vegetation. It is evident from the results presented that the incorporation of additional information from the middle infrared bands lengthens the distance over which the values of these modeling parameters remain correlated. This may be indicative of the robustness in these parameters that although they initially exhibit less correlation, underlying correlations do exist. These underlying correlations could be attributable to the ability of these parameters to model some underlying large-scale vegetation process, such as moisture transfer, in a way which improves their modeling over those exhibited by the modeling parameters which do not incorporate middle infrared data.

7.1.3.3 Multi-Scale Analysis

Through an examination of the degree of spatial correlation in the modeling parameters at different scales it is possible to conclude how the results of analysis vary with scale and determine whether it is either advisable to conduct analysis at another spatial resolution.

One conclusion is that the LAI estimation relationships are both scale dependent and sensor specific. Therefore applying the relationships derived for SPOT directly to MODIS imagery is unadvisable. This conclusion is supported by LAI estimates from MODIS data not following the same distribution as those for SPOT for needleleaf and broadleaf vegetation. Even applying the relationships derived for SPOT at a given scale to SPOT imagery resampled to another scale causes degradation of the precision and accuracy associated with the estimation model.

Another conclusion derived from the multi-scale analysis is that the input modeling parameters used in this study exhibit spatial correlation over a variety of lag distances and that these relationships are highly dependent on the spatial resolution of the imagery. This is evident from the comparison of the spatial statistical analysis of the input parameters from coarser resolution imagery against those of the initially derived parameters from finer scale imagery. Coarser resolution imagery evidences spatial correlation over lag distances where the initial SPOT imagery has already deteriorated into complete spatial randomness.

7.2 Recommendations

After reviewing the conclusions of the success and achievements of this research relative to its initial goals, there are several pertinent recommendations for those wishing to conduct further research related to the remote LAI estimation. Recommendations are also provided for those wishing to apply similar methods to those utilized within this study to obtain LAI estimates to serve as input parameters to process models of various types.

7.2.1 Recommendations Related to Remote LAI Estimation

One recommendation for further research, regarding remote LAI estimation is to expand the current focus from LAI estimation for pure stands to LAI estimation for stands composed of heterogeneous vegetation types. This would involve the performance of *in-situ* LAI measurements in forests within heterogeneous stands of both needleleaf and broadleaf vegetation. T techniques such as spectral mixture analysis or fuzzy classification could then be implemented within the plots to determine the relative composition of each vegetation type. These composition estimates could then be used to estimate LAI.

Another recommendation for further research is the further investigation of linear spectral mixture analysis techniques for broadleaf vegetation. To have observed such a disparity between the efficacy of linear spectral mixture analysis between vegetation types is intriguing and further investigation is necessary to determine whether these results are anomalous or are indicative of an underlying effect that limits linear spectral mixture analysis in broadleaf canopies. The observed inefficacy of linear spectral mixture analysis may be due to non-linear scattering in broadleaf canopies, which should be investigated.

It is also recommended that investigations be performed related to the use of remote LAI estimates in climatic and environmental models, particularly related to gas-exchange. Similar sensitivity analyses to those conducted for hydrological models could help to determine the sensitivity of these models to error in LAI estimates and whether the current techniques yield sufficient accuracy for their utilization as input parameters in such models.

Comparison of spatial correlation values for various modeling parameters over a range of spatial scales allows for the determination of whether an optimal scale for analysis exists and to select an appropriate scale for analysis given the constraints of the implementation. Further investigations to determine robust relationships at coarser scales could be generated through the use of estimation models at higher resolution with a subsequent downsampling and regression analysis similar to that performed in chapters 5 and 6.

7.2.2 Recommendations Related to Use of Remote LAI Estimates in Process Models

The most important recommendation for users of remote estimation techniques who are wishing to obtain LAI estimates for input into process models is that they be cognizant of the limitations and the requirements of the estimation techniques and the process models.

The relevant application of a remote estimation model is limited by the degree of sensor-specificity and scale dependence it exhibits. Therefore, it is recommended that investigation be performed as to the scale-dependence of that model, prior to its use for a landscape. If any model is to be applied on a different sensor than the one for which it has originally been derived the performance of a comparison is recommended to examine the variability of modeling parameters given any differences between the two imaging systems.

In order for meaningful results to be obtained for a process model, input parameters require a certain degree of accuracy and precision. It is recommended that when any process model is selected for application that the user be acquainted with the accuracy and precision required for LAI estimates within that model. It is then recommended that the user examine the factors influencing the quality of the specified estimation model over the landscape in question to determine whether that particular model will provide LAI estimates that satisfy the accuracy and precision requirements necessitated by the process model.

8 Bibliography

Alavi, G., Jansson,P., Hallgren,J. and Bergholm,J. "Interception of a Dense Spruce Forest, Performance of a Simplified Canopy Water Balance Model." <u>Nordic Hydrology</u> 32 4/5 (2001): 265-284.

Bailey, T. and Gatrell, A. <u>Interactive Spatial Data Analysis.</u> Essex: Pearson Education Press, 1995.

Baldocchi, D., Hicks, B. and Camara,P. "A Canopy Stomatal Resistance Model for Gaseous Deposition to Vegetated Surfaces." <u>Atmospheric Environment</u> 21 1 (1987):91-101.

Baret, F. and Guyot, G. "TSAVI: A Vegetation Index which Minimizes Soil Brightness Effects on LAI and APAR Estimation." <u>Proceeding of the 12th Canadian Symposium on Remote Sensing</u> 3 (1989): 1355-1358

Baret, F. and Guyot, G. "Potentials and Limits of Spectral vegetation indices for LAI and APAR Assessment." <u>Remote Sensing of Environment</u> 35 (1991): 161-173.

Barclay, H. "Conversion of Total Leaf Area to Projected Leaf Area in Lodgepole Pine and Douglas Fir." <u>Tree Physiology</u> 18 (1998): 185-193.

Bouman, B. "Accuracy of Estimating the LAI from Spectral vegetation indices Derived from Crop Reflectance Characteristics, a Simulation Study" <u>International Journal of Remote Sensing</u> 13 16 (1992): 3069-3084.

Bonan, G. "Importance of LAI and Forest Type when Estimating Photosynthesis in Boreal Forests." <u>Remote Sensing of Environment</u> 43 (1993): 303-314.

Brown, L., Chen, J., Leblanc, S. and Cihlar, J. "A Shortwave Infrared Modification to the Simple Ratio for LAI Retrieval in Boreal Forests: An Image and Model Analysis." <u>Remote Sensing of Environment</u> 71 (2000): 16-25.

Carlyle-Moses,D. and Price,A. "An Evaluation of the Gash Interception Model in a Northern Hardwood Stand." Journal of Hydrology 214 (1999): 103-110.

Chen, J. "Canopy Architecture and Remote Sensing of the Fraction of Photosynthetically Active Radiation Absorbed by Boreal Conifer Forests." IEEE Transactions on Geoscience and Remote Sensing 34 6 (1996): 1353-1368.

Chen, J. "Evaluation of Spectral vegetation indices and a Modified Simple Ratio for Boreal Applications." Canadian Journal of Remote Sensing 22 3 (1996): 229-242.

Chen, J. and Cihlar, J. "Quantifying the Effect of Canopy Architecture on Optical Measurements of LAI Using Two Gap Size Analysis Methods." IEEE Transactions on Geoscience and Remote Sensing 33 3 (1995): 777-787.

Clevers, J. "The Application of a Weighted Infrared-Red Vegetation Index for Estimating Leaf Area Index by Correcting for Soil Moisture." Remote Sensing of Environment 29 (1989): 25-37.

Eklundh,L., Hall, K., Eriksson, H., Ardo, J. and Pilesjo, P. "Investigating the Use of Landsat Thematic Mapper Data for Estimation of Forest LAI in Southern Sweden." Canadian Journal of Remote Sensing 29 3 (2003): 349-362.

Eklundh, L., Harrie, L. and Kuusk A. "Investigating Relationships between Landsat ETM+ Sensor Data and LAI in a Boreal Conifer Forest." Remote Sensing of Environment 78 (2001): 239-251.

Environment Canada, "Canadian Climate Normals 1971-2000." 22 Feb, 2004. 24 March, 2005. http://www.climate.weatheroffice.ec.gc.ca/climate_normals

Fernandes, R., Miller, J., Chen, J. and Rubinstein, I. "Evaluating Image-Based Estimates of LAI in Boreal Conifer Stands over a Range of Scales Using High-Resolution CASI Imagery." Remote Sensing of Environment 89 (2004): 200-216.

Fernandes, R., Miller, J., Hu, B. and Rubinstein, I. "A Multi-Scale Approach to Mapping Effective LAI in Boreal Picea Mariana Stands Using High Spatial Resolution CASI Imagery." <u>International Journal of Remote Sensing</u> 23 18 (2002): 3547-3568.

Franklin, S., Lavigne, M., Deuling, M., Wulder,M. and Hunt, E. "Estimation of Forest LAI Using Remote Sensing and GIS Data for Modeling Net Primary Production." <u>International Journal of Remote Sensing</u> 18 16 (1997): 3459-3471.

Friedl, M., Davis, F., Michaelsen, J. and Moritz, M. "Scaling and Uncertainty in the Relationship Between the NDVI and Land Surface Biophysical Variables: An Analysis Using a Scene Simulation Model and Data from FIFE." <u>Remote Sensing of Environment</u> 54 (1995): 233-246.

Gower, S. and Norman, J. "Rapid Estimation of LAI in Conifer and Broad-Leaf Plantations." <u>Ecology</u> 72 5 (1991): 1896-1900.

Gower, S., Kucharik, C. and Norman,J. "Direct and Indirect Estimation of LAI, f_{APAR} and Net Primary Production of Terrestrial Ecosystems." <u>Remote Sensing of Environment</u> 70 (1999): 29-51.

Gluck, M. and Rempel, R. "The Effect of Spatial Resolution on Landscape Measurements of Post Disturbance Vegetation." <u>EARSEL Advances in Remote Sensing</u> 4 4 (1996): 170-176

Hall, R., Davidson, D. and Peddle, D. "Ground and Remote Estimation of Leaf Area Index in Rocky Mountain Forest Stands, Kananaskis, Alberta." <u>Canadian Journal of Remote Sensing</u> 29 3 (2003): 411-427.

Hedstrom,N. and Pomeroy,J. "Measurements and Modeling of Snow Interception in the Boreal Forest" <u>Hydrological Processes</u> 12 (1998): 1611-1625.

Henry, J. <u>Canada's Boreal Forest.</u> Washington: Smithsonian Institution Press, 2002.

Hu, B., Miller, J., Chen, J. and Hollinger, A. "Retrieval of the Canopy LAI in the BOREAS Flux Tower Sites Using Linear Spectral Mixture Analysis" <u>Remote Sensing of Environment</u> 89 (2004): 176-188.

Huber, A. and Iroume, A. "Variability of Annual Rainfall Partitioning for Different Sites and Forest Covers in Chile." <u>Journal of Hydrology</u> 248 (2001): 78-92.

Huete, A. "A Soil-Adjusted Vegetation Index (SAVI)" <u>Remote Sensing of Environment</u> 25 (1988): 295-309.

Jordan, C. "Derivation of Leaf Area Index from Quality of Light on the Forest Floor." <u>Ecology</u> 50 (1969) : 663-666.

Kergoat, L. "A Model for Hydrological Equilibrium of LAI on a Global Scale." <u>Journal of Hydrology</u> 212-213 (1998):268-286.

Kite,G. and Spence,C. "Land Cover, NDVI, LAI and Evapotranspiration in Hydrological Modeling" <u>Application of Remote Sensing in Hydrology (Proceedings of the Second International Workshop NHRI Symposium</u> 14 October (1994): 223-239.

Kogan,F., Gitelson,A.,Zakarin,E., Spivak, L. and Lebed,L. "AVHRR-Based Spectral Vegetation Index for Quantitative Assessment of Vegetation State and Productivity: Calibration and Validation" <u>Photogrammetric Engineering and Remote Sensing</u> 69 8 (2003): 899-906.

Kollenberg, C. and O'Hara, K. "Leaf and Tree Increment Dynamic of Even-Aged and Multi-Aged Lodgepole Pine Stands in Montana" <u>Canadian Journal of Forest Research</u> 29 6 (1999): 687-695

Kucharik, C., Norman, J. and Gower, S. "Measurements of Leaf Orientation, Light Distribution and Sunlit Leaf Area in a Boreal Aspen Forest" <u>Agricultural and Forest Meteorology</u> 91 (1998): 127-148.

Leblanc, S., Chen, J. and Kwong, M. "Tracing Radiation and Architecture of Canopies: Trac Manual" 2.1.3 (2002) 1-25.

Nemani, R., Pierce, L., Running, S. and Band, L. "Forest Ecosystem Processes at the Watershed Scale: Sensitivity to Remotely-Sensed LAI Estimates." International Journal of Remote Sensing 14 13 (1993): 2519-2534.

Peddle, D., Brunke, S. and Hall, F. "A Comparison of Spectral Mixture Analysis and Ten Spectral Vegetation Indices for Estimating Boreal Forest Biophysical Information from Airborne Data." Canadian Journal of Remote Sensing 27 6 (2001):627-635.

Peddle, D., Hall, F. and LeDrew, E. "Spectral Mixture Analysis and Geometric-Optical Reflectance Modeling of Boreal Forest Biophysical Structure." Remote Sensing of Environment 67 (1999): 288-297.

Peddle, D. and Johnson, R. "Spectral Mixture Analysis of Airborne Remote Sensing Imagery for Improved Prediction of LAI in Mountainous Terrain, Kananaskis Alberta." Canadian Journal of Remote Sensing 26 3 (2000):177-188.

Peterson, D., Spanner, M., Running, S. and Teuber, K. "Relationship of Thematic Mapper Simulator Data to LAI of Temperate Needleleaf Forests." Remote Sensing of Environment 22 (1987): 323-341.

Phinn, S., Stow, D. and Van Mouwerik, D. "Remotely Sensed Estimates of Vegetation Structural Characteristics in Restored Wetlands, Southern California." Photogrammetric Engineering and Remote Sensing April (1999): 485-493.

Pierce, L. and Running, S. "Rapid Estimation of Needleleaf Forest LAI Using a Portable Integrating Radiometer." Ecology 69 6 (1988): 1762-1767.

Pomeroy,J., Parviainen, J., Hedstrom,N. and Gray,D. "Coupled Modeling of Forest Snow Interception and Sublimation." <u>Hydrological Processes</u> 12 (1998): 2317-2337.

Pontailler, J., Hymus, G. and Drake, B. "Estimation of LAI Using Ground-Based Remote Sensed NDVI Measurements: Validation and Comparison with Two Indirect Techniques." <u>Canadian Journal of Remote Sensing</u> 29 3 (2003): 381-387.

Price, A., Dunham, K., Carleton, T. and Band, L. "Variability of Water Fluxes through the Black Spruce (*Picea Mariana*): Canopy and Feather Moss (*Pleurozium Schreberi*): Carpet in the Boreal Forest of Northern Manitoba." <u>Journal of Hydrology</u> 196 (1997): 310-323.

Rautiainen,M., Stenberg,P., Nilson, T., Kuusk, A. and Smolander, H. "Application of a Forest Reflectance Model in Estimating LAI of Scots Pine Stands Using Landsat-7 ETM Reflectance Data." <u>Canadian Journal of Remote Sensing</u> 29 3 (2003):314-323.

Richardson, A. and Wiegand, C. "Distinguishing Vegetation from Soil Background Information." <u>Remote Sensing of Environment</u> 8 (1977): 307-312.

Reese, H., Lillesand, T., Nagel,D., Stewart,J., Goldmann,R., Simmons, T., Chipman,J. and Tessar,P. "Statewide Land Cover Derived from Multiseasonal Landsat TM Data A Retrospective of the WISCLAND Project" <u>Remote Sensing of Environment</u> 82 (2002):224-237.

Rock, B., Vogelmann, J., Williams, D., Voglemann and Hoshizaki, T. "Remote Detection of Forest Damage." <u>Bio Science</u> 36 (1986): 439 pp.

Rouse, J., Haas, R., Schell, J. and Deering, D. "Monitoring Vegetation Systems in the Great Plains with ERTS." <u>Proceedings of the Third Earth Resources Technology Satellite-1 Symposium</u> SP-351 (1973) 3010-3017

Running S. and Coughlan J. "A General Model of Forest Ecosystem Processes for Regional Applications. I. Hydrologic Balance, Canopy Gas Exchange and Primary Production Processes." Ecological Modeling 42 (1988): 125-154.

Running, S. and Gower, S. "FOREST-BGC, A General Model of Forest Ecosystem Processes for Regional Applications: II. Dynamic Carbon Allocation and Nitrogen Budgets." Tree Physiology 9 (1991): 147-160.

Schlerf, M., Atzberger, C., Vohland, M., Buddenbaum, H., Seeling, S. and Hill, J. "Derivation of Forest LAI from Multi- and Hyperspectral Remote Sensing Data." *New Strategies for European Remote Sensing,* Ed. Oluik, Rotterdam: Millipress, 2005, 253-261.

Seed, E. and King, D. "Shadow Brightness and Shadow Fraction Relations with Effective LAI: Importance of Canopy Closure and View Angle in Mixedwood Boreal Forest." Canadian Journal of Remote Sensing 29 3 (2003): 324-335.

Spanner,M., Pierce,L., Peterson,D. and Running,S. "Remote Sensing of Temperate Needleleaf Forest LAI: The Influence of Canopy Closure, Understory Vegetation and Background Reflectance." International Journal of Remote Sensing 11 1 (1990): 95-111.

Stenberg, P., Nilson, T., Smolander, H. and Voipio, P. "Gap Fraction Based Estimation of LAI in Scots Pine Stands Subjected to Experimental Removal of Branches and Stems." Canadian Journal of Remote Sensing 29 3 (2003): 363-370.

Van Dijk,A. and Bruijnzeel,L. "Modeling Rainfall Interception by Vegetation of Variable Density Using an Adapted Analytical Model: Part 1. Model Description." Journal of Hydrology 247 (2001): 230-238.

Videma, O., Garcia-Haro, J. and Segarra, D. "Monitoring Forest Regrowth Rates After Fires with Multitemporal Landsat TM Imagery." EARSEL Advances in Remote Sensing 4 4 (1996):

145-154.

Walsh,S., Moody,A., Allen, T. and Brown,D. "Scale Dependence of NDVI and Its Relationship to Mountainous Terrain". *Scale and Remote Sensing and GIS*, Ed. Quattrochi, D and Goodchild, M., Boca Raton: Lewis Publishers,1997. 27-55.

Walter,J.,Fournier,R., Soudani,K. and Meyer,E. "Integrating Clumping Effects in Forest Canopy Structure: An Assessment through Hemispherical Photographs." <u>Canadian Journal of Remote Sensing</u> 29 3 (2003): 388-410.

Watson, D. "Comparative Physiological Studies on the Growth of Field Crops: I. Variation in Net Assimilation Rate and Leaf Area between Species and Varieties and within and between Years." <u>Annals of Botany</u> 41 (1947): 41-76.

Watson,J., Vertessy, R. and Grayson,R. "Large-Scale Modeling of Forest Hydrological Processes and Their Long-Term Effect on Water Yield." <u>Hydrological Processes</u> 13 (1999): 689-700

Zhang,L., Moran, M. and Brook,J. "A Comparision of Models to Estimate In-Canopy Photosynthetically Active Radiation and their Influence on Canopy Stomatal Resistance" <u>Atmospheric Environment</u> 35 26 (2001): 4463-4470.

Appendix A: Plot Location Algorithm Code

```
/////////////////////////////////////////////////////////////////////////////////////////////////////////////////////////////////////////
// Filename:Main.cpp
// Author:David McAllister
// Date:October 6,2004

#include "Matrix.hpp"
#include "Functions.h"

void main()
{
    //Define the output file streams
    ofstream out1;
    out1.open("Final.txt");
    out1.setf(ios::fixed);
    out1.setf(ios::showpoint);
    out1.precision(2);

    //Reads in the input file matrix of initial corner coordinates
    char *cFileName="Coords.txt";
    Matrix<double> mdCoords= mdReadIn(cFileName);
    mdCoords.redim(mdCoords.nRows()+1,mdCoords.nCols());
    mdCoords[mdCoords.nRows()-1][0]=mdCoords[0][0];
    mdCoords[mdCoords.nRows()-1][1]=mdCoords[0][1];

    //Compute mean azimuth and orient ourselves toward the corner
    double dAzimuth=dGetAzimuth(mdCoords);
    dAzimuth-=dPi/4.0;

    double dX=0.0;
    double dY=0.0;
    double dDist=pow(1800,0.5);
    double dArea=dPolArea(mdCoords);
    int iRowCount=0;

    //Determine the centroid coordinates
    for(int iRow=0;iRow<mdCoords.nRows()-1;iRow++)
    {

    dX=dX+(mdCoords[iRow][0]+mdCoords[iRow+1][0])*(mdCoords[iRow][0]*mdCoords[iR
ow+1][1]-mdCoords[iRow+1][0]*mdCoords[iRow][1]);

    dY=dY+(mdCoords[iRow][1]+mdCoords[iRow+1][1])*(mdCoords[iRow][0]*mdCoords[iR
ow+1][1]-mdCoords[iRow+1][0]*mdCoords[iRow][1]);
```

```
    }

    dX=dX/(6.0*dArea);
    dY=dY/(6.0*dArea);

    //Output the centroid coordinates
    out1 << dX << " " << dY << endl;

    //Compute the new corner coordinates
    Matrix<double> mdNewCoords=mdCoords;
    mdNewCoords.redim(mdNewCoords.nRows()-1,mdNewCoords.nCols());

    for(iRow=0;iRow<mdNewCoords.nRows();iRow++)
    {
        mdNewCoords[iRow][0]=dX+dDist*sin(dAzimuth);
        mdNewCoords[iRow][1]=dY+dDist*cos(dAzimuth);
        dAzimuth+=dPi/2.0;
    }

    //Print the new corner coordinates to an output file
    mdNewCoords.print(out1);
}


///////////////////////////////////////////////////////////////////////////////////////////////////////////////////////////////////
// Filename: Functions.cpp
// Author:David McAllister
// Date:September 23,2004

#include "Functions.h"

Matrix<double> mdReadIn(char* cFileName)
{
    //Define and open the input file stream
    ifstream if1;
    if1.open(cFileName);

    //Define and read in the row and column number variables
    int iRowNum=0;
    int iColNum=0;
    if1 >> iRowNum >> iColNum;

    //Define matrix and temporary storage variables
    Matrix<double> mdRead(iRowNum,iColNum);
    double dTempStore = 0.0;
```

```cpp
//Read in the values from the text file and insert them into the Matrix
for(int iRowIter=0; iRowIter<iRowNum;iRowIter++)
{
    for(int iColIter=0;iColIter<iColNum;iColIter++)
    {
            if1 >> dTempStore;
            mdRead[iRowIter][iColIter]=dTempStore;
    }
}

//Return the matrix that was read in
return mdRead;
}

double dPolArea(Matrix<double> &mdCoords)
{
    double dArea=0.0;

    for(int iRow=0;iRow<mdCoords.nRows()-1;iRow++)
    {

    dArea=dArea+0.5*(mdCoords[iRow][0]*mdCoords[iRow+1][1]-mdCoords[iRow+1][0]*md
Coords[iRow][1]);
    }

    return dArea;

}

double dGetAzimuth(Matrix<double> &mdCoords)
{
    //Define azimuth variables
    double dAzSum=0.0;
    double dAzimuth=0.0;

    //Compute azimuth between adjoining points
    for(int iRow=0;iRow<mdCoords.nRows()-1;iRow++)
    {

    dAzimuth=atan2(mdCoords[iRow+1][0]-mdCoords[iRow][0],mdCoords[iRow+1][1]-mdCo
ords[iRow][1])+double(iRow)*dPi/2.0;

        //Ensure angle is from 0 to 2Pi
        while(dAzimuth<0.0)
        {
                dAzimuth+=2.0*dPi;
```

```cpp
		}

		while(dAzimuth>2.0*dPi)
		{
			dAzimuth-=2.0*dPi;
		}

		dAzSum+=dAzimuth;
	}

	double dMeanAz=dAzSum/double(mdCoords.nRows()-1);

	return dMeanAz;
}

/////////////////////////////////////////////////////////////////////////////////////////////////////////////////////////////////
// FileName:Functions.h
// Author:David McAllister
// Date:Sept 22,2004


#ifndef FUNCTIONS_H
#define FUNCTIONS_H

#include<fstream.h>
#include<math.h>
#include "Matrix.hpp"
#include "ErrorGrids.h"

const double dPi=3.14159265;

//Computes the azimuth given the initial coords
double dGetAzimuth(Matrix<double> &mdCoords);

//Reads the data in the specified file into a matrix of type double
Matrix<double> mdReadIn(char *cFileName);

//Computes the area contained within a given set of points
double dPolArea(Matrix<double> &mdCoords);


#endif FUNCTIONS_H
/////////////////////////////////////////////////////////////////////////////////////////////////////////////////////////////////
```